

NONLINEAR AEROELASTIC ANALYSIS OF AIRCRAFT WING-WITH-STORE
CONFIGURATIONS

A Dissertation

by

KIUN KIM

Submitted to the Office of Graduate Studies of
Texas A&M University
in partial fulfillment of the requirements for the degree of

DOCTOR OF PHILOSOPHY

May 2004

Major Subject: Aerospace Engineering

NONLINEAR AEROELASTIC ANALYSIS OF AIRCRAFT WING-WITH-STORE
CONFIGURATIONS

A Dissertation

by

KIUN KIM

Submitted to Texas A&M University
in partial fulfillment of the requirements
for the degree of

DOCTOR OF PHILOSOPHY

Approved as to style and content by:

Thomas W. Strganac
(Chair of Committee)

Paul Cizmas
(Member)

Johnny Hurtado
(Member)

Luis San Andres
(Member)

Walter E. Haisler
(Head of Department)

May 2004

Major Subject: Aerospace Engineering

ABSTRACT

Nonlinear Aeroelastic Analysis of
Aircraft Wing-with-Store Configurations. (May 2004)

Kiun Kim,

B.S., Inha University, M.S., Inha University

Chair of Advisory Committee: Dr. Thomas W. Strganac

The author examines nonlinear aeroelastic responses of air vehicle systems. Herein, the governing equations for a cantilevered configuration are developed and the methods of analysis are explored. Based on the developed nonlinear bending-bending-torsion equations, internal resonance, which is possible in future air vehicles, and the possible cause of limit cycle oscillations of aircraft wings with stores are investigated. The nonlinear equations have three types of nonlinearities caused by wing flexibility, store geometry and aerodynamic stall, and retain up to third-order nonlinear terms. The internal resonance conditions are examined by the Method of Multiple Scales and demonstrated by time simulations. The effect of velocity change for various physical parameters and stiffness ratio is investigated through bifurcation diagrams derived from Poinaré maps. The dominant factor causing limit cycle oscillations is the stiffness ratio between in-plane and out-of-plane motion.

To my father in heaven

ACKNOWLEDGMENTS

I wish to express my sincere appreciation to my parents and to all my advisors including my mentor, Dr. Strganac. Regardless of their ages or positions, they are my advisors. As the proverb says, a penny and penny stacked will be a great amount, my work could not be finished without their support. Although my children are very young, they also have given me an impetus to continue my study.

I am especially indebted to my advisor, Dr. Strganac for his teaching, guidance, and support during all phases of this research. Also, I would like to thank my committee members, Dr. Luis San Andres, Dr. Paul Czimas and Dr. Johnny Hurtado for their valuable comments and time spent in reviewing my primary manuscript.

Dr. Patrick Miller, who is an associate professor at Stevens Institute of Technology, and Professor Eusebius Doedel, who is at California Institute of Technology, are acknowledged for their valuable time spent in answering my questions about DsTool and AUTO2000, respectively.

There are two special guys, KS Kim and JS Kim that I must not forget. Many problems with my computer, including the installation of nonlinear softwares, were resolved by KS Kim. Although I am senior to JS Kim, who is a graduate student at Penn State, he is very familiar with the development of nonlinear equations of motion. His assistance was very helpful in developing the nonlinear equations.

Finally, I am thankful to my wife, Myounghee and to our children, Jinho and Sunho. Time in and time out, they encouraged me and provided me with many chances to think about what I have to do. For more than four years, my wife has been very busy supporting my family. Without my wife's sacrifice, I could not have finished my work.

TABLE OF CONTENTS

CHAPTER		Page
I	INTRODUCTION	1
	A. Statement of Problem	1
	B. Literature Review	3
	C. Objective and Scope of the Dissertation	10
II	NONLINEAR EQUATIONS OF MOTION	14
	A. Kinematics and Euler Angles	14
	B. Taylor-Series Expansions and Ordering Scheme	20
	C. Aerodynamics	21
	D. Nonlinear Equations of Motion	23
	1. Nondimensional Bending-Bending-Torsion	26
	2. Bending-Torsion	32
III	NONLINEAR APPROACHES	36
	A. Time Simulation	36
	B. Perturbation Methods	37
	C. Nonlinear Software Packages DsTool and AUTO(a Con- tinuation Method)	57
	D. Phase Plane Analysis and Poincaré Maps	59
IV	SYSTEMS WITH QUADRATIC NONLINEARITIES	69
	A. Equations of Motion for a Wing with Quadratic Nonlinearities	69
	B. Analysis by the Method of Multiple Scales	72
	1. Uncoupling Process in Aeroelastic Systems	73
	a. Process I	73
	b. Process II	75
	2. Approximation	77
	a. IR condition 1 $\omega_1 = 2\omega_3$	82
	b. IR condition 2: $\omega_1 = \omega_2 + \omega_3$	85
	C. Benchmark Wing Models	88
	1. The Effects of Wing Span	91
	D. Time Simulation	94
	1. Case I (L=20 ft): $\omega_2 = 2\omega_3$	95

CHAPTER	Page
2. Case II (L=36ft): $\omega_1 = 2\omega_3$	98
3. Case III (L=60ft): $\omega_1 = \omega_2 + \omega_3$	102
E. Discussion	106
V BENDING-TORSION DYNAMICS OF A CANTILEVER WING WITH CUBIC NONLINEARITIES	109
A. Equations of Motion	110
B. Flutter Analysis	111
C. Poincaré Map and Bifurcation Diagram	112
D. Effect of External Store	126
E. Discussion	130
VI BENDING-BENDING-TORSIONAL MOTION	132
A. Systems with only Aerodynamic Nonlinearities	132
1. Equations of Motion	133
2. Analysis by the Method of Multiple Scales	135
3. Numerical Simulations and Bifurcation Analysis	138
B. Systems with Structural Nonlinearities	143
1. Equations of Motion	144
2. Analysis by the Method of Multiple Scales	145
3. Numerical Simulations and Bifurcation Analysis	152
C. The System with Store Nonlinearities	153
1. Equations of Motion	153
2. Analysis by the Method of Multiple Scales	155
3. Numerical Simulations and Bifurcation Analysis	155
D. The System with All Nonlinearities	156
1. Equations of Motion	156
2. Analysis by the Method of Multiple Scales	158
3. Numerical Simulation and Bifurcation Analysis	159
E. Discussion	170
VII CONCLUSIONS	174
REFERENCES	177
APPENDIX I	184
APPENDIX II	212

CHAPTER	Page
APPENDIX III	220
VITA	273

LIST OF TABLES

TABLE		Page
I	System Properties for the NATAm	89
II	System Properties for the HGW	90
III	Natural Frequencies for the HGW	92
IV	Natural Frequencies for the HGW with a Store	93
V	Uncoupled Bending and Torsion Frequencies for the Selected Three Cases	93
VI	Possible Frequency Combination for Case I ($V = 0$)	97
VII	Possible Frequency Combination for Case II ($L = 36$ ft & $V = 0$ ft/sec)	101
VIII	Response Characteristics at $Vr = 0.95$	114
IX	Order of Terms Used in the Hodges-Dowell Equations ²²	200
X	Order of Terms Used in the Pai & Nayfeh Equations ¹²	201

LIST OF FIGURES

FIGURE		Page
1	Undeformed wing coordinate systems	15
2	Deformed wing coordinate systems	16
3	Quasi-steady aerodynamics	22
4	Spring pendulum	39
5	Time simulation of spring pendulum	40
6	Modal response of spring pendulum for an initial condition, $(a_1, a_2) = (0.01, 0.01)$	44
7	Frequency-Amplitude curves for the Duffing Equation	50
8	Phase portraits for the Duffing Equation ($k=0.0, \Gamma = 0$)	52
9	Bifurcation diagram obtained by the Method of Harmonic Balance	57
10	Bifurcation diagram obtained by AUTO (the maximum)	58
11	Bifurcation diagram(2) obtained by AUTO(L2-norm)	59
12	Phase portraits for the Duffing Equations obtained by DsTool: (a) $\Gamma = 0.2$ (b) $\Gamma = 0.28$ (c) $\Gamma = 0.29$ (d) $\Gamma = 0.5$	60
13	Phase portrait for the Van der Pol Equation	61
14	Bifurcation diagram(1) of Poincaré maps for the Duffing Equation	63
15	Bifurcation diagram(2) of Poincaré maps for the Duffing Equation	63
16	Time simulations, phase portraits, and Poincaré maps of the Duffing Oscillator for $k = 0.3, \omega = 1.2, \Gamma = 0.2(\text{period} - 1)$	65
17	Frequency content for $k = 0.3, \omega = 1.2, \Gamma = 0.2(\text{period} - 1)$	65

FIGURE	Page
18	Time simulations, phase portraits, and Poincaré maps of the Duffing Oscillator for $k = 0.3, \omega = 1.2, \Gamma = 0.28(\textit{period} - 2)$ 66
19	Time simulations, phase portraits, and Poincaré maps of the Duffing Oscillator for $k = 0.3, \omega = 1.2, \Gamma = 0.29(\textit{period} - 4)$ 66
20	Frequency content for $k = 0.3, \omega = 1.2, \Gamma = 0.28(\textit{period} - 2)$ 67
21	Time simulations, phase portraits, and Poincaré maps of the Duffing Oscillator for $k = 0.3, \omega = 1.2, \Gamma = 0.5(\textit{period} - 1)$ 68
22	Frequency content for $k = 0.3, \omega = 1.2, \Gamma = 0.5(\textit{period} - 1)$ 68
23	Frequencies vs. wing span(L) for the NATAm wing model 91
24	Frequencies vs. wing span(L) for the HGW 94
25	Simulation for Case I (L=20ft & V=0 ft/sec) 96
26	Frequency content for Case I (L=20ft & V=0 ft/sec) 96
27	Simulation for Case I (L=20 ft & V = 50 ft/sec) 99
28	Frequency content for Case I (L=20 ft & V=50 ft/sec) 99
29	Time histories for Case II (L=36 ft & V=0 ft/sec) 100
30	Frequencies content for Case II (L=36 ft & V =0 ft/sec) 101
31	Time histories for Case II (L=36 ft& V=50 ft/sec) 103
32	Frequencies content for Case II (L=36 ft& V =50 ft/sec) 103
33	Simulation results for Case III (L=60 ft & V=0 ft/sec) 104
34	Frequency content for Case III (L=60 ft& V=0 ft/sec) 105
35	Approximation for Case III (L=60 ft & V=5 ft/sec) 106
36	Simulation results for Case III (L=60 ft& V=5 ft/sec) 107
37	Frequency content for Case III (L=60 ft & V=5 ft/sec) 107

FIGURE	Page
38	V-f and V-g plots 111
39	Simulation results at $V_r = 0.85$ 112
40	Simulation results at $V_r = 1.05$ 113
41	Simulation results at $V_r = .95$ 115
42	Phase portrait and Poincaré map at $V_r = 0.95$ 115
43	Bifurcation diagram for Case BT2 (A) 117
44	Simulation results for Case BT2 ($V_r = 1.15$) 117
45	Phase portrait and Poincaré map for Case BT2 ($V_r = 1.15$) 118
46	Bifurcation diagram for Case BT7 119
47	(a) Phase portrait and Poincaré map and (b) simulation results for Case BT7 ($V_r = 0.78$) 120
48	(a) Phase portrait and Poincaré map and (b) simulation results for Case BT7 ($V_r = 0.96$) 121
49	Phase portrait and Poincaré map for Case BT7 ($V_r = 0.81$) 123
50	Phase portrait for Case BT7 ($V_r = 0.89$) 123
51	Poincaré map for Case BT7 ($V_r = 0.89$) 124
52	Bifurcation diagram for a sample case (AUTO2000) 124
53	Bifurcation diagram for a sample case (Poincare map)) 125
54	Simulation results for a sample case: (a) $V=24\text{m/sec}$ (Left) (b) $V =28\text{m/sec}$ (right) 126
55	Bifurcation diagram for Case BT7 ($x_s=0.5\text{b}$) 127
56	Three dimensional bifurcation diagram for several store masses (BT7) 128

FIGURE	Page
57	Three dimensional bifurcation diagram for variation store inertia(BT7) 129
58	Three dimensional bifurcation diagram for variation x_s (BT7) 129
59	Three dimensional bifurcation diagram for variation z_s (BT7)) 130
60	V-f and V-g plots for a wing with an external store (BBT1) 138
61	Bifurcation diagram for a wing with aerodynamic nonlinearities (w_{max}) 139
62	Bifurcation diagram for a wing with aerodynamic nonlinearities (a_{max}) 140
63	Time histories for a wing with aerodynamic nonlinearities (Vr=1.1) . 141
64	Phase portrait and Poincare maps for a wing with aerodynamic nonlinearities(Vr=1.1) 142
65	Phase portrait and Poincare maps for a wing with aerodynamic nonlinearities(Vr=0.9) 142
66	FFT for a wing with aerodynamic nonlinearities: (a) Vr=0.85(Left, Upper), (b) Vr=0.95(Right, Upper), (c) Vr=1.05(Left, Lower), (d) Vr=1.15(Right, Lower) 143
67	Bifurcation diagram for a wing (w_{max}) 153
68	Bifurcation diagram for a wing (α_{max}) 154
69	Bifurcation diagram for a wing [$M_s = 0.1mL$, $I_{sy} = 0.1I_yL$, $x_s = z_s = 0.0$, and $\beta_z = 44$],(w_{max}) 159
70	Bifurcation diagram for a wing [$M_s = 0.2mL$, $I_{sy} = 0.1I_yL$, $x_s = -0.2b$, $z_s = 0.0$, $\beta_z = 44$],(w_{max}) 160
71	Bifurcation diagram for a wing [Store parameters $M_s = 0.2mL$, $I_{sy} = 0.1I_yL$, $x_s = -0.2b$, $z_s = 0.0$, $\beta_z = 44$],(α_{max}) 161
72	Bifurcation diagram for a wing [$M_s = 0.3mL$, $I_{sy} = 0.1I_yL$, $x_s = -0.2b$, $z_s = 0.0$, $\beta_z = 44$],(w_{max}) 162

FIGURE	Page
73	Subcritical Bifurcation for a wing [$M_s = 0.3mL$, $I_{sy} = 0.1I_yL$, $x_s = -0.2b$, $z_s = 0.0$, $\beta_z = 44$],(w_{max}) 162
74	Time histories of w for various initial conditions and velocities: $V_r = 0.8$ (Left) and $V_r = 0.9$ (Right) 164
75	Time history and frequency content for two initial conditions IC2 (lower) and IC3(upper) [$M_s = 0.3mL$, $I_{sy} = 0.1I_yL$, $x_s =$ $-0.2b$, $z_s = 0.0$, $\beta_z = 44$],(w_{max}) 165
76	Three dimensional spectral map (or Waterfall plot) for an initial condition IC3 [$M_s = 0.3mL$, $I_{sy} = 0.1I_yL$, $x_s = -0.2b$, $z_s = 0.0$, $\beta_z = 44$],($w - motion$) 166
77	Three dimensional spectral map (or Waterfall plot) for an initial condition IC3 [$M_s = 0.3mL$, $I_{sy} = 0.1I_yL$, $x_s = -0.2b$, $z_s = 0.0$, $\beta_z = 44$],($\alpha - motion$) 166
78	Bifurcation diagram for a wing [$M_s = 0.2mL$, $I_{sy} = 0.3I_yL$, $x_s =$ $-0.2b$, $z_s = 0.0$, $\beta_z = 44$],(w_{max}) 167
79	Bifurcation diagram for a wing [$M_s = 0.2mL$, $I_{sy} = 0.1I_yL$, $x_s =$ $-0.4b$, $z_s = 0.0$, $\beta_z = 44$],(w_{max}) 167
80	Bifurcation diagram for a wing [$M_s = 0.2mL$, $I_{sy} = 0.1I_yL$, $x_s =$ $-0.2b$, $z_s = 0.3b$, $\beta_z = 44$],(w_{max}) 168
81	Bifurcation diagram for a wing [$M_s = 0.2mL$, $I_{sy} = 0.3I_yL$, $x_s =$ $-0.2b$, $z_s = 0.3b$, $\beta_z = 44$],(w_{max}) 169
82	Bifurcation diagram for a wing [$M_s = 0.2mL$, $I_{sy} = 0.1I_yL$, $x_s =$ $-0.2b$, $z_s = 0.0b$, $\beta_z = 10$],(w_{max}) 169
83	Bifurcation diagram for a wing [$M_s = 0.2mL$, $I_{sy} = 0.1I_yL$, $x_s =$ $-0.2b$, $z_s = 0.0b$, $\beta_z = 10$, α_{max}] 170
84	Bifurcation diagram for a wing [$M_s = 0.2mL$, $I_{sy} = 0.3I_yL$, $x_s =$ $-0.2b$, $z_s = 0.0b$, $\beta_z = 44$],(w_{max}) 171
85	Bifurcation diagram for a wing [$M_s = 0.2mL$, $I_{sy} = 0.3I_yL$, $x_s =$ $-0.2b$, $z_s = 0.0b$, $\beta_z = 10$],(α_{max}) 171

FIGURE		Page
86	Euler Angles and the derivatives of displacements	187
87	A differential element of the beam	191

CHAPTER I

INTRODUCTION

A. Statement of Problem

Aeroelasticity is the study of the interaction of aerodynamics, elasticity, and dynamics. Flutter is the classic aeroelastic instability and, based on linear theories, the stable flight region is routinely identified. Because a margin of safety is introduced in that region, the aircraft may not experience any unstable situations in the flight envelope. However, some aircraft have experienced Limit Cycle Oscillation (LCO) which maintains the amplitude during flight tests. Linear approaches do not provide an adequate explanation for this response. According to linear theory, the responses must be decayed. In addition, new designs with highly flexible wings are expected in future air vehicles, and the corresponding motion will not be fully described by a linear theory because the increased flexibility may cause nonlinearities. These two situations require a nonlinear aeroelastic analysis capability.

A persistent aeroelastic problem is Limit Cycle Oscillation which has been observed in high-performance aircraft, such as the F-5, F-16, F-111, and F/A-18.¹⁻³ Historical LCO examples and safe flight test methods are presented by Norton.⁴ It is stated that the LCO of the F-16 have been reported from the earliest days of prototype flight tests. LCOs are observed over a wide range of Mach numbers, from subsonic through transonic to supersonic conditions. Abort criteria for flight operation have been suggested in order to prevent possible damage because the phenomena is not fully understood. It is important to determine the characteristics of LCO responses

The journal model is *AIAA Journal*.

because they observed at velocity less than the flutter speed.

The term LCO is used to describe these unusual responses, because the aeroelastic response does not diverge, but maintains the amplitude with periodic characteristics. Other terms, such as divergent LCO, limit cycle flutter, and limited amplitude flutter, also are used to describe the unusual aeroelastic response.³ Denegri,¹ Denegri and Cutchins⁵ introduced other terminologies, including both typical LCO and non-typical LCO. The use of these various terms indicates that the phenomena is not understood fully.

For typical LCOs, the amplitude is constant at stabilized flight conditions. But, for non-typical LCO's, the amplitude progressively increases with Mach number and dynamic pressure. Bunton and Denegri³ describe a possible explanation of the phenomena, and attempt to use classical linear flutter analysis to correlate to flight test results, including the LCO response. However the LCO amplitude and LCO onset velocity can not be provided by linear analysis.

Most traditional fighter aircraft have relatively low aspect ratio wings on the order of 2-3, but the wings of certain future uninhabited air vehicles will be very flexible due to high aspect ratios on the order of 30 or more. Very complex responses are expected due to this flexibility. Although existing aeroelastic tools are useful in identifying the traditional aircraft stability, they cannot provide enough information regarding the aeroelastic stability of future air vehicles. The large deformation response expected in the highly flexible wing will cause nonlinear phenomena, such as limit cycle oscillations, chaotic motion, and internal resonance. However, the related results have not yet been adequately obtained.

Although in-plane wing motion may be negligible in traditional aircraft having low aspect ratio wings, it should be considered in the case of air vehicles with high aspect ratio wings. It will be shown that bending and torsional frequencies are proportional to “ $1/\text{span}$ ” and “ $1/\text{span}^2$ ”, respectively. An increase of aspect ratio reduces the frequency ratio between bending and torsional motions. Consequently, the frequency ratio may have a significant role in the nonlinear responses through nonlinear coupling terms. Quadratic and cubic nonlinearities may provide various autoparametric (internal) resonance conditions.

The advantages of simplified linear approaches are not present in nonlinear analysis. Linearized formulations are often used in some case to simplified nonlinear problem in the frequency domain. But, in order to fully explore the nonlinear characteristics, it is deemed necessary to perform the analysis in the time domain. In order to perform the nonlinear aeroelastic analysis, development of the proper nonlinear equations of motion is required, and useful solution approaches must be considered.

B. Literature Review

Nonlinear responses of aeroelastic systems reveal not only unstable linear responses including flutter, but also stable responses of interest such as limit cycle oscillations and chaotic motions. Internal resonance may be possible under certain circumstances. Aeroelastic system nonlinearities may be caused by aerodynamic nonlinearities, such as transonic aerodynamic and stall effects, and structural nonlinearities. The structural nonlinearities can be divided into two categories: distributed and concentrated. A nonlinearity caused by large deformation belongs to the distributed category, and

friction and freeplay are examples of the concentrated nonlinearity. An aeroelastic system with any nonlinearity may be solved by using various nonlinear approaches.

For systems with a concentrated nonlinearity, the Method of Harmonic Balance or the so-called Describing Function Approach is useful. Using the Describing Function Approach, the nonlinear term can be replaced by an equivalent stiffness. Because the modified equation is linear, existing aeroelastic methodologies such as the *k method* and *P-k method* can be used for analysis, and the characteristics of the nonlinear system can be identified. Tang and Dowell⁶ used this approach in their nonlinear analysis. A freeplay-type nonlinearity is linearized by this method. Kim and Lee⁴¹ adopted this technique to solve the nonlinear aeroelastic problem for a flexible airfoil with a concentrated nonlinearity. Applying this method to the structural freeplay nonlinearity, they obtained an equivalent linear system. Although Tang and Kim considered different systems, they observed that a freeplay structural nonlinearity leads to a bounded response such as LCO and chaotic motion.

In order to determine the source of the LCO responses observed in flight tests, researchers suggest various possibilities. A structural damping sources are suggested by Chen et al.⁸ as a possible cause of LCO motion on the F-16. Their research focused on the LCOs at a relatively low Mach number. They compared several store configurations and showed that although the natural frequencies and mode shapes were very similar to each other, small differences in either aerodynamic or structural characteristics might cause LCO response. By using nonlinear statistical techniques, flight test data were analyzed by Stearman et al.^{2,9} They focused on the LCOs of the F/A-18 and F-111. Using a mathematical model having the form of the Forced Mathieu-Hill equations, they showed that both combination and parametric resonances could occur.

Similar instabilities may be present in the experiments of Cole.¹⁰ Torsional instabilities, possibly related to resonance, were observed in wind tunnel tests. The unexpected torsional instability occurred at a dynamic pressure well below the expected flutter conditions as predicted by a linear method. Oh et al.¹¹ suggested that a two-to-one internal resonance might be responsible for this instability. They determined the linear natural frequencies and the mode shapes of a cantilever metallic plate, and experimentally showed that an antisymmetric vibration mode was excited by a 2:1 internal resonance mechanism. To explain the experimental results, they referred to the study of Pai and Nayfeh¹² in which nonlinear beam theory was used. Oh et al.¹¹ concluded that the nonlinear beam theory was essential to the complete study of the nonlinear structure. Though resonance and bifurcation characteristics were studied using this theory, aerodynamic loads were not considered in their effort.

Gillatt¹³ investigated the presence of internal resonance in the aeroelastic systems. To study the effects of aerodynamic nonlinearities, a quasi-steady aerodynamic stall model was used. In these studies, the stall model was represented by a cubic function. Gillatt showed that a 3:1 internal resonance is possible. Thompson et al.,^{14,15} Ko et al.,¹⁶ O'Neil et al.¹⁷ and Block et al.¹⁸ considered nonlinear aeroelastic effects through wind tunnel experiments with the Nonlinear Aeroelastic Test Apparatus (NATA). Investigations of wing section models provided validation to their studies of nonlinear aeroelastic mechanisms. Thompson¹⁵ studied the effects of structural and store configuration nonlinearities. Thompson showed that although store-induced kinematic nonlinearities may appear to be negligible, these nonlinearities introduce behavior that would not be present in linear systems. These studies were based on a rigid typical wing section model which is mounted to a flexible support and restricted to

two degree-of-freedom motion. Owing to the simplicity of an airfoil model, many nonlinear aeroelastic analyses were performed by using a typical section.

Thus, it was meaningful to extend the study from a section model to a continuous wing model with nonlinearities, such as aerodynamic, structural, and store configuration nonlinearities. Tang and Dowell¹⁹ studied the aeroelastic response of a high-aspect ratio wing. The structural nonlinearity was expressed by the Hodges-Dowell equation,¹⁹ and the ONERA stall model¹⁹ was used to describe the nonlinear aerodynamics. They showed that the onset of the LCO was dependent on a balance between stall aerodynamics and structural nonlinear forces. In their study, LCO responses were theoretically and experimentally captured. They showed by analysis that the stall aerodynamics dominated the considered model. Although a tip mass was attached to the model, the role of the tip mass was not explicitly explained. If the in-plane motion was neglected, the nonlinear coupling terms would vanish. Patil and Hodges²⁰ performed nonlinear aeroelastic analysis of a complete aircraft with high aspect-ratio wings. LCOs were observed, but the amplitude was beyond practical limitations. In their study, store effects were not considered and the existence of internal resonance was not studied.

Tang and Dowell¹⁹ produced meaningful results, but their formulation could be improved. They used semi-experimental aerodynamics (ONERA stall model), for which it was not easy to perform analytical analysis. Cubic nonlinear terms were required to describe the stall phenomena with the ONERA stall model. It was not easy to explicitly identify the imbalance between the order of structural nonlinearities and aerodynamic nonlinearities.

Kim and Strganac²¹ studied LCOs for a cantilever wing-with-store with three possible nonlinearities: aerodynamic, structural, and store-induced. When these three nonlinearities were combined, LCOs were observed at speeds below the flutter velocity. This study was limited to special conditions, such as wing velocity and store properties. The equations used were not suitable for a high aspect ratio wing, since in-plane motion was neglected.

In order to improve the understanding of nonlinear aeroelastic systems, proper nonlinear equations and appropriate solution approaches are required. Hodges and Dowell²² provide nonlinear equations with quadratic nonlinearities for twisted non-uniform rotor blades. Dowell, Traybar and Hodges²³ examined the Hodges-Dowell equation to evaluate the equation. According to their experimental results, systematic differences between theory and experiment occur for large deflections because the theory contains only quadratic nonlinearities. Hodges, Crespo da Silva and Peters²⁴ show that the nonlinear equations governing flexural deformation should also include all nonlinear terms up through third order.

A more accurate set of equations than those of Hodges and Dowell²² are provided by Rosen and Fiedmann.²⁵ Although the equations are very similar to those of Hodges and Dowell,²² the predicted responses are in much better agreement with experimental results obtained by Dowell *et al.*²³ This improvement is due to attributed to additional higher order nonlinear terms. Rosen²⁶ obtained improved numerical results by adding some cubic nonlinearities. At first, Rosen²⁵ expected that the most important applications is in the field of aeroelasticity of helicopter rotor blades. However, their later publications show that they focused on the investigation of the nonlinear

behavior of beams, not wings.

Another set of equations were derived by Crespo da Silva and Glynn.²⁷ They adopted the extended form of Hamilton's principle. Their purpose was to formulate a set of mathematically consistent nonlinear equations. Although cubic terms were not shown explicitly in their curvature terms, these developed equations fully included the contributions due to nonlinear curvature and nonlinear inertia. Using the developed equations, they performed nonlinear analysis of a fixed-free beam.²⁸ They showed that nonlinear curvature terms play a significant role in the nonlinear flexural response of the beam when compared to nonlinear inertia terms. Their equations were extended to the case of composite beams by Pai and Nayfeh.¹² For the case of an isotropic beam, the equations were simpler than those of Crespo da Silva et. al. By applying an ordering scheme, inertia terms having higher order were dropped. The equations contain structural coupling terms and include both quadratic and cubic nonlinearities due to curvature and inertia. For various systems having different material properties, degrees-of-freedom, and exciting conditions, their equations were used to provide solutions. For isotropic beams possessing flexural-flexural-torsional motion, they showed that one-to-one and two-to-one internal resonances are possible. These results were cited by Oh and Nayfeh¹¹ to explain their experimental results. The equation has the assumption that the beam has no pre-twist angle, and the mass center and elastic axes coincide. This assumption is a primary reason that these equations are not popular in the field of aeroelasticity, as a major source of coupling is eliminated.

Although the Describing Function Approach is a powerful method for solving systems with a concentrated nonlinearity, it is not easy to extend the approach to the

system with multiple and/or distributed nonlinearities. Consequently, many nonlinear aeroelastic problems are solved in the time domain. To solve the second-order differential equations in the time domain, they are transformed into a set of first-order differential equations in state-space. By using numerical integration methods, such as the Runge-Kutta method, the modified equations can be solved. Based on the results, system characteristics can be identified. The time history directly shows the behavior of the system. Because the nonlinear responses depend upon the initial conditions and given parameters, many simulations are required to fully characterize responses. Unfortunately, many characteristics might not be determined without analysis

Phase plane analysis including phase portraits may provide intuitive insights about the nature of the nonlinear system. Phase portraits are used by Tang and Dowell¹⁹ and Oh and Nayfeh¹¹ to show LCO responses and 2:1 internal resonances, respectively. Similar characteristics can be detected by using Poincaré maps. The number of fixed points of Poincaré maps indicates the number of periodic components included in the nonlinear response. The signal showing the possibility of 2:1 internal resonance can be denoted by two fixed points, and a simple LCO response can be expressed by a single fixed point in the phase plane. For forced vibration systems, Poincaré maps may provide additional information about frequency content included in the response. But the map for autonomous system, including aeroelastic systems, may only provide relative frequency, since these systems do not have any exciting force and frequency. In order to identify frequency content, the Fourier spectrum of signal should be examined.

The use of the perturbation method may guide nonlinear analysis of response characteristics of the considered system. In the field of nonlinear vibrations, the Method

of Multiple Scales is used. Using the method, Crespo da Silva and Glynn²⁸ analyzed the nonlinear resonant forced oscillations of a fixed-free beam, and Pai and Nayfeh showed that internal resonances are possible in nonlinear beam systems. Gilliatt and Strganac introduced this concept into the field of aeroelasticity. They showed that 3:1 internal resonance is possible, and that the characteristics of 3:1 internal resonance are identified in the Fourier spectrum of responses.

C. Objective and Scope of the Dissertation

Based on the literature review and recent studies by the author,²⁹ the following research activities are proposed.

First, in order to improve the understanding of nonlinear aeroelastic responses, the first step must be the proper development of the nonlinear equations of motion. The nonlinear equations will be analyzed using the approaches shown in the literatures.^{30,31} Numerical simulation, perturbation methods and nonlinear softwares such as DsTool³² and AUTO³³ will be included in those approaches. The nonlinear structural model will be the foundation of the entire research program. From a comprehensive literature search and the recent studies by this investigator, an improved nonlinear structural model will be developed, in which the in-plane motion will be included. Although in-plane motion is negligible in traditional aircraft with low aspect-ratio wings, it must not be neglected in a system with high aspect-ratio wings.

Using the extended version of Hamilton's principle, the nonlinear equations of motion

will be derived. After the nonlinear equations are constructed, dimensional analysis will be performed. Through a process of nondimensionalization, the important dimensionless parameters governing the responses of the system will be identified, and some higher order terms may be eliminated. Consequently, proper equations of motion will be established. The final nonlinear equations will include all nonlinear terms up through third order.

Dimensional analysis will be performed to the nonlinear equations. Through a process of nondimensionalization, the important dimensionless parameters governing the responses of the system could be identified, and some higher order terms may be excluded as a consequence. The final nonlinear equations will consider all nonlinear terms up through third order.

Second, in contrast to linear systems, the nonlinear system may show multiple equilibrium points, limit cycles, bifurcations and chaos. In order to understand a complex nonlinear system, one needs to utilize several approaches to fully analyze all nonlinear characteristics. Therefore, a comprehensive solution methodology is proposed as a major research topic. For a specified initial condition and/or parameter, the time history, Poincaré map, and Fourier spectrum can provide meaningful results. However, these approaches are not effective to examine global characteristics and/or the effects of any parameter. The bifurcation diagram is a very useful tool to concisely denote the change in characteristics when parameters are varied. The bifurcation diagram consists of fixed points. These fixed points can be detected by Poincaré maps and/or a continuation method.

Using the fixed points obtained from the Poincaré maps, bifurcation analyses have

been performed in the author's recent work. Although meaningful results are generated through this approach, it has limitations. A more enhanced approach tool is required, because there are many parameters, and the nonlinear responses depend on the initial conditions. To effectively study the characteristics of nonlinear aeroelastic systems, a dynamic system toolkit, DsTool³² and AUTO will be also examined. DsTool is a computer program for the interactive investigation of dynamical systems. Through some well-known examples including the Duffing Equation, the bifurcation capability of DsTool will be evaluated. Because DsTool may reveal weakness in special cases, such as the physics present in aeroelastic systems, additional tools will be also considered, if necessary. Then, bifurcation analysis for the aeroelastic system will be performed. Another useful approach is found in perturbation methods, such as the Method of Multiple Scales. Because blind simulation may generate limited and/or inaccurate results, and requires much computational time to get adequate results, theoretical analysis is necessary. In particular, internal resonance phenomena are usually explored by using the Method of Multiple Scales.

There are several parameters, such as velocity, initial conditions, wing geometry and store configuration that are of interest. In particular, the effect of in-plane contributions will be studied in detail. In this research, resonance analysis will be also performed because internal resonance may be caused by the nonlinear coupling terms. Especially, it will be explored what specific terms lead to the subcritical bifurcations. For a wing with very high aspect ratios, it is also of value to explore resonance and other bifurcation characteristics. Based on this prior discussion, the following two topics are proposed as primary objectives:

1. Equations of motion - Development of a nonlinear structural model for a cantilever wing with store

- Include in-plane bending, out-of-plane motion and torsion motion
- Include a rigid store model with kinematic nonlinearities
- Maintain consistency in higher order nonlinearities
- Include nonlinear aerodynamics with subsonic stall

2. Solution Approaches - Development of effective and verified solution methodologies.

- Time simulation
- Nonlinear analysis of equations, including bifurcation analysis and resonance analysis
- Comprehensive parametric studies (e.g., the effects of individual and combined nonlinearities, flow velocity, and initial conditions)

CHAPTER II

NONLINEAR EQUATIONS OF MOTION

A. Kinematics and Euler Angles

A cantilever wing with an external store is shown in Fig. 1. This wing has constant length L and mass m per unit length. As shown in Figs. 1 and 2, the wing is initially straight. The relationship between the undeformed shape and the deformed shape can be described with several coordinate systems; one inertially fixed frame, $N : \{O, X, Y, Z\}$ and two local frames, $E : \{Ow, \xi, \eta, \zeta\}$ and $B\{Os, \xi_0, \eta_0, \zeta_0\}$.

The extended Hamilton's principle³⁴ is

$$\int_{t_0}^{t_f} (\delta T_T + \delta W_T) dt = 0. \quad (2.1)$$

When only potential forces are being applied, the Hamilton's principle is enough to describe the behavior of the considered system. But, if there happen to be non-conservative forces, then the extended Hamilton's principle should be adopted. Here, T_T and W_T are the kinetic energy and the virtual work for the total system, respectively. The subscript 'T' means total system. W_T consists of the potential energy (V_T), and the work caused by constraint forces and aerodynamic forces. The kinetic energy and the potential energy can be simplified by the Lagrangian function, $L_T = T_T - V_T$. Using these terms, the principle can be rewritten as

$$\int_{t_0}^{t_f} (\delta L_T + \delta W_A) dt = 0 \quad (2.2)$$

In this expression, the last item δW_A is introduced to express the work by aerodynamic forces. The Lagrangian function can be divided into two parts; wing and store, i.e.

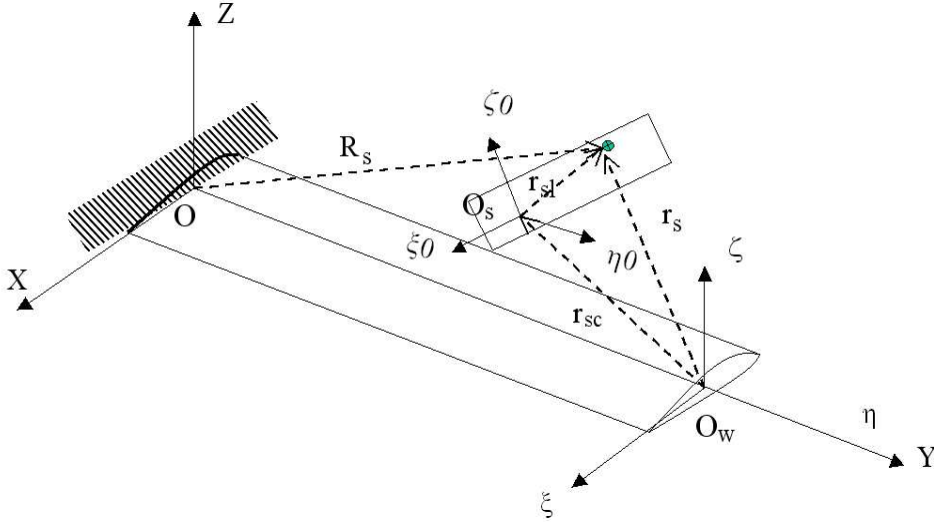


Fig. 1. Undeformed wing coordinate systems

$L_T = L_w + L_s$. The subscripts w and s mean ‘wing’ and ‘store’, respectively. Using the inertial vector R_W representing the position of the wing segment of length \hat{s} , the kinetic energy of the whole wing is represented as

$$\begin{aligned}
 T_W &= \frac{1}{2} \int_0^L \int \int_A \rho_W \dot{R}_W \cdot \dot{R}_W d\hat{s} \\
 &= \frac{1}{2} \int_0^L \int \int_A \rho_W \dot{R}_e \cdot \dot{R}_e d\hat{s} + \int_0^L \int \int_A \rho_W \dot{R}_e \cdot \dot{r}_w d\hat{s} + \frac{1}{2} \int_0^L \int \int_A \rho_W \dot{r}_w \cdot \dot{r}_w d\hat{s} \\
 &= T_{w1} + T_{w2} + T_{w3}
 \end{aligned} \tag{2.3}$$

Because $R_W = R_e + r_w$, the kinetic energy is divided into three parts as shown in Eq.(2.3). The first two terms in this equation represent the translational kinetic energy, and the third term represents the rotational kinetic energy. When the elastic axis does not have any offset distance from the center of mass, the second term should be zero. Introducing some definitions such as mass and moment of inertia which are defined in Appendix A, we obtain

$$T_W = \frac{1}{2} \int_0^L m (\dot{u}^2 + \dot{v}^2 + \dot{w}^2) d\hat{s} + \int_0^L m (\dot{T}_{11} \dot{u}^2 + \dot{T}_{12} \dot{v}^2 + \dot{T}_{13} \dot{w}^2) d\hat{s}$$

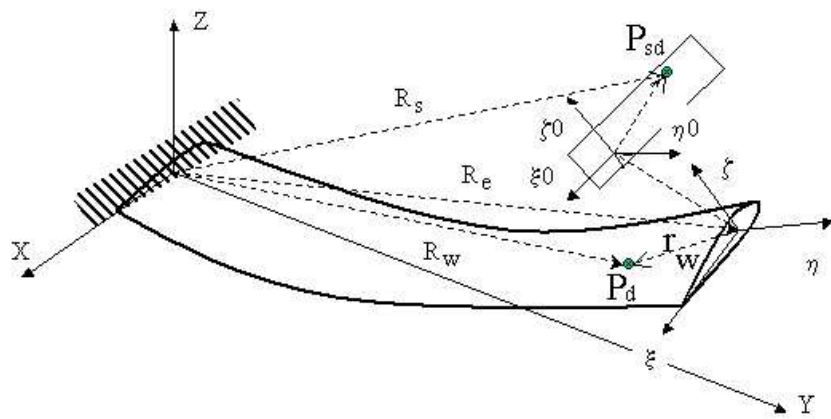


Fig. 2. Deformed wing coordinate systems

$$+\frac{1}{2} \int_0^L \left(I_\xi \omega_\xi^2 + I_\eta \omega_\eta^2 + I_\zeta \omega_\zeta^2 \right) d\hat{s} \quad (2.4)$$

Here, the T_{ij} shown in the second integration are components of the direction cosine matrix, and the ω_k are angular velocities. Definitions for these terms are given in Appendix A.

The potential energy caused by bending and torsion is expressed as

$$V_W = \frac{1}{2} \rho D \rho = \frac{1}{2} D_\xi \rho_\xi^2 + \frac{1}{2} D_\eta \rho_\eta^2 + \frac{1}{2} D_\zeta \rho_\zeta^2 \quad (2.5)$$

where ρ and D are curvatures and stiffnesses, respectively. D_η is the torsional stiffness, and the other stiffnesses D_ξ and D_ζ are the principal bending stiffnesses.

The kinetic energy for the external store is similarly defined as

$$\begin{aligned} T_s &= T_{s1} + T_{s2} + T_{s3} \\ &= \frac{1}{2} \int_0^L M_s \left(\dot{u}^2 + \dot{v}^2 + \dot{w}^2 \right) \delta(y - y_s) d\hat{s} \\ &\quad + \int_0^L M_s \left(\begin{array}{c} (x_s \dot{T}_{11} + z_s \dot{T}_{31}) \dot{u}^2 + (x_s \dot{T}_{12} + z_s \dot{T}_{32}) \dot{v}^2 \\ (+x_s \dot{T}_{13} + z_s \dot{T}_{33}) \dot{w}^2 \end{array} \right) \delta(y - y_s) d\hat{s} \\ &\quad + \frac{1}{2} \int_0^L \left(I_{s\xi} \omega_{s\xi}^2 + I_{s\eta} \omega_{s\eta}^2 + I_{s\zeta} \omega_{s\zeta}^2 \right) \delta(y - y_s) d\hat{s} \end{aligned} \quad (2.6)$$

Here the subscript s means ‘store’. Definitions for these terms are given in Appendix A.

From these energy expressions, it is realized that the Lagrangians are simply expressed as

$$\begin{aligned} L_T &= T_W + T_s - V_W \\ &= L_T(\rho_{\xi,\eta,\zeta}, \omega_{\xi,\eta,\zeta}, \dot{u}, \dot{v}, \dot{w}, \text{etc.}) \\ &= L_T(\dot{u}, \dot{v}, \dot{w}, \phi, \theta, \psi, \dot{\phi}, \dot{\theta}, \dot{\psi}, \phi', \theta', \psi') \end{aligned} \quad (2.7)$$

Using this expression, the variation of L_T can be rewritten as

$$\begin{aligned} \delta L_T = & \frac{\partial L_T}{\partial u} \dot{u} + \frac{\partial L_T}{\partial v} \dot{v} + \frac{\partial L_T}{\partial w} \dot{w} + \frac{\partial L_T}{\partial \phi} \dot{\phi} + \frac{\partial L_T}{\partial \theta} \dot{\theta} + \frac{\partial L_T}{\partial \psi} \dot{\psi} \\ & + \frac{\partial L_T}{\partial \dot{\phi}} \dot{\phi} + \frac{\partial L_T}{\partial \dot{\theta}} \dot{\theta} + \frac{\partial L_T}{\partial \dot{\psi}} \dot{\psi} + \frac{\partial L_T}{\partial \phi'} \dot{\phi}' + \frac{\partial L_T}{\partial \theta'} \dot{\theta}' + \frac{\partial L_T}{\partial \psi'} \dot{\psi}' \end{aligned} \quad (2.8)$$

where the partial derivatives of L_T are defined in Appendix A. The work done by aerodynamic loads are expressed in the following variational form

$$\delta W_A = Q_u \delta u + Q_v \delta v + Q_w \delta w + Q_\theta \delta \theta \quad (2.9)$$

In the above expression, the loads Q_q ($q = u, v, w, \theta$) include aerodynamic loads.

We now consider an inextensibility constraint which is stated in Appendix A given by

$$c_w \equiv (1 + u')^2 + v'^2 + w'^2 - 1 = 0 \quad (2.10)$$

Its variation is

$$\delta c_w = -u' \delta u' - v' \delta v' - w' \delta w' \quad (2.11)$$

So, for general non-zero λ

$$\lambda \delta c_w = \lambda (-u' \delta u' - v' \delta v' - w' \delta w') \quad (2.12)$$

The consideration of this inextensibility constraint modifies Eq. 2.2 to become

$$\int_{t_0}^{t_f} (\delta L_T + \delta W_A + \lambda c_w) dt = 0 \quad (2.13)$$

Substituting the variational expressions into the extended Hamilton's principle, we obtain

$$\begin{aligned}
\delta I_T = & \int_{t_0}^{t_f} \int_0^L \left\{ -\frac{d}{dt} \frac{\partial L_T}{\partial \dot{u}} u - \frac{\partial L_T}{\partial v} v - \frac{d}{dt} \frac{\partial L_T}{\partial \dot{w}} w + \frac{\partial L_T}{\partial \phi} \delta \phi + \frac{\partial L_T}{\partial \theta} \delta \theta + \frac{\partial L_T}{\partial \psi} \delta \psi \right. \\
& - \frac{d}{dt} \frac{\partial L_T}{\partial \dot{\phi}} \delta \phi - \frac{d}{dt} \frac{\partial L_T}{\partial \dot{\theta}} \delta \theta - \frac{d}{dt} \frac{\partial L_T}{\partial \dot{\psi}} \delta \psi - \frac{d}{d\hat{s}} \frac{\partial L_T}{\partial \phi'} \delta \phi - \frac{d}{d\hat{s}} \frac{\partial L_T}{\partial \theta'} \delta \theta - \frac{d}{d\hat{s}} \frac{\partial L_T}{\partial \psi'} \delta \psi \left. \right\} d\hat{s} \\
& - \lambda_p (-u' \delta u' - v' \delta v' - w' \delta w') + Q_u \delta u + Q_v \delta v + Q_w \delta w + Q_\theta \delta \theta \\
& + \left[\frac{\partial L_T}{\partial \phi'} \phi + \frac{\partial L_T}{\partial \theta'} \theta + \frac{\partial L_T}{\partial \psi'} \psi \right]_0^L dt
\end{aligned} \tag{2.14}$$

Because ϕ and ψ are functions of u' , v' and w' as shown in Appendix A, the terms having ϕ and ψ must be expressed in terms of the real deformation. The virtual variations $\delta \phi$ and $\delta \psi$ are

$$\begin{aligned}
\delta \phi &= \frac{\partial \phi}{\partial u'} \delta u' + \frac{\partial \phi}{\partial v'} \delta v' + \frac{\partial \phi}{\partial w'} \delta w' \\
\delta \psi &= \frac{\partial \psi}{\partial u'} \delta u' + \frac{\partial \psi}{\partial v'} \delta v' + \frac{\partial \psi}{\partial w'} \delta w'
\end{aligned} \tag{2.15}$$

After substituting the above variation expressions and performing the integration by parts, Eq.(2.14) can be rewritten as

$$\begin{aligned}
\delta I_T = & \int_{t_0}^{t_f} \left\{ \int_0^L \left\{ \left(\frac{\partial L_T}{\partial u} - \frac{d}{dt} \frac{\partial L_T}{\partial \dot{u}} \right) \delta u - \left(\frac{\partial L_T}{\partial v} - \frac{d}{dt} \frac{\partial L_T}{\partial \dot{v}} \right) \delta v + \left(\frac{\partial L_T}{\partial w} - \frac{d}{dt} \frac{\partial L_T}{\partial \dot{w}} \right) \delta w \right. \right. \\
& + \frac{\partial}{\partial \hat{s}} \left[A_\phi \frac{\partial \phi}{\partial u'} + A_\psi \frac{\partial \psi}{\partial u'} - \lambda_p u' \right] \delta u + Q_u \delta u \\
& + \frac{\partial}{\partial \hat{s}} \left[A_\phi \frac{\partial \phi}{\partial v'} + A_\psi \frac{\partial \psi}{\partial v'} - \lambda_p (1 + v') \right] \delta v + Q_v \delta v \\
& + \frac{\partial}{\partial \hat{s}} \left[A_\phi \frac{\partial \phi}{\partial w'} + A_\psi \frac{\partial \psi}{\partial w'} - \lambda_p w' \right] \delta w + Q_w \delta w \\
& \left. + A_\theta \delta \theta + Q_\theta \delta \theta \right\} d\hat{s} + B.C's \left. \right\} dt
\end{aligned} \tag{2.16}$$

In Eq. (2.16), the function $A_q (q = \phi, \theta, \psi)$ is

$$A_q \equiv \frac{\partial L_w}{\partial q} - \frac{\partial}{\partial t} \left(\frac{\partial L_w}{\partial \dot{q}} \right) - \frac{\partial}{\partial t} \left(\frac{\partial L_w}{\partial \dot{q}} \right) \tag{2.17}$$

The terms $\delta u, \delta v, \delta w$ and $\delta \theta$ are independent and arbitrary. Thus, the following equations of motion are obtained from the nontrivial solution.

$$\begin{aligned}
& - \left(\frac{\partial L_T}{\partial u} - \frac{d}{dt} \frac{\partial L_T}{\partial \dot{u}} \right) + \frac{\partial}{\partial \hat{s}} \left[A_\phi \frac{\partial \phi}{\partial u'} + A_\psi \frac{\partial \psi}{\partial u'} - \lambda_p u' \right] + Q_u = 0 \\
& - \left(\frac{\partial L_T}{\partial v} - \frac{d}{dt} \frac{\partial L_T}{\partial \dot{v}} \right) + \frac{\partial}{\partial \hat{s}} \left[A_\phi \frac{\partial \phi}{\partial v'} + A_\psi \frac{\partial \psi}{\partial v'} - \lambda_p (1 + v') \right] + Q_v = 0 \\
& - \left(\frac{\partial L_T}{\partial w} - \frac{d}{dt} \frac{\partial L_T}{\partial \dot{w}} \right) + \frac{\partial}{\partial \hat{s}} \left[A_\phi \frac{\partial \phi}{\partial w'} + A_\psi \frac{\partial \psi}{\partial w'} - \lambda_p w' \right] + Q_w = 0 \\
& A_\theta + Q_\theta = 0
\end{aligned} \tag{2.18}$$

B. Taylor-Series Expansions and Ordering Scheme

Each term shown in Eq.(2.18) can be expanded in polynomial form. Initially, the order of four variables u, v, w, ϕ and their derivatives is $O(\epsilon)$. Their final order will be estimated in the final step. The ϵ is assumed as a small dimensionless parameter ($\epsilon \ll 1$). Although some terms, such as the axial deformation u and the rotary inertia terms could be $O(\epsilon^2)$, they are treated as $O(\epsilon)$ at this point. In the normalized final expressions, some higher order terms greater than $O(\epsilon^3)$ will be removed.

For the inextensional case, the axial motion should be restricted, and the following relation can be obtained from Eq. (2.10).

$$v' = \sqrt{1 - (u'^2 + w'^2)} - 1 = -\frac{1}{2} (u'^2 + w'^2) + H.O.T \tag{2.19}$$

Here, H.O.T means 'Higher-Order Terms' and they are neglected in the following formulation. The corresponding Lagrangian multiplier is obtained from the second expression of Eq. (2.18)

$$\lambda_p \approx \int_L^s m \left[-\frac{1}{2} \int_0^s (u'^2 + w'^2) \ddot{} - m e \ddot{u}' \right] ds + (I_1 w' \ddot{w}' + I_3 u' \ddot{u}')$$

$$-(D_1 w' w''' + D_3 u' u''') + H.O.T \quad (2.20)$$

If the in-plane motion can be neglected, and the inertia terms have higher order, then it can be simplified as

$$\lambda_p \approx \int_L^s m \left[-\frac{1}{2} \int_0^s (w'^2) \ddot{\cdot} \right] ds - (D_1 w' w''') + H.O.T \quad (2.21)$$

C. Aerodynamics

In order to perform aeroelastic analysis, the external load terms are replaced by the quasi-steady aerodynamics^{35,13} as follows,

$$Q_w = L_{QS} = \pi \rho b^2 V \dot{\alpha} + \rho V^2 b C_{L\alpha} (\alpha_{eff} - c_3 \alpha_{eff}^3) \quad (2.22)$$

$$Q_\alpha = M_{QS} = -\pi \rho b^2 V b \left(\frac{1}{2} - a \right) \dot{\alpha} + \rho V^2 b^2 C_{m\alpha} (\alpha_{eff} - c_3 \alpha_{eff}^3) \quad (2.23)$$

where the subscript ‘*QS*’ means the aerodynamics are described by the quasi-steady (QS) aerodynamics. The first term in these expressions describes a damping in pitch. In Eq. (2.22), ρ is the air density, V is the free-stream velocity, b is the semi-chord length. Lift and moment coefficients are represented by $C_{L\alpha}$ and $C_{m\alpha}$, respectively. A nonlinear parameter c_3 is introduced to describe the stall nonlinearity. As shown in Eq. (2.22), the stall nonlinearity is expressed by cubic terms. Although the quasi-steady aerodynamics is relatively simple, it is useful to obtain analytical solutions. In nonlinear aeroelastic analysis, the analytical solutions obtained from perturbation methods may effectively guide the analysis. Additionally, from Eq. (2.22) we can identify the fact that the stall model is described by the third order nonlinearities. Thus, the other nonlinear terms should have up to third order terms.

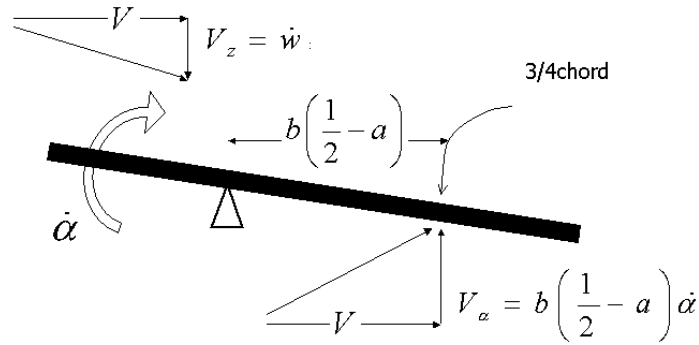


Fig. 3. Quasi-steady aerodynamics

The effective angle of attack α_{eff} is defined by

$$\alpha_{eff}^3 = \left[\alpha - \frac{1}{V} \dot{w} + \frac{b}{V} \left(\frac{1}{2} - a \right) \dot{\alpha} \right]^3 \quad (2.24)$$

As shown in Eq. (2.24) and Fig. 3, quasi-steady aerodynamics uses the effective angle of attack (AoA) induced by velocities. The downwash V_z increases the AoA. Angular velocity about the elastic axis leads to an AOA that varies along the wing. The upwash V_α at the $3/4c$ is used.³⁶ This equation for α_{eff} is limited to $\alpha_{eff} \approx \pm 11deg.$. Because stall occurs rather suddenly and abruptly, aerodynamic load terms are removed when the angle of attack exceeds the stall angle. The stall model presented herein is attributed to Gilliatt's paper¹³ in which the stall model is developed by fitting a curve to wind tunnel data for the NACA 0012. The lift coefficient is expressed as follows,

$$C_L = C_{L\alpha}(\alpha - c_3\alpha^3) = 7.074\alpha - 64.3064\alpha^3$$

From this formulation, the coefficient c_3 is defined as follows,

$$c_3 = 0.00034189 \left(\frac{180}{\pi} \right)^3 \frac{1}{C_{L\alpha}}$$

D. Nonlinear Equations of Motion

The terms in Eq. (2.18) are evaluated one by one. Based on the inextensionality condition, the v' is expressed in terms of u' and w' as shown in Eq. (2.19). The Lagrangian multiplier λ is defined by Eq. (2.20). The loads $Q_q (q = u, w, \theta)$ are described by the quasi-steady aerodynamics with the stall model in the previous section. The partial derivatives shown in Eq. (2.18) are defined in Appendix A. In this process, Taylor-Series expansion and the ordering scheme are applied, and the higher order terms are neglected. Substituting these results into Eq. (2.18), we obtain the following bending-bending-torsion equations having the third order nonlinearities.

$$\begin{aligned} m\ddot{u} + D_z u^{IV} + M_s(\ddot{u} + z_s \ddot{\alpha})\delta(y - y_s) &= G_u \\ m\ddot{w} - me\ddot{\alpha} + D_x w^{IV} + M_s(\ddot{w} - x_s \ddot{\alpha})\delta(y - y_s) \\ &\quad - \pi \rho b^2 V \dot{\alpha} + \rho V b C_{L\alpha} \left[\dot{w} - V\alpha - b\left(\frac{1}{2} - a\right)\dot{\alpha} \right] = G_w \\ I_y \ddot{\alpha} - me\ddot{w} - D_y \alpha'' + \left[(I_{sy} + M_s(x_s^2 + z_s^2)) \ddot{\alpha} - M_s x_s \ddot{w} + M_s z_s \ddot{u} \right] \delta(y - y_s) \\ &\quad + \pi \rho b^2 V b \left(\frac{1}{2} - a\right) \dot{\alpha} + \rho V b^2 C_{m\alpha} \left[\dot{w} - V\alpha - b\left(\frac{1}{2} - a\right)\dot{\alpha} \right] = G_\alpha \end{aligned} \quad (2.25)$$

In the above equations, linear terms are written on the left-hand side, and the corresponding nonlinear terms are simply expressed by G_u , G_w , and G_α . Details of the nonlinear components are shown in the following expressions

$$\begin{aligned} G_u &= D_y (\alpha' w'')' - D_z \left[u' (u' u'' + w' w'')' \right]' \\ &\quad + (D_z - D_x) \left[(w'' \alpha + u'' \alpha^2)' - w''' \int_0^s u'' w' ds \right]' + I_z \ddot{u}'' \end{aligned}$$

$$\begin{aligned}
& - \left\{ \frac{1}{2} u' \int_L^s m \left[\int_o^{\hat{s}} (w'^2 + u'^2) ds \right]^{\bullet\bullet} d\hat{s} - me u' \int_L^s \ddot{u}' ds \right\}' \\
& + me \left[\frac{1}{2} (\alpha^2 - w'^2)^{\bullet\bullet} - (u'\ddot{u} + w'\ddot{w}') \right] + \frac{1}{2} me \left[(w'^2 + u'^2 + \alpha^2) \right]^{\bullet} \\
& + \left[\frac{1}{2} M_s x_s (\alpha^2 - w'^2)^{\bullet\bullet} + M_s z_s \left(\int_0^s w'' u' ds \right)^{\bullet\bullet} \right] \delta(y - y_s) \quad (2.26)
\end{aligned}$$

$$\begin{aligned}
G_w &= -D_y (\alpha' u'')' - D_x \left[w' (w' w'' + u' u'') \right]' \\
& + (D_z - D_x) \left[(u'' \alpha - w'' \alpha^2)' + u''' \int_0^s w'' u' ds \right]' + I_x \ddot{w}'' \\
& - \left\{ \frac{1}{2} w' \int_L^s m \left[\int_o^{\hat{s}} (w'^2 + u'^2) ds \right]^{\bullet\bullet} d\hat{s} - me w' \int_L^s \ddot{u}' ds \right\}' + me \left[\int_0^s w' u'' ds \right]^{\bullet\bullet} \\
& + \left[M_s x_s \left(\int_0^s w' u'' ds \right)^{\bullet\bullet} + M_s z_s (\alpha \dot{\alpha} + w' \dot{w}') \right] \delta(y - y_s) \\
& - \rho V^2 b C_{L\alpha} c_3 \alpha_{eff}^3 \quad (2.27)
\end{aligned}$$

$$\begin{aligned}
G_\alpha &= -(D_z - D_x) \left[(w''^2 - u''^2) \alpha - w'' u'' \right] \\
& + I_y \left[\left(\int_0^s w'' u' ds \right)^{\bullet\bullet} - (\dot{w}' u') \right] + (I_z - I_x) \left[(\dot{w}'^2 - \dot{u}'^2) \alpha - \dot{u}' \dot{w}' \right] \\
& + me \left\{ -\frac{1}{2} \ddot{w} (w'^2 + \alpha^2) + \frac{1}{2} w' \left(\int_0^s (w'^2 + u'^2) ds \right)^{\bullet\bullet} + \ddot{u} \left(\alpha - \int_0^s w'' u' ds \right) \right\} \\
& + M_s \ddot{w} \left[-\frac{1}{2} x_s (w'^2 + \alpha^2) + z_s \left(\alpha - \int_0^s w'' u' ds \right) + z_s u' w' \right] \delta(y - y_s) \\
& + M_s \ddot{u} \left[x_s \left(\alpha - \int_0^s w'' u' ds \right) + \frac{1}{2} z_s (\alpha^2 + u'^2) \right] \delta(y - y_s) \\
& + M_s \left\{ x_s z_s (-\dot{u}'^2 + 2\dot{u}' \dot{w}' \alpha) - \frac{1}{2} \left[\int_0^s (w'^2 + u'^2) \right]^{\bullet\bullet} (x_s w' - z_s u') \right\} \delta(y - y_s) \\
& + \left\{ I_{sy} \left[\left(\int_0^s w'' u' ds \right)^{\bullet\bullet} - (\dot{w}' u') \right] + (I_{sz} - I_{sx}) \left[(\dot{w}'^2 - \dot{u}'^2) \alpha - \dot{u}' \dot{w}' \right] \right\} \delta(y - y_s) \\
& - \rho V^2 b^2 C_{m\alpha} c_3 \alpha_{eff}^3 \quad (2.28)
\end{aligned}$$

When the aerodynamic loads are replaced by the forcing functions, the mass imbalance terms are removed and the store terms are excluded; the Eqs. (2.26)~(2.28) could be reduced as follows,

$$m\ddot{u} + D_z u^{IV} = D_y (\alpha' w'')' - D_z \left[u' (u' u'' + w' w'') \right]'$$

$$\begin{aligned}
& +(D_z - D_x) \left[(w''\alpha + u''\alpha^2)' - w''' \int_0^s u''w' ds \right]' + I_z \ddot{u}'' \\
& - \left\{ \frac{1}{2} u' \int_L^s m \left[\int_0^{\hat{s}} (w'^2 + u'^2) ds \right]'' d\hat{s} \right\}' \\
& + Q_u^*
\end{aligned} \tag{2.29}$$

$$\begin{aligned}
m\ddot{w} + D_x w^{IV} &= -D_y (\alpha' u'')' - D_x [w' (w'w'' + u'u'')]'' \\
& +(D_z - D_x) \left[(u''\alpha - w''\alpha^2)' + u''' \int_0^s w''u' ds \right]' + I_x \ddot{w}'' \\
& - \left\{ \frac{1}{2} w' \int_L^s m \left[\int_0^{\hat{s}} (w'^2 + u'^2) ds \right]'' d\hat{s} \right\}' \\
& + Q_w^*
\end{aligned} \tag{2.30}$$

$$\begin{aligned}
I_y \ddot{\alpha} - D_y \alpha'' &= -(D_z - D_x) [(w''^2 - u''^2)\alpha - w''u''] \\
& + I_y \left[\left(\int_0^s w''u' ds \right)'' - (\dot{w}'u')^\bullet \right] + (I_z - I_x) [(\dot{w}'^2 - \dot{u}'^2)\alpha - \dot{u}'\dot{w}'] \\
& + Q_\alpha^*
\end{aligned} \tag{2.31}$$

These reduced expressions could be compared with those of Crespo da Silva and Glynn,²⁷ and those of Pai and Nayfeh.¹² In this comparison, we must remember their assumptions. Crespo da Silva and Glynn²⁷ formulated a set of mathematically consistent nonlinear equations of motion. This means that they included all expressions with order-three polynomial nonlinearities. Thus, there are many inertia terms in their original equations. When they applied their equations to a fixed-free beam with lateral excitation,²⁸ they applied a simplifying assumption that the effect of the distributed mass moments of inertia is negligible. Thus, the mass moment of inertia terms are removed from their resulting equations. Because Pai and Nayfeh¹² accounted for composite beams, we must set $D_{12} = D_{13} = D_{23}$ terms in their equations equal to zero to compare with the nonlinear equations for uniform isotropic beams. They have a few moment of inertia terms. By applying the ordering scheme, many

higher order inertia terms are removed. The moment of inertia terms are treated as second-order quantities. These three sets of nonlinear equations for uniform isotropic beams are identical when the mass imbalance terms and the store terms are removed from Eqs.(2.26)~(eq:Ga), the ordering scheme is applied to those of Crespo da Silva and Glynn,²⁷ and the condition $D_{12} = D_{13} = D_{23} = 0$ is applied to those of Pai and Nayfeh.¹²

1. Nondimensional Bending-Bending-Torsion

Nondimensionalized equations are beneficial in comparing relative magnitude and identifying important parameters dominating the responses of the considered system. Although it is required as the first step in perturbation analysis, it is also recommended to perform this process before analyzing the given problem.

In order to get nondimensionalized equations, the dependent variables u, v, w , and the independent variable t , are made dimensionless by introducing the characteristic length (L) and the characteristic time, $\sqrt{\frac{mL^4}{D_x}}$. The characteristic time adopted in this study is inversely proportioned to the system's natural frequency. Using these characteristic terms, the dependent variables and system parameters are written in nondimensional form as follows,

$$\begin{aligned}
 u^* &= \frac{u}{L}, & w^* &= \frac{w}{L}, & e^* &= \frac{e}{L}, & t^* &= t\sqrt{\frac{mL^4}{D_x}}, \\
 I_x^* &= \frac{I_x}{mL^2}, & I_y^* &= \frac{I_y}{mL^2}, & I_z^* &= \frac{I_z}{mL^2}, \\
 \beta_y &= \frac{D_y}{D_x}, & \beta_z &= \frac{D_z}{D_x}, & \mu^* &= \frac{\pi\rho b^2}{m}, & V^* &= \frac{V}{V_F}\sqrt{D_x/mL^2}, \\
 M_x^* &= \frac{M_s}{mL}, & x_s^* &= \frac{x_s}{L}, & z_s^* &= \frac{z_s}{L}, \\
 I_{sx}^* &= \frac{I_{sx}}{mL^3}, & I_{sy}^* &= \frac{I_{sy}}{mL^3}, & I_{sz}^* &= \frac{I_{sz}}{mL^3}
 \end{aligned} \tag{2.32}$$

Now, the nonlinear equations of motion for a cantilever wing with an external store can be rewritten in nondimensional form as follows. For ease of notation in the following analysis, the ‘*’ superscripts in the three motion and time variables, u , w , α , and t are omitted.

$$\begin{aligned}
& \frac{\partial^2 u}{\partial t^2} + \beta_z \frac{\partial^4 u}{\partial s^4} + \left[M_s^* \left(\frac{\partial^2 u}{\partial t^2} + z_s^* \frac{\partial^2 \alpha}{\partial t^2} \right) \right] L\delta(y - y_s) \\
= & \beta_y \frac{\partial}{\partial s} \left(\frac{\partial \alpha}{\partial s} \frac{\partial^2 w}{\partial t^2} \right) - \beta_z \frac{\partial}{\partial s} \left[\frac{\partial u}{\partial s} \frac{\partial}{\partial s} \left(\frac{\partial u}{\partial s} \frac{\partial^2 u}{\partial s^2} + \frac{\partial w}{\partial s} \frac{\partial^2 w}{\partial s^2} \right) \right] \\
& + (\beta_z - 1) \frac{\partial}{\partial s} \left[\frac{\partial}{\partial s} \left(\frac{\partial^2 w}{\partial s^2} \alpha + \frac{\partial^2 u}{\partial s^2} \alpha^2 \right) - \frac{\partial^3 w}{\partial s^3} \int_0^s \frac{\partial^2 u}{\partial s^2} \frac{\partial w}{\partial s} ds \right] + I_z^* \left(\frac{\partial^4 u}{\partial t^2 \partial s^2} \right) \\
& - \frac{\partial}{\partial s} \left\{ \frac{1}{2} \frac{\partial u}{\partial s} \left[\int_1^s \left(\frac{\partial w^2}{\partial s} + \frac{\partial u^2}{\partial s} \right) ds \right] - e^* \frac{\partial u}{\partial s} \int_1^s \frac{\partial^3 u}{\partial t^2 \partial s} ds \right\} \\
& + e^* \left[\frac{1}{2} \frac{\partial^2}{\partial t^2} \left(\alpha^2 - \frac{\partial w^2}{\partial s} \right) - \frac{\partial}{\partial s} \left(\frac{\partial u}{\partial s} \frac{\partial u^2}{\partial t^2} + \frac{\partial w}{\partial s} \frac{\partial^2 w}{\partial t^2} \right) \right] \\
& + M_s^* x_s^* \left[\frac{1}{2} \frac{\partial^2}{\partial t^2} \left(\frac{\partial u^2}{\partial s} + \alpha^2 \right) \right] L\delta(y - y_s) + M_s^* z_s^* \frac{\partial^2}{\partial t^2} \left(\int_0^s \frac{\partial^2 w}{\partial s^2} \frac{\partial u}{\partial s} ds \right) L\delta(y - y_s)
\end{aligned} \tag{2.33}$$

$$\begin{aligned}
& \frac{\partial^2 w}{\partial t^2} - e^* \frac{\partial^2 \alpha}{\partial t^2} + \frac{\partial^4 w}{\partial s^4} + \left[M_s^* \left(\frac{\partial^2 w}{\partial t^2} - x_s^* \frac{\partial^2 \alpha}{\partial t^2} \right) \right] L\delta(y - y_s) \\
& - \mu^* V^* \frac{\partial \alpha}{\partial t} + \mu \frac{C_{L\alpha}}{\pi} V^* \left[\frac{1}{b^* V^*} \frac{\partial w}{\partial t} - \alpha - V^* \left(\frac{1}{2} - a \right) \frac{\partial \alpha}{\partial t} \right] \\
= & -\beta_y \frac{\partial}{\partial s} \left(\frac{\partial \alpha}{\partial s} \frac{\partial^2 u}{\partial t^2} \right) - \frac{\partial}{\partial s} \left[\frac{\partial w}{\partial s} \frac{\partial}{\partial s} \left(\frac{\partial w}{\partial s} \frac{\partial^2 w}{\partial s^2} + \frac{\partial u}{\partial s} \frac{\partial^2 u}{\partial s^2} \right) \right] \\
& + (\beta_z - 1) \frac{\partial}{\partial s} \left[\frac{\partial}{\partial s} \left(\frac{\partial^2 u}{\partial s^2} \alpha + \frac{\partial^2 w}{\partial s^2} \alpha^2 \right) + \frac{\partial^3 u}{\partial s^3} \int_0^s \frac{\partial^2 w}{\partial s^2} \frac{\partial u}{\partial s} ds \right] + I_z^* \left(\frac{\partial^4 w}{\partial t^2 \partial s^2} \right) \\
& - \frac{\partial}{\partial s} \left\{ \frac{1}{2} \frac{\partial w}{\partial s} \left[\int_1^s \frac{\partial^2}{\partial t^2} \int_0^s \left(\frac{\partial w^2}{\partial s} + \frac{\partial u^2}{\partial s} \right) ds ds - e^* \frac{\partial u}{\partial s} \int_1^s \left(\frac{\partial^3 u}{\partial t^2 \partial s} \right) ds \right] \right\} \\
& - e^* \left[\frac{1}{2} \frac{\partial^2}{\partial t^2} \left(\alpha^2 - \left(\frac{\partial w}{\partial s} \right)^2 \right) - \frac{\partial}{\partial s} \left(\frac{\partial u}{\partial s} \frac{\partial^2 u}{\partial t^2} + \frac{\partial w}{\partial s} \frac{\partial^2 w}{\partial t^2} \right) \right] \\
& + M_s^* z_s^* \frac{\partial}{\partial t} \left[\frac{\partial w}{\partial s} \left(\frac{\partial^2 w}{\partial s \partial t} + \alpha \frac{\partial \alpha}{\partial t} \right) \right] L\delta(y - y_s) + M_s^* x_s^* \frac{\partial^2}{\partial t^2} \left(\int_0^s \frac{\partial^2 u}{\partial s^2} \frac{\partial w}{\partial s} ds \right) L\delta(y - y_s)
\end{aligned}$$

$$-\mu \frac{C_{L\alpha}}{\pi} V^{*2} c_3 \alpha_{eff}^3 \quad (2.34)$$

$$\begin{aligned}
& \frac{\partial^2 \alpha}{\partial t^2} - \frac{e^*}{I_y^*} \frac{\partial^2 w}{\partial t^2} - \frac{1}{I_y^*} \beta_y \frac{\partial^2 \alpha}{\partial s^2} \\
& + \frac{1}{I_y^*} \left[\left(I_{sy}^* + M_S^* z_s^{*2} + M_S^* x_s^{*2} \right) \frac{\partial^2 \alpha}{\partial t^2} + M_s^* \left(-x_s^* \frac{\partial^2 w}{\partial t^2} + z_s^* \frac{\partial^2 u}{\partial t^2} \right) \right] L\delta(y - y_s) \\
& - \frac{1}{I_y^*} \mu b^* \left(\frac{1}{2} - a \right) V^* \frac{\partial \alpha}{\partial t} + \frac{1}{I_y^*} \mu \frac{C_{m\alpha}}{\pi} V^{*2} \left[\frac{1}{V^*} \frac{\partial w}{\partial t} - \alpha - b^* \left(\frac{1}{2} - a \right) \frac{1}{V^*} \frac{\partial \alpha}{\partial t} \right] \\
= & -(\beta_z - 1) \left[\left(\frac{\partial^2 w^2}{\partial s^2} - \frac{\partial^2 u^2}{\partial s^2} \right) \alpha - \frac{\partial^2 w}{\partial s^2} \frac{\partial^2 u}{\partial s^2} \right] \\
& + I_y^* \left[\frac{\partial^2}{\partial t^2} \int_0^s \left(\frac{\partial^2 w}{\partial s^2} + \frac{\partial^2 u}{\partial s^2} \right) ds - \frac{\partial}{\partial t} \left(\frac{\partial^2 w}{\partial t \partial s} \frac{\partial u}{\partial s} \right) \right] \\
& + (I_z^* - I_x^*) \left[\left(\frac{\partial^2 w^2}{\partial t \partial s} - \frac{\partial^2 u^2}{\partial t \partial s} \right) \alpha - \frac{\partial^2 w}{\partial t \partial s} \frac{\partial^2 u}{\partial t \partial s} \right] \\
& + e^* \left[-\frac{1}{2} \frac{\partial^2 w}{\partial t^2} \left(\frac{\partial w^2}{\partial s} + \alpha^2 \right) + \frac{1}{2} \frac{\partial^2}{\partial t^2} \int_0^s \left(\frac{\partial^2 w}{\partial s^2} + \frac{\partial^2 u}{\partial s^2} \right) ds \frac{\partial w}{\partial s} \right] \\
& + e^* \frac{\partial^2 u}{\partial t^2} \left(\alpha - \int_0^s \frac{\partial^2 w}{\partial s^2} \frac{\partial u}{\partial s} ds \right) \\
& + M_s^* \frac{\partial^2 w}{\partial t^2} \left[-\frac{1}{2} x_s^* \left(\frac{\partial w^2}{\partial s} + \alpha^2 \right) + z_s^* \left(\alpha - \int_0^s \frac{\partial^2 w}{\partial s^2} \frac{\partial u}{\partial s} ds + \frac{\partial w}{\partial s} \frac{\partial u}{\partial s} \right) \right] L\delta(y - y_s) \\
& + M_s^* \frac{\partial^2 u}{\partial t^2} \left[x_s^* \left(\alpha - \int_0^s \frac{\partial^2 w}{\partial s^2} \frac{\partial u}{\partial s} ds \right) + \frac{1}{2} z_s^* \left(\frac{\partial u^2}{\partial s} + \alpha^2 \right) \right] L\delta(y - y_s) \\
& + M_s^* x_s^* z_s^* \left[-\frac{\partial^2 u^2}{\partial t \partial s} + 2\alpha \frac{\partial^2 u}{\partial t \partial s} \frac{\partial^2 w}{\partial t \partial s} \right] L\delta(y - y_s) \\
& + M_s^* \left[\frac{1}{2} \frac{\partial^2}{\partial t^2} \int_0^s \left(\frac{\partial^2 w}{\partial s^2} + \frac{\partial^2 u}{\partial s^2} \right) ds \left(x_s^* \frac{\partial w}{\partial s} - z_s^* \frac{\partial u}{\partial s} \right) \right] L\delta(y - y_s) \\
& + (I_{sz}^* - I_{sx}^*) \left[\left(\frac{\partial^2 w^2}{\partial t \partial s} - \frac{\partial^2 u^2}{\partial t \partial s} \right) \alpha - \frac{\partial^2 w}{\partial t \partial s} \frac{\partial^2 u}{\partial t \partial s} \right] \\
& + I_{sy}^* \left[\frac{\partial^2}{\partial t^2} \int_0^s \frac{\partial^2 w}{\partial s^2} \frac{\partial u}{\partial s} ds - \frac{\partial}{\partial t} \left(\frac{\partial^2 w}{\partial t \partial s} \frac{\partial u}{\partial s} \right) \right] L\delta(y - y_s) \\
& - \mu \frac{C_{m\alpha}}{\pi} V^{*2} c_3 \alpha_{eff}^3
\end{aligned} \quad (2.35)$$

By using the Galerkin method, the corresponding ordinary differential equations (ODEs) can be obtained from the above partial differential equations. The variables are expressed in series form as follows:

$$u^*(s, t) = \sum_{i=1}^{\infty} U_i(s)u_i, \quad (2.36)$$

$$w^*(s, t) = \sum_{j=1}^{\infty} W_j(s)w_j, \quad (2.37)$$

$$\alpha^*(s, t) = \sum_{k=1}^{\infty} A_k(s)\alpha_k \quad (2.38)$$

In these expressions, the capitalized terms, U_i , W_j and A_k represent the shape functions derived from a vibrating, nonrotating cantilever beam, and they are defined as follows,³⁴

$$\begin{aligned} U_i(s) = F_i(s) &= \cosh(\beta_i s) - \cos(\beta_i s) - \sigma_i [\sinh(\beta_i s) - \sin(\beta_i s)] \\ W_j(s) = F_j(s) &= \cosh(\beta_j s) - \cos(\beta_j s) - \sigma_j [\sinh(\beta_j s) - \sin(\beta_j s)] \\ &= \cosh(\beta_i \frac{\tilde{s}}{L}) - \cos(\beta_i \frac{\tilde{s}}{L}) - \sigma_i \left[\sinh(\beta_i \frac{\tilde{s}}{L}) - \sin(\beta_i \frac{\tilde{s}}{L}) \right] \\ A_k(s) &= \sqrt{2} \sin(\gamma_k s) \end{aligned} \quad (2.39)$$

The $F_i(s)$ and $A_k(s)$ are for bending and torsion motion, respectively. Here, β_i is a root of the characteristic equation for pure bending,

$$1 + \cos(\beta) \cosh(\beta) = 0 \quad (2.40)$$

and σ_i is defined as follows

$$\sigma_i = \frac{\cosh(\beta_i) + \cos(\beta_i)}{\sinh(\beta_i) + \sin(\beta_i)} \quad (2.41)$$

γ_k is a root of the characteristic equation for pure torsion motion $\sin(\gamma_k) = 0$.

Substituting the expanded variables and applying the Galerkin procedure, we obtain

the following ordinary-differential equations.

$$\begin{aligned}
& C_{uw1}\ddot{u}_i + \beta_z C_{uw2}u_i + M_s^* (C_{us1}\ddot{u}_i + z_s^* C_{us2}\ddot{\alpha}_k) \\
= & \beta_y C_{uw3}\alpha_k w_j - \beta_z [C_{uw4}u_i u_p u_q + C_{uw5}u_i w_j w_p] \\
& + (\beta_z - 1) [(C_{uw6}w_j \alpha_k + C_{uw7}u_i \alpha_k \alpha_p) - C_{uw8}w_j u_i u_p] + I_z^* C_{uw9}\ddot{u}_i \\
& - [C_{uw10}u_i (\ddot{w}_j w_p + \dot{w}_j \dot{w}_p) + C_{uw11}u_i (\ddot{u}_p u_q + \dot{u}_p \dot{u}_q)] \\
& + e^* C_{uw21}u_i \ddot{u}_p \\
& + e^* \left[\frac{1}{2} (C_{uw22}\alpha_k \ddot{\alpha}_p - C_{uw23}w_j \ddot{w}_p) - C_{uw24}u_i \ddot{u}_p - C_{uw25}w_j \ddot{w}_p \right] \\
& + M_s^* x_s^* [C_{us3}(\ddot{u}_i u_p + \dot{u}_i \dot{u}_p) + C_{us4}(\ddot{\alpha}_k \alpha_p + \dot{\alpha}_k \dot{\alpha}_p)] \\
& + M_s^* z_s^* [C_{us5}(\ddot{w}_j u_i + 2\dot{w}_j \dot{u}_i + \ddot{u}_i w_j)] \tag{2.42}
\end{aligned}$$

$$\begin{aligned}
& C_{ww1}\ddot{w}_j - e^* C_{we1}\ddot{\alpha}_k + C_{ww2}w_j + M_s^* (C_{ws1}\ddot{w}_j - x_s^* C_{ws2}\ddot{\alpha}_k) \\
& - \mu * V^* C_{wa1}\dot{\alpha}_k + \mu \frac{C_{L\alpha_k}}{\pi} V^* \left[\frac{1}{b^* V^*} C_{wa2}\dot{w} - C_{wa3}\alpha - V^* \left(\frac{1}{2} - a \right) C_{wa4}\dot{\alpha} \right] \\
= & -\beta_y C_{ww3} (\alpha_k u_i) - [C_{ww4}w_j (w_p w_q) + C_{ww5}w_j (u_i u_p)] \\
& + (\beta_z - 1) [(C_{ww6}u_i \alpha_k - C_{ww7}w_j \alpha_k \alpha_p) + C_{ww8}u_i w_j u_p] + I_z^* C_{ww9}\ddot{w}_j \\
& - [C_{ww10}w_j (\ddot{w}_p w_q + \dot{w}_p \dot{w}_q) + C_{ww11}w_j (\ddot{u}_i u_p + \dot{u}_i \dot{u}_p)] - e^* C_{ww22}w_j \ddot{u}_i \\
& - e^* C_{ww23}u_i \ddot{w}_j \\
& + M_s^* z_s^* [C_{ws3}(\ddot{w}_j w_p + \dot{w}_j \dot{w}_p) + C_{ws4}(\ddot{\alpha}_k \alpha_p + \dot{\alpha}_k \dot{\alpha}_p)] \\
& + M_s^* x_s^* [C_{ws5}(\ddot{u}_i w_j + 2\dot{u}_i \dot{w}_j + \ddot{w}_j u_i)] \\
& - \mu \frac{C_{L\alpha}}{\pi} V^{*2} c_3 \int_0^s W_r \alpha_{eff}^3 ds \tag{2.43}
\end{aligned}$$

$$\begin{aligned}
& C_{aw1}\ddot{\alpha}_k - \frac{e^*}{I_y^*} C_{ae1}\ddot{w}_j - \frac{1}{I_y^*} \beta_y C_{aw2}\alpha_k \\
& + \frac{1}{I_y^*} \left[(I_{sy}^* + M_s^* z_s^{*2} + M_s^* x_s^{*2}) \ddot{\alpha}_k + M_s^* (-x_s^* \ddot{w}_j + z_s^* \ddot{u}) \right]
\end{aligned}$$

$$\begin{aligned}
& -\frac{1}{I_y^*} \mu b^* \left(\frac{1}{2} - a \right) V^* C_{aa1} \dot{\alpha}_k \\
& + \frac{1}{I_y^*} \mu \frac{C_{m\alpha k}}{\pi} V^{*2} \left[\frac{1}{V^*} C_{aa2} \dot{w} - C_{aa3} \alpha_k - b^* \left(\frac{1}{2} - a \right) \frac{1}{V^*} C_{aa4} \dot{\alpha} \right] \\
= & -\frac{1}{I_y^*} (\beta_z - 1) [(C_{aw3} w_j w_p - C_{aw4} u_i u_p) \alpha_k - C_{aw5} w_j u_i] \\
& + \frac{1}{I_y^*} I_y^* [C_{aw6} (\ddot{w}_j u_i + 2\dot{w}_j \dot{u}_i + w_j \ddot{u}_i) - C_{aw7} (\dot{w}_j \dot{u}_i + \ddot{w}_j u_i)] \\
& + \frac{1}{I_y^*} (I_z^* - I_x^*) [(C_{aw8} \dot{w}_j \dot{w}_p - C_{aw9} \dot{u}_i \dot{u}_p) \alpha_k - C_{aw10} \dot{u}_i \dot{w}_j] \\
& + \frac{1}{I_y^*} \frac{1}{2} e^* [-\ddot{w}_j (C_{aw22} w_p w_q + C_{aw23} \alpha_k \alpha_p) + C_{aw24} w_j \ddot{w}_p w_q + C_{aw25} u_i \ddot{u}_p] \\
& + \frac{1}{I_y^*} e^* \ddot{u}_i (C_{aw26} \alpha_k - C_{aw27} u_p w_j) \\
& + \frac{1}{I_y^*} M_s^* \ddot{w}_j \left[-\frac{1}{2} x_s^* (C_{as4} w_p w_q + C_{as5} \alpha_k \alpha_p) + z_s^* (C_{as6} \alpha_k - C_{as7} w_p u_i + C_{as8} u_i w_p) \right] \\
& + \frac{1}{I_y^*} M_s^* \ddot{u}_i \left[x_s^* (C_{as9} \alpha_k - C_{as10} w_j u_p) + \frac{1}{2} z_s^* (C_{as11} \alpha_k \alpha_p + C_{as12} u_p u_q) \right] \\
& - \frac{1}{I_y^*} M_s^* x_s^* z_s^* [-C_{as13} \dot{u}_i \dot{u}_p + 2C_{as14} \dot{u}_i \dot{w}_j \alpha_k] \\
& - \frac{1}{I_y^*} M_s^* x_s^* [C_{as15} (\ddot{w}_j w_p + \dot{w}_j \dot{w}_p) w_p + C_{as16} (2\ddot{u}_i u_p + 2\dot{u}_i \dot{u}_p) w_j] \\
& - \frac{1}{I_y^*} M_s^* z_s^* [C_{as17} (\dot{w}_j w_p + \dot{w}_j \dot{w}_p) u_i + C_{as18} (2\ddot{u}_i u_p + 2\dot{u}_i \dot{u}_p) u_q] \\
& + \frac{1}{I_y^*} (I_{sz}^* - I_{sx}^*) [(C_{as19} \dot{w}_j \dot{w}_p - C_{as20} \dot{u}_i \dot{u}_p) \alpha_k - C_{as21} \dot{u}_i \dot{w}_j] \\
& + \frac{1}{I_y^*} I_{sy}^* [C_{as22} (\ddot{w}_j u_i + 2\dot{w}_j \dot{u}_i + w_j \ddot{u}_i) - C_{as23} (\dot{w}_j \dot{u}_i + \ddot{w}_j u_i)] \\
& - \frac{1}{I_y^*} \mu \frac{C_{m\alpha}}{\pi} V^{*2} c_3 \int_0^1 \alpha_{eff}^3 ds
\end{aligned} \tag{2.44}$$

These equations could be written in matrix form as

$$[M_L] \begin{Bmatrix} \ddot{u} \\ \ddot{w} \\ \ddot{\alpha} \end{Bmatrix} + [C_L] \begin{Bmatrix} \ddot{u} \\ \ddot{w} \\ \ddot{\alpha} \end{Bmatrix} + [K_L] \begin{Bmatrix} \ddot{u} \\ \ddot{w} \\ \ddot{\alpha} \end{Bmatrix}$$

$$= [M_{NL}] \begin{Bmatrix} \ddot{u} \\ \ddot{w} \\ \ddot{\alpha} \end{Bmatrix} + [C_{NL}] \begin{Bmatrix} \dot{u} \\ \dot{w} \\ \dot{\alpha} \end{Bmatrix} + [K_{NL}] \begin{Bmatrix} u \\ w \\ \alpha \end{Bmatrix} \quad (2.45)$$

The matrices shown in Eq. 2.45 are defined in Appendix A.

2. Bending-Torsion

If the in-plane bending rigidity is relatively high, then the effects of the in-plane bending can be neglected. Because aeroelastic analysis for conventional aircraft may be performed under this assumption, the nonlinear BBT equations are reduced to the bending-torsion (BT) equations. The following equations are dimensional.

$$\begin{aligned} & m\ddot{w} - me\ddot{\alpha} + D_x w^{IV} + M_s(\ddot{w} - x_z \ddot{\alpha})\delta(y - y_s) \\ & - \pi \rho b^2 V \dot{\alpha} + \rho b V C_{L\alpha} \left[\dot{w} - V\alpha - b \left(\frac{1}{2} - a \right) \dot{\alpha} \right] \\ = & -D_x [w'(w'w'')] + (D_x - D_z)[w''\alpha^2]'' + I_x \ddot{w}'' - \frac{1}{2} m \left[w' \int_L^s \left(\int_0^s w'^2 ds \right)'' ds \right]' \\ & - me \left(\frac{1}{2} \dot{\alpha} w'^2 + \alpha w' \dot{w}' + \frac{1}{2} \alpha^2 \dot{\alpha} \right)' + me \left[-\frac{1}{2} (w'^2)'' \alpha - \frac{1}{2} \int_0^s (w'^2)'' ds \alpha' + (\ddot{w}\alpha w')' \right] \\ & - M_s x_s \left(\frac{1}{2} \dot{\alpha} w'^2 + \alpha w' \dot{w}' + \frac{1}{2} \alpha^2 \dot{\alpha} \right)' \delta(y - y_s) + M_s z_s (w' \dot{w}' + \alpha \dot{\alpha})' \delta(y - y_s) \\ & - \rho b V^2 C_{L\alpha} c_3 \alpha_{eff}^3 \end{aligned} \quad (2.46)$$

$$\begin{aligned} & I_y \ddot{\alpha} - me \ddot{w} - D_y \alpha'' + [(I_{sy} + M_s x_s^2 + M_s z_s^2) \ddot{\alpha} - M_s x_s \ddot{w}] \delta(y - y_s) \\ & + \pi \rho b^2 V b \left(\frac{1}{2} - a \right) \dot{\alpha} + \rho b^2 V C_{m\alpha} \left[\dot{w} - V\alpha - b \left(\frac{1}{2} - a \right) \dot{\alpha} \right] \\ = & (I_z - I_x) \dot{w}'^2 \alpha - (D_z - D_x) w''^2 \alpha \\ & + \frac{1}{2} me \left[-\ddot{w}(w'^2 + \alpha^2) + \left(\int_0^s w'^2 ds \right)'' w' \right] \\ & + (I_{sz} - I_{sx}) \dot{w}'^2 \alpha \delta(y - y_s) \\ & + \frac{1}{2} M_s x_s \left[-\ddot{w}(w'^2 + \alpha^2) + \left(\int_0^s w'^2 ds \right)'' w' \right] \delta(y - y_s) + M_s z_s \ddot{w} \alpha \delta(y - y_s) \end{aligned}$$

$$-\rho b^2 V^2 C_{m\alpha} c_3 \alpha_{eff}^3 \quad (2.47)$$

In the above expressions, e , x_s and z_s are not treated as $O(\epsilon)$ terms. Thus, there are additional nonlinear terms. In Appendix B, two sets of nonlinear bending-torsion equations are presented. In Appendix B, a constraint equation allowing the elimination of the in-plane bending terms is considered in the first set of nonlinear bending-torsion equations. Applying the Galerkin method to these two partial differential equations, we obtain

$$\begin{aligned} & C_{ww1}\ddot{w}_j - e^* \ddot{\alpha}_k + C_{wwq}w_j + M_s^* (C_{ws1}\ddot{w}_j - x_s^* C_{ws2}\ddot{\alpha}_k) \\ & - \mu * V^* C_{wa1}\dot{\alpha}_k + \mu \frac{C_{L\alpha k}}{\pi} V^* \left[\frac{1}{b^* V^*} \dot{w} - \alpha - V^* \left(\frac{1}{2} - a \right) \dot{\alpha} \right] \\ = & - [C_{ww4}w_j(w_p w_q)] \\ & + (\beta_z - 1) [(-C_{ww7}w_j \alpha_k \alpha_p)] + I_z^* C_{ww9}\ddot{w}_j \\ & - [C_{ww10}w_j(\ddot{w}_p w_q + \dot{w}_p \dot{w}_q)] \\ & + M_s^* z_s^* [C_{ws3}(\ddot{w}_j w_p + \dot{w}_j \dot{w}_p) + C_{ws4}(\ddot{\alpha}_k \alpha_p + \dot{\alpha}_k \dot{\alpha}_p)] \\ & - \mu \frac{C_{L\alpha}}{\pi} V^{*2} c_3 \int_0^s W_r \alpha_{eff}^3 ds \end{aligned} \quad (2.48)$$

$$\begin{aligned} & C_{aw1}\ddot{\alpha}_k - \frac{e^*}{I_y^*} \ddot{w}_j + \frac{1}{I_y^*} \beta_y C_{aw2} \alpha_k \\ & + \frac{1}{I_y^*} \left[(I_{sy}^* + M_s^* z_s^{*2} + M_s^* x_s^{*2}) \ddot{\alpha}_k + M_s^* (-x_s^* \ddot{w}_j + z_s^* \ddot{u}) \right] \\ & - \frac{b^* \mu}{I_y^*} \left(\frac{1}{2} - a \right) V^* C_{aa1} \dot{\alpha}_k + \frac{\mu}{I_y^*} \frac{C_{m\alpha}}{\pi} V^{*2} \left[\frac{1}{V^*} C_{aa2} \dot{w} - C_{aa3} \alpha_k - \left(\frac{1}{2} - a \right) \frac{b^*}{V^*} C_{aa4} \dot{\alpha} \right] \\ = & - \frac{1}{I_y^*} (\beta_z - 1) [C_{aw3} w_j w_p \alpha_k] \\ & + \frac{1}{I_y^*} (I_z^* - I_x^*) [(C_{aw8} \dot{w}_j \dot{w}_p) \alpha_k] \\ & + \frac{1}{I_y^*} \frac{1}{2} e^* [-\ddot{w}_j (C_{aw22} w_p w_q + C_{aw23} \alpha_k \alpha_p) + C_{aw24} \dot{w}_j \dot{w}_p w_q + C_{aw25} u_i \ddot{u}_p] \end{aligned}$$

$$\begin{aligned}
& + \frac{1}{I_y^*} e^* \ddot{u}_i (C_{aw26} \alpha_k) \\
& + \frac{1}{I_y^*} M_s^* \ddot{w}_j \left[-\frac{1}{2} x_s^* (C_{as4} w_p w_q + C_{as5} \alpha_k \alpha_p) + z_s^* (C_{as6} \alpha_k) \right] \\
& + \frac{1}{I_y^*} M_s^* \ddot{u}_i \left[x_s^* (C_{as9} \alpha_k) + \frac{1}{2} z_s^* (C_{as11} \alpha_k \alpha_p) \right] \\
& - \frac{1}{I_y^*} M_s^* x_s^* [C_{as15} (\ddot{w}_j w_p + \dot{w}_j \dot{w}_p) w_p] \\
& + \frac{1}{I_y^*} (I_{sz}^* - I_{sx}^*) [(C_{as19} \dot{w}_j \dot{w}_p) \alpha_k] \\
& - \frac{1}{I_y^*} \mu \frac{C_{m\alpha}}{\pi} V^{*2} c_3 \int_0^1 \alpha_{eff}^3 ds
\end{aligned} \tag{2.49}$$

Depending upon the purpose of study, the second-order (w.r.t. time) expressions are maintained or transformed into first-order expressions. In order to perform nonlinear aeroelastic analysis in the time domain, these equations are transformed into state space as

$$\{\dot{q}\} = [SM]\{q\} \tag{2.50}$$

The state vector $\{q\}$ will have different components depending upon the system, such as

$$q = [w_j \ \alpha_k \ \dot{w}_j \ \dot{\alpha}_k]^T \tag{2.51}$$

$$q = [u_i \ w_j \ \alpha_k \ \dot{u}_i \ \dot{w}_j \ \dot{\alpha}_k]^T \tag{2.52}$$

In these expressions, $[SM]$ is the system matrix, from which the aeroelastic frequencies and damping values are obtained. The system matrix and two other matrices, $[M_{T2}]$ and $[CK]$, are defined as follows,

$$\begin{aligned}
[SM] &= -[M_{T2}]^{-1}[CK] \\
[M_{T2}] &= \begin{bmatrix} I & 0 \\ 0 & M_T \end{bmatrix}
\end{aligned}$$

$$[CK] = \begin{bmatrix} 0 & -I \\ K_T & C_T \end{bmatrix} \quad (2.53)$$

where $[M_T] = [M_L] - [M_{NL}]$, $[C_T] = [C_L] - [C_{NL}]$, and $[K_T] = [K_L] - [K_{NL}]$. These matrices are defined in Appendix A.

CHAPTER III

NONLINEAR APPROACHES

Nonlinear aeroelastic phenomena are observed in wind tunnel and flight tests. These cannot be explained by linear aeroelastic theories. In order to understand the characteristics of a nonlinear system, it is proposed to use several approaches because there is not one universal method that can be used to analyze all nonlinear mechanical systems. Furthermore, the nonlinear methodologies used for aeroelastic systems are limited. Thus, we must extend the nonlinear approaches to aeroelastic systems. Time simulation, perturbation methods, continuation methods, and numerical methods such as Poincaré map, and Fast Fourier Transformation (FFT) are considered in this chapter as nonlinear approaches. In this process, the effect of any parameter can be effectively expressed through bifurcation diagrams. One of the main purposes of this research is to detect LCO responses and to identify the primary sources of LCO responses. Bifurcation diagrams serve this purpose. The LCO response is represented by a Hopf bifurcation. Bifurcation diagrams can be generated by various approaches, such as perturbation methods, software packages (such as AUTO and DsTool), and Poincaré maps. Depending upon the approach, the obtained bifurcation diagrams may appear somewhat different from each other. This difference is considered in this chapter. Another main research topic is to investigate possible nonlinear phenomena of the wing system having a high aspect ratio. In order to study the possible internal resonance mechanism, the Method of Multiple Scales is considered.

A. Time Simulation

Direct time simulation is beneficial in understanding the characteristics of nonlinear systems. A set of first-order ordinary differential equations, as shown in Chapter II,

can be directly solved by using a number of numerical methods. It does not matter whether the system is aeroelastic or otherwise, nor whether the system is linear or nonlinear. In using perturbation methods, solutions for a system with complex nonlinearities cannot be easily obtained and/or there may not be analytical solutions for some nonlinear systems. These difficulties do not exist in direct time simulations. Additionally, the time simulation will provide a more accurate solution than any other solution obtained by approximate approaches.

A fourth-order Runge-Kutta method is used by Lee et al.,³⁷ Poirel³⁸ and Tang *et al.*³⁹ for simulation. Because a constant time step is adopted in this Runge-Kutta method, it is useful to analyze the frequency content of nonlinear signals. Poirel and Price³⁸ used the time step increment as the smaller of either 1/128 of the lowest uncoupled natural frequency, or 1/5 of the noise correction time. Kim^{40,41} used a fifth-order Runge-Kutta method because a fourth-order Runge-Kutta method requires a very large number of iterations. If the time step is not small enough, then the predicted response may diverge numerically. Depending upon the status of responses, the time step is adjustable in the fifth-order Runge-Kutta method. This method is adopted in Matlab. One disadvantage of the fifth-order method is that this method may not provide proper frequency content because the time increment is not constant.

B. Perturbation Methods

Direct time simulation can provide accurate results for nonlinear systems. But, because the nonlinear responses depend upon the given initial conditions, there may be an infinite number of cases. Without any guidance, the blind simulation approach

requires too many time simulations to fully obtain useful results, and may result in inaccurate conclusions. Approximate solutions based on perturbation methods may guide the time simulation. Although Lee et al³⁷ introduced the Describing Function Technique as one of solution techniques to solve nonlinear aeroelastic systems, it is appropriate for the system with concentrate nonlinearities such as freeplay. Because the nonlinearities considered in this paper are not concentrated, but distributed, other approaches are needed such as the Method of Multiple Scales and the Method of Harmonic Balance. Although, the Describing Function Technique is sometimes called the Method of Harmonic Balance, they are slightly different in that the nonlinearities are linearized in the Describing Function Method.

Another interesting nonlinear phenomena, internal resonance, can be analyzed by the Method of Multiple Scales. For example, when a wing span is increased, the frequency ratio between bending and torsional motions is changed. For a cantilever beam, the natural frequencies³⁵ can be expressed as

$$\omega_{bending} = \left(\frac{\beta_j}{L}\right)^2 \sqrt{\frac{EI}{m}}, \quad \omega_{torsion} = \left(\frac{(2k-1)\pi}{2L}\right) \sqrt{\frac{GJ}{I_y}} \quad (3.1)$$

where $j = 1, 2, 3, \dots$, $k = 1, 2, 3, \dots$ and $\beta_1 = 1.8751$. Although the stiffnesses are specified, the frequency ratio can be changed by a change in wing span, L . At a certain wing span condition, the ratio could be commensurable, that is, the two frequencies satisfy a condition $m\omega_{bending} + n\omega_{torsion} = 0$ for integers m and n . In aeroelastic systems, the aeroelastic frequencies are changed by the velocity condition. Under this situation, internal resonance may occur.

In order to obtain approximate solution showing internal resonance, the Method of Multiple Scales is used. One of well-known examples of internal resonance³¹ is a spring pendulum as shown in Fig. 4. A mass m is attached to a spring that is swinging in a

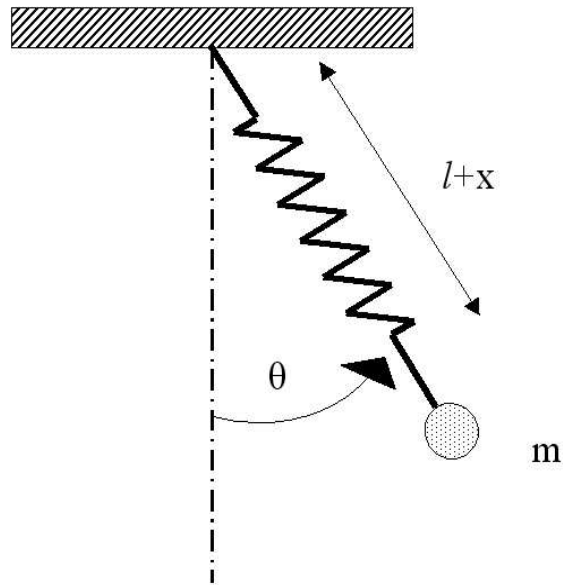


Fig. 4. Spring pendulum

vertical plane. Substituting the following kinetic and potential energies for the spring pendulum system into the Lagrangian equations

$$T = \frac{1}{2}m [\dot{x}^2 + (l+x)^2\dot{\theta}^2] \quad (3.2)$$

$$V = \frac{1}{2}kx^2 + mg(l+x)(1 - \cos\theta) - mgx \quad (3.3)$$

we obtained the following equations of motion.

$$\ddot{x} + \omega_2^2 x - (l+x)\dot{\theta}^2 - g \cos\theta = 0 \quad (3.4)$$

$$\ddot{\theta} + \frac{g \sin\theta + 2\dot{x}\dot{\theta}}{l+x} = 0 \quad (3.5)$$

where $\omega_2^2 = k/m$. Each equation has nonlinear terms including cos and sin terms.

When all nonlinear terms are neglected, the linear equations do not have any coupling term. Thus, the linear equations could not be used to explain the fact that when $\omega_2 \approx 2\omega_1$ the spring mode with frequency ω_2 and the pendulum mode with

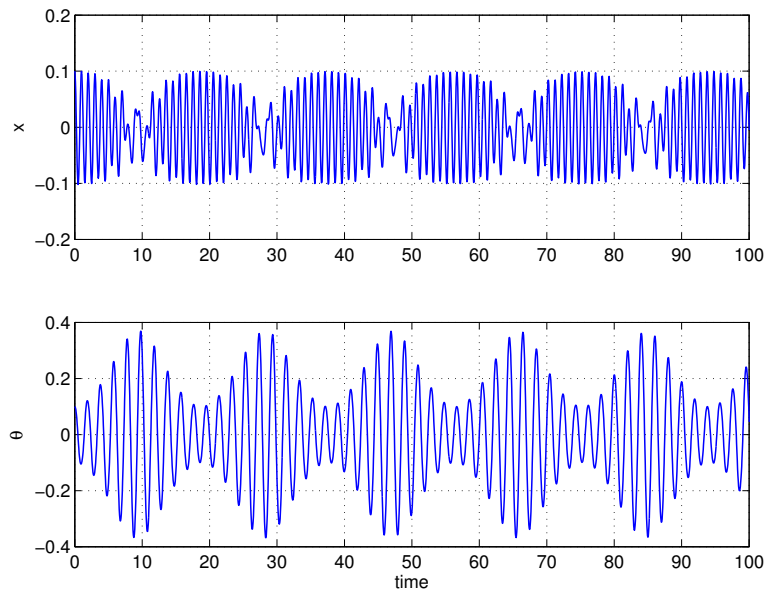


Fig. 5. Time simulation of spring pendulum

frequency $\omega_1 = \sqrt{g/l}$ are coupled as shown in Fig. 5. The results shown in Fig. 5 are obtained from Eqs. (3.4) and (3.5). Because the frequencies satisfy $m\omega_2 + n\omega_1 = 0$ when $m = 1$ and $n = 2$, the frequencies are commensurable. Figure 5 shows the modulation in which the energy in the system is exchanged continuously between the two modes.

Gilliatt¹³ shows that for the case of initial condition ($x_i \neq 0.0, \theta_i = 0.0$) the internal resonance mechanism is not observed. In the spring pendulum system, the spring mode has a quadratic nonlinear term, $\dot{\theta}^2$, and the pendulum mode has a quadratic term consisting of the spring mode(x) and the pendulum mode(θ). Nayfeh and Mook³¹ showed modulated responses for a conservative two-degree-of-freedom system with quadratic nonlinearities. The presented two cases showed that the modulation shape is affected by the initial conditions. In these two examples, the initial value for the motion that has a quadratic nonlinear term, consisting of two different motions, is not zero. These results showed that the internal resonance could not be

detected easily without any guidance provided by any perturbation method such as the Method of Multiple Scales.

Using the Method of Multiple Scales, this internal resonance mechanism is investigated. The solutions of Eqs. (3.4) and (3.5) are assumed as follows,

$$x = \epsilon x_1(T_0, T_1, T_2, \dots) + \epsilon^2 x_2(T_0, T_1, T_2, \dots) + \dots \quad (3.6)$$

$$\theta = \epsilon \theta_1(T_0, T_1, T_2, \dots) + \epsilon^2 \theta_2(T_0, T_1, T_2, \dots) + \dots \quad (3.7)$$

where $T_n = \epsilon t$. In these expressions, T_1 is a slow scale showing the envelop of the original responses, or a fast scale T_0 . The original equations of motion are rewritten by using the new independent variables T_n as follows,

$$\begin{aligned} \frac{d}{dt} &= D_0 + \epsilon D_1 + \epsilon^2 D_2 + \dots \\ \frac{d^2}{dt^2} &= D_0^2 + 2\epsilon D_0 D_1 + \epsilon^2 (D_1^2 + 2D_0 D_1) + \dots \end{aligned} \quad (3.8)$$

where $D_n = \partial/\partial T_n$. Substituting Eqs. (3.6) and (3.7) into Eqs. (3.4) and (3.5), applying Eq. (3.8), and equating like powers of ϵ , we obtains the following order equaitons

Order(ϵ) :

$$\begin{aligned} D_0^2 x_1 + \omega_1^2 x_1 &= 0 \\ D_0^2 \theta_1 + \omega_2^2 \theta_1 &= 0 \end{aligned} \quad (3.9)$$

Order(ϵ^2) :

$$\begin{aligned} D_0^2 x_2 + \omega_1^2 x_2 &= l (D_0 \theta_1)^2 - 2D_0 D_1 x_1 - \frac{1}{2} g \theta_1^2 \\ D_0^2 \theta_2 + \omega_2^2 \theta_2 &= \frac{1}{l} \omega_2^2 x_1 \theta_1 - 2D_0 D_1 \theta_1 - \frac{2}{l} D_0 x - 1D_0 \theta_1 \end{aligned} \quad (3.10)$$

The solution of the first-order equation Eq. (3.9) is

$$\begin{aligned} x_1 &= A_x(T_1)e^{i\omega_1 T_0} + \bar{A}_x(T_1)e^{-i\omega_1 T_0} \\ \theta_1 &= A_\theta(T_1)e^{i\omega_2 T_0} + \bar{A}_\theta(T_1)e^{-i\omega_2 T_0} \end{aligned} \quad (3.11)$$

where \bar{A}_x and \bar{A}_θ denote the complex conjugate of A_x and A_θ , respectively. Substituting the solution into the second-order equation having non-homogeneous terms leads to

$$\begin{aligned} D_0^2 x_2 + \omega_1^2 x_2 &= -2i\omega_1 D_1 A_x e^{i\omega_1 T_0} - \frac{3}{2} g A_\theta^2 e^{2i\omega_2 T_0} + g A_\theta \bar{A}_\theta + cc \\ D_0^2 \theta_2 + \omega_2^2 \theta_2 &= \frac{1}{l} \omega_2 (\omega_\theta + 2\omega_x) A_x A_\theta e^{i(\omega_1 + \omega_2) T_0} - \frac{1}{l} \omega_2 (\omega_\theta - 2\omega_x) A_x A_\theta e^{i(\omega_2 - \omega_1) T_0} \\ &\quad - 2i\omega_\theta D_1 A_\theta e^{i\omega_2 T_0} + cc \end{aligned} \quad (3.12)$$

where cc implies the complex conjugate of the whole expression on the right-hand side. The particular solution for these second-order equation are obtained for constant A_x and A_θ as follows,

$$x_2 = \frac{1}{\omega_\theta} g A_\theta \bar{A}_\theta - \frac{3g A_\theta^2}{2(\omega_1 + 2\omega_2)(\omega_1 - 2\omega_2)} + cc \quad (3.13)$$

$$\theta_2 = -\frac{\omega_2(\omega_2 + 2\omega_1)}{l\omega_1(\omega_1 + 2\omega_2)} A_x A_\theta e^{i(\omega_1 + \omega_2) T_0} - \frac{\omega_\theta(\omega_2 - 2\omega_1)}{l\omega_1(\omega_1 - 2\omega_\theta)} \bar{A}_x B_\theta e^{i(\omega_1 - \omega_2) T_0} + cc \quad (3.14)$$

Because the second-order equation for the spring mode (x_2) has a square term, the corresponding solution may have a non-oscillatory term without an exponential function. These solutions show that the denominator approaches infinity as ω_1 approaches $2\omega_2$. It is the 2:1 internal resonance condition.

In the 2:1 internal resonance case in which $\omega_1 \approx 2\omega_2$, a detuning parameter σ is introduced. We let

$$\omega_1 - 2\omega_2 = \epsilon\sigma \quad (3.15)$$

and let A_x and A_θ be functions of T_1 , rather than being constants. Using Eq. (3.15), Eq. (3.12) could be rewritten. In the resulting equations, the secular term which make the expansion of x and θ nonperiodic and/or nonconvergent are then removed. Consequently, the following solvability conditions are obtained.

$$2i\omega_1 D_1 A_x = -\frac{3}{2}g A_\theta^2 e^{-i\sigma T_1} \quad (3.16)$$

$$2i\omega_2 D_1 A_\theta = \frac{1}{l}\omega_2(\omega_2 - 2\omega_1)A_x \bar{A}_\theta e^{-i\sigma T_1} \quad (3.17)$$

Introducing polar notation, A_x and A_θ are rewritten as follows,

$$A_x(T_1) = \frac{1}{2}a_1 e^{-i\phi_x}$$

$$A_\theta(T_1) = \frac{1}{2}a_1 e^{-i\phi_\theta}$$

where a_1 , a_2 , ϕ_x and ϕ_θ are functions of T_1 .

Substituting these expressions for A_x and A_θ into the solvability conditions and separating the real and imaginary parts give the following expressions.

$$\dot{a}_1 = -\frac{3g}{8\omega_1}a_2^2 \cos \gamma \quad (3.18)$$

$$a_1 \dot{\phi}_x = \frac{3g}{8\omega_1}a_2^2 \sin \gamma \quad (3.19)$$

$$\dot{a}_2 = \frac{\omega_2 - 2\omega_1}{4l}a_1 a_2 \cos \gamma \quad (3.20)$$

$$\dot{\phi}_\theta = \frac{\omega_2 - 2\omega_1}{4l}a_1 \sin \gamma \quad (3.21)$$

where $\gamma = \phi_x - 2\phi_\theta + \sigma T_1$. Because these expressions have γ terms and γ is related to ϕ terms, ϕ terms are eliminated from these expressions. The result is of the form

$$\dot{a}_1 = -\frac{3g}{8\omega_1}a_2^2 \cos \gamma \quad (3.22)$$

$$a_1 \dot{\phi}_x = \frac{3g}{8\omega_1}a_2^2 \sin \gamma \quad (3.23)$$

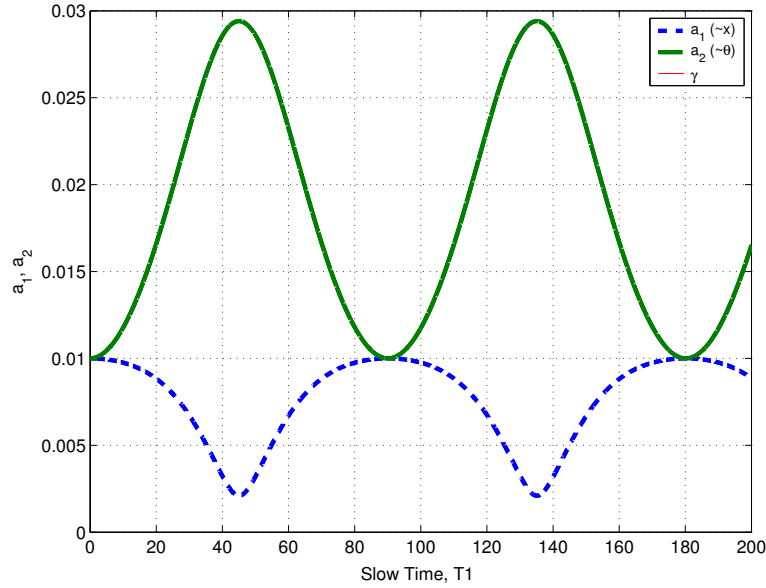


Fig. 6. Modal response of spring pendulum for an initial condition, $(a_1, a_2) = (0.01, 0.01)$

$$\dot{\gamma} = \frac{3g}{8\omega_1} \frac{a_2^2}{a_1} \sin \gamma - 2 \frac{3g}{8\omega_1} a_1 \sin \gamma + \sigma \quad (3.24)$$

By integrating these equations, we obtain the nonlinear modal amplitudes a_1 and a_2 for the spring mode and the pendulum mode, respectively, and the pseudo-phase,³¹ γ .

For an initial condition, the modal amplitudes are shown in Fig. 6. It can be seen from this figure that there is the amplitude modulation showing an energy exchange between the two modes. It is the main characteristic of the internal resonance response. For $T_1 < 45$, the amplitude of a_1 decreases, but a_2 increases. In the next time region $45 < T_1 < 90$, this trend is reversed. This type of modulating motion is caused by the internal resonance mechanism. If there is no damping, then the amplitudes are maintained and the amplitude of one mode is maximum when the amplitude of the other mode is minimum. From figures 5 and 6, we realized that the approximation obtained from the Method of Multiple Scales provide enough information about the

internal resonance. Thus, the Method of Multiple Scales will be used to analyze the internal resonance of aeroelastic systems.

Bifurcation diagrams are very effective expressions for investigating the effect of system parameters. The usefulness of two perturbation methods is studied through the well-known Duffing equation.

$$\ddot{u} + \beta^2 u + \epsilon(2\mu\dot{u} + \alpha u^3) = 2\epsilon f \cos \omega t. \quad (3.25)$$

Bifurcation diagrams for this system are obtained by using the Method of Multiple Scales (MMS) and the Method of Harmonic Balance (MHB). Because the exact solution for nonlinear systems is rare, perturbation methods are usually used for understanding the system.

In order to apply MMS to the given equation, new independent variables $T_n = \epsilon^n t$ ($n = 0, 1, 2, \dots$) is introduced and the independent variable u is perturbed as follows,

$$u = u_o + \epsilon u_1 + \epsilon^2 u_2 + \dots$$

where ϵ is a bookkeeping parameter. Substituting these new terms and variables into Eq. (3.25), we could get

$$\begin{aligned} 2\epsilon f \cos \omega t &= \left(D_0^2 + 2\epsilon D_0 D_1 \right) (u_o + \epsilon u_1 + \dots) + \beta^2 (u_o + \epsilon u_1) \\ &\quad + \epsilon [2\mu (D_0 + \epsilon D_1 + \dots) (u_o + \epsilon u_1 + \dots) + \alpha (u_o + \epsilon u_1 + \dots)] \\ &= \left[D_0^2 u_o + \beta^2 u_o \right] \\ &\quad + \epsilon \left[D_0^2 u_1 + \beta^2 u_1 + 2D_0 D_1 u_o + 2\mu D_0 u_o + \alpha u_o^3 \right] + O(\epsilon^2) \end{aligned} \quad (3.26)$$

where $D_n = \partial/\partial T_n$, $T_n = \epsilon^n t$ and ϵ is a small, dimensionless parameter with the same order as the amplitudes. Equating the coefficients of ϵ^0 and ϵ gives the following

equations.

$$O(\epsilon^0) : D_0^2 u_0 + \beta^2 u_0 = 0 \quad (3.27)$$

$$O(\epsilon^1) : D_0^2 u_1 + \beta u_1 = -2D_0 D_1 u_0 - 2\mu D_0 u_0 - \alpha u_0^3 + 2\epsilon \Gamma \cos \omega t \quad (3.28)$$

The solution of Eq.(3.27) is

$$u_0 = A_1(T_1)e^{i\beta T_0} + \bar{A}_1(T_1)e^{-i\beta T_0} \quad (3.29)$$

Putting this solution into Eq.(3.28), we obtain an expression in slow time scale T_1 .

To this end, the following expressions are used

$$\begin{aligned} D_0 D_1 u_0 &= \frac{\partial}{\partial T_0} \frac{\partial}{\partial T_1} \left(A_1(T_1)e^{i\beta T_0} + \bar{A}_1(T_1)e^{-i\beta T_0} \right) \\ &= i\beta A_1' e^{i\beta T_0} + cc \\ D_0 u_0 &= \frac{\partial}{\partial T_0} \left(A_1(T_1)e^{i\beta T_0} + \bar{A}_1(T_1)e^{-i\beta T_0} \right) \\ &= i\beta A_1(T_1)e^{i\beta T_0} + cc \\ u_0^3 &= \left(A_1(T_1)e^{i\beta T_0} + \bar{A}_1(T_1)e^{-i\beta T_0} \right)^3 \\ &= A_1^3(T_1)e^{i3\beta T_0} + 3A_1^2 \bar{A}_1(T_1)e^{i\beta T_0} + cc \\ \cos \omega t &= \frac{1}{2} \left(e^{i\omega t} + e^{-i\omega t} \right) \end{aligned} \quad (3.30)$$

From Eq. (3.30) we find

$$\begin{aligned} D_0^2 u_1 + \beta^2 u_1 &= -2 \left(i\beta A_1' e^{i\beta T_0} \right) - 2\mu \left(i\beta A_1 e^{i\beta T_0} \right) \\ &\quad - \alpha \left(A_1^3 e^{i3\beta T_0} + 3A_1^2 \bar{A}_1 e^{i\beta T_0} \right) + 2\frac{1}{2} \left(e^{i\omega t} \right) + cc \\ &= e^{i\beta t} \left(-2A_1' i\beta - 2\mu A_1 i\beta - 3\alpha A_1^2 \bar{A}_1 \right) + f e^{i\omega t} - \alpha A_1^3 e^{i3\beta T_0} + cc. \end{aligned} \quad (3.31)$$

For Eq.(3.31), there are two possibilities; either A_1 is constant or a function of T_1 . The first case, the case of constant A_1 , is considered. In this case, some parametric resonance cases can be detected. Because A_1 is a constant, A_1' in Eq.(3.31) is zero. The corresponding particular solution can be expressed as follows,

$$u_{1p} = g_1 e^{i\beta t} + g_2 e^{i\omega t} + g_3 e^{i3\beta t} \quad (3.32)$$

Substituting this particular solution into the left hand side of Eq.(3.31), the left-hand side of the equation can be rewritten as follows.

$$g_1 (\beta^2 - \beta^2) e^{i\beta t} + g_2 (\beta^2 - \omega^2) e^{i\omega t} + g_3 (\beta^2 - 9\beta^2) e^{i3\beta t} \quad (3.33)$$

The first term provides a trivial solution and the third term has a coefficient $-8\beta^2$. Comparing the other terms with the right-hand side of Eq.(3.31), g_i terms are determined.

$$g_2 = \frac{f}{\beta^2 - \omega^2}, \quad g_3 = \frac{\alpha A_1^3}{8\beta}. \quad (3.34)$$

This result shows that resonance may occur at a conditions $\beta = \Omega$.

In the second case, A_1 is not a constant, but a function of T_1 . Because a resonance is expected at a condition $\beta = \omega$ as shown in Eq. (3.34), a detuning parameter σ is introduced. Further, the exciting frequency ω is such that

$$\omega = \beta + \epsilon\sigma. \quad (3.35)$$

Substituting Eq.(3.35) into Eq. (3.31) gives

$$\begin{aligned} D_0^2 u_1 + \beta^2 u_1 &= e^{i\beta t} \left(-2A_1' i\beta - 2\mu A_1 i\beta - 3\alpha A_1^2 \bar{A}_1 \right) + f e^{i(\beta+\epsilon\sigma)t} - \alpha A_1^3 e^{i3\beta T_0} + cc. \\ &= e^{i\beta T_0} \left(-2A_1' i\beta - 2\mu A_1 i\beta - 3\alpha A_1^2 \bar{A}_1 + f e^{i\epsilon\sigma T_0} \right) - \alpha A_1^3 e^{i3\beta T_0} + cc. \\ &= e^{i\beta T_0} \left(-2A_1' i\beta - 2\mu A_1 i\beta - 3\alpha A_1^2 \bar{A}_1 + f e^{i\sigma T_1} \right) - \alpha A_1^3 e^{i3\beta T_0} + cc. \end{aligned}$$

$$(3.36)$$

where cc represent the complex conjugate. Let

$$A_1(T_1) = \frac{1}{2}a(T_1)e^{i\phi(T_1)} \quad (3.37)$$

then, taking the derivative with respect to T_1 yields

$$A_1' = \frac{\partial A_1}{\partial T_1} = \frac{1}{2}a'e^{i\phi} + \frac{1}{2}ai\phi'e^{i\phi} \quad (3.38)$$

Using Eqs. (3.37) and (3.38), Eq. (3.36) can be rewritten.

$$\begin{aligned} D_0^2 u_1 + \beta^2 u_1 &= e^{i\beta T_0} \left[-2 \left(\frac{1}{2}a'e^{i\phi} + \frac{1}{2}ai\phi'e^{i\phi} \right) i\beta \right] \\ &\quad + e^{i\beta T_0} \left[-2\mu \left(\frac{1}{2}ae^{i\phi} \right) i\beta - 3\alpha \left(\frac{1}{2}ae^{i\phi} \right)^2 \left(\frac{1}{2}ae^{-i\phi} \right) + fe^{i\sigma T_1} \right] \\ &\quad - \alpha \left(\frac{1}{2}ae^{i\phi} \right)^3 e^{i3\beta T_0} + cc. \\ &= e^{i\beta T_0} e^{i\phi} \left[-a'i\beta + a\phi'\beta - \mu ai\beta - \frac{3}{8}\alpha a^3 + fe^{i\sigma T_1} e^{-i\phi} \right] \\ &\quad - \alpha \left(\frac{1}{2}ae^{i\phi} \right)^3 e^{i3\beta T_0} + cc. \\ &= e^{i\beta T_0} e^{i\phi} \left[-a'i\beta + a\phi'\beta - \mu ai\beta - \frac{3}{8}\alpha a^3 + fe^{i\gamma} \right] \\ &\quad - \alpha \left(\frac{1}{2}ae^{i\phi} \right)^3 e^{i3\beta T_0} + cc. \\ &= e^{i\beta T_0} e^{i\phi} \left[-a'i\beta + a\phi'\beta - \mu ai\beta - \frac{3}{8}\alpha a^3 + f(\cos \gamma + i \sin \gamma) \right] \\ &\quad - \alpha \left(\frac{1}{2}ae^{i\phi} \right)^3 e^{i3\beta T_0} + cc. \end{aligned} \quad (3.39)$$

Here, $\gamma = (\sigma T_1 - \phi)$. The solvability condition is formed by the term having $e^{i\beta T_0}$. The secular terms causing unbounded responses are eliminated by equating the secular

terms to zero. Then, we can separate the equation into real and imaginary parts.

$$\begin{aligned} \text{Im.} & : -\beta(a' + a\mu) + f \sin \gamma = 0 \\ \text{Re.} & : a\beta\phi' - \frac{3}{8}\alpha a^3 + f \cos \gamma = 0 \end{aligned} \quad (3.40)$$

Using $\gamma = (\sigma T_1 - \phi)$, ϕ' can be replaced by γ' , and the first expression can be reorganized as follows.

$$\begin{aligned} a\beta\gamma' & = a\beta\sigma - a\beta\phi' \\ & = a\beta\sigma - \left(\frac{3}{8}\alpha a^3 - f \cos \gamma \right) \\ a' & = -a\mu + \frac{f}{\beta} \sin \gamma \end{aligned} \quad (3.41)$$

This system Eq.(3.41) is a planner autonomous dynamical system. For this case, the steady-state solution can be analytically obtained as shown in the next section. But, in other cases, it is not easy to get analytical solutions. In those cases, this kind of equation Eq.(3.41) should be solved by another approach.

The fixed point (or equilibrium point) (a_0, γ_0) of this system are given as follows. By letting $a' = \gamma' = 0$, the following condition is obtained

$$0 = -a\mu + \frac{f}{\beta} \sin \gamma, \text{ or } a\mu\beta = f \sin \gamma \quad (3.42)$$

$$0 = a\beta\sigma - \left(\frac{3}{8}\alpha a^3 - f \cos \gamma \right), \text{ or } -a\beta\sigma + \frac{3}{8}\alpha a^3 = f \cos \gamma \quad (3.43)$$

By squaring and adding we find that a_0 satisfies

$$\begin{aligned} (a_0\mu\beta)^2 + \left(-a_0\beta\sigma + \frac{3}{8}\alpha a_0^3 \right)^2 & = f^2 (\cos^2 \gamma + \sin^2 \gamma) \\ a_0^2 \left[\mu^2\beta^2 + \left(-\beta\sigma + \frac{3}{8}\alpha a^2 \right)^2 \right] & = f^2 \end{aligned} \quad (3.44)$$

Equation (3.44) is an implicit equation for the amplitude of the response a_0 as a

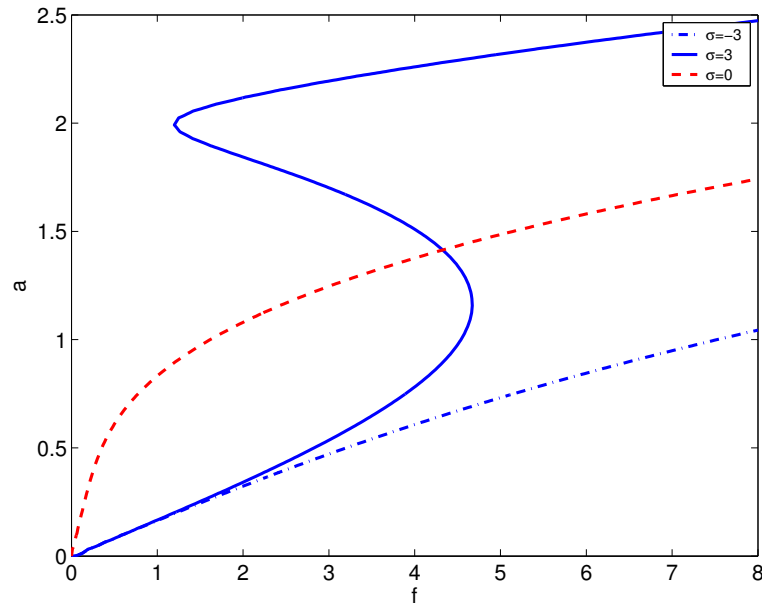


Fig. 7. Frequency-Amplitude curves for the Duffing Equation

function of the external detuning σ (i.e. the exciting frequency) and the amplitude of the excitation f . It is called the frequency-response equation. For various σ , the frequency-amplitude curves are depicted in Fig. 7. It can be seen from Fig. 7 that for a system with a hardening cubic spring ($\alpha > 0$) multiple solutions are possible when the exciting frequency is greater than the natural frequency ($\sigma \propto \omega - \beta > 0$) [see the rigid line]. In other frequency conditions, there is only one solution as represented by the dashed line and the dash-dot line.

The following Duffing equation is analyzed by using the Method of Harmonic Balance.

$$\ddot{u} + k\dot{u} + \beta u + u^3 = \Gamma \cos \omega t. \quad (3.45)$$

The coefficient that is associated with linear term β is negative. To determine equilibrium points, the autonomous system ($\Gamma = 0$) is studied. Equilibrium points and their stabilities are determined. From equation (3.45) and the equilibrium condition

$\dot{y} = 0$, the following expression for the equilibrium points is obtained.

$$u(u^2 + \beta) = 0 \quad (3.46)$$

From this condition, the following equilibrium points are obtained. The number of points depends upon the value of β .

$$u_E = 0, \quad u_E = \pm 1 \quad \text{for } \beta = -1 \quad (3.47)$$

$$u_E = 0 \quad \text{for } \beta = 1 \quad (3.48)$$

In order to estimate the stability at the equilibrium points, the second order differential equation is transformed into two first-order differential equation.

$$\begin{aligned} \dot{u} &= y = f_1(u, y) \\ \dot{y} &= -ky - \beta u - u^3 = f_2(u, y) \end{aligned} \quad (3.49)$$

The Jacobian matrix for this system is

$$[J] = J_{ij} = \frac{\partial f_i}{\partial q_j} = \begin{bmatrix} 0 & 1 \\ -\beta - 3u^2 & -k \end{bmatrix}, \quad (3.50)$$

where $q_1 = u$, and $q_2 = y$. The corresponding eigenvalues can be obtained from the following expression,

$$eig.[J] = |J - \lambda I| = \begin{bmatrix} 0 - \lambda & 1 \\ -\beta - 3u^2 & -k - \lambda \end{bmatrix} = \lambda^2 + k\lambda + (\beta + 3u^2) = 0 \quad (3.51)$$

or

$$\lambda = \frac{1}{2} \left[-k \pm \sqrt{k^2 - 4(\beta + 3u^2)} \right] \quad (3.52)$$

At the first equilibrium point $(x, y)_{E_1} = (0, 0)$, the eigenvalues are $-k \pm \sqrt{k^2 - 4\beta}$.

For a case of $\beta = 1$ the eigenvalues are either real with negative sign ($k > 2$) or

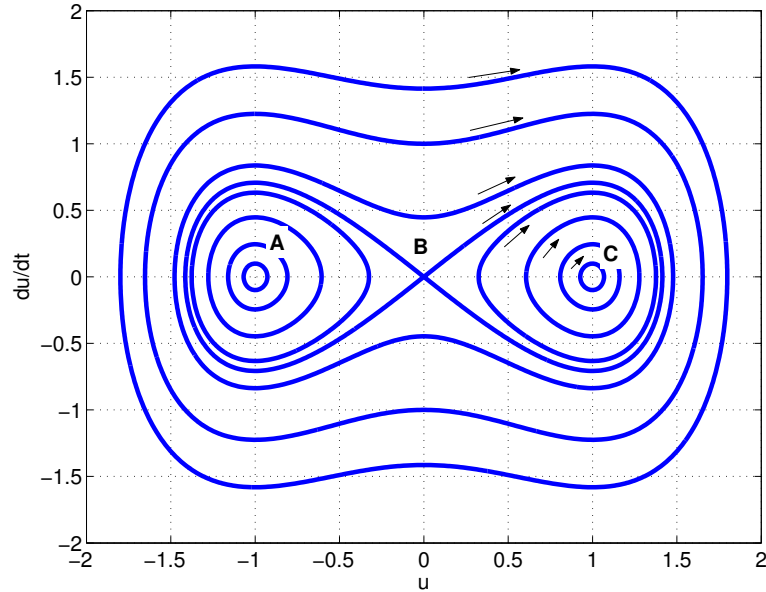


Fig. 8. Phase portraits for the Duffing Equation ($k=0.0, \Gamma = 0$)

complex with negative real part ($k < 2$). These represent stable node or stable spiral. For $\beta = -1$ there are three equilibrium points. Because the corresponding eigenvalues are real with opposite sign at the point $(u, y)_{E_1} = (0, 0)$, the point represent a saddle. At the other equilibrium points $(u, y)_{E_{2,3}} = (\pm 1, 0)$, the eigenvalues are $-k \pm \sqrt{k^2 - 8}$. Depending upon the value of k , they could be either complex conjugate with two negative real values for $k^2 - 8 < 0$ and real with negative sign for $k^2 - 8 > 0$. These points represent either stable spiral or stable node. For the case of no damping and no external force, ($k = 0.0$ and $\Gamma = 0$), phase portraits are shown in Fig. 8. As shown in this figure, there are three equilibrium points, $(0,0)$ and $(\pm 1, 0)$. The first point, $B=(0,0)$ is a saddle, and the other two points, A and C are centers.

In the above analysis, the effects of the exciting force are not included. By setting $\Omega = \omega t$, the non-autonomous system Eq. (3.45) can be changed to an autonomous system. One approximation, the Method of Harmonic Balance is used to study the effect of the exciting force.

It is assumed that the amplitudes are 'slowly varying', so that in the subsequent their second derivatives can be neglected. Also, harmonics of order higher than one will be neglected in the approximation.

Let

$$\begin{aligned}
u(t) &= c(t) + a(t) \cos \omega t + b(t) \sin \omega t \\
\dot{u}(t) &= \dot{c}(t) + (\dot{a} + b\omega) \cos \omega t + (\dot{b} - a\omega) \sin \omega t \\
\ddot{u}(t) &= \ddot{c}(t) + (\ddot{a} + 2b\omega - a\omega^2) \cos \omega t + (\ddot{b} - 2a\omega - b\omega^2) \sin \omega t \\
u^3 &= c^3 + \frac{3}{2}c(a^2 + b^2) + 3b[c^2 + \frac{1}{4}(a^2 + b^2)] \sin \omega t \\
&\quad + 3a[c^2 + \frac{1}{4}(a^2 + b^2)] \cos \omega t + H.O.T.
\end{aligned} \tag{3.53}$$

Substituting Eq. (3.53) into Eq.(3.45), and equating the coefficients of $\cos \omega t$, $\sin \omega t$ and constant $c(t)$, gives the following expressions

$$\begin{aligned}
\ddot{c} + k\dot{c} - c + c^3 + \frac{3}{2}c(a^2 + b^2) &= 0 \\
(\ddot{a} + 2\dot{b}\omega - a\omega^2) + k(\dot{a} + b\omega) - a + 3a[c^2 + \frac{1}{4}(a^2 + b^2)] &= \Gamma \\
(\ddot{b} - 2a\omega - b\omega^2) + k(\dot{b} - a\omega) - b + 3b[c^2 + \frac{1}{4}(a^2 + b^2)] &= 0
\end{aligned} \tag{3.54}$$

Based on the initial assumption, second-order differential terms \ddot{a} and \ddot{b} are neglected.

Thus,

$$\ddot{c} + k\dot{c} = -c(c^2 - 1 + \frac{3}{2}r^2) \tag{3.55}$$

$$k\dot{a} + 2\dot{b}\omega = -a(-1 - \omega^2 + 3c^2 + \frac{3}{4}r^2) - kb\omega + \Gamma_o \tag{3.56}$$

$$-2\dot{a}\omega + k\dot{b} = -b(-1 - \omega^2 + 3c^2 + \frac{3}{4}r^2) + k\omega a \tag{3.57}$$

where $r^2 = a^2 + b^2$. If we further define

$$\dot{c} = d, \tag{3.58}$$

then, we have the following new expression from Eqs. (3.55), (3.58) and

$$\dot{d} = -kd - c(c^2 - 1 + \frac{3}{2}r^2) \quad (3.59)$$

Thus, these equations are rewritten in matrix form as follows,

$$\begin{bmatrix} k & 2\omega & 0 & 0 \\ -2\omega & k & 0 & 0 \\ 0 & 0 & 1 & 0 \\ 0 & 0 & 0 & 1 \end{bmatrix} \begin{bmatrix} \dot{a} \\ \dot{b} \\ \dot{c} \\ \dot{d} \end{bmatrix} = \begin{bmatrix} -a(-1 - \omega^2 + 3c^2 + \frac{3}{4}r^2) - k\omega b + \Gamma \\ -b(-1 - \omega^2 + 3c^2 + \frac{3}{4}r^2) + k\omega b \\ d \\ -c(c^2 - 1 + \frac{3}{2}r^2) - kd \end{bmatrix} \quad (3.60)$$

The steady-state solution for the approximation can be determined by setting $d()/dt = 0$, which is also the condition for equilibrium points. At this point, it is meaningful to review the concepts for invariant manifolds, steady-state solution, and equilibrium points. There are three kinds of invariant manifolds: equilibrium points, centers, and limit cycles. Because they stay at the point forever or return to their original position, they represent a steady-state solution for the considered system. From the original differential equation, it is easy to determine the equilibrium points because Duffing's equation is relatively simple. Unless eigenvalues are pure imaginary, the linearized stability fully represents the response characteristics of the nonlinear system. To identify a Hopf bifurcation, the birth of a limit cycle, additional analysis is required, but this process is not simple. Especially, the equilibrium points are obtained under the condition that there is no external force term. By introducing a parameter $\Omega = \omega t$, the following expression can be obtained from the original Duffing equation.

$$\begin{aligned} \dot{u} &= y \\ \dot{y} &= -ky - \beta u - u^3 + \Gamma \cos \Omega \\ \dot{\Omega} &= \omega \end{aligned} \quad (3.61)$$

Because $d()/dt = 0$ at equilibrium points, y and ω should be zero; otherwise, Ω must be constant. The number of equilibrium points can be determined by the following expression

$$-\beta u - u^3 + \Gamma \cos \Omega = 0. \quad (3.62)$$

Depending upon β, Γ and Ω , the number of equilibrium point may be changed from one to three.

The approximation may be beneficial in that the steady-state solution may include limit cycles. The obtained steady-state solution is either zero or non-zero. Because the solution corresponds to the amplitude and/or phase angle of the response, the zero amplitude means a equilibrium point, and the non-zero values represent either centers or limit cycles. In numerical simulation, the unstable solutions cannot be easily detected, but they can be identified in the steady-state solution of the approximation. For Duffing's equation, the steady-state solution of the approximation can be obtained analytically. But, in practice, it is not easy to obtain the analytical solution. So, it is required to use a continuation method, which consists of predictor (Pseudo-Arclength method) and corrector (Newton-Raphson method).

In order to obtain the steady-state solution for Eq. (3.60), the derivative terms are set to zero i.e., $(\cdot) = 0$. Thus,

$$\begin{pmatrix} 0 \\ 0 \\ 0 \\ 0 \end{pmatrix} = \begin{pmatrix} -a(-1 - \omega^2 + 3c^2 + \frac{3}{4}r^2) - k\omega b + \Gamma \\ -b(-1 - \omega^2 + 3c^2 + \frac{3}{4}r^2) + k\omega b \\ d \\ -c(c^2 - 1 + \frac{3}{2}r^2) - kd \end{pmatrix} \quad (3.63)$$

or

$$\begin{pmatrix} -\Gamma \\ 0 \\ 0 \end{pmatrix} = \begin{pmatrix} -a(\beta^2 - \omega^2 + 3c^2 + \frac{3}{4}r^2) - k\omega b \\ -b(\beta^2 - \omega^2 + 3c^2 + \frac{3}{4}r^2) + k\omega b \\ -c(c^2\beta^2 + \frac{3}{2}r^2) \end{pmatrix} \quad (3.64)$$

where, $r^2 = a^2 + b^2$. Because the first and second expressions of Eqs. (3.63) and (3.64) have similar terms, the expressions can be combined by squaring and adding them. The following expression is obtained.

$$r^2 \left[\left(\beta - \omega^2 + 3c^2 + \frac{3}{4}r^2 \right)^2 + k^2\omega^2 \right] = \Gamma^2. \quad (3.65)$$

If the linear restoring force term has negative sign, $\beta = -1$, then the obtained result coincides with the Eq.(13.23) in J&S's book. From the third row of Eq.(3.64) and Eq.(3.65), we can generate the following two types of solutions.

$$TYPE I : c = 0, r^2 \left[\left(\beta - \omega^2 + \frac{3}{4}r^2 \right)^2 + k^2\omega^2 \right] = \Gamma^2 \quad (3.66)$$

$$TYPE II : c = 1 - \frac{3}{2}r^2, r^2 \left[\left(\beta - \omega^2 - \frac{15}{4}r^2 \right)^2 + k^2\omega^2 \right] = \Gamma^2 \quad (3.67)$$

Using the obtained approximate solutions Eq. (3.66) , a bifurcation diagram is generated. Bifurcation diagrams for the case $k = 0.3, \omega = 1.2$ are shown in Fig. 9. Later, this bifurcation diagram will be compared with the diagram based on the Poincaré map. From these bifurcation diagrams, we can easily realize the effect of Γ . This figure shows that $r = 0$ and $\Gamma = 0$ at the point $P1$. If $r = 0$, then a and b must be zero because of $r^2 = a^2 + b^2$. But, the point $B(u, \dot{u}) = (0, 0)$ is a saddle point as shown in Fig. 8. It implies that the response will not stay at the point $P1$. The Γ region including the two points $P2$ and $P3$ has three solutions. Usually, all of three solutions could not be stable solutions. Thus, at least one solution is unstable.

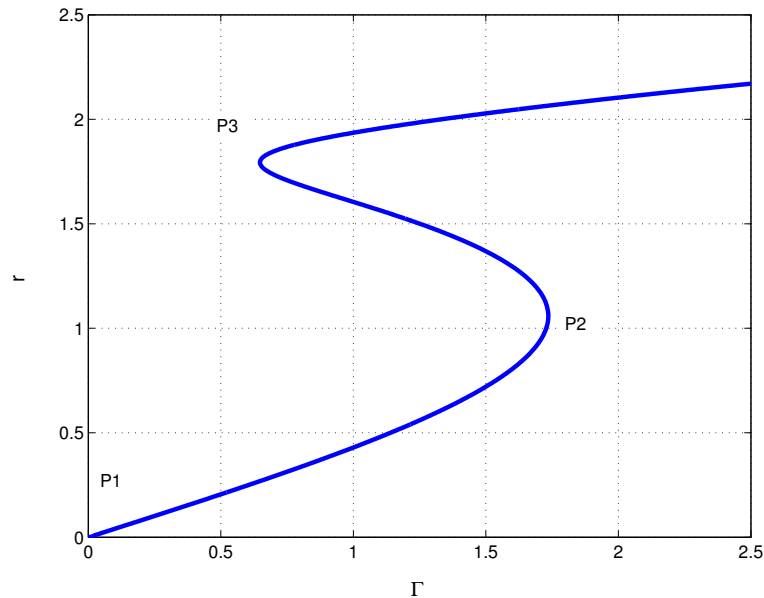


Fig. 9. Bifurcation diagram obtained by the Method of Harmonic Balance

C. Nonlinear Software Packages DsTool and AUTO(a Continuation Method)

The bifurcation diagram shown in Fig. 9 gives us meaningful information. However, these analytical solutions can be obtained only for special systems. Therefore, we need alternatives to generate bifurcation diagrams. Software packages such as DsTool³² and AUTO³³ have the ability to generate bifurcation diagrams for nonlinear systems.

Lee et al.³⁷ reviewed some nonlinear approaches for aeroelastic systems. AUTO is included in his review. According to Lee, AUTO can perform a limited bifurcation analysis of a system of ordinary differential equations. The fact that the original equations is approximated in AUTO could be one of reasons. The continuation method adopted in AUTO consists of Newton-Raphson method and Pseudo Arclength method

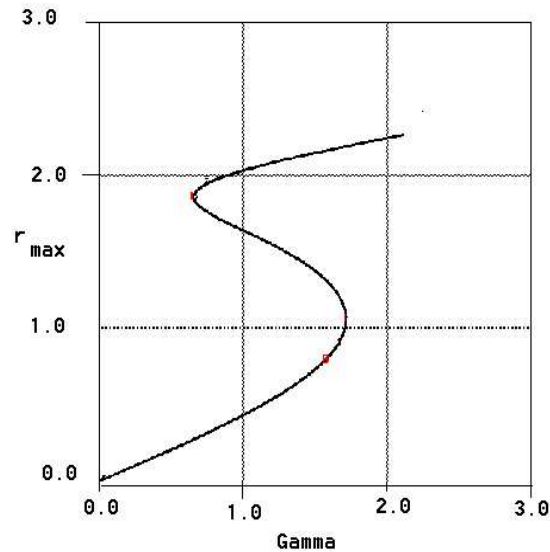


Fig. 10. Bifurcation diagram obtained by AUTO (the maximum)

as a predictor and a corrector, respectively.⁴² In this process, the Jacobian matrix is used. Because the Jacobian matrix is the matrix of the first partial derivatives of the system matrix, the obtained solution is approximate.

In order to obtain bifurcation diagrams for Duffing's equation with an exciting force, a nonlinear oscillator is added to describe the desired periodic forcing. A bifurcation diagram for Duffing's equation is shown in Fig. 10. The y-axis represents the maximum values of responses. The shape of this diagram is very similar with the diagram obtained by MHB. It means that AUTO may provide an acceptable approximate solution. More accurate solutions could be obtained from the L2-norm, not the maximum as shown in Fig. 11. The initial point at $\Gamma = 0$ is moved from 'zero' in Fig. 10 to 'one' in Fig. 11.

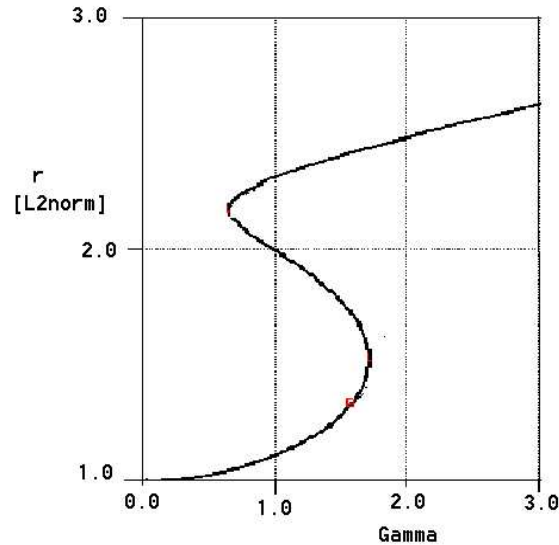


Fig. 11. Bifurcation diagram(2) obtained by AUTO(L2-norm)

Using DsTool, Phase portraits for the Duffing equation are generated. The results for various Γ are shown in Fig. 12. According to the User's Manual for DsTool, a Dynamic System Toolkit with an Interactive Graphical Interface, Hopf bifurcation can be obtained by using four different methods. But, the present version of DsTool have lost the ability to build the bifurcation diagram including Hopf bifurcation.

D. Phase Plane Analysis and Poincaré Maps

Although bifurcation diagrams can be obtained by using perturbation methods and continuation methods included in AUTO, they cannot provide all information about the considered nonlinear system. For the Duffing equation, bifurcation diagrams could be obtained by using the Method of Harmonic Balance and the Method of Multiple Scales. The obtained diagrams are very simple as shown in Fig. 9 and

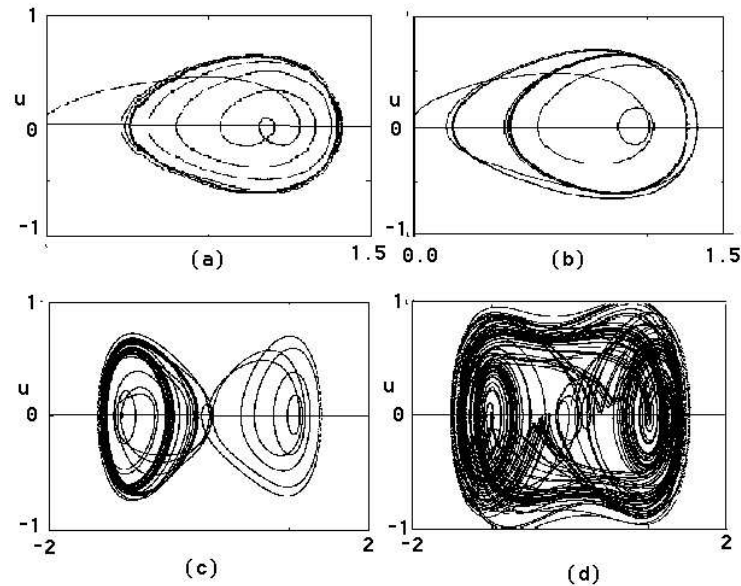


Fig. 12. Phase portraits for the Duffing Equations obtained by DsTool: (a) $\Gamma = 0.2$ (b) $\Gamma = 0.28$ (c) $\Gamma = 0.29$ (d) $\Gamma = 0.5$

books written by Jordan and Smith,³⁰ and Balanchandra and Nayfeh.⁴² The approximate solution shows that there are stable and unstable equilibrium points. Although period-2 responses and chaotic motions, etc. are included in the responses, these kinds of response characteristics cannot be identified from the approximation. In order to capture these responses, other approaches are required. Many researchers have investigated LCO and periodic motions by using phase portraits and Poincaré maps. A limit cycle is defined as an isolated closed curve in the phase plane.⁴³ The periodic nature of the motion and the limiting nature of the cycle are described by the words ‘closed’ and ‘isolated’, respectively. The ‘isolated’ curve implies that the nearby trajectories converge to the cycle or diverge from it. Although there are many closed curves in Fig. 8, they are not limit cycles because they are not isolated. If the curve has only one-period, the corresponding Poincaré map has only one fixed point. Depending upon the period of the response represented by the curve, the number of

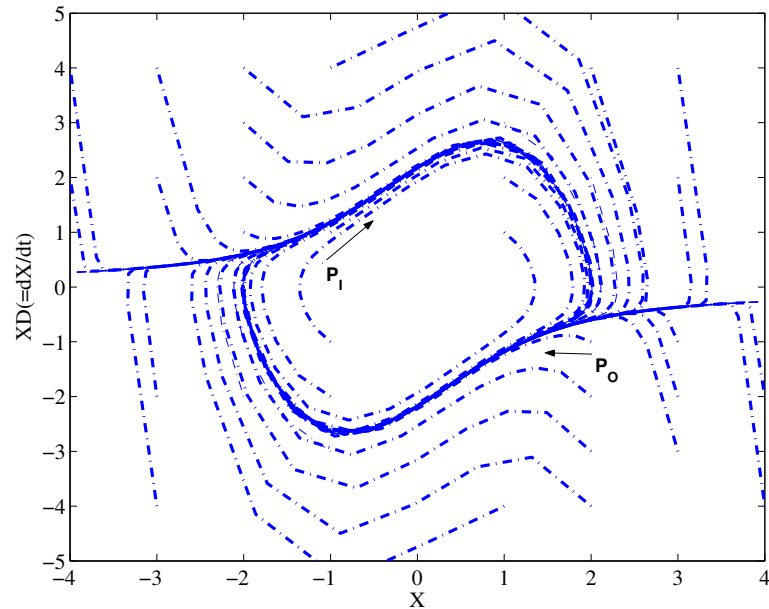


Fig. 13. Phase portrait for the Van der Pol Equation

fixed points may change. In the phase plane, each curve represents a possible motion, and each point is an instantaneous state of the system. The curves are phase trajectories⁴⁴ or, simply, trajectories. A display of a number of such trajectories in the phase plane is called a phase portrait of the original differential equation. Typically, we show a select number of cases to avoid confusion. A phase portrait for the Van der Pol equation is shown in Fig. 13. In this figure, phase trajectories are denoted by ‘dash-dot line’. In the region $-2 < X < 2$, a closed curve could be identified. Because many dash-dot lines are duplicated, it looks like a solid line. The nearby trajectories including the trajectories stated from points P_I and P_O converge to the closed curve. Thus, the closed isolated curve is a limit cycle.

Mathematically, a map can be viewed as a time-sampled sequence of data.⁴⁵ If there is a sampling rule in place, then the map can be called as a Poincaré map. For a forced vibration problem, the sampling rule usually is based on the period of the exciting force because the responses depend upon the force, especially the frequency

and amplitude of the external force. Unfortunately, aeroelastic systems are usually autonomous. Because there is not any periodic input, we must define other sampling rules. For the case of the Van der Pol equation, the limit cycle is represented by one fixed point on Poincaré map.

Using Poincaré maps, we generate bifurcation diagrams. Because the Duffing Equation has an external force, the first sampling rule is the period of the exciting force. In order to generate a bifurcation diagram, it is assumed that the simulation achieves a steady-state. Thus, the corresponding Poincaré map in this state provides the fixed points. The obtained bifurcation diagram is depicted in Fig. 14. In this figure, the number of fixed points represents the periodicity of the responses. If there are n -fixed points at a Γ , then it means that the responses at the specified Γ condition consists of n periodic functions. It can be seen from Figs. 9 and 14 that they appear to have different behavior. It is noted that one difference is due to the y-axis data on these bifurcation diagrams. In the bifurcation diagram generated by perturbation methods, the y-axis corresponds to the maximum amplitude of responses. However, in the bifurcation diagram based on the Poincaré map, the y-axis does not guarantee the maximum amplitude, but may be an intermediate value. To satisfy the maximum condition, we define another sampling rule $\dot{u} = 0$. Because of this new sampling rule, one periodic motion is represented by two fixed points. It implies that there will be two situations satisfying the sampling condition $\dot{u} = 0$ when the sign of response changes from ‘positive(+)’ to ‘negative(-)’, vice versa. By applying this new sampling rule, another bifurcation diagram is obtained as shown in Fig. 15. These two bifurcation diagrams show that depending upon the sampling rule the shape of bifurcation diagrams based on Poincaré maps appears changed. Simply, the information presented in the diagrams is slightly modified. In order to compare with the previous bifurcation diagram, Fig. 9, the bifurcation diagram is expressed by the dashed line

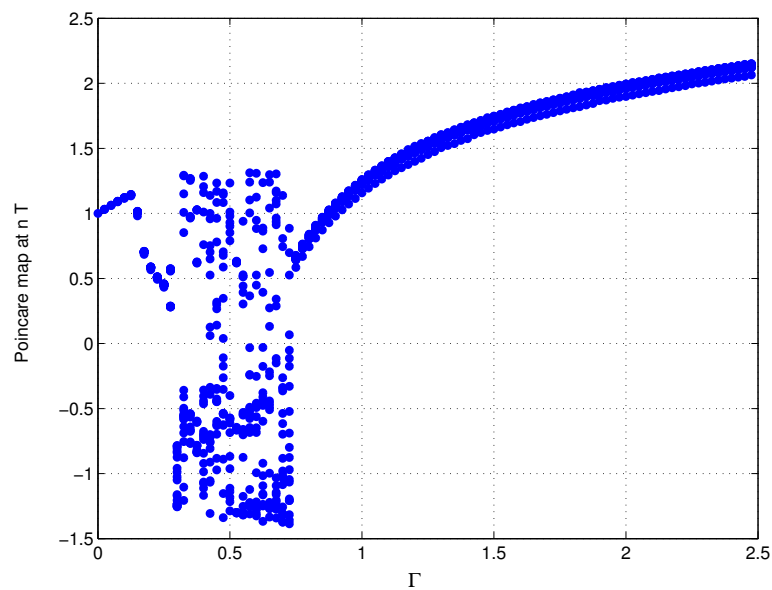


Fig. 14. Bifurcation diagram(1) of Poincaré maps for the Duffing Equation

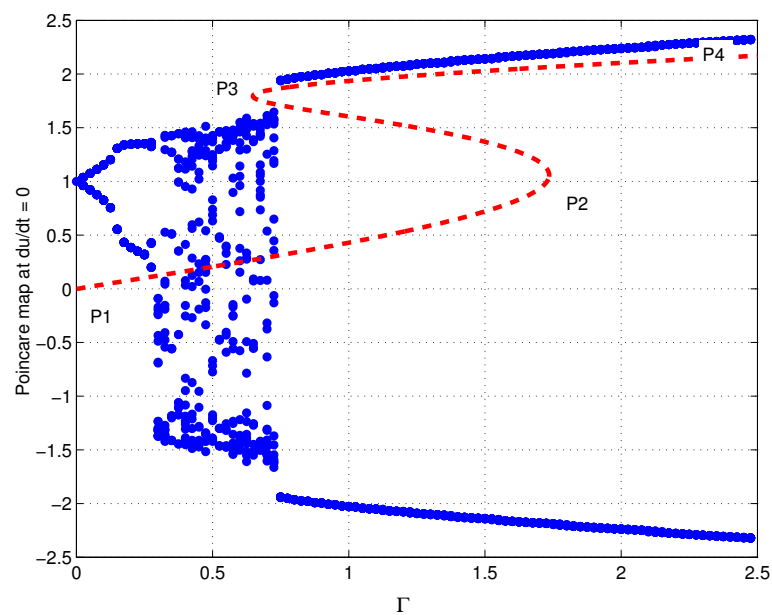


Fig. 15. Bifurcation diagram(2) of Poincaré maps for the Duffing Equation

in Fig. 15. As shown in this figure, the amplitudes in the range from P3 to P4 are very close each other. But, in the other area, the shapes of bifurcation diagrams are different. In the region $0.28 < \Gamma < 0.73$, period doubling phenomena and chaotic motion exist.³⁰ Time simulations, phase portraits, and Poincaré maps of the Duffing Oscillator for $k = 0.3, \omega = 1.2, \Gamma = 0.2$ are shown in Fig. 16. The initial condition used is $(u, \dot{u}) = (0.0, 0.01)$. This condition applied to the other cases having different Γ . Time histories for u and \dot{u} are shown in the left-hand side. Although the initial u is '0.0(zero)', it oscillates with respect to '1.0' because the point $(0,0)$ is an unstable equilibrium point and the point $(1.0,0.0)$ is one of stable equilibrium points as shown in Fig. 8. Periodicity of the responses could be identified from the phase portrait and Poincaré map. Depending upon the sampling rule, the meaning of the fixed points are different. When a sampling rule $t = nT + t_0$ based on the period of exciting force T is applied, there is only one fixed point as shown in the upper side. For another sampling rule $du/dt = 0.0$, two fixed points are appeared as shown in the lower side. Regardless of the adopted sampling rule, the result shows a period-1 motion. This result could be supported by the frequency content as shown in Fig. 17. There is only one peak frequency(P1) showing one-period motion. Although there is one more peak, P0, it has zero frequency which implies statical movement from $u = 0$ to $u = 1$.

The responses for two conditions $\Gamma = 0.28, 0.29$ show that the number of fixed points are increased as Γ is increased. Although the value of Γ is slightly increased, the responses are different as shown in Figs. 18 and 19. The response for $\Gamma = 0.28$ makes a closed circle around a equilibrium point $(1,0)$, but the another response for $\Gamma = 0.29$ make another bounded response which includes another equilibrium point $(-1,0)$. Because the number of fixed points for $\Gamma = 0.28$ is two (or four), it could be expected that the response consists of two frequency components. When we

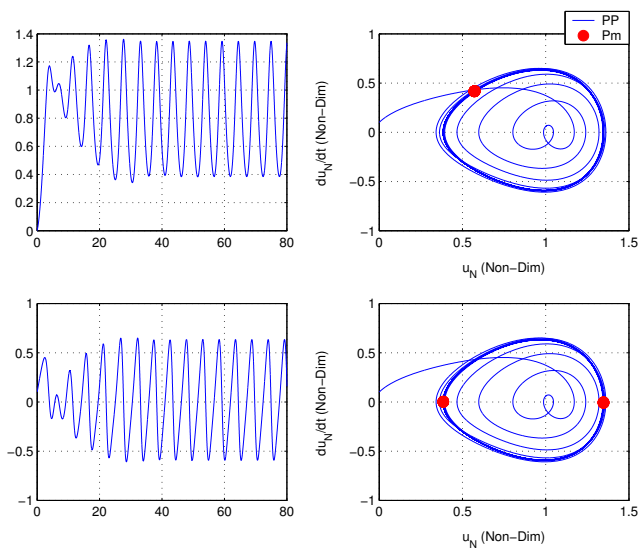


Fig. 16. Time simulations, phase portraits, and Poincaré maps of the Duffing Oscillator for $k = 0.3, \omega = 1.2, \Gamma = 0.2(\text{period} - 1)$

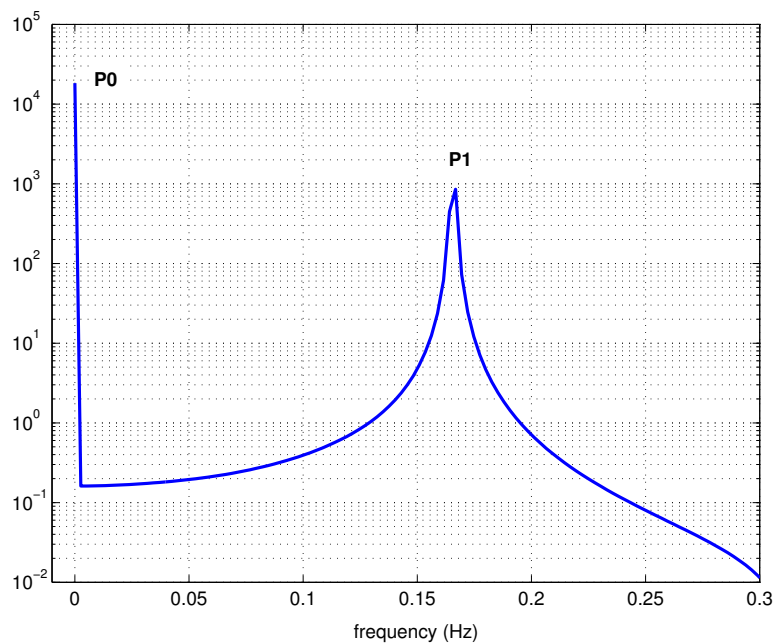


Fig. 17. Frequency content for $k = 0.3, \omega = 1.2, \Gamma = 0.2(\text{period} - 1)$

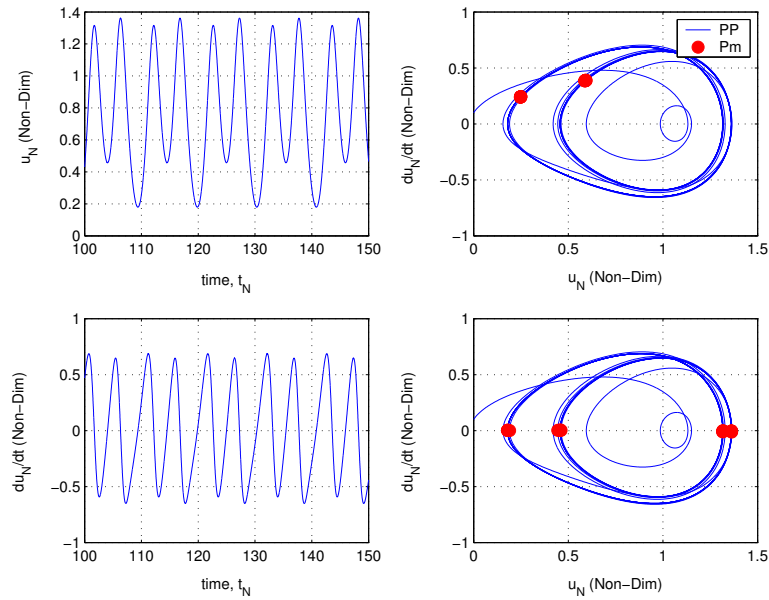


Fig. 18. Time simulations, phase portraits, and Poincaré maps of the Duffing Oscillator for $k = 0.3, \omega = 1.2, \Gamma = 0.28$ (period = 2)

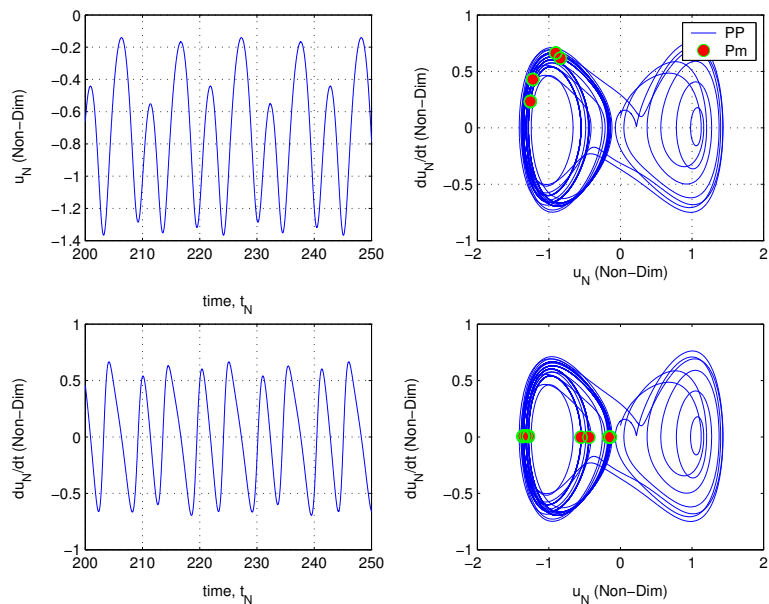


Fig. 19. Time simulations, phase portraits, and Poincaré maps of the Duffing Oscillator for $k = 0.3, \omega = 1.2, \Gamma = 0.29$ (period = 4)

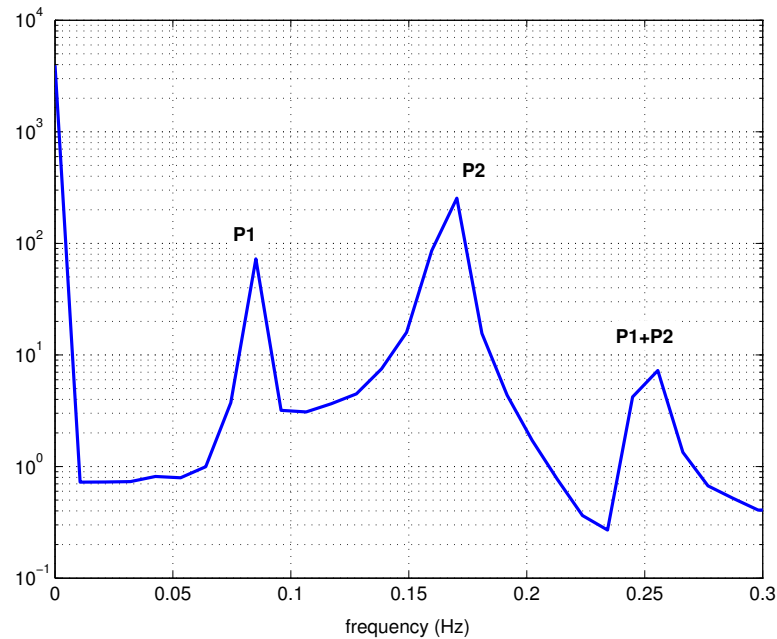


Fig. 20. Frequency content for $k = 0.3, \omega = 1.2, \Gamma = 0.28(\text{period} - 2)$

checked the frequency content for this case, it could be seen that there are three peak frequencies as shown in Fig. 20. But, it could be said that there are two frequency components 'P1' and 'P2' because the last peak 'P1+P2' implies the combination of 'P1' and 'P2'.

One more interesting response is shown in Fig. 21 and 22. There are many Poincaré maps regardless of the sampling rules. The frequency content is also complex. Indeed, there is no fixed points and the result shows one example of a strange attractor. Although multiple periodic motions are included in these responses, they should be fully investigated in that they are bounded and not unstable responses. These kinds of responses are not captured by perturbation methods alone, the bifurcation diagram based on the Poincaré fixed points is a useful tool for analysis.

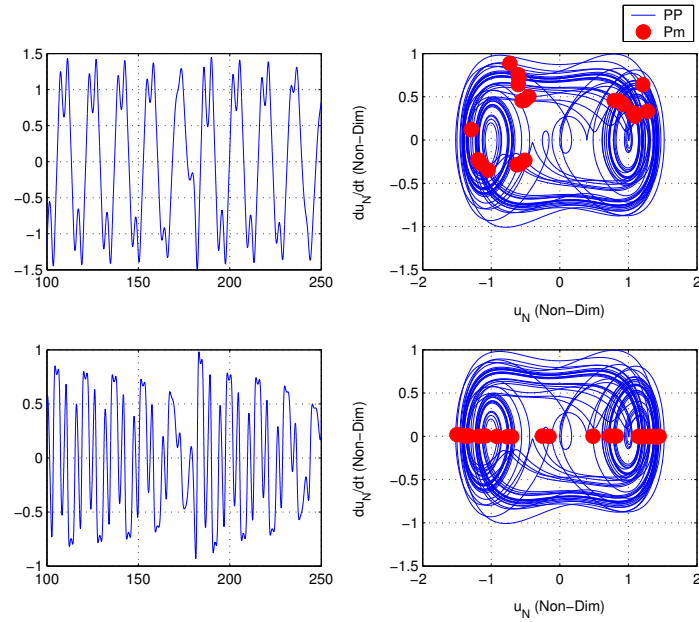


Fig. 21. Time simulations, phase portraits, and Poincaré maps of the Duffing Oscillator for $k = 0.3, \omega = 1.2, \Gamma = 0.5(\text{period} - 1)$

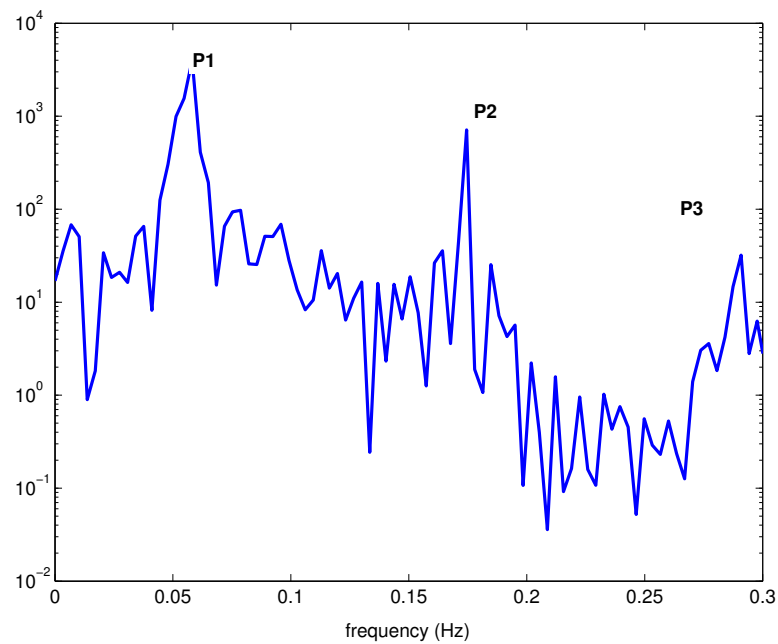


Fig. 22. Frequency content for $k = 0.3, \omega = 1.2, \Gamma = 0.5(\text{period} - 1)$

CHAPTER IV

SYSTEMS WITH QUADRATIC NONLINEARITIES

In this chapter, we examine a wing system in which quadratic nonlinearities are considered. In the bending-bending-torsion equations, third-order nonlinear terms are neglected. Consequently, the equations have only quadratic nonlinear terms. The quadratic nonlinearities are caused by wing flexibilities. The Method of Multiple Scales (MMS) is applied to the equations, and some approximate solutions are obtained. In this process, two approaches to uncouple the system are considered. At least two internal resonance conditions are found by the MMS. The possibility of internal resonance (IR) is examined through a wing model based on the Nonlinear Aeroelastic Test Apparatus (NATA) and the Heavy Goland Wing (HGW). When wing span increases, two wing models satisfying the resonance conditions are obtained from the HGW. The anticipated resonance conditions are examined through time simulation and analyses of Fast Fourier Transforms.

A. Equations of Motion for a Wing with Quadratic Nonlinearities

When third order nonlinear terms and store terms are neglected, a simpler form of the nonlinear bending-bending-torsion(BBT) equations is obtained. No aerodynamic nonlinear terms and store nonlinear terms exist because they consist of third order terms. To maintain the consistency in nonlinear order terms, the third order terms in nonlinear structural terms are also removed. The resulting BBT equations are as follows,

$$C_{uw1}\ddot{u}_i + \beta_z C_{uw2}u_i = \beta_y C_{uw3}\alpha_k w_j + (\beta_z - 1)(C_{uw6}w_j\alpha_k) \quad (4.1)$$

$$\begin{aligned}
& C_{ww1}\ddot{w}_j - e^*\ddot{\alpha}_k + C_{wwq}w_j - \mu * V^* C_{wa1}\dot{\alpha}_k \\
& + \mu \frac{C_{L\alpha}}{\pi} V^* \left[\frac{1}{b^* V^*} \dot{w}_j C_{wa2} - \alpha_k C_{wa3} - V^* \left(\frac{1}{2} - a \right) \dot{\alpha}_k C_{wa4} \right] \\
& = -\beta_y C_{ww3} (\alpha_k u_i) + (\beta_z - 1) (C_{ww6} u_i \alpha_k)
\end{aligned} \tag{4.2}$$

$$\begin{aligned}
& C_{aw1}\ddot{\alpha}_k - \frac{e^*}{I_y^*} \ddot{w}_j + \frac{1}{I_y^*} \beta_y C_{aw2} \alpha_k - \frac{1}{I_y^*} \mu b^* \left(\frac{1}{2} - a \right) V^* C_{aa1} \dot{\alpha}_k \\
& + \frac{1}{I_y^*} \mu \frac{C_{m\alpha}}{\pi} V^{*2} \left[\frac{1}{V^*} C_{aa2} \dot{w}_j - C_{aa3} \alpha_k - b^* \left(\frac{1}{2} - a \right) \frac{1}{V^*} C_{aa4} \dot{\alpha}_k \right] \\
& = -(\beta_z - 1) [-C_{aw5} w_j u_i]
\end{aligned} \tag{4.3}$$

where the terms having the superscript ‘*’ are defined in Chapter II, and the coefficient terms such as C_{ww1} , C_{aw1} and C_{aw5} are defined in Appendix A. For ease of notation, the superscript * which is used to denote that the t , u , and w terms are nondimensionalized is omitted. These equations are obtained from Eqs. (2.42), (2.43) and (2.44) by neglecting higher order terms and all store terms. In future air vehicles, the external store may not be a mandatory option. And, because it is the first attempt to investigate the internal resonance (IR) in the bending-bending-torsional aeroelastic system, a simpler wing system without store terms is considered. From Eqs.(4.1),(4.2), and (4.3), the linear mass and stiffness matrices are expressed as follows,

$$[M_L] \{\ddot{q}\} = \begin{bmatrix} C_{ww1} & 0 & 0 \\ 0 & C_{ww1} & -e^* C_{we1} \\ 0 & -\frac{e^*}{I_y^*} C_{ae1} & C_{aw1} \end{bmatrix} \begin{Bmatrix} \ddot{u}_i \\ \ddot{w}_i \\ \ddot{\alpha}_i \end{Bmatrix} \tag{4.4}$$

$$[C_L] \{\dot{q}\} = \begin{bmatrix} 0 & 0 & 0 \\ 0 & C^{22} & C^{23} \\ 0 & C^{32} & C^{33} \end{bmatrix} \begin{Bmatrix} \dot{u}_i \\ \dot{w}_i \\ \dot{\alpha}_i \end{Bmatrix} = \begin{bmatrix} 0 & 0 & 0 \\ 0 & C_{a2}^{22} & -C_{a1}^{23} - C_{a4}^{23} \\ 0 & C_{a2}^{32} & C_{a1}^{33} - C_{a4}^{33} \end{bmatrix} \begin{Bmatrix} \dot{u}_i \\ \dot{w}_i \\ \dot{\alpha}_i \end{Bmatrix} \tag{4.5}$$

$$[K_L] \{q\} = \begin{bmatrix} \beta_z C_{uw2} & 0 & 0 \\ 0 & C_{ww2} & -\mu \frac{C_{L\alpha_k}}{\pi} V^* C_{wa3} \\ 0 & 0 & -\frac{1}{I_y^*} \beta_y C_{aw2} - \frac{1}{I_y^*} \mu \frac{C_{m\alpha_k}}{\pi} V^{*2} C_{aa3} \end{bmatrix} \begin{Bmatrix} u_i \\ w_i \\ \alpha_i \end{Bmatrix} \quad (4.6)$$

where $\{q\}$ represents the system variables, $\{q\} = \{u, w, \alpha\}$ and the coefficients are defined as follows,

$$C_{a1}^{23} = \mu V^* C_{wa1} \quad (4.7)$$

$$C_{a2}^{22} = \mu \frac{C_{L\alpha}}{\pi} \frac{V^*}{b^*} C_{wa2} \quad (4.8)$$

$$C_{a4}^{23} = \mu \frac{C_{L\alpha}}{\pi} V^* \left(\frac{1}{2} - a \right) C_{wa4} \quad (4.9)$$

$$C_{a1}^{33} = \mu \frac{1}{I_y^*} b^* \left(\frac{1}{2} - a \right) V^{*2} C_{aa1} \quad (4.10)$$

$$C_{a2}^{32} = \mu \frac{1}{I_y^*} \frac{C_{m\alpha}}{\pi} \left(\frac{1}{2} - a \right) V^* C_{aa2} \quad (4.11)$$

$$C_{a4}^{33} = \mu \frac{1}{I_y^*} \frac{C_{m\alpha}}{\pi} b^* \left(\frac{1}{2} - a \right) V^* C_{aa4} \quad (4.12)$$

As shown in the above expressions, these matrices have coupling terms and they are not symmetric. Depending upon the order of the parameters e^* and V^* , the coupling terms may be treated as higher order terms and relocated to the right-hand side, where all damping terms and nonlinear terms are placed.

In the case of small e^* , the mass imbalance terms can be removed from the linear mass matrix and relocated to the right-hand side. For example, for a wing with high aspect ratio, the order of e^* could be less than the order of ϵ . If the relative velocity V^* has the order of ϵ , the coupling terms in the stiffness matrix can be placed on the right-hand side. When these two cases are valid, there are no requirements to remove the coupling terms. Simply, by relocating these terms to the right-hand side, we can apply the Method of Multiple Scales. But, in this study, we have a special interest

in the velocity range close to the flutter velocity. Therefore, the coupling term in the stiffness matrix is not relocated. Additionally, because the mass imbalance terms are one of the important factors in aeroelastic systems, the mass matrix having the imbalance terms is also considered. The approximations will be examined in a later section.

B. Analysis by the Method of Multiple Scales

A number of nonlinear beam problems are solved by the Method of Multiple Scales (MMS).^{12,28,42} These beams are not coupled by linear terms, but coupled by nonlinear terms only. Because the lowest order equations consist of the linear parts of the nonlinear equations, the order equations do not have any coupling terms in this study, and the corresponding solutions can be easily identified. Substituting the solutions of the lowest order equations into the first non-homogeneous order equations which include nonlinear terms, we can solve the nonlinear equations and obtain approximate solutions for the nonlinear system.

In aeroelastic systems, linear coupling terms usually exist. They are caused by mass imbalance and aerodynamic forces as shown in Eqs. (4.1), (4.2) and (4.3). Usually, the mass imbalance terms lead to symmetric components in the mass matrix, but the effects of aerodynamic forces may lead to nonsymmetric matrices in stiffness matrix. In order to keep the benefit of MMS, these coupling terms should be properly removed from the lowest order equations. Two processes are considered to uncouple the linear mass and stiffness matrices. After that, the MMS is applied to the uncoupled equations and approximate solutions could be obtained from the first non-homogeneous order equations. The solutions show that there are two possible internal resonances.

1. Uncoupling Process in Aeroelastic Systems

a. Process I

As the first decoupling procedure, the simplest case is considered. The mass imbalance terms are not included in the mass matrix shown in the left-hand side, but relocated to the right-hand side. For this simplified case, the equations consisting of linear mass and stiffness matrices are

$$\begin{bmatrix} C_{uw1} & 0 & 0 \\ 0 & C_{ww1} & 0 \\ 0 & 0 & C_{a\omega 1} \end{bmatrix} \begin{Bmatrix} \ddot{u}_i \\ \ddot{w}_i \\ \ddot{\alpha}_i \end{Bmatrix} + \begin{bmatrix} \beta_z C_{uw2} & 0 & 0 \\ 0 & C_{ww2} & -\mu \frac{C_{L\alpha_k}}{\pi} V^* C_{wa3} \\ 0 & 0 & -\frac{\beta_y}{I_y^*} C_{a\omega 2} - \frac{\mu}{I_y^*} \frac{C_{m\alpha_k}}{\pi} V^{*2} C_{aa3} \end{bmatrix} \begin{Bmatrix} u_i \\ w_i \\ \alpha_i \end{Bmatrix} = 0 \quad (4.13)$$

Although the stiffness matrix, $[K]_L$, is not symmetric, the eigenvalues are still real at the velocity condition less than the flutter velocity. Therefore, linearly independent eigenvectors may be found.

Harmonic motion is assumed of the form

$$\{q\} = \{A_q\} e^{i\omega t}, \quad \text{for } q = u, w, \alpha \quad (4.14)$$

where $\{A_q\}$ is a column of unknown amplitudes and ω is the frequency. Substituting Eq. (4.14) into Eq.(4.13), and letting $\lambda = \omega^2$, we obtain

$$[K - \lambda M] \{q\} = 0$$

or, with substitution

$$\begin{bmatrix} \beta_z C_{uw1} & 0 & 0 \\ 0 & C_{ww2} - \lambda C_{ww1} & -K_{a3}^{23} \\ 0 & 0 & \beta_z / I_y^* C_{aw2} K_{a3}^{33} - \lambda C_{aw1} \end{bmatrix} \begin{Bmatrix} A_u \\ A_w \\ A_\alpha \end{Bmatrix} = \begin{Bmatrix} 0 \\ 0 \\ 0 \end{Bmatrix} \quad (4.15)$$

where

$$\begin{aligned} K_{a3}^{23} &= \mu \frac{C_{L\alpha}}{\pi} V^{*2} \\ K_{a3}^{33} &= \frac{1}{I_y^*} \mu \frac{C_{m\alpha}}{\pi} V^{*2} C_{aa3}. \end{aligned} \quad (4.16)$$

The corresponding characteristic equation is

$$\Delta = (\beta_z C_{uw2} - \lambda C_{uw1}) (C_{ww2} - \lambda C_{ww1}) (\beta_y / I_y^* C_{aw2} - K_{a3}^{33} - \lambda C_{aw1}) = 0 \quad (4.17)$$

and the solutions for λ are

$$\begin{aligned} \lambda_1 &= \beta_z \frac{C_{uw2}}{C_{uw1}} \\ \lambda_2 &= \frac{C_{ww2}}{C_{ww1}} \\ \lambda_3 &= \frac{\beta_y C_{aw2}}{I_y^* C_{aw1}} - \frac{K_{a3}^{33}}{C_{aw1}} \end{aligned} \quad (4.18)$$

The associated eigenvectors $\{A_i\}$, ($i = 1, 2, 3$), are obtained by substituting these eigenvalues into Eq.(4.15). Each mode is scaled by equating the amplitude of one of the components to one. The modal matrix, $[P]$ is defined as follows,

$$[P] = [\{A_1\}\{A_2\}\{A_3\}] = \begin{bmatrix} 1 & 0 & 0 \\ 0 & 1 & \tau \\ 0 & 0 & 1 \end{bmatrix} \quad (4.19)$$

where

$$\tau = -\frac{\beta_z C_{aw2} \pi + \mu C_{ma} V^{*2} C_{aa2}}{\pi * I_y^* C_{aw1}}. \quad (4.20)$$

Because $[K]$ is not symmetric, the modal matrix is not orthogonal. Thus,

$$[P]^{-1} \neq [P]^T$$

This property is verified through the following matrix product,

$$[P][P]^T = \begin{bmatrix} 1 & 0 & 0 \\ 0 & 1 & 1 \\ 0 & 1 & 1 + \tau^2 \end{bmatrix}, \quad [P][P]^{-1} = \begin{bmatrix} 1 & 0 & 0 \\ 0 & 1 & 0 \\ 0 & 0 & 1 \end{bmatrix} = [I] \quad (4.21)$$

Thus, the matrices on the left-hand side are expanded as

$$[P]^{-1}[M_L][P] = \begin{bmatrix} 1 & 0 & 0 \\ 0 & 1 & 0 \\ 0 & 0 & 1 \end{bmatrix} \quad (4.22)$$

$$[P]^{-1}[K_L][P] = \begin{bmatrix} \omega_u^2 & 0 & 0 \\ 0 & \omega_w^2 & 0 \\ 0 & 0 & \omega_\alpha^2 \end{bmatrix} \quad (4.23)$$

These matrices are uncoupled. After applying the coordinate transformation, $\{q\} = [P]\{\eta\}$, the equations of motion are pre-multiplied by $[P]^{-1}$, and lead to uncoupled equations of motion.

b. Process II

In the second process, the mass imbalance terms exist on the left-hand side. In this case, the mass and stiffness matrices are shown in Eq.(4.4). Assuming harmonic

motion of the form

$$\{q\} = \{A_q\}e^{i\omega t}$$

and substituting this expression into the following linear expression,

$$[M_L]\{q\}'' + [K_L]\{q\} = 0 \quad (4.24)$$

where $[M_L]$ and $[K_L]$ are defined in Eq.(4.4), leads to the following characteristic equation,

$$(\beta_z C_{uw2} - \lambda C_{uw1}) (A\lambda^2 + B\lambda + C) = 0. \quad (4.25)$$

In the above equation, the coefficients are defined as

$$\begin{aligned} A &= C_{ww1}C_{aw1} - \frac{e^*}{I_y^*}C_{ae1}e^*C_{we1} \\ B &= -C_{ww2}C_{aw1} - C_{ww1} \left(\frac{\beta_y}{I_y^*}C_{aw2} - K_{a3}^{33} \right) + \frac{e^*}{I_y^*}C_{ae1}K_{aw3}^{23} \\ C &= C_{ww2} \frac{\beta_y}{I_y^*}C_{aw2} \end{aligned} \quad (4.26)$$

From the characteristic equation, Eq.(4.25), the obtained eigenvalues are

$$\begin{aligned} \lambda_1 &= \beta_z \frac{C_{uw2}}{C_{uw1}} \\ \lambda_{2,3} &= \frac{-B \pm \sqrt{B^2 - 4AC}}{2A} \end{aligned} \quad (4.27)$$

and the corresponding eigenvectors are

$$[P] = \begin{bmatrix} 1 & 0 & 0 \\ 0 & \tau_1 + \tau_2 & \tau_1 - \tau_2 \\ 0 & 1 & 1 \end{bmatrix} \quad (4.28)$$

where $\tau_1 = -B/2A$, $\tau_2 = \sqrt{B^2 - 4AC}/2A$. This modal matrix is not orthogonal because $[K]$ is not symmetric. From the following matrix product,

$$[P][P]^{-1} = \begin{bmatrix} 1 & 0 & 0 \\ 0 & 1 & 0 \\ 0 & 0 & 1 \end{bmatrix} = [I] \quad (4.29)$$

$$[P][P]^T = \begin{bmatrix} 1 & 0 & 0 \\ 0 & 1 + (\tau_1 + \tau_2)^2 & 1 + (\tau_1 + \tau_2) * (\tau_1 - \tau_2) \\ 0 & 1 + (\tau_1 + \tau_2) * (\tau_1 - \tau_2) & 1 + (\tau_1 - \tau_2)^2 \end{bmatrix} \quad (4.30)$$

the property $[P]^{-1} \neq [P]^T$ could be verified.

2. Approximation

Although two processes are used to uncouple the linear mass and stiffness matrices, the first process is adopted because it is less complex. When the linear terms are decoupled, the corresponding solutions of the expressions having the lowest order can be simplified. Because the mass imbalance terms are higher order terms, they are placed in right-hand side, where nonlinear and damping terms appear. If they remain on the left-hand side, the decoupling process should be changed.

The modal matrix $[P]$ as shown in Eq. (4.19) is used to uncouple the nonlinear equations and the coordinate is related by the following transformation,

$$\begin{Bmatrix} u \\ w \\ \alpha \end{Bmatrix} = \begin{bmatrix} 1 & 0 & 0 \\ 0 & 1 & 1 \\ 0 & 0 & \tau \end{bmatrix} \begin{Bmatrix} \eta_a \\ \eta_b \\ \eta_c \end{Bmatrix}$$

or,

$$\{q\} = [P]\{\eta\} \quad (4.31)$$

After applying this transformation, the nonlinear equations are pre-multiplied by $[P]^{-1}$. In this process, the matrices on the left-hand side are diagonalized as shown in Eqs. (4.22) and (4.23). The matrices on the right-hand side are defined as follows,

$$[P]^{-1}[M_e][P] = \begin{bmatrix} 0 & 0 & 0 \\ 0 & \bar{M}_e^{22} & \bar{M}_e^{23} \\ 0 & \bar{M}_e^{32} & 0 \end{bmatrix} = \begin{bmatrix} 0 & 0 & 0 \\ 0 & \frac{1}{\tau I_y^*} e^* C_{ae1} & -e^* C_{we1} \tau \\ 0 & -\frac{1}{\tau I_y^*} e^* C_{ae1} & 0 \end{bmatrix} \quad (4.32)$$

$$\begin{aligned} [P]^{-1}[C][P] &= \begin{bmatrix} 0 & 0 & 0 \\ 0 & \bar{C}^{22} & \bar{C}^{23} \\ 0 & \bar{C}^{32} & \bar{C}^{33} \end{bmatrix} \\ &= \begin{bmatrix} 0 & 0 & 0 \\ 0 & C^{22} - \frac{1}{\tau} C^{32} & (C^{22} + \tau * C^{23}) - \frac{1}{\tau} (C^{32} + \tau C^{33}) \\ 0 & \frac{1}{\tau} C^{32} & \frac{1}{\tau} (C^{32} + \tau C^{33}) \end{bmatrix} \end{aligned} \quad (4.33)$$

$$[P]^{-1}\{NL_\eta\} = \left\{ \begin{array}{l} C_{NLu} \tau (\eta_b \eta_c + \eta_c^2) \\ C_{NLw} \tau \eta_a \eta_c - \frac{1}{\tau} C_{NLa} (\eta_a \eta_b + \eta_a \eta_c) \\ \frac{1}{\tau} C_{NLa} (\eta_a \eta_b + \eta_a \eta_c) \end{array} \right\} \quad (4.34)$$

The full uncoupled equations are written in matrix form as

$$[I] \{\ddot{\eta}\} + [\Lambda] \{\eta\} = - [\bar{M}e] \{\ddot{\eta}\} - [\bar{C}] \{\dot{\eta}\} - \{NL(\eta)\} \quad (4.35)$$

Here, $[I]$ is a unit matrix and $[\Lambda]$ is a diagonal matrix with aeroelastic frequencies.

In these matrices, the following notations are introduced to simplify the expressions.

$$C_{NLu} = \beta_z C_{uw3} + (\beta_z - 1) C_{uw6} \quad (4.36)$$

$$C_{NLw} = -\beta_z C_{ww3} + (\beta_z - 1) C_{ww6} \quad (4.37)$$

$$C_{NL\alpha} = \frac{1}{I_y^*}(\beta_z - 1)C_{aw5} \quad (4.38)$$

We seek an approximate solution of the above transformed nonlinear equations of the form

$$\begin{aligned} \eta(T_0, T_1; \epsilon) &= \eta_0(T_0, T_1) + \epsilon\eta_1(T_0, T_1) + \dots \\ \dot{\eta}(T_0, T_1; \epsilon) &= D_0\eta_{x0} + \epsilon(D_0\eta_{x1} + D_1\eta_{x0}) + \dots \\ \ddot{\eta}(T_0, T_1; \epsilon) &= D_0^2\eta_{x0} + 2\epsilon D_0D_1\eta_{x0} + \epsilon D_0^2\eta_{x1} + \dots \end{aligned} \quad (4.39)$$

In this expression, T_0 is a fast time scale characterizing motions with the aeroelastic frequencies and $T_1 = \epsilon t$ is a slow scale characterizing the modulations of the amplitudes and phases. The envelop of the actual response could be identified through the slow time scale. The derivatives with respect to time t can be rewritten in terms of partial derivatives with respect to the new scales T_0 and T_1 .

In order to facilitate the analysis, the linear mass imbalance terms and damping terms are perturbed by ϵ to the nonlinear portion of the equations as follows,

$$[I] \{\ddot{\eta}\} + [\Lambda] \{\eta\} = -\epsilon [\bar{M}e] \{\ddot{\eta}\} - \epsilon [\bar{C}] \{\dot{\eta}\} - \epsilon \{NL(\eta)\} \quad (4.40)$$

Substituting Eq.(4.39) into Eq.(4.40), and equating coefficients of like powers of ϵ , gives the following sets of equations:

Order(ϵ^0),

$$\begin{aligned} D_0^2\eta_{a0} + \omega_1^2\eta_{a0} &= 0 \\ D_0^2\eta_{b0} + \omega_2^2\eta_{b0} &= 0 \\ D_0^2\eta_{c0} + \omega_3^2\eta_{c0} &= 0 \end{aligned} \quad (4.41)$$

Order(ϵ^2),

$$\begin{aligned}
D_0^2 \eta_{a1} + \omega_1^2 \eta_{a1} &= -2D_0 D_1 \eta_{a0} + C_{NLu} \tau (\eta_{b0} \eta_{c0} + \eta_{c0}^2) \\
D_0^2 \eta_{b1} + \omega_1^2 \eta_{b1} &= -2D_0 D_1 \eta_{b0} - \overline{M} e^{22} D_0^2 \eta_{b0} - \overline{M} e^{23} D_0^2 \eta_{c0} \\
&\quad - \overline{C} e^{22} D_0 \eta_{b0} - \overline{C} e^{23} D_0 \eta_{c0} + C_{NLw} \tau \eta_{a0} \eta_{c0} \\
&\quad - \frac{1}{\tau} C_{NLa} \tau (\eta_{a0} \eta_{b0} + \eta_{a0} \eta_{c0}) \\
D_0^2 \eta_{c1} + \omega_1^2 \eta_{c1} &= -2D_0 D_1 \eta_{c0} - \overline{M} e^{32} D_0^2 \eta_{b0} \\
&\quad - \overline{C} e^{32} D_0 \eta_{b0} - \overline{C} e^{33} D_0 \eta_{c0} + \frac{1}{\tau} C_{NLa} (\eta_{a0} \eta_{b0} + \eta_{a0} \eta_{c0}) \quad (4.42)
\end{aligned}$$

The solutions of Eq. (4.41) can be expressed as follows.

$$\eta_{x0} = A_k(T_1) e^{i\omega_k T_0} + \overline{A}_k(T_1) e^{-i\omega_k T_0} \quad (4.43)$$

Substituting these solutions into Eq. (4.42), we obtain the following results,

$$\begin{aligned}
D_0^2 \eta_{a1} + \omega_1^2 \eta_{a1} &= -2i\omega_1 A_1' e^{i\omega_1 T_0} \\
&\quad + C_{NLu} \tau (A_2 A_3 e^{i(\omega_2 + \omega_3) T_0} + A_2 \overline{A}_3 e^{i(\omega_2 - \omega_3) T_0} + A_3^2 e^{i2\omega_3 T_0} + A_3 \overline{A}_3) \\
&\quad + cc \\
D_0^2 \eta_{b1} + \omega_1^2 \eta_{b1} &= -2i\omega_2 A_2' e^{i\omega_2 T_0} \\
&\quad - \overline{M} e^{22} (-\omega_2^2) A_2 e^{i\omega_2 T_0} - \overline{M} e^{23} (-\omega_3^2) A_3 e^{i\omega_3 T_0} \\
&\quad - \overline{C} e^{22} (i\omega_2) A_2 e^{i\omega_2 T_0} - \overline{C} e^{23} (i\omega_3) A_3 e^{i\omega_3 T_0} \\
&\quad + C_{NLw} \tau A_2 A_3 e^{i(\omega_2 + \omega_3) T_0} + A_2 \overline{A}_3 e^{i(\omega_2 - \omega_3) T_0} \\
&\quad - \frac{1}{\tau} C_{NLa} (A_1 A_2 e^{i(\omega_1 + \omega_2) T_0} + A_1 \overline{A}_2 e^{i(\omega_1 - \omega_2) T_0} + A_1 A_3 e^{i(\omega_1 + \omega_3) T_0} \\
&\quad + A_1 \overline{A}_3 e^{i(\omega_1 - \omega_3) T_0}) \\
D_0^2 \eta_{c1} + \omega_1^2 \eta_{c1} &= -2i\omega_3 A_3' e^{i\omega_3 T_0} \\
&\quad - \overline{M} e^{32} (-\omega_3^2) A_3 e^{i\omega_3 T_0}
\end{aligned}$$

$$\begin{aligned}
& -\bar{C}^{32}(i\omega_2)A_2e^{i\omega_2T_0} - \bar{C}^{33}(i\omega_3)A_3e^{i\omega_3T_0} \\
& + \frac{1}{\tau}C_{NLa} (A_1A_2e^{i(\omega_1+\omega_2)T_0} + A_1\bar{A}_2e^{i(\omega_1-\omega_2)T_0} + A_1A_3e^{i(\omega_1+\omega_3)T_0} \\
& + A_1\bar{A}_3e^{i(\omega_1-\omega_3)T_0})
\end{aligned} \tag{4.44}$$

where cc represents the complex conjugate, and the prime implies differentiation with respect to T_1 . For constant A_k , ($k = 1, 2, 3$), the particular solutions of Eq. (4.44) are expressed as follows,

$$\begin{aligned}
\eta_{ap} &= \frac{C_{NLu}A_2A_3}{[\omega_1 + (\omega_2 + \omega_3)T_0][\omega_1 - (\omega_2 + \omega_3)T_0]}e^{i(\omega_2+\omega_3)T_0} + \dots + \frac{C_{NLu}A_3^2}{\omega_1 - 2\omega_3}e^{2i\omega_3T_0} \\
\eta_{bp} &= -\frac{C_{NLa}A_1A_3}{\tau[\omega_2 - (\omega_1 - \omega_3)][\omega_2 - (\omega_1 - \omega_3)]}e^{i(\omega_1-\omega_3)T_0} + \dots \\
\eta_{cp} &= \frac{C_{NLa}A_1\bar{A}_2}{\tau[\omega_3 - (\omega_1 - \omega_2)][\omega_3 - (\omega_1 - \omega_2)]}e^{i(\omega_1-\omega_2)T_0} + \dots \frac{C_{NLa}A_1\bar{A}_3}{\tau(2\omega_3 - \omega_1)}e^{i(\omega_1-\omega_3)T_0}
\end{aligned} \tag{4.45}$$

where, '...', represents many other terms which do not cause any resonance phenomenon. Note, when $\omega_1 = 2\omega_3$, the denominator of the last term of η_{ap} and η_{cp} is zero. Also, the denominator of the first term shown in each particular solution is zero when $\omega_1 \simeq \omega_2 + \omega_3$. Therefore, the following two resonance conditions, at which the denominator will be zero or close to zero, are identified.

$$\omega_1 : \omega_3 \simeq 2 : 1 \tag{4.46}$$

$$\omega_1 \simeq \omega_2 + \omega_3 \tag{4.47}$$

At this point, it should be noted that these internal resonance conditions are caused by the aerodynamic coupling terms in the stiffness matrix. Although the details of the process does not appear in this dissertation, the same internal resonance conditions are predicted by applying Process II.

a. IR condition 1 $\omega_1 = 2\omega_3$

The first internal resonance may occur when $\omega_1 : \omega_3 \simeq 2 : 1$. Introducing the detuning parameter σ , and substituting it into the Eq. (4.44), we can investigate the characteristics of responses at the 2:1 internal resonance condition. The detuning parameter for this case is defined by

$$\omega_1 = 2\omega_3 + \epsilon\sigma \quad (4.48)$$

By inserting this expression into Eq. (4.44), we obtain additional secular terms (or resonance terms). Because the terms $e^{(i\omega_1 T_0)}$, $e^{(i\omega_2 T_0)}$, and $e^{(i\omega_3 T_0)}$ produce secular terms in the first, second, and third equation in Eq. (4.44), respectively, the following terms are also secular terms.

$$e^{2\omega_3 T_0} = e^{(\omega_1 - \epsilon\sigma)T_0} = e^{\omega_1 T_0} e^{-\sigma T_1} \quad (4.49)$$

$$e^{(\omega_1 - \omega_3)T_0} = e^{(2\omega_3 + \epsilon\sigma - \omega_3)T_0} = e^{(\omega_3 + \epsilon\sigma)T_0} = e^{\omega_3 T_0} e^{\sigma T_1} \quad (4.50)$$

Substituting Eq.(4.49) into Eq.(4.44), and eliminating the terms producing secular terms, the following solvability conditions are obtained.

$$-2i\omega_1 A_1' + C_{nlu}\tau A_3^2 e^{-i\sigma T_1} = 0 \quad (4.51)$$

$$-2i\omega_2 A_2' + \overline{M}e^{-22}\omega_2^2 A_2 - \overline{C}^{22}i\omega_2 A_2 = 0 \quad (4.52)$$

$$-2i\omega_3 A_3' - \overline{C}^{33}i\omega_3 A_3 + \frac{1}{\tau}C_{nla}A_1 \bar{A}_3 e^{i\sigma T_1} = 0 \quad (4.53)$$

In order to express the terms $A_k(T_1)$, it is convenient to introduce the following polar notation,

$$A_k(T_1) = \frac{1}{2}a_k e^{i\phi}$$

for $k = 1, 2, 3$ where a_k and ϕ are real functions of T_1 . Substituting the polar form into the solvability conditions, and separating the real and imaginary parts, we obtain

$$\begin{aligned}\omega_1 a_1 \phi'_1 + \frac{1}{4} C_{nlu} \tau a_3^2 \cos(\gamma) &= 0 \\ -\omega_1 a'_1 + \frac{1}{4} C_{nlu} \tau a_3^2 \sin(\gamma) &= 0\end{aligned}\quad (4.54)$$

$$\begin{aligned}\omega_2 a_2 \phi'_2 + \frac{1}{2} \overline{M} e^{-22} \omega_2^2 &= 0 \\ -\omega_2 a'_2 - \frac{1}{2} \overline{C}^2 2\omega_2 a_2 &= 0\end{aligned}\quad (4.55)$$

$$\begin{aligned}\omega_3 a_3 \phi'_3 + \frac{1}{4\tau} C_{nla} a_1 a_3 \cos(\gamma) &= 0 \\ -\omega_3 a'_3 - \frac{1}{2} \overline{C}^3 3\omega_3 a_3 + \frac{1}{4\tau} C_{nla} a_1 a_3 \sin(\gamma) &= 0\end{aligned}\quad (4.56)$$

where $\gamma = 2\phi_3 - \phi_1 - \sigma T_1$, and γ is considered a pseudo-phase angle. Eliminating ϕ_1 and ϕ_3 from Eqs.(4.54) and (4.56), we obtain

$$\gamma' = -\frac{1}{2\tau\omega_3 a_3} C_{nla} a_1 a_3 \cos(\gamma) + \frac{1}{4\omega_1 a_1} C_{nlu} \tau a_3^2 \cos(\gamma) - \sigma \quad (4.57)$$

Integrating these equations over the slow time scale, T_1 , we can investigate the response characteristics of a system with the frequency ratio $\omega_1 \simeq 2\omega_3$.

The equilibrium points of the system correspond to steady oscillation (i.e. constant solutions), and can be obtained by setting the prime terms in Eqs.(4.54)-(4.57) to zero, that is $a'_1 = a'_2 = a'_3 = \phi'_2 = \gamma' = 0$. Thus,

$$\omega_1 a'_1 = 0 = \frac{1}{4} C_{nlu} \tau a_3^2 \sin(\gamma) \quad (4.58)$$

$$\omega_2 a'_2 = 0 = -\frac{1}{2} \overline{C}^{22} \omega_2 a_2 \quad (4.59)$$

$$\omega_3 a_3' = 0 = -\frac{1}{2}\bar{C}^{33}\omega_3 a_3 + \frac{1}{4\tau}C_{nla}a_1 a_3 \sin(\gamma) \quad (4.60)$$

$$-\omega_2 a_2 \phi_2' = 0 = \frac{1}{2}\bar{M}e^{22}\omega_2^2 a_2 \quad (4.61)$$

$$\gamma' = 0 = -\frac{1}{2\tau\omega_3 a_3}C_{nla}a_1 a_3 \cos(\gamma) + \frac{1}{4\omega_1 a_1}C_{nlu}\tau a_3^2 \cos(\gamma) - \sigma \quad (4.62)$$

In the above expressions, the \bar{C}^{ij} terms have positive or negative values depending upon the velocity condition. From Eq. (4.59), the following expression is obtained.

$$a_2(T_1) = e^{-\bar{C}_{22}/2T_1}$$

If \bar{C}_{22} is negative, then a_2 will go to infinity. This condition corresponds to the flutter condition. Otherwise, it goes to zero. For positive coefficients ($-\bar{C}_{22} > 0$), Eqs. (4.59) and (4.61) show that a_2 should be zero. If the velocity will not exceed the flutter condition, then the responses will be damped according to the linear theory.

The γ terms are eliminated from Eqs. (4.58) and (4.60) by multiplying $\frac{1}{4\tau}C_{nla}a_1$ and $\frac{1}{4}C_{nlu}\tau a_3$, respectively, and subtracting sin term from the resulting expressions. Thus,

$$\begin{aligned} & \left[\frac{1}{4}C_{nlu}\tau a_3^2 \sin(\gamma) \right] \frac{1}{4\tau}C_{nla}a_1 - \left[-\frac{1}{2}\bar{C}^{33}\omega_3 a_3 + \frac{1}{4\tau}C_{nla}a_1 a_3 \sin(\gamma) \right] \frac{1}{4}C_{nlu}\tau a_3 \\ & = -\frac{1}{2}\bar{C}^{33}\omega_3 a_3 \frac{1}{4}C_{nlu}\tau a_3 = 0 \end{aligned} \quad (4.63)$$

This expression shows that a_3 should be zero. When $a_3 = 0$ is applied to other expressions such as Eqs. (4.59), and (4.62), they are automatically satisfied. This solution represents a trivial solution and corresponds to the solution of the linear system.

According to Nayfeh,³¹ when there is an internal resonance and the coefficients of a_1 and a_3 have opposite signs, the equations provide self-sustained oscillations in spite

of the presence of damping. For the considered aeroelastic systems, the aerodynamic damping terms \bar{C}^{ij} have positive values and the corresponding nonlinear coefficients, such as C_{nlx} , $x = u, w, \alpha$, are positive. Therefore, self-sustained oscillations will not occur. For non-zero a_3 , it can be seen from Eq.(4.58) that $\sin\gamma$ should be zero (or $\gamma = n\pi$, $n = 0, 1, 2, \dots$). Applying this γ condition into Eq.(4.62), we obtain

$$-\frac{1}{2\tau\omega_3}C_{nla}a_1^2 \cos(\gamma) + \frac{1}{4\omega_1}C_{nlu}\tau a_3^2 \cos(\gamma) - \sigma a_1 = 0. \quad (4.64)$$

or

$$-\frac{1}{2\tau\omega_3}C_{nla}a_1^2 + \frac{1}{4\omega_1}C_{nlu}\tau a_3^2 - \sigma a_1 = 0. \quad (4.65)$$

This result shows that self-sustained oscillations may be possible. But one is reminded that the above condition, $\gamma = n\pi$, can be satisfied by Eq. (4.59). On the other hand, to cause self-sustained oscillation, the term \bar{C}^{33} should be zero.

b. IR condition 2: $\omega_1 = \omega_2 + \omega_3$.

Another internal resonance condition is $\omega_1 \simeq \omega_2 + \omega_3$. Let

$$\omega_1 = \omega_2 + \omega_3 + \epsilon\sigma$$

Using this expression, the following terms are rewritten as follows,

$$A_2 A_3 e^{i(\omega_2 + \omega_3)T_0} = A_2 A_3 e^{i(\omega_1 - \epsilon\sigma)T_0} = A_2 A_3 e^{i\omega_1 T_0} e^{-\sigma T_1} \quad (4.66)$$

$$A_1 \bar{A}_3 e^{i(\omega_1 - \omega_3)T_0} = A_1 \bar{A}_3 e^{i(\omega_2 + \epsilon\sigma)T_0} = A_1 \bar{A}_3 e^{i\omega_2 T_0} e^{\sigma T_1} \quad (4.67)$$

$$A_1 \bar{A}_2 e^{i(\omega_1 - \omega_2)T_0} = A_1 \bar{A}_2 e^{i(\omega_3 - \epsilon\sigma)T_0} = A_1 \bar{A}_2 e^{i\omega_3 T_0} e^{-\sigma T_1} \quad (4.68)$$

Substituting these solutions into Eq. (4.42), we obtain the following results,

$$D_0^2 \eta_{a1} + \omega_1^2 \eta_{a1} = -2i\omega_1 A_1' e^{i\omega_1 T_0} + C_{NLU}\tau A_2 A_3 e^{i\omega_1 T_0} e^{-\sigma T_1} + cc$$

$$+NST \quad (4.69)$$

$$\begin{aligned} D_0^2 \eta_{b1} + \omega_1^2 \eta_{b1} &= \left(-2i\omega_2 A_2' + \overline{M} e^{22} (\omega_2^2) A_2 - \overline{C}^{22} (i\omega_2) A_2 \right) e^{i\omega_2 T_0} \\ &\quad - \frac{1}{\tau} C_{NL a} (A_1 \bar{A}_3 e^{i\omega_2 T_0} e^{\sigma T_1} + cc + NST) \end{aligned} \quad (4.70)$$

$$\begin{aligned} D_0^2 \eta_{c1} + \omega_1^2 \eta_{c1} &= \left(-2i\omega_3 A_3' - \overline{C}^{33} (i\omega_3) A_3 \right) e^{i\omega_3 T_0} \\ &\quad + \frac{1}{\tau} C_{NL a} (A_1 \bar{A}_2 e^{i\omega_3 T_0} e^{-\sigma T_1}) + cc + NST \end{aligned} \quad (4.71)$$

where cc and NST represent the complex conjugate and the non-secular terms, respectively, and the prime implies differentiation with respect to T_1 . Let

$$A_k = \frac{1}{2} a_k e^{i\phi_k}$$

Substituting this expression into the secular terms shown in Eqs. (4.69), (4.70), and (4.71), and separating real and imaginary parts, we obtain the following equations.

$$a_1' \omega_1 = -\frac{1}{2} a_1 \bar{C}^{11} \omega_1 + \frac{1}{4} C_{NL u} \tau a_2 a_3 \sin \gamma \quad (4.72)$$

$$a_2' \omega_2 = -\frac{1}{2} a_2 \bar{C}^{22} \omega_2 + \frac{1}{4} C_{NL a} \tau a_1 a_3 \sin \gamma \quad (4.73)$$

$$a_3' \omega_3 = -\frac{1}{2} a_3 \bar{C}^{33} \omega_3 - \frac{1}{4} C_{NL a} \tau a_1 a_2 \sin \gamma \quad (4.74)$$

and

$$\begin{aligned} \gamma' &= - \left[-\frac{1}{4a_1 \omega_1} C_{NL u} \tau a_2 a_3 \cos \gamma \right] \\ &\quad + \left[-\frac{1}{2a_2 \omega_2} a_2 \overline{M} e^{22} \omega_2^2 + \frac{1}{4a_2 \omega_2 \tau} C_{NL a} a_1 a_3 \cos \gamma \right] \\ &\quad + \left[-\frac{1}{4a_3 \omega_3 \tau} C_{NL a} a_1 a_2 \cos \gamma \right] - \sigma \end{aligned} \quad (4.75)$$

In Eq. (4.72), the term \bar{C}^{11} represents the damping coefficient and it is assumed that \bar{C}^{11} is zero. But, \bar{C}^{11} is included in Eq.(4.72) because the structural damping for any

real system is not zero, and the aerodynamic damping may exist if aerodynamic loads are included in the in-plane motion.

The steady-state solution satisfies

$$a'_1 = a'_2 = a'_3 = \gamma' = 0. \quad (4.76)$$

Thus, the corresponding responses are described by the following expressions:

$$a'_1\omega_1 = 0 = -\frac{1}{2}a_1\bar{C}^{11}\omega_1 + \frac{1}{4}C_{NLu}\tau a_2 a_3 \sin \gamma \quad (4.77)$$

$$a'_2\omega_2 = 0 = -\frac{1}{2}a_2\bar{C}^{22}\omega_2 + \frac{1}{4}C_{NLa}\tau a_1 a_3 \sin \gamma \quad (4.78)$$

$$a'_3\omega_3 = 0 = -\frac{1}{2}a_3\bar{C}^{33}\omega_3 - \frac{1}{4}C_{NLa}\tau a_1 a_2 \sin \gamma \quad (4.79)$$

and

$$\begin{aligned} \gamma' = 0 = & - \left[-\frac{1}{4a_1\omega_1}C_{NLu}\tau a_2 a_3 \cos \gamma \right] \\ & + \left[-\frac{1}{2a_2\omega_2}a_2\overline{Me}^{22}\omega_2^2 + \frac{1}{4a_2\omega_2\tau}C_{NLa}a_1 a_3 \cos \gamma \right] \\ & + \left[-\frac{1}{4a_3\omega_3\tau}C_{NLa}a_1 a_2 \cos \gamma \right] - \sigma \end{aligned} \quad (4.80)$$

Multiplying Eqs.(4.73) and (4.74) by $\frac{1}{4}C_{NLa}\tau a_1 a_2$ and $\frac{1}{4}C_{NLa}\tau a_1 a_3$, respectively, and adding the results gives the following expression

$$\begin{aligned} & -\frac{1}{2}a_2\bar{C}^{22}\omega_2\frac{1}{4}C_{NLa}\tau a_1 a_2 - \frac{1}{2}a_3\bar{C}^{33}\omega_3\frac{1}{4}C_{NLa}\tau a_1 a_3 \\ & = -a_1\tau\frac{1}{8}\bar{C}^{22}\omega_2 C_{NLa} \left\{ a_2^2 + \frac{\bar{C}^{33}\omega_3}{\bar{C}^{22}\omega_2}C_{NLa}a_3^2 \right\} = 0. \end{aligned} \quad (4.81)$$

This expression shows that if \bar{C}^{22} and \bar{C}^{33} have opposite signs, a_2 and a_3 may have non-zero values. For any velocity condition greater than the flutter condition, this situation is possible. But, for a velocity less than the flutter velocity, a_2 and a_3 must be zero.

C. Benchmark Wing Models

In order to study internal resonance, benchmark wing models with representative physical properties are considered. As shown in Tables I and II, two possible wing models are presented. The system parameters for the first wing model shown in Table I are based on the NATA model⁴⁶ with modification, thus, it is named ‘NATAm’. The second wing model is the Heavy Goland Wing (HGW). The system parameters are shown in II. This wing is developed for a transonic flutter analysis.⁴⁷ Beran^{48,49} added a tip store and studied store-induced limit cycle oscillations.

Future air vehicles such as Uninhabited Air Vehicles (UAVs) may have high aspect ratio wings. The increased wing span will affect the natural frequencies of the system. For a uniform cantilever beam, the uncoupled bending and torsion frequencies are defined as

$$\omega_u = \left(\frac{\beta}{L}\right)^2 \sqrt{\frac{D_z}{m}} = \left(\frac{\beta}{L}\right)^2 \sqrt{\frac{EIz}{m}} \quad (4.82)$$

$$\omega_w = \left(\frac{\beta}{L}\right)^2 \sqrt{\frac{D_x}{m}} = \left(\frac{\beta}{L}\right)^2 \sqrt{\frac{EIx}{m}} \quad (4.83)$$

$$\omega_\alpha = \left(\frac{\lambda}{L}\right) \sqrt{\frac{D_y}{I_y}} = \left(\frac{\lambda}{L}\right) \sqrt{\frac{GJ}{I_y}} \quad (4.84)$$

where u , w , and α represent in-plane bending, out-of-plane bending, and torsional responses, respectively. β and λ are defined in Chapter II. As shown in these expressions, the effect of the wing span (L) on the bending and torsion motion is different from each other. Therefore, it is expected that the bending and the torsional frequencies may intersect as the wing span is increased.

Table I. System Properties for the NATAm

Property	Value	Remark
<i>Wing</i>		
Span (L)	1.2 m	Reference Length
Chord (c)	0.27 m	
mass per unit length (m)	1.973 kg/m	
mass moment of inertia (I_y)	0.0527 kg m	$I_o + m(CG - ea)^2$
bending rigidity (EI)	476.9 N m ²	D_x
torsional rigidity (GJ)	3.988 N m ²	D_y
<i>Store</i>		
mass (Ms)	0.394 kg	
moment of inertia ($I_{s,y}$)	0.0056 kg m ²	
moment of inertia ($I_{s,x}$)	5.265×10^{-5} kg m ²	

Table II. System Properties for the HGW

Property	Value	Remark
<i>Wing</i>		
Span (L)	20 ft	Reference Length
Chord	6 ft	
ea & c.g.	2 ft & 2.6 ft	
mass per unit length (m)	11.249 slugs/ft	
first mass moment of inertia (S)	6.7494 slugs ft/ft	$m(ea - cg)$
mass moment of inertia (I_y)	29.2196	$I_o + m(cg - ea)^2$
bending rigidity (EI)	23.647×10^6 lb ft ²	D_x
torsional rigidity (GJ)	2.3988×10^6 lb ft ²	D_y
<i>Store</i>		
mass, Ms	22.496 slugs	
moment of inertia ($I_{s,y}$)	50.3396 slug-ft ²	
moment of inertia ($I_{s,x}$)	0.0	Assumed

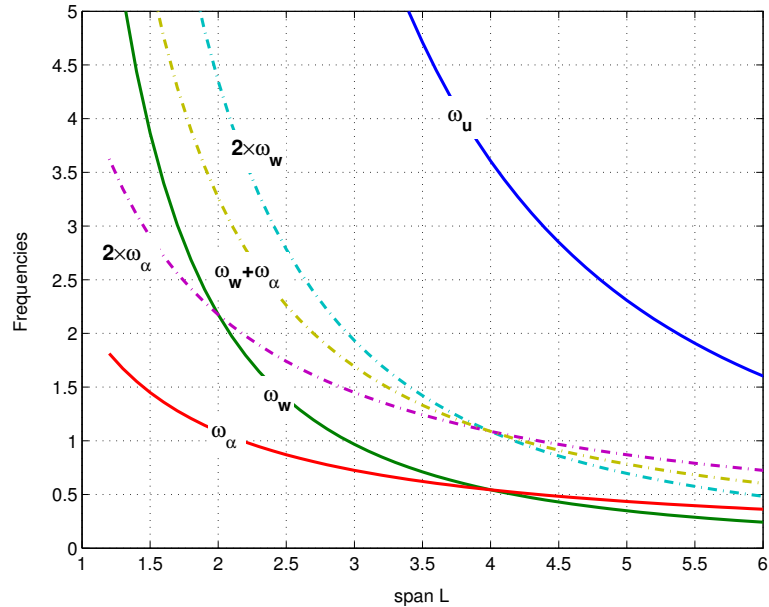


Fig. 23. Frequencies vs. wing span(L) for the NATAm wing model

1. The Effects of Wing Span

For the NATAm wing, the effect of the wing span is depicted in Fig. 23. In this figure, the stiffness ratio $\beta_z = D_z/D_x$ is 44. This ratio is adopted from Tang and Dowell's model.¹⁹ The stiffness ratios are not shown in the papers dealing with the NATA model and the HGW model,^{13,46,48} because the in-plane bending motion is not included in these papers. Because Tang et al. adopted the NACA 0012 airfoil, and they made an experimental wing. The wing includes a precision ground flat steel spar, 2×33 flanges which are distributed along the wingspan and centerline of the spar, and 18 pieces of NACA 0012 airfoil plate uniformly distributed along the spar. The presented stiffness ratio could be a realistic value. The stiffness ratio $\beta_z = 44$, could be reasonable for the NATAm wing which also has the NACA 0012 airfoil.

In Fig. 23, the natural frequencies are depicted by solid lines, and the multiplied

Table III. Natural Frequencies for the HGW

Mode	Beran ⁴⁸	Present	Remark
1	1.97 Hz	1.974 Hz	1 st Bending
2	4.05 Hz	3.932 Hz	1 st Torsion
3	9.65 Hz	-	
4	13.4 Hz	-	

and/or combined frequencies are represented by dashed lines. In order to obtain internal resonance (IR) models, we must determine the points satisfying the frequency condition for IR. As shown in the figure, the frequency ω_u does not interact with any other curve. The anticipated IR conditions could not be found in Fig. 23.

Another possible IR model is studied with the HGW model. The HGW is designed for the transonic flutter analysis. Using the quasi-steady aerodynamics adopted in this dissertation, the responses at transonic region cannot be properly predicted. But, for a relatively low velocity region (low subsonic), it was shown by Beran⁴⁹ that the quasi-steady aerodynamics could produce reasonable results. Therefore, the HGW could be considered as an IR model in the relatively low velocity area.

Using the data shown in Table II, the natural frequencies are obtained. These frequencies are shown in Table III and Table IV. When the wing span is changed, the frequency ratio is changed. As shown in Table III and IV, the first torsional frequency is twice that of the first bending frequency. Because two cases of internal resonances, $\omega_u \simeq 2 \times \omega_\alpha$ and $\omega_u \simeq \omega_w + \omega_\alpha$, are identified by the Method of Multiple Scales, the corresponding conditions should be identified.

Table IV. Natural Frequencies for the HGW with a Store

Mode	Beran ⁴⁸	Present	Remark
1	1.69 Hz	1.714 Hz	1 st Bending
2	3.05 Hz	3.031 Hz	1 st Torsion
3	9.17 Hz	-	
4	10.8 Hz	-	

Table V. Uncoupled Bending and Torsion Frequencies for the Selected Three Cases

L	ω_u	ω_w	ω_α	Remark
20	13.4544 Hz	2.0283 Hz	3.5748 Hz	No resonance
36	4.1525 Hz	3.9334 Hz	1.9860 Hz	$\omega_u \approx 2 \times \omega_\alpha$
60	1.4948 Hz	0.2253 Hz	1.1916 Hz	$\omega_u \approx \omega_w + \omega_\alpha$

For a case of $\beta_z = D_z/D_x = 44$, the effect of the wing span is depicted in Fig. 24. In this figure, the natural frequencies are expressed as solid lines, and the frequencies $2\omega_w$, $2\omega_\alpha$, and $\omega_w + \omega_\alpha$, are denoted by dash-dots. These lines intersect at three points of interest. These three cases are examined. It can be seen from Fig. 24 that three cases are selected such as $L \approx 20\text{ft}$, $L \approx 36\text{ft}$, and $L \approx 60\text{ft}$. The first case ($L = 20\text{ft}$) is a non-resonance case. Internal resonances will be investigated in the other two cases ($L = 36\text{ft}$, and $L = 60\text{ft}$). Uncoupled bending and torsion frequencies for these three cases are summarized in Table. V. As shown in Table V, the frequencies do not satisfy exactly the internal resonance conditions. In aeroelastic systems, the aeroelastic frequencies depend upon the velocity. Because aeroelastic frequencies may decrease as the velocity increases, the frequency differences, $\omega_u - 2 \times \omega_\alpha$ and $\omega_u - (\omega_w + \omega_\alpha)$,

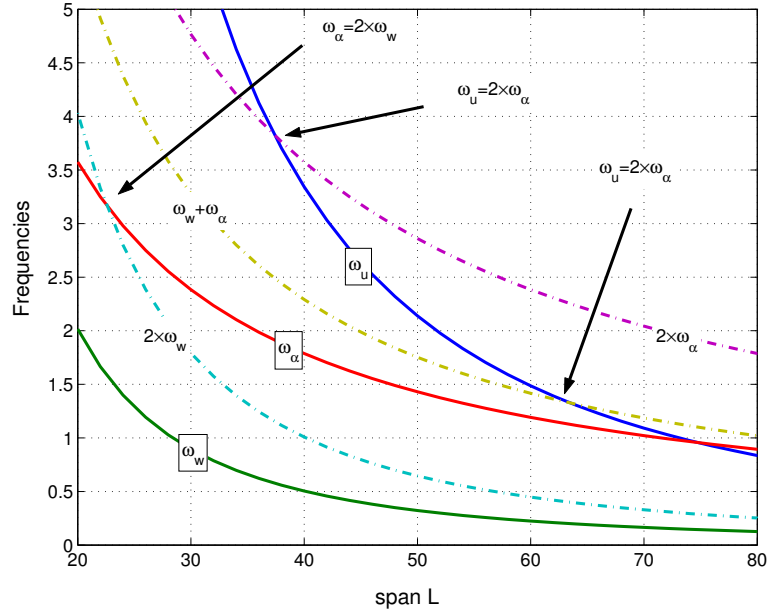


Fig. 24. Frequencies vs. wing span(L) for the HGW

are slightly greater than zero and the internal resonance conditions could be satisfied at relatively low velocities. Therefore, the quasi-steady aerodynamics is useful at this velocity region. These three cases with different wing spans are named as Case I, II, and III, and will be analyzed in the following sections.

D. Time Simulation

As mentioned in the previous section, the internal resonance of a wing with high aspect ratio is studied through the modified HGW models. The models have different wing spans. For a case of $\beta_z = 44$, we obtain the following coefficients,

$$C_{NLu} = \beta_y C_{uw3} + (\beta_z - 1) C_{uw6} = 216.01$$

$$C_{NLw} = -\beta_y C_{ww3} + (\beta_z - 1) C_{ww6} = 217.34$$

$$C_{NL\alpha} = (\beta_z - 1) C_{aw5} = 216.71$$

$$I_y^* = \frac{I_y}{mL^2} = \frac{29.219}{11.249 \times 60^2} = 0.00072153 \quad (4.85)$$

where $C_{uw3} = C_{ww3} = -6.5975$, $C_{uw6} = C_{ww6} = 5.0389$, $C_{wa5} = 5.0389$ are used, and β_y is 0.10106. It can be said that the quadratic nonlinear terms are dominated by β_z because the terms including β_z are relatively large. The effect of β_y on the above nonlinear terms is negligibly small. These values will be applied to the three cases.

1. Case I (L=20 ft): $\omega_2 = 2\omega_3$

As a reference case, the original wing with $L = 20$ ft is considered. Although the frequency ratio is very similar to one of the internal resonance cases, the motions are different since the in-plane motion is involved in the 2:1 IR mechanism. Therefore, no internal resonance is anticipated in Case I. Verifications for this case are performed by Beran *et al.*⁴⁹ From the Fig.5 shown in their paper, it is realized that the two modes used in current analysis are nearly identical to the first bending and torsion modes, obtained through finite element analysis.⁴⁸ Additionally, the Fig.6 shown in their paper⁴⁹ shows identical results.

The response for an example condition is shown in Fig. 25. In order to identify the interaction between the modes, frequency content is investigated. The frequency content is shown in Fig. 26. The initial conditions are $(u, w, \alpha) = (0.01, 0.02, 0.1)$ and the free stream velocity is zero. Because there are not any aerodynamic terms and the structural damping is zero, the amplitudes of responses are constant. From the the out-of-plane bending responses, we can see a slowly varying amplitude. But it is not ease to identify whether or not the torsional response has a slowly varying amplitude. The response characteristics are investigated through the frequency content as shown in Fig. 26. The Fourier Fast Transforms (FFTs) for u , w , and α

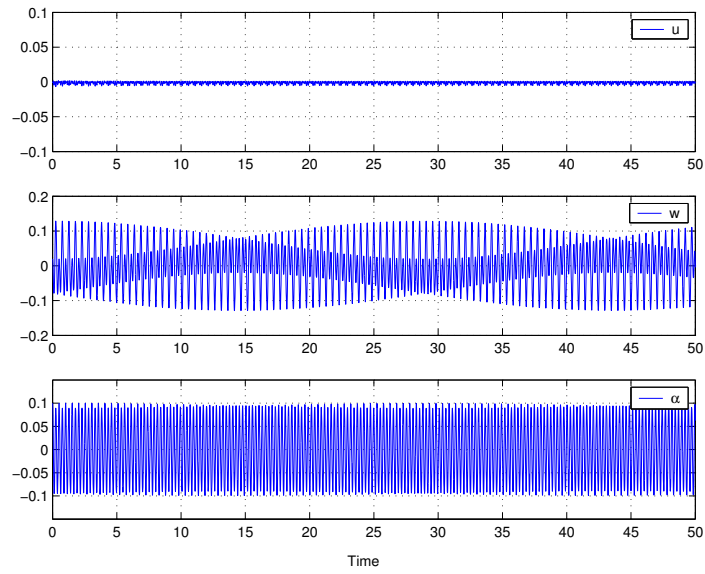


Fig. 25. Simulation for Case I ($L=20\text{ft}$ & $V=0\text{ ft/sec}$)

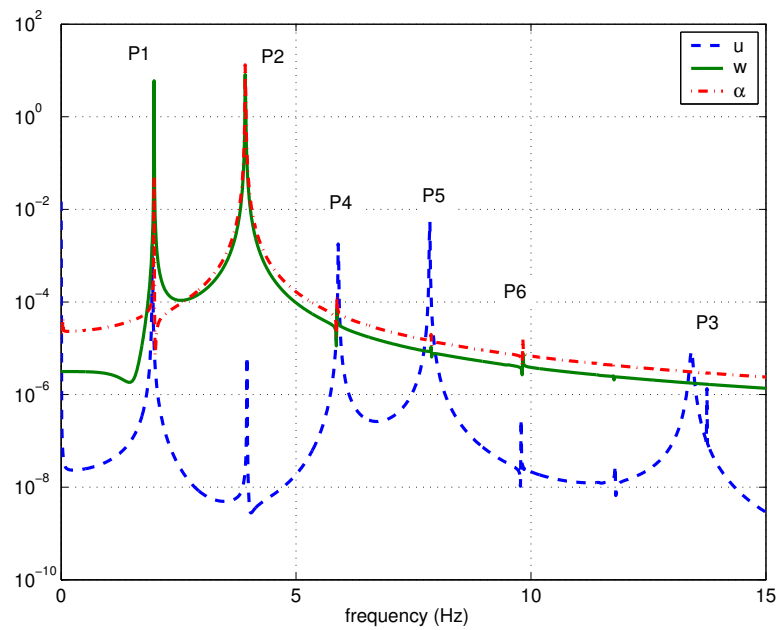


Fig. 26. Frequency content for Case I ($L=20\text{ft}$ & $V=0\text{ ft/sec}$)

Table VI. Possible Frequency Combination for Case I ($V = 0$)

Peak No.	Frequency[Hz]	Possible Combination
1	1.977	$\omega_w = 1.9739$
2	3.918	$\omega_\alpha = 3.9322$
-	3.955	$2\omega_w = 3.9477$
4	5.896	$\omega_w + \omega_\alpha = 5.9061$
5	7.849	$2\omega_\alpha = 7.8644$
6	9.827	$\omega_u - \omega_\alpha = 9.5222$
-	11.792	$\omega_u - \omega_w = 11.48$
3	13.415	$\omega_\alpha = 13.4544$

are represented by ‘dashed-line’, ‘dash-dot’, and ‘solid line’, respectively. Among the several peak frequencies denoted by $P_i (i = 1, 2, \dots, 6)$, the natural frequencies are P_1 , P_2 , and P_3 . The other peak points, P_4 , P_5 , and P_6 , are caused by the properties of three natural frequencies. Using the following product of trigonometric functions, these peaks, P_4 , P_5 , and P_6 , are explained

$$\cos \omega_A \cos \omega_B = \frac{1}{2} (\cos(\omega_A - \omega_B) + \cos(\omega_A + \omega_B)).$$

This expression shows that there are 4 different frequency combinations such as $(\omega_A - \omega_B)$, $(\omega_A + \omega_B)$, $2\omega_A$, and $2\omega_B$. The peak frequencies shown in Fig. 26 and the possible combination of frequencies are summarized in Table VI. From Table VI, it can be seen that the peak frequencies shown in Fig. 26 consist of natural frequencies and their combination. The out-of-plane bending response (w) has two dominant peak frequencies, P_1 and P_2 . Because the magnitudes of these two frequencies are similar, the response shows a slowly varying amplitude which type of motion is referred to as

beating. It is caused by the linear coupling terms, that is the mass imbalance terms. The out-of-plane bending motion is coupled with the torsional motion in this case. Although the torsional motion has two peak points, $P1$ and $P2$, $P2$ is the dominant frequency. At this point, it is required to focus on the peak ‘P1’. At ‘P1’, the frequency content for the torsional response shows a negative peak while the peak at ‘P2’ is positive. The negative peak can be seen explicitly on the figure at the bottom of page 99. This peak, which is close to zero amplitude, means that the point is the nodal point for the mode corresponding to the frequency ‘P1’. Thus, it is not easy to identify explicitly the effect of the frequency component ‘P1’ in the response for α . The in-plane bending motion has several peak points, but the magnitudes of these peak points are relatively small. The effect of these peak frequencies is not identified in Fig. 25. This result implies that the bending motion is strongly affected by the torsional motion, but the effect of the bending mode on the torsional motion is weak. But, it is not easy to identify any possibility of internal resonance from Figs. 25 and 26.

For another velocity condition, $V = 50$, simulation results and frequency content are shown in Figs. 27 and 28. As mentioned in the previous case, the negative peak can be seen explicitly from Fig. 28. All responses are decayed as shown in Fig. 27. The frequency spectrum for this example ($V = 50$) is simpler than the previous example. These results also show there is not any internal resonance between the in-plane bending and the torsional responses.

2. Case II ($L=36\text{ft}$): $\omega_1 = 2\omega_3$

In order to investigate 2:1 internal resonance, a wing having a wing span $L = 36\text{ft}$ is considered. For a velocity condition $V = 0$, the simulation results and frequency

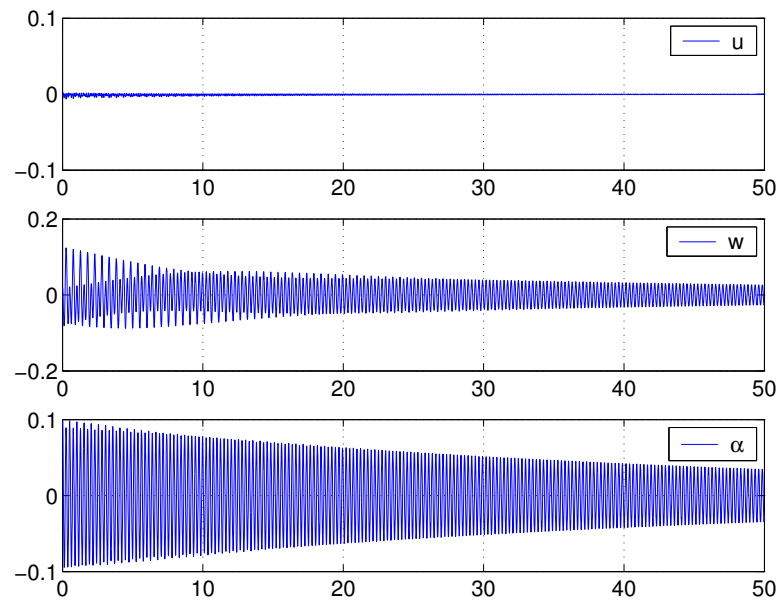


Fig. 27. Simulation for Case I ($L=20$ ft & $V = 50$ ft/sec)

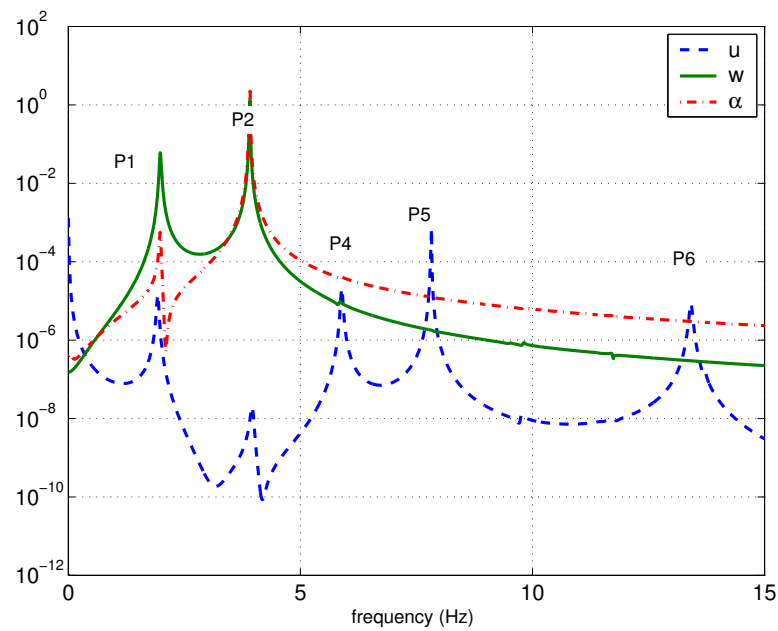


Fig. 28. Frequency content for Case I ($L=20$ ft & $V=50$ ft/sec)

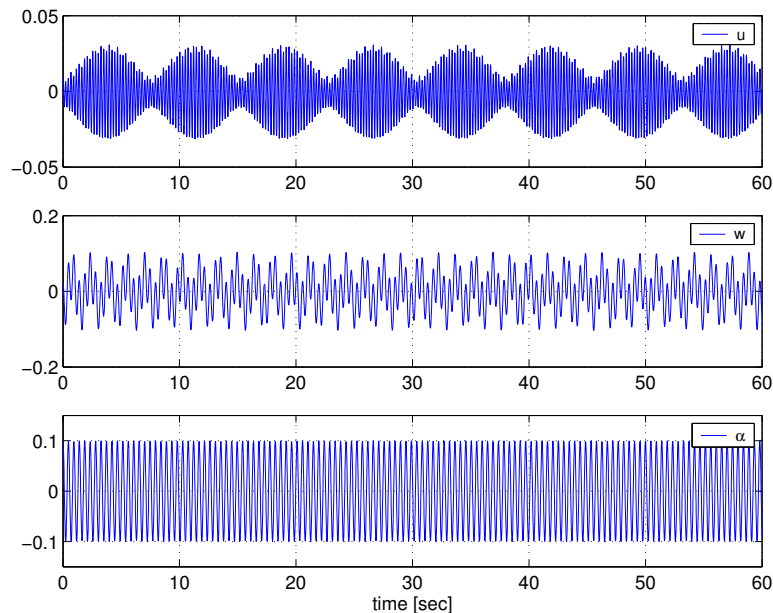


Fig. 29. Time histories for Case II ($L=36$ ft & $V=0$ ft/sec)

content are shown in Figs. 29 and 30, respectively. An interesting shape of response can be seen from the in-plane bending motion. The amplitude of u is periodically changed. Although the out-of-plane bending motion shows somewhat different responses from Case I, it is not easy to identify the interaction between u and w . More detailed characteristics are investigated through the frequency content as shown in Fig. 30. The torsional response has one dominant peak frequency, $P2$, and the envelop of the response is almost constant. The out-of-plane bending motion has two dominant peaks, $P1$ and $P2$, and the envelop of response is continuously changed. The in-plane bending response has several peaks, but the dominant peaks are $P3$ and $P7$. The peak frequency, $P3$, is the primary aeroelastic frequency of the in-plane bending motion, but $P7$ corresponds to $2 \times \omega_\alpha$ as shown in Table VII. The equation for the in-plane bending motion is

$$C_{uu}1\ddot{u} + \beta_z u = C_{NLu} w \alpha. \quad (4.86)$$

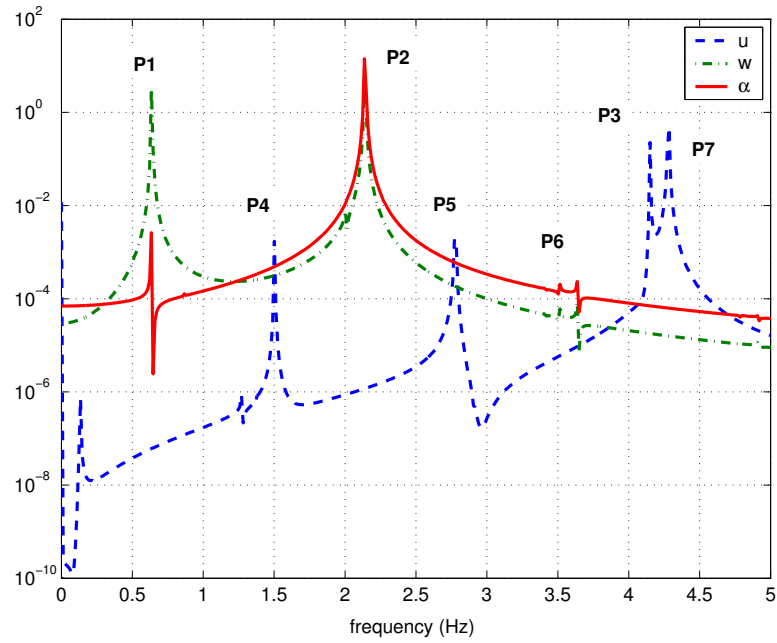


Fig. 30. Frequencies content for Case II ($L=36$ ft & $V = 0$ ft/sec)

Table VII. Possible Frequency Combination for Case II ($L = 36$ ft & $V = 0$ ft/sec)

Peak No.	Frequency[Hz]	Possible Combination
1	0.635	$\omega_w = 0.6217$
-	1.269	$2\omega_w = 1.2434$
4	1.501	$\omega_\alpha - \omega_w = 1.5189$
-	2.	$\omega_u - \omega_\alpha = 2.0119$
2	2.136	$\omega_\alpha = 2.1406$
5	2.775	$\omega_w + \omega_\alpha = 2.7624$
6	3.645	$\omega_u - \omega_w = 3.5308$
3	4.15	$\omega_u = 4.1525$
7	4.285	$2\omega_\alpha = 4.2813$

As expected by the approximation, modulated responses between the in-plane bending and torsional modes are seen in Fig. 31. The frequency ratio between the in-plane motion and the torsion motion is close to 2. Observe, when α amplitude decreases, u amplitude increases, and vice versa. Because the system has positive damping, the torsional response goes to zero, and the in-plane bending motion converges to non-zero amplitude because of zero-damping in the in-plane bending motion. Another interesting phenomenon is seen: the results imply that unidirectional energy flow⁵⁰ is possible. This can be the basis of a new strategy for suppressing flutter.⁵⁰ As shown in Fig. 32, the frequency content for Case II is different from that for Case I. In the non-resonance case (Case I), the dominant components are caused by the out-of-plane bending and torsional motion and the effect of the in-plane motion is negligible as shown in Fig. 28. But, in Case II, the effect of u is increased when the velocity is increased, although the in-plane motion is excited indirectly by the internal resonance mechanism. As shown in Fig. 32, the two peaks $P2$ and $P3$ have similar order of magnitude but the magnitude of the out-of-plane bending ($P1$) is relatively small. This result shows that when two modes, u and α , are involved in the internal resonance mechanism, the responses are dominated by the two modes and the effect of the other mode w is relatively small.

3. Case III ($L=60\text{ft}$): $\omega_1 = \omega_2 + \omega_3$

Another internal resonance phenomenon occurs at a frequency condition, $\omega_1 \approx \omega_2 + \omega_3$. This frequency condition occurs at $L = 60\text{ft}$. This internal resonance case is different from Case II, in that all three modes are involved in the internal resonance mechanism.

When the free stream velocity is zero, the simulation results are shown in Fig. 33. It can be clearly seen that the in-plane bending mode and the torsional mode are

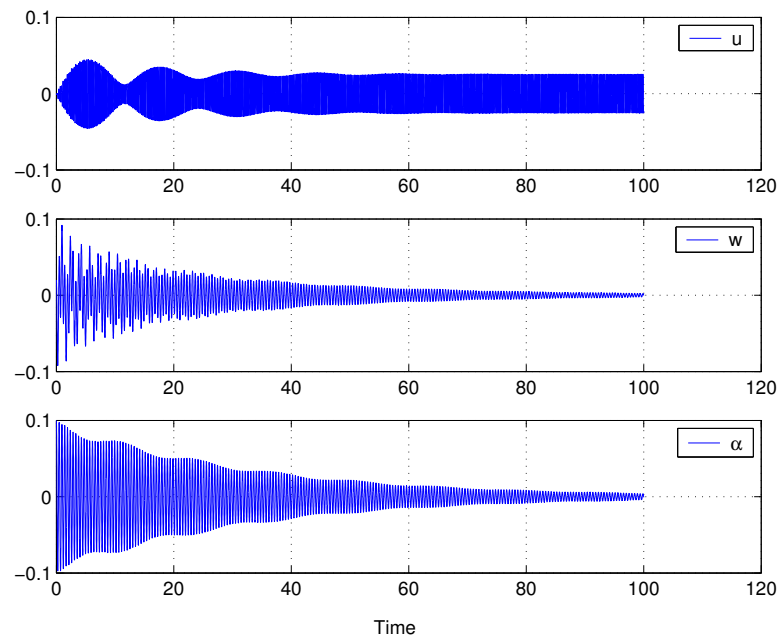


Fig. 31. Time histories for Case II ($L=36$ ft & $V=50$ ft/sec)

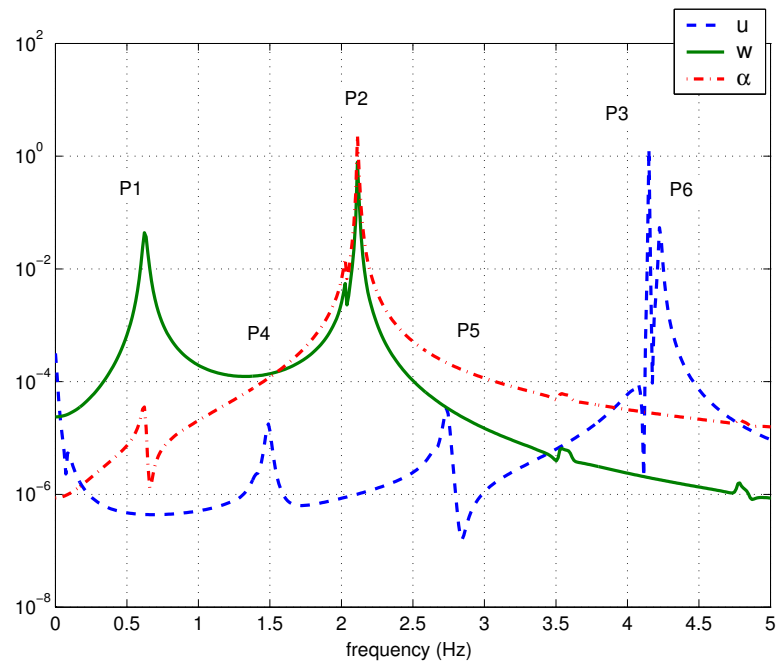


Fig. 32. Frequencies content for Case II ($L=36$ ft & $V=50$ ft/sec)

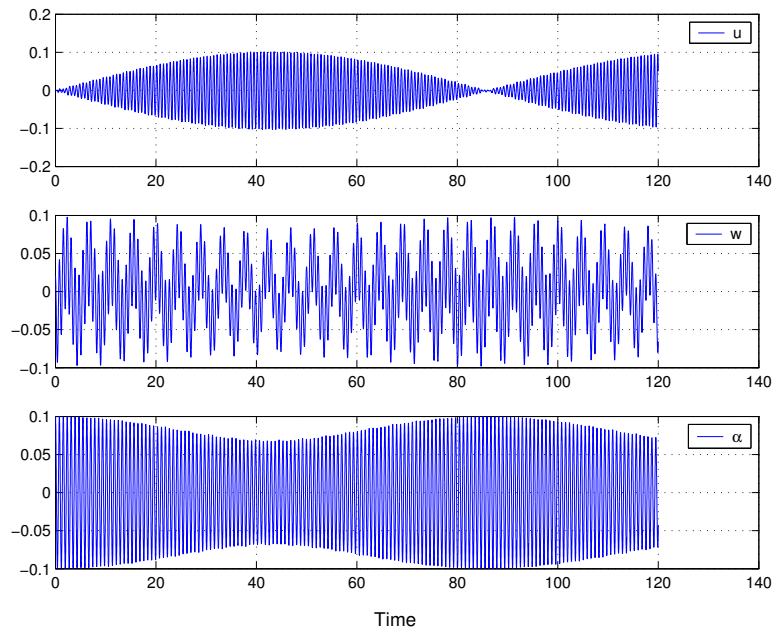


Fig. 33. Simulation results for Case III (L=60 ft & V=0 ft/sec)

modulated. The envelop of the out-of-plane bending motion is very similar with that of the torsional motion. As shown in Fig. 34, the frequencies for u and α motions do not satisfy the commensurable condition, $m\omega_u + n\omega_\alpha = 0$, where m and n are integers. Because the three frequencies satisfy a commensurable condition, $\omega_u \approx \omega_w + \omega_\alpha$, and the responses are modulated, it is an internal resonance. It is meaningful to review Eqs. (4.1), (4.2), (4.3) and the particular solution, Eq. (4.45). In Eq. (4.45), the terms causing the resonance condition $\omega_u \approx \omega_w + \omega_\alpha$ are related directly to the nonlinear coupling terms as follows,

$$C_{uw1}\ddot{u}_i + \beta_z C_{uw2}u_i = C_{NLu}w_j\alpha_k \quad \sim e^{i(\omega_w + \omega_\alpha)T_o} \quad (4.87)$$

$$C_{ww1}\ddot{w}_j - e^*\ddot{\alpha}_k + C_{wwq}w_j = C_{NLw}u_i\alpha_k \quad \sim e^{i(\omega_u - \omega_\alpha)T_o} \quad (4.88)$$

$$C_{aw1}\ddot{\alpha}_k - \frac{e^*}{I_y^*}\ddot{w}_j + \frac{1}{I_y^*}\beta_y C_{aw2}\alpha_k = C_{NL\alpha}w_ju_i \quad \sim e^{i(\omega_u - \omega_w)T_o} \quad (4.89)$$

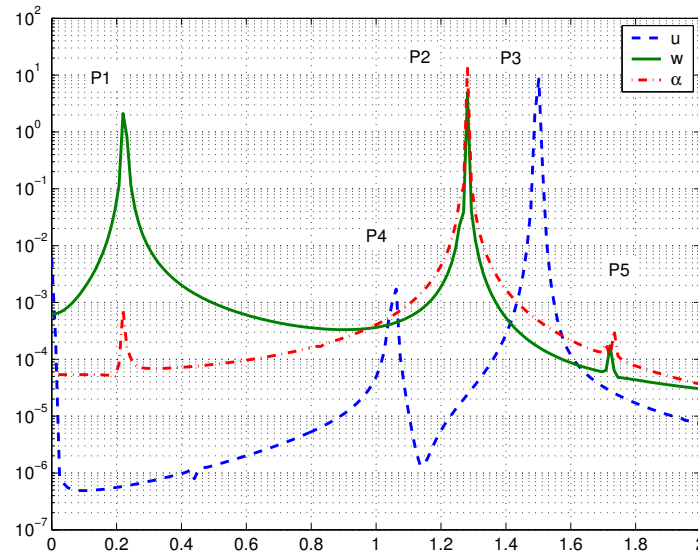


Fig. 34. Frequency content for Case III ($L=60$ ft & $V=0$ ft/sec)

As shown in the above formulations, there is no aerodynamic terms. Contrast to the previous resonance condition (Case II), this resonance is caused by the nonlinear coupling terms without any linear coupling term related to aerodynamics.

Another example with non-zero velocity is considered. Using the approximate solution, an envelope of the responses are generated as shown in Fig. 35. In this figure, the x-axis is the slow scale, T_1 . It can be seen from this figure that the two bending modes are in-phase, but the torsional motion shows amplitude-modulated response. In the previous example (Fig. 33), it was difficult to identify the modulated response of the out-of-bending motion. But, the modulated responses for the three modes could be easily detected from Fig. 35. As shown in Fig. 36, the bending modes are synchronized with each other, and the torsional motion has about 180 deg. of phase angle, with respect to the bending motions. Because of aerodynamic damping, the out-of-plane bending and the torsional motions are decayed continuously. Although

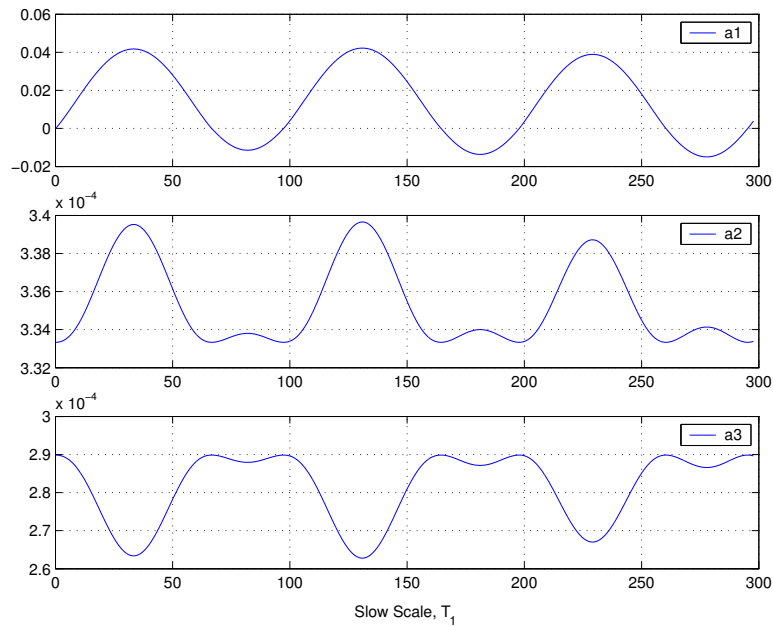


Fig. 35. Approximation for Case III ($L=60$ ft & $V=5$ ft/sec)

there are many peak frequencies in Fig. 37, the dominant components are located around three points $P1$, $P2$ and $P3$.

E. Discussion

Although these examples are limited, they show illustrative results. When a wing has high aspect ratios and flexibility, the wing may experience new phenomena such as internal resonance. Depending upon the stiffness ratio, the wing span, and aerodynamics, possible internal resonance conditions are different. For a specified stiffness ratio, $\beta_z = 44$, two different internal resonance conditions, $\omega_u = 2 \times \omega_\alpha$ and $\omega_u = \omega_w + \omega_\alpha$, are observed for different wing spans, $L = 36$ ft and $L = 60$ ft, respectively. The first resonance is related to the linear coupling term caused by aerodynamics. The second resonance is possible whether there is linear aerodynamic terms or not because this resonance is dominated by nonlinear coupling terms. The in-plane bending mode is

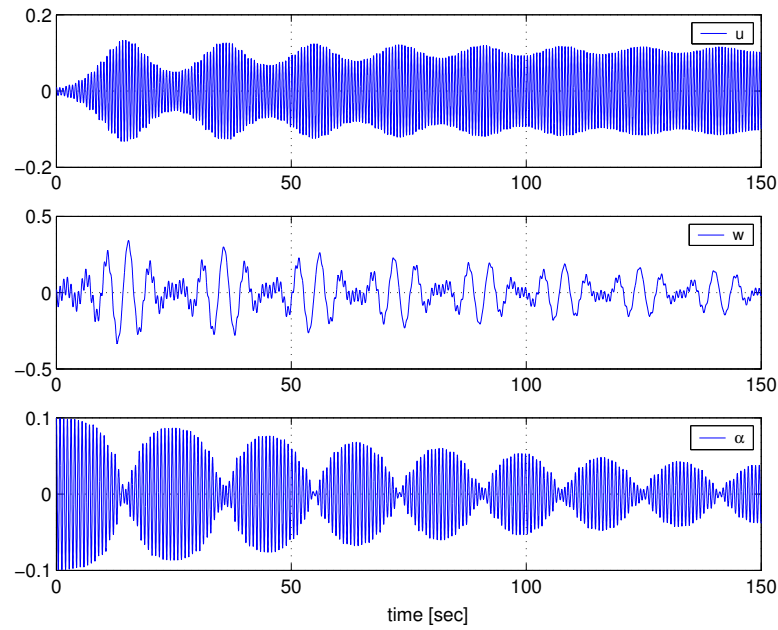


Fig. 36. Simulation results for Case III ($L=60$ ft & $V=5$ ft/sec)

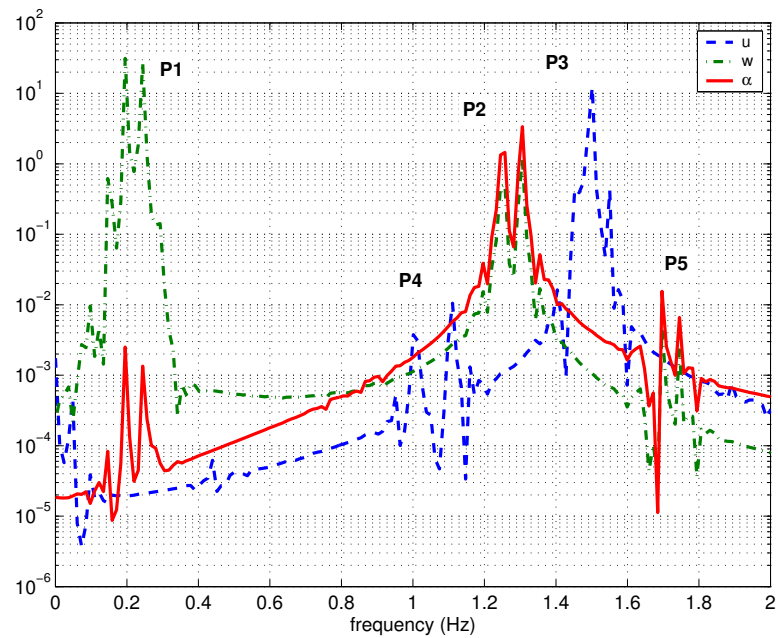


Fig. 37. Frequency content for Case III ($L=60$ ft & $V=5$ ft/sec)

included in both resonance cases. Additionally, the characteristics of unidirectional energy transfer may be used as a new strategy for suppressing flutter.

CHAPTER V

BENDING-TORSION DYNAMICS OF A CANTILEVER WING WITH CUBIC
NONLINEARITIES

Typically, aeroelastic characteristics of conventional aircraft are described by the out-of-plane bending and torsion. The bending-torsion equations are used to investigate LCO responses. The considered cantilever wing has three types of nonlinearities: structural nonlinearity caused by large wing flexibility, aerodynamic stall nonlinearity, and store-induced nonlinearity. All these nonlinearities have up to the third order nonlinear terms. Because the LCOs are observed at a velocity less than the linear flutter velocity, we focus on the the velocity region $V_r = V/V_F < 1.0$. Because the nonlinear aerodynamics are described by the quasi-steady aerodynamics with stall model, the NATAm wing model is considered.

To investigate the response characteristics, phase portraits and Poincaré maps are examined to determine the key features of the response for a given nonlinear system. The effects of the velocity change are depicted in bifurcation diagrams. This study consists of two separate steps. First, the effects of individual and combined nonlinearities are studied. Then, the sensitivity of store parameters is considered. Because the linear flutter velocity, V_F is changed by the given configuration conditions, the relative velocity, V_r for the given configuration is introduced. To study the LCOs at a velocity less than the linear flutter velocity, $V_r = 0.95$ is used as the reference case for comparison. It should be stated that V_F is configuration dependent; thus, as results are compared, the actual flutter velocity may be lower even if the ratio, V_r is higher.

A. Equations of Motion

It is assumed that the in-plane bending stiffness is so high that the in-plane motion and the associated coupling can be neglected. Hence, the following bending-torsion equations are obtained from Eqs. 2.46 and 2.47.

$$\begin{aligned}
& m\ddot{w} - me\ddot{\alpha} + D_x w^{IV} + M_s(\ddot{w} - x_z \ddot{\alpha})\delta(y - y_s) \\
& - \pi \rho b^2 V \dot{\alpha} + \rho b V C_{L\alpha} \left[\dot{w} - V\alpha - b \left(\frac{1}{2} - a \right) \dot{\alpha} \right] \\
& = -D_x [w'(w'w'')] + (D_x - D_z)[w''\alpha^2]'' + I_x \ddot{w}'' - \frac{1}{2}m \left[w' \int_L^s \left(\int_0^s w'^2 ds \right)'' ds \right]' \\
& - me \left(\frac{1}{2} \dot{\alpha} w'^2 + \alpha w' \dot{w}' + \frac{1}{2} \alpha^2 \dot{\alpha} \right) \bullet + me \left[-\frac{1}{2} (w'^2)'' \alpha - \frac{1}{2} \int_0^s (w'^2)'' ds \alpha' + (\ddot{w} \alpha w')' \right] \\
& - M_s x_s \left(\frac{1}{2} \dot{\alpha} w'^2 + \alpha w' \dot{w}' + \frac{1}{2} \alpha^2 \dot{\alpha} \right) \bullet \delta(y - y_s) + M_s z_s (w' \dot{w}' + \alpha \dot{\alpha}) \bullet \delta(y - y_s) \\
& - \rho b V^2 C_{L\alpha} c_3 \alpha_{eff}^3
\end{aligned} \tag{5.1}$$

$$\begin{aligned}
& I_y \ddot{\alpha} - me \ddot{w} - D_y \alpha'' + [(I_{sy} + M_s x_s^2 + M_s z_s^2) \ddot{\alpha} - M_s x_s \ddot{w}] \delta(y - y_s) \\
& + \pi \rho b^2 V b \left(\frac{1}{2} - a \right) \dot{\alpha} + \rho b^2 V C_{m\alpha} \left[\dot{w} - V\alpha - b \left(\frac{1}{2} - a \right) \dot{\alpha} \right] \\
& = (I_z - I_x) \dot{w}'^2 \alpha - (D_z - D_x) w''^2 \alpha \\
& + \frac{1}{2} me \left[-\ddot{w} (w'^2 + \alpha^2) + \left(\int_0^s w'^2 ds \right)'' w' \right] \\
& + (I_{sz} - I_{sx}) \dot{w}'^2 \alpha \delta(y - y_s) \\
& + \frac{1}{2} M_s x_s \left[-\ddot{w} (w'^2 + \alpha^2) + \left(\int_0^s w'^2 ds \right)'' w' \right] \delta(y - y_s) + M_s z_s \ddot{w} \alpha \delta(y - y_s) \\
& - \rho b^2 V^2 C_{m\alpha} c_3 \alpha_{eff}^3
\end{aligned} \tag{5.2}$$

The ordinary differential equations (ODEs) are obtained by applying the Galerkin's procedure to Eqs. 5.1 and 5.2. In this chapter, the shape function for the torsional mode is $A_k(s) = \sin(\gamma_k s)$ which is a maximum at wing tip. It is assumed that the aeroelastic responses are dominated by the first bending and torsion. And, all modes

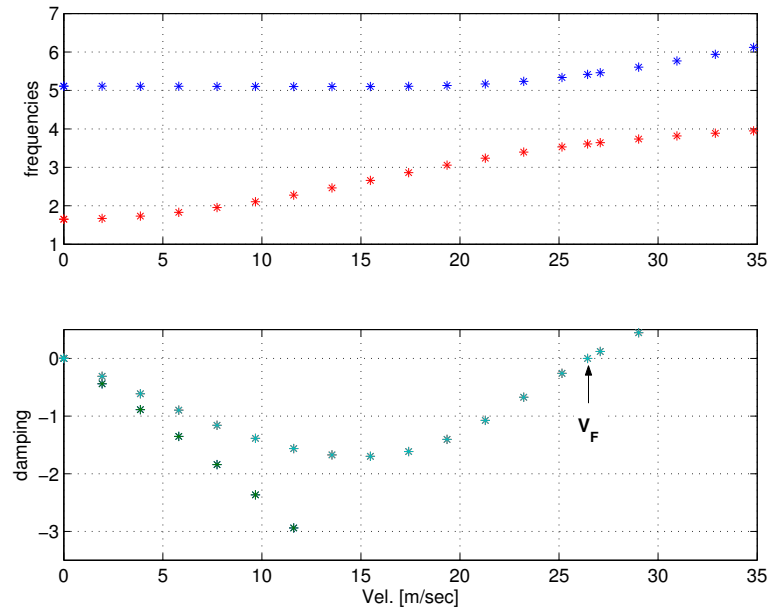


Fig. 38. V-f and V-g plots

that are not directly excited by external loads or indirectly excited by any resonance mechanism decay with time.⁵¹ Thus, in order to focus on the interaction between the bending motion and the torsional behavior, only one mode in each motion is used to describe the responses. In this situation, the equations of motion may be expressed without summation signs and the subscripts 'j' and 'k' shown in the out-of-plane bending and torsion equations.

B. Flutter Analysis

To estimate the effects of nonlinear terms, linear flutter analysis is briefly performed. In a linear aeroelastic system, the dynamic characteristics may be distinguished by the relative velocity with respect to the flutter velocity, V_F . For a system specified by the system parameters shown in Table I. As shown in Fig. 38, the flutter velocity is 26.44 m/sec at which damping is zero. When the system does not have any store,

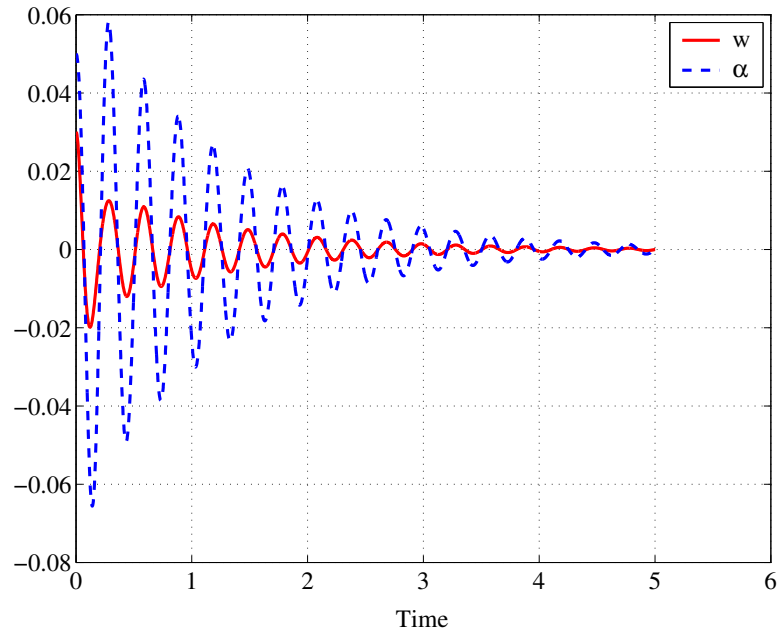


Fig. 39. Simulation results at $V_r = 0.85$

the corresponding flutter velocity is 26.36 m/sec. When a velocity less than V_F ($V_r = 0.85$), the responses decay as shown in Fig. 39. Eventually, the responses decay to zero. For velocities greater than V_F , the responses will increase as shown in Fig. 40. As shown in Fig. 38, the aeroelastic frequencies for the bending and torsion motions are different at these velocity conditions $V_r = 0.85$ and 1.05. But, the responses show that the two modes are synchronized. It is one of characteristics of aeroelastic responses.

C. Poincaré Map and Bifurcation Diagram

Because there are three types of nonlinearities with various combinations, 8 possible cases are studied; one linear case and 7 combinations of the three types of nonlinearities. The case number has two characters 'BT' to show these cases are valid only for the bending-torsion problem. In order to check the existence of LCO at any velocity

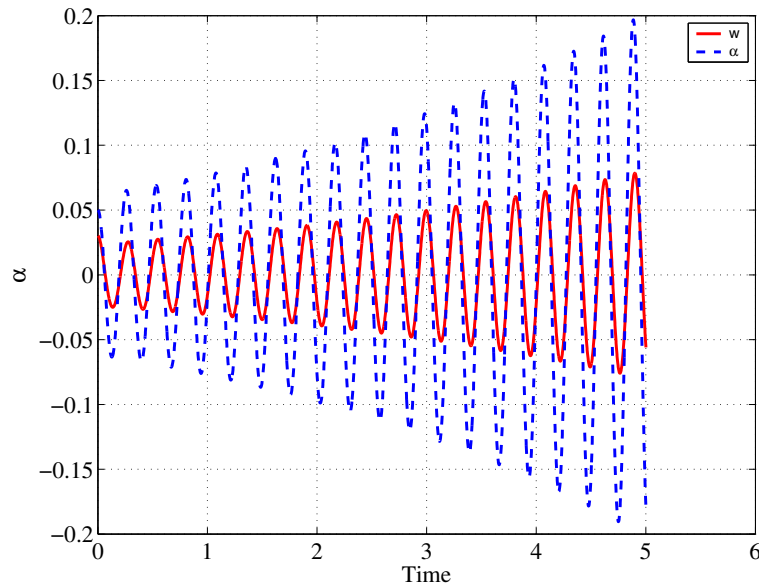


Fig. 40. Simulation results at $Vr = 1.05$

less than V_F , a velocity condition, V_r 0.95 is adopted as a reference case. Because the closed orbits in phase portraits represent periodic motions, phase portraits are used to check the existence of LCOs. The response characteristics are summarized in Table VIII. In the table, the characters ‘W’, ‘A’, and ‘S’ are used to show the nonlinearity included in the cases. The case ‘BT7’ having three ‘W’, ‘A’ and ‘S’ means that the system has the structural nonlinearities caused by wing(W) flexibility, the aerodynamic (A) stall nonlinearity, and the store(S)-induced nonlinearity. As shown in this table, LCO type responses are observed for those cases with structural nonlinearities.

When a system has only store nonlinearities, the responses are very similar with those in linear analysis. For a velocity less than flutter, the motion decays as shown in Fig. 39, and the response grows at a velocity greater than flutter as shown in Fig. 40.

At $V_r=0.95$, the response characteristics of some cases with structural nonlin-

Table VIII. Response Characteristics at $Vr = 0.95$

Case No.	Case ID	Responses
-	Linear	Decay
BT1	W	LCO
BT2	A	Decay
BT3	S	Decay
BT4	W+A	LCO
BT5	W+S	LCO
BT6	A+S	Decay
BT7	W+A+S	LCO

earities are very similar to each other. Therefore, phase portraits and time histories for a representative case are depicted in Fig. 41. The time histories show that the amplitudes of responses are maintained. In this case, the store parameters are $M_s = 0.1mL, I_{sy} = 0.1I_yL, xs = -0.2b$, and $zs = 0.0b$. The corresponding phase portraits and Poincaré maps are shown in Fig. 42. In this figure, phase portrait is expressed by a solid line, and Poincaré maps are depicted by a symbol ‘O’. From the phase portrait, an isolated closed orbit can be identified. This closed orbit represents a periodic motion⁴⁴ as shown in Fig. 41. This type of periodic motion is represented by two fixed points, A_F and B_F . These figures show that for any case having structural nonlinearities, LCO type responses are possible at a velocity less than V_F .

Although phase portraits provide useful information about LCO type responses, it is not easy to represent summarized characteristics in such a figure. In order to investigate the effects of velocity change and relative motions between bending deflection

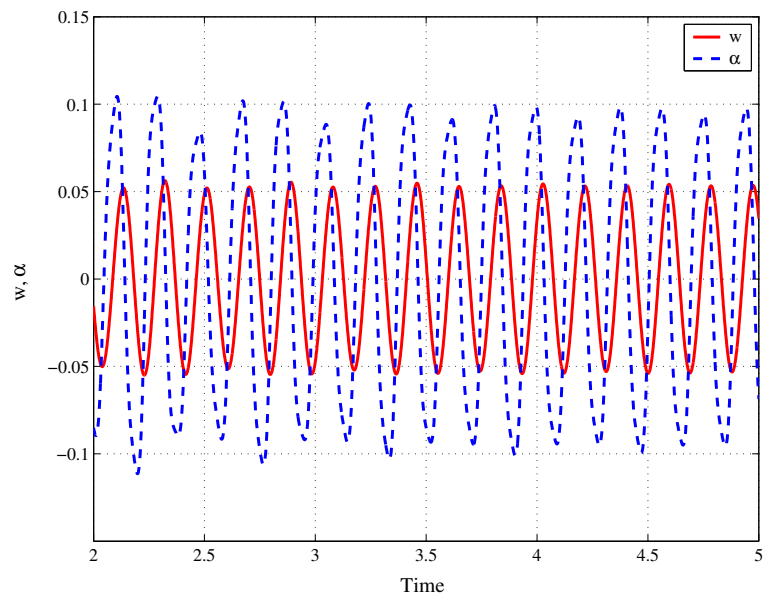


Fig. 41. Simulation results at $Vr = .95$

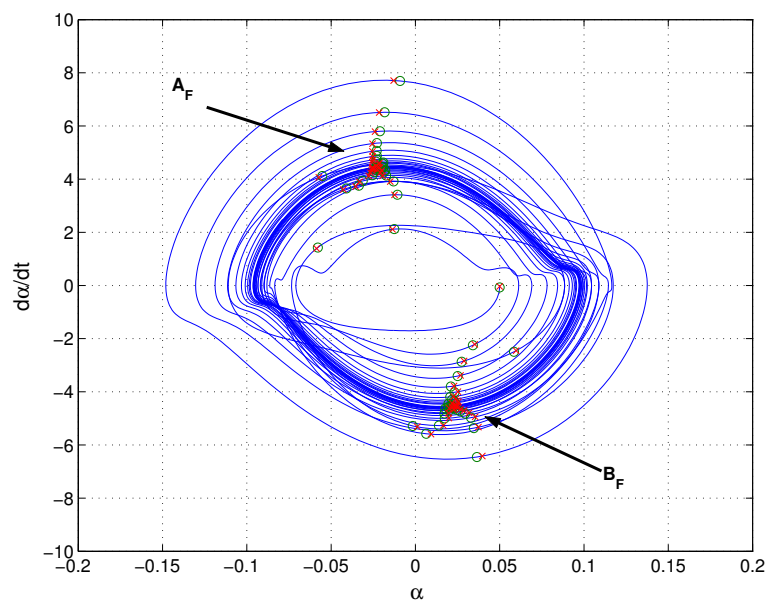


Fig. 42. Phase portrait and Poincaré map at $Vr = 0.95$

and torsional response, Poincaré maps and bifurcation diagrams are introduced.

For a forced vibration system, a Poincaré map can be generated by a sampling rule based on the exciting period. Because in aeroelastic systems, steady-state responses are possible without any exciting force, other sampling rules are required. To generate the bifurcation diagram of pitch amplitude and a Poincaré map of pitch motion, Kim⁴⁰, and Kim et al.⁴¹ used two sampling rules: $\dot{\alpha} = 0$ (the velocity of the pitch angle is zero) condition and $h = 0.0$ (bending deflection is zero), respectively. In this dissertation, another sample rule, $\dot{w} = 0$, is adopted to generate Poincaré maps of pitch motion. By applying this new rule, equilibrium points at which $\dot{\alpha} = \dot{w} = 0$ could be detected in a Poincaré map. If the fixed points in the Poincaré map have $\dot{\alpha} = 0$, then the points are equilibrium points.

By using the fixed points shown in Poincaré maps for various velocity conditions, bifurcation diagrams are generated. Bifurcation diagram for a case with only aerodynamic nonlinearities are shown in Fig. 43. As shown in Fig. 43, the number of fixed points are changed by the velocity conditions; one fixed point at a velocity less than $V_r < 1$ and two fixed points at $V_r > 1$. The one fixed point in a region of $V_r < 1$ means that the responses go to zero as shown in Fig. 39. But the two fixed points at a velocity greater than V_F imply that the response has a limit cycle oscillation as shown in Fig. 44 and Fig. 45. As shown in Fig. 45, the corresponding phase portraits and Poincaré map show closed orbit(s) and fixed points, respectively. In Fig. 45, A_F and B_F are fixed points. For a case with only store nonlinearities, the corresponding bifurcation diagram simply shows only one point regardless of the velocity condition. For a velocity condition $V_r < 1$, the responses decay to zero in a manner similar to Fig. 39, and for a velocity condition $V_r > 1$ the responses grow in a manner similar

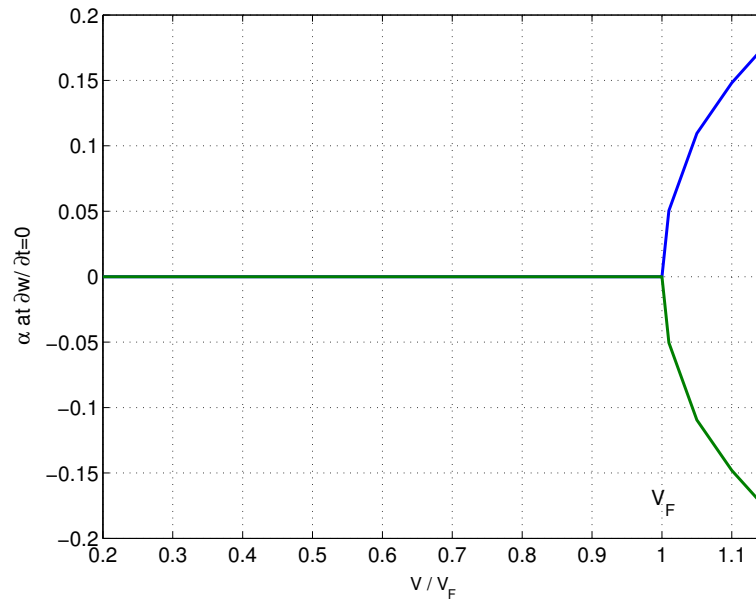


Fig. 43. Bifurcation diagram for Case BT2 (A)

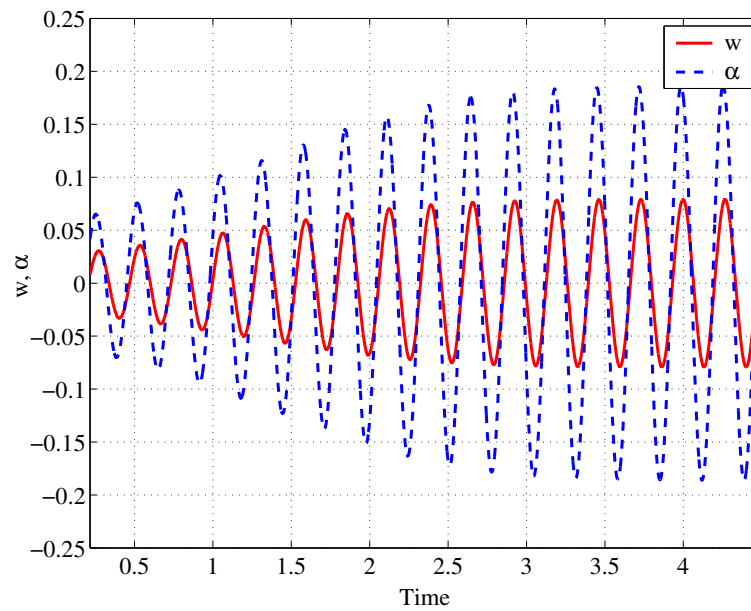


Fig. 44. Simulation results for Case BT2 ($V_r = 1.15$)

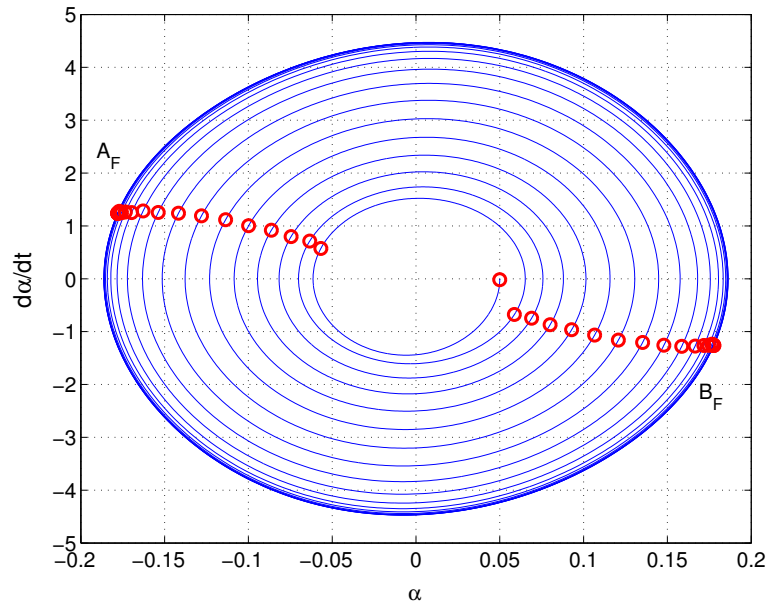


Fig. 45. Phase portrait and Poincaré map for Case BT2 ($V_r = 1.15$)

to Fig. 40.

Based on the results presented in Table VIII, the effects of velocity change in some cases with structural nonlinearities are studied. At first, a case with only structural nonlinearity is considered. The aerodynamic loads remain linear in this case. For the studies intended to focus on only structural nonlinearity, the torsional response exceeds the stall angle (0.1920 rad). The torsional angle is so high that linear aerodynamics does not care. This situation must be improved by adding a nonlinear aerodynamic model. Thus, a combined case including the aerodynamic and store-induced nonlinearities is considered to investigate the effects of the velocity change

The bifurcation diagram for a case in which all three forms of nonlinearity are considered is shown in Fig. 46. As shown in this figure, there are various fixed points with different magnitudes of the alpha amplitude for $V_r < 1$. These fixed points mean

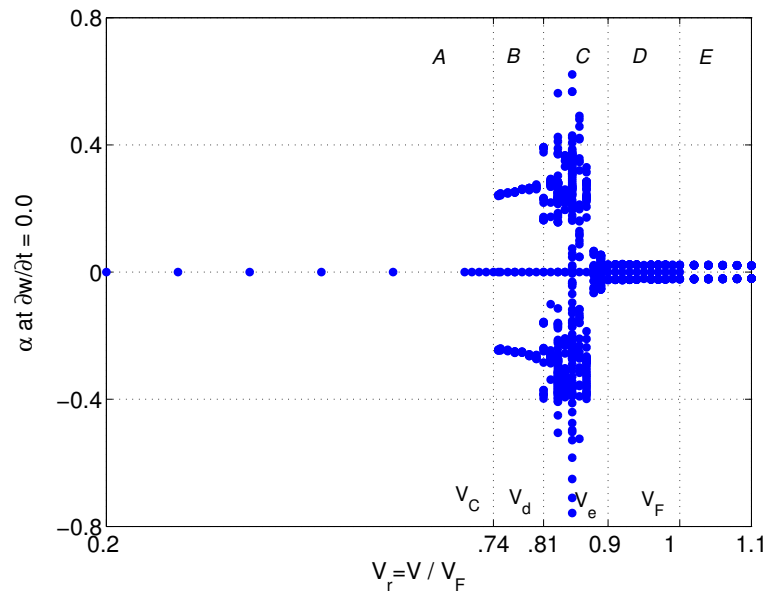


Fig. 46. Bifurcation diagram for Case BT7

that LCO type responses are possible in the velocity range $V_r < 1$. For $V_r < V_C$, the responses go to zero. For $V_C < V_r < V_F$, there are at least three fixed points including a fixed point with zero alpha. The existence of a zero fixed point implies that the responses may be damped out depending upon the initial conditions. For small initial conditions, the response goes to zero, but larger initial conditions may cause the response to go to other fixed points with non-zero amplitudes. This kind of subcritical bifurcation characteristic is maintained in this velocity region. The bifurcation diagram may be sub-divided into several regions. Three fixed points appear in the region B and D. In region C, the fixed points exceed 3. Although the number of fixed points shown in regions B & D are the same, the amplitudes are different. As shown in Figs. 47 and 48, these regions have different characteristics. From the Poincaré maps shown in Figs. 48 and 48, it is easy to identify the position of the fixed points A_F , B_F , and C_F . The two fixed points A_F and B_F represent a periodic motion. One A_F (or one B_F) means that the bending motion and the torsional motion have

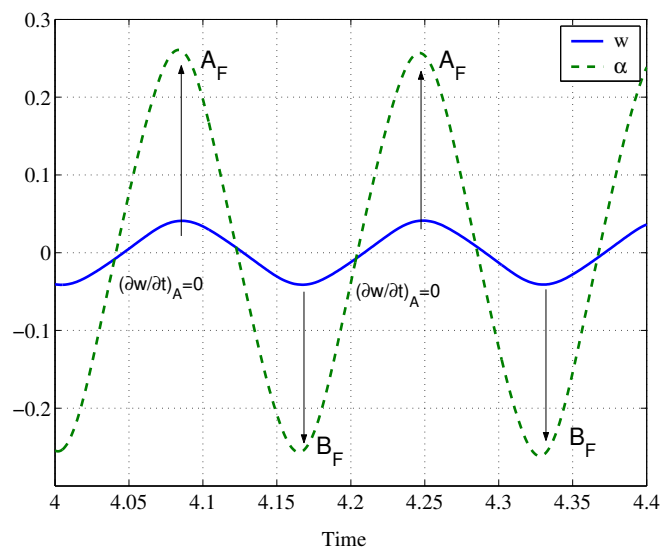
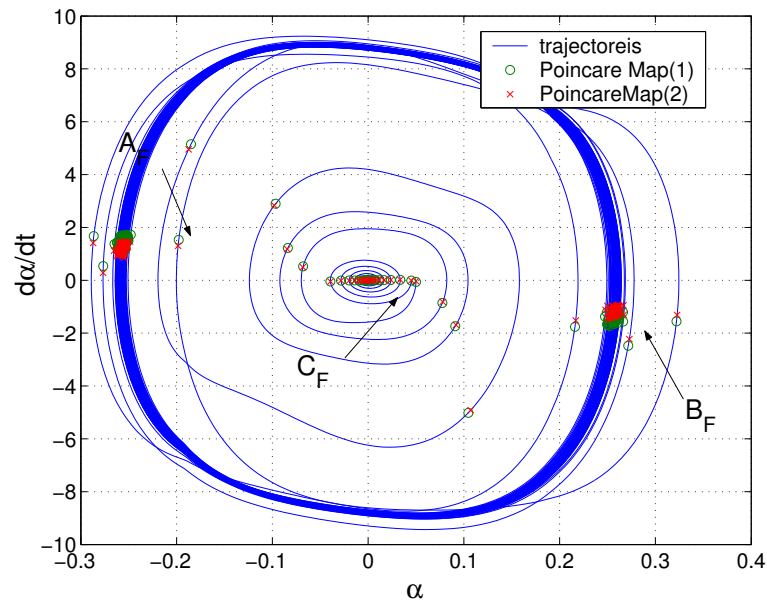


Fig. 47. (a) Phase portrait and Poincaré map and (b) simulation results for Case BT7 ($V_r = 0.78$)

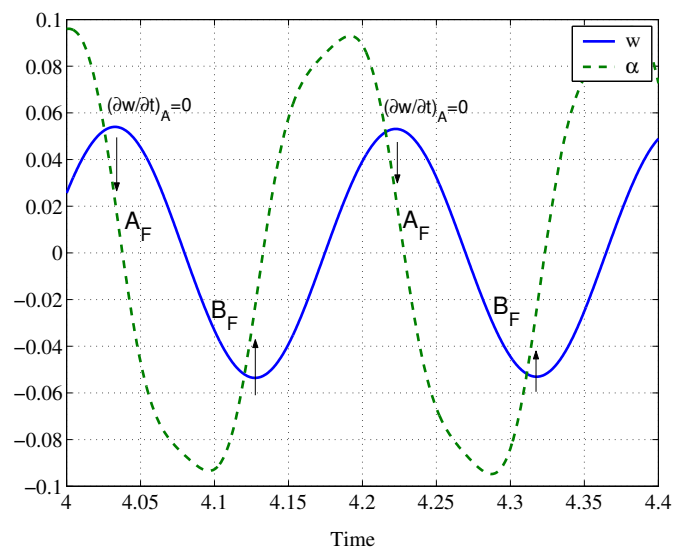
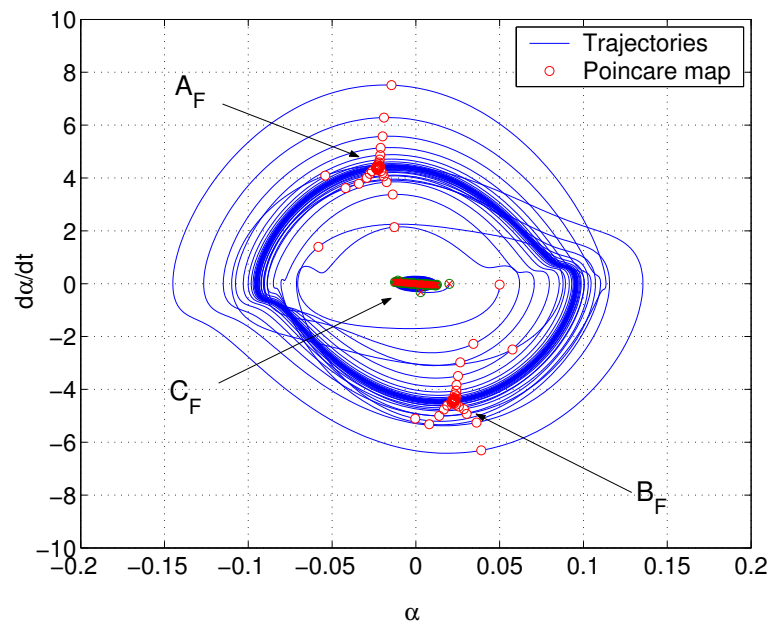


Fig. 48. (a) Phase portrait and Poincaré map and (b) simulation results for Case BT7 ($V_r = 0.96$)

a same (nonlinear) period. As shown in Fig. 48(b), the time interval between A_F is the same as the period of $\dot{w}_A = 0.0$. The third fixed point, C_F corresponds to a damped motion. Depending upon the initial conditions, the responses either go to zero or show LCO (subcritical bifurcation) behavior.

The two fixed points A_F and B_F included in Fig. 48(a) are close to $\dot{\alpha} = 0.0$, but the fixed points shown in Fig. 48(a) are close to the maximum $\dot{\alpha}$. Because the sampling condition is ' $\dot{w} = 0.0$ ', the fixed points close to zero means that the relative phase angle between the bending motion and torsional motion are close to zero as shown in Fig. 48(b). But the other case having almost maximum $\dot{\alpha}$ shows that the two motions have almost a 90-degree phase angle as shown in Fig. 48(b). Although bending motion is not explicitly shown in these figures, the relative characteristic of the bending motion can be identified from the Poincaré map.

In region C, two interesting responses are included as shown in Figs. 49, 50 and 51. At a velocity close to V_d , the nonlinear frequency ratio is almost 3 as shown in Fig. 49. In this figure, there are 3 points associated with A_{FS} and 3 points associated with B_{FS} . This means that the period of the bending motion is 3 times of the torsional period. For another velocity close to V_e , quasi-periodic motion is observed as shown in Fig. 51. As shown in Fig. 51, the fixed points lie in a circular shape. This type of Poincaré map may occur when the ratio of the frequencies is not a rational number.

The bifurcation diagram based on Poincaré map is examined by Chetan.⁵² He used the software package AUTO2000³³ for continuation and bifurcation problems in ordinary differential equations. The AUTO2000 bifurcation diagram is depicted in Fig. 52 The store parameters are $M_s = 0.394$, $I_{sy} = 0.0056$, $x_s = -0.027$, and $z_s = 0.0$,

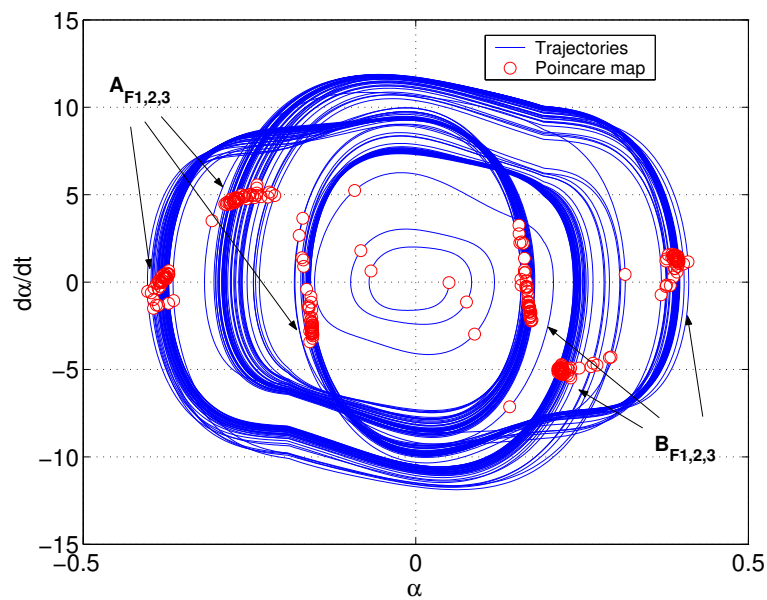


Fig. 49. Phase portrait and Poincaré map for Case BT7 ($V_r = 0.81$)

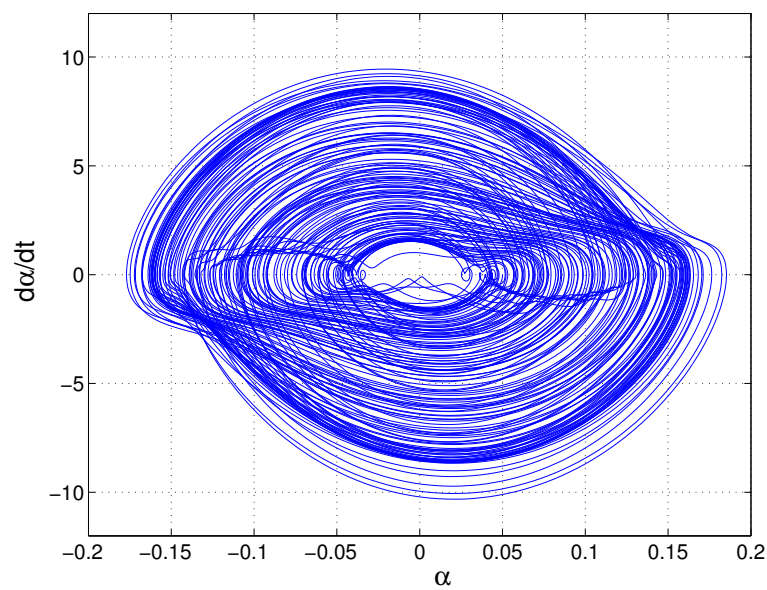


Fig. 50. Phase portrait for Case BT7 ($V_r = 0.89$)

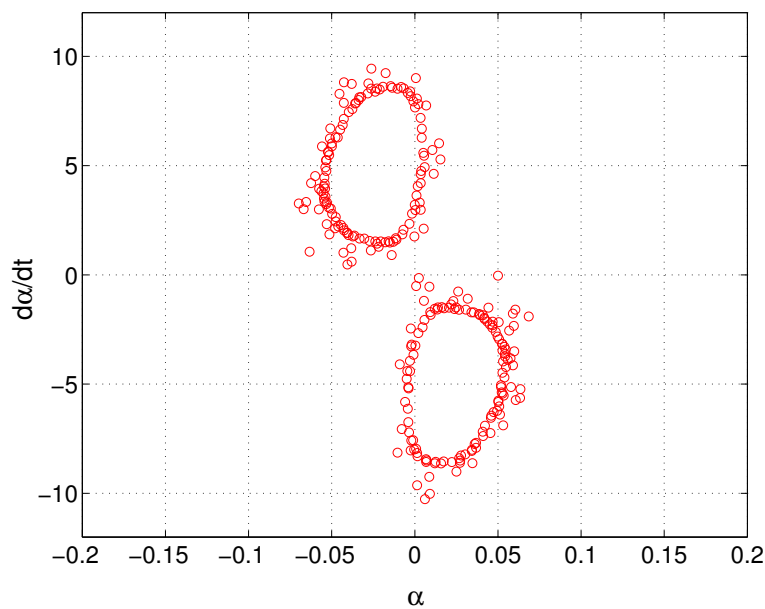


Fig. 51. Poincaré map for Case BT7 ($V_r = 0.89$)

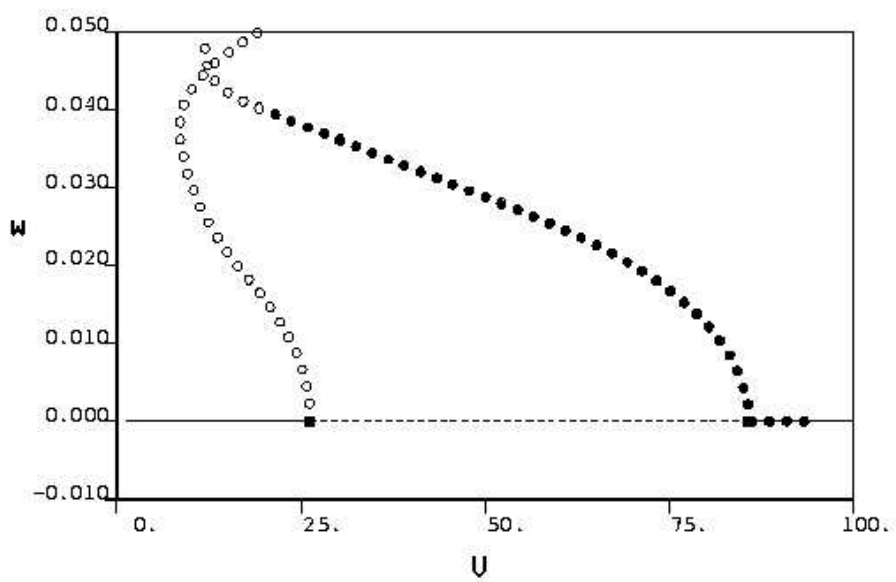


Fig. 52. Bifurcation diagram for a sample case (AUTO2000)

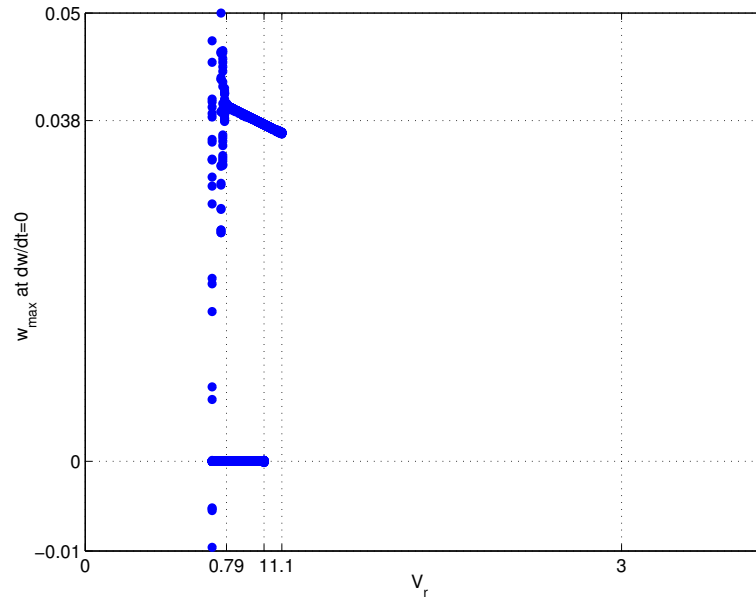


Fig. 53. Bifurcation diagram for a sample case (Poincare map)

and the stiffness ratio $\beta_z = 12^2$ are used in his analysis. The obtained flutter velocity is $V_F = 26.2$ m/sec. The y-axis is w_{max} . The filled square is a Hopf bifurcation which corresponds to the flutter velocity. In the bifurcation diagram, the Stable equilibrium points are denoted by the solid line, and the dashed line represents unstable equilibrium points. The maximum amplitude of response is given by circles. The filled circle represents stable periodic solution. The unstable solution is depicted by an empty circle. The corresponding bifurcation diagram of Poincare maps is depicted in Fig. 53. The x-axis is normalized by the flutter velocity ($V_F = 26.21$ m/sec) and the y-axis is w_{max} . The existence of stable periodic solutions below flutter velocity are confirmed by numerical simulation. For the velocity range $0.7 < V_r < 1.1$, the Poincare maps are appeared in the figure. Although the presented data are limited, it can be seen that their shapes are analogous to each other. The similarity is examined through the stable periodic solutions. For two specific velocity conditions $V = 24$ and 28 ,

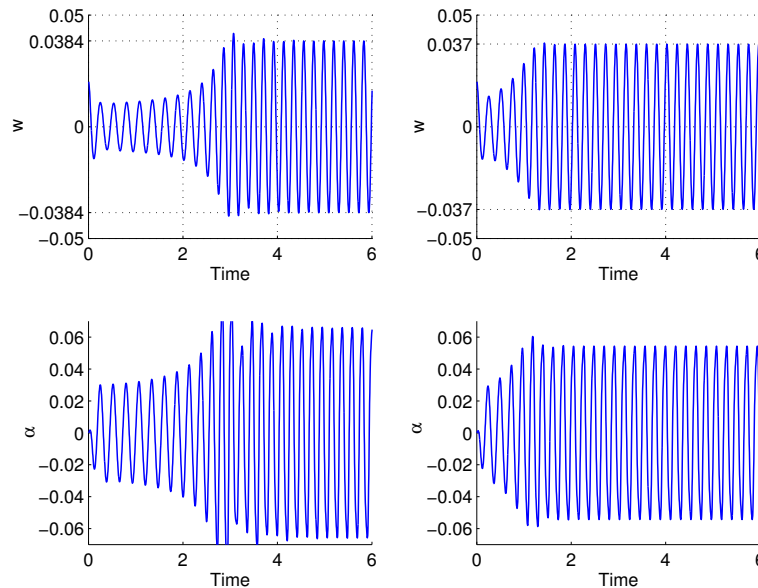


Fig. 54. Simulation results for a sample case: (a) $V=24\text{m/sec}$ (Left) (b) $V =28\text{m/sec}$ (right)

time histories are depicted in Fig. 54. According to Chetan,⁵² w_{max} at these velocity conditions, $V = 24$ and $V = 28$ are ‘0.0386’ and ‘0.0367’, respectively. The maximum amplitudes of w are ‘0.384($V=24$)’ and ‘0.037($V=28$)’. These amplitudes are almost same as those obtained by Chetan. Thus, it is shown that bifurcation analyses based on the numerical simulations and Poincaré maps may provide comparable results.

D. Effect of External Store

The effect of store parameters is investigated. The considered store parameters are store mass, inertia and positions. The store mass and inertia are expressed by using the wing mass term mL and wing inertia term I_yL , respectively. The store position x_s and z_s are scaled by the semi-chord length b . In this section, the reference store parameters are $M_s = 0.1mL$, $I_s y = 0.1I_yL$, $x_s = 0.0b$ and $z_s = 0.0b$. Only one store parameter is changed at a time.

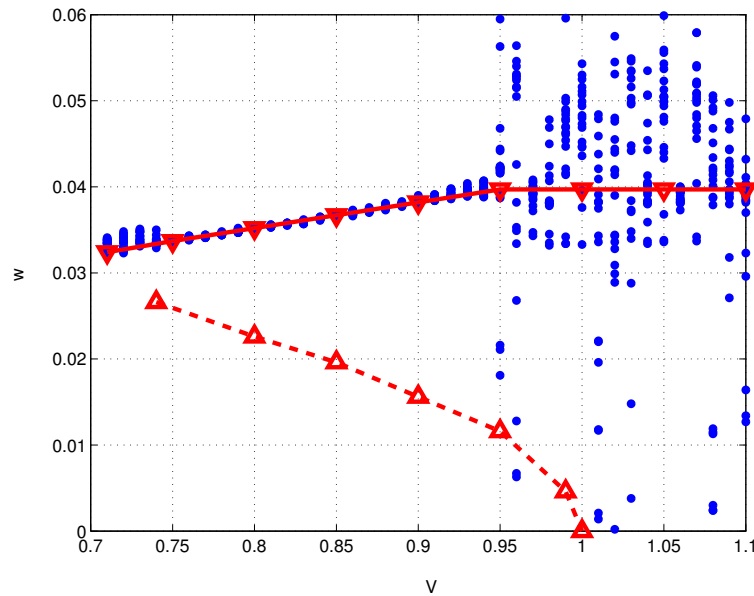


Fig. 55. Bifurcation diagram for Case BT7 ($x_s=0.5b$)

In order to investigate the effect of the store parameter, the bifurcation diagrams consisting of many points are simplified. For a case of $x_s = 0.5b$, a bifurcation diagram is shown in Fig. 55. In this figure, the original bifurcation diagram consists of dots and the simplified version is represented by lines with triangle symbols. Another dashed line showing unstable periodic solution is added in Fig. 55 to show the sub-critical bifurcation characteristics.

Using bifurcation data for some store mass conditions, a three-dimensional bifurcation diagram is generated as shown in Fig. 56. The two-dimensional bifurcation diagrams for several store masses are combined in this 3D bifurcation diagram by adding one more axis representing the store parameter. An underlying contour plot for the stable non-zero fixed points is also included in the diagram to further describe the characteristics of the bifurcation. Although the store mass is increased to

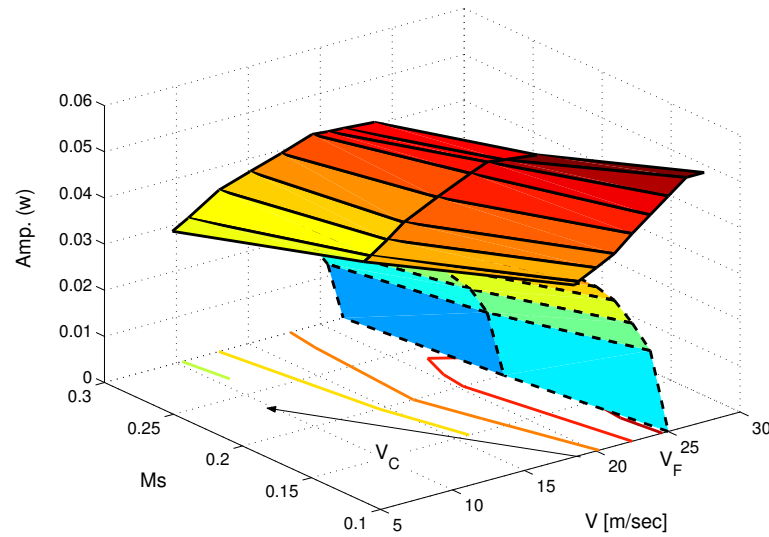


Fig. 56. Three dimensional bifurcation diagram for several store masses (BT7)

$M_s = 0.3mL$, the cross section of the bifurcation diagram for various store masses is similar. As shown in Fig. 56, the flutter velocity, V_F , is slightly reduced, but the V_C is moved to a relatively low velocity.

For an increase in store inertia (I_{sy}), the bifurcation pattern changes as shown in Fig. 57. Main bifurcation characteristics are changed. When the store inertia is increased, the velocities V_F and V_C increase. This result is opposite to that for the store mass (Fig. 56). The effects of the store positions of center of mass, x_s and z_s are depicted in Figs. 58 and 59, respectively. Regardless of the increased value, the amplitude is increased. When the store position z_s is changed from 0.0 to 0.5b, changes in V_C and V_F are too small to differentiate. For a change in the positive x_s , the velocities V_C and V_F decrease. Yet, they increase when the position has negative value. Depending upon the direction, the effects of x_s are reversed.

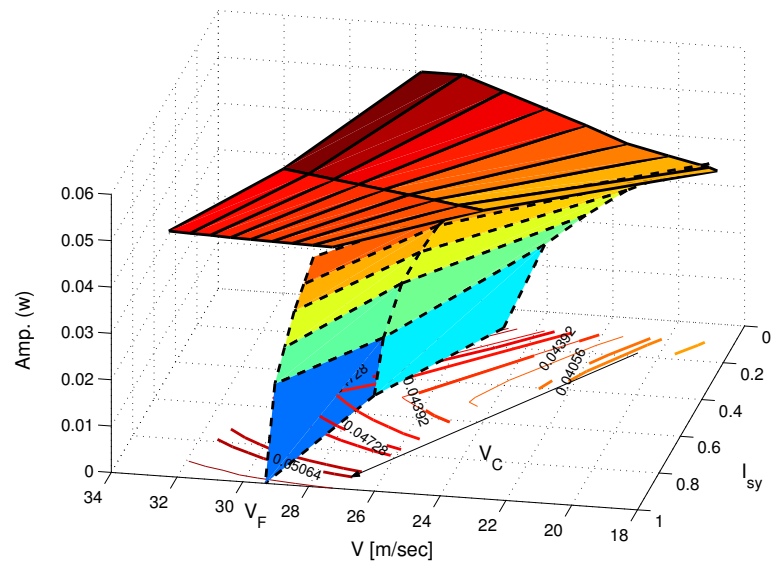


Fig. 57. Three dimensional bifurcation diagram for variation store inertia(BT7)

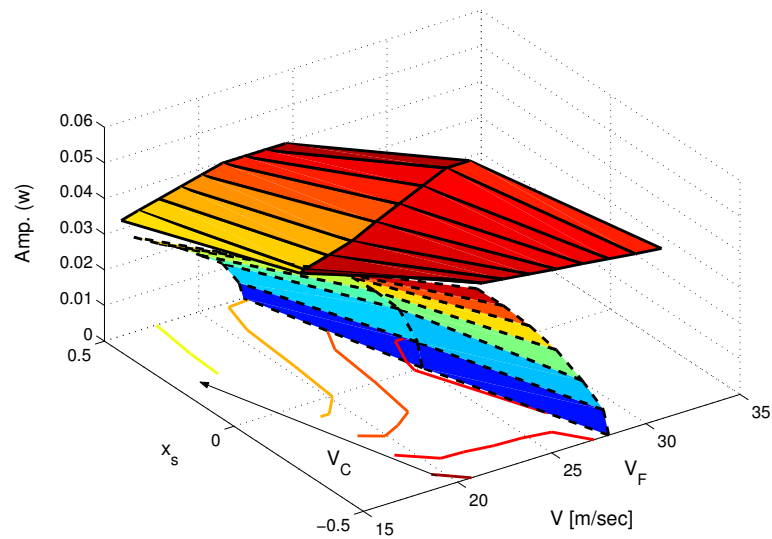


Fig. 58. Three dimensional bifurcation diagram for variation x_s (BT7)

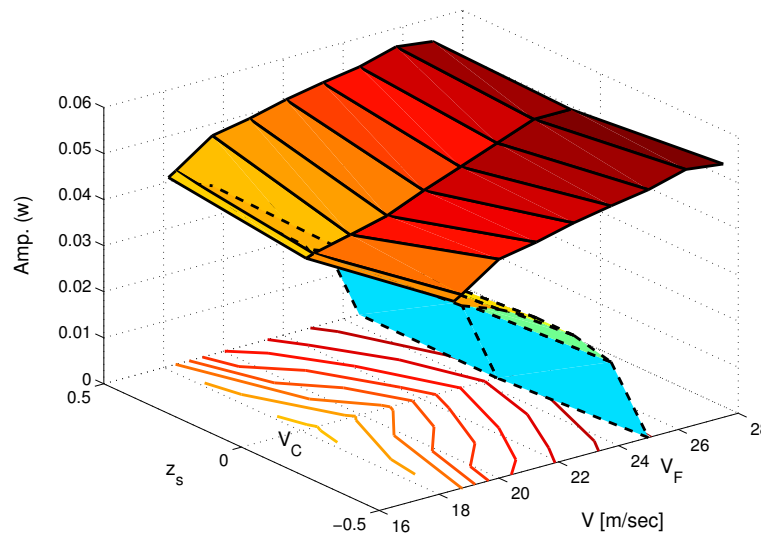


Fig. 59. Three dimensional bifurcation diagram for variation z_s (BT7))

E. Discussion

By using phase portrait and Poincaré maps, bifurcation diagrams are generated. The result is verified through a software package AUTO2000. Existing nonlinear aeroelastic literature dealing with a cantilever wing adopts either only quadratic nonlinearities or does not consider any external store in their systems. The cantilever wing model used in this dissertation has an external store, and cubic nonlinearities are included in the wing model. Interesting results are obtained using this model. The first meaningful result is the presence of a subcritical bifurcation. This result implies that LCO responses are possible at a velocity less than the flutter velocity and, depending upon the initial conditions, the nonlinear responses either decay to zero amplitude or migrate to other equilibrium points with non-zero amplitudes. There are limit cycle oscillations. Additional meaningful results are generated by the presence of store. Although store position z_s may show insignificant change in the subcritical bifurcation, the other parameters, such as M_s , I_{sy} and x_s , cause remarkable changes. When

the store mass, M_s is increased, LCOs are observed at relatively low velocity. But the opposite tendency is caused by an increase in store inertia, I_{sy} ; in which case LCOs occurred at relatively high velocity conditions. Depending upon the relative position (forward or aft of the elastic axis) of the store, x_s , the velocity at which LCOs are observed is increased or decreased. When x_s is forward, the velocity is increased, but the aft position reduces the velocity.

CHAPTER VI

BENDING-BENDING-TORSIONAL MOTION

Using the bending-bending-torsional (BBT) equations of motion derived in Chapter II, nonlinear responses of wing systems are investigated for nonlinearities up to the third order in this chapter. The wing, having three types of nonlinearities - structural, store kinematics and aerodynamic nonlinearities - is treated. In chapter V, the bending-torsion (BT) systems were considered. The BT systems having cubic nonlinearities do not have quadratic nonlinear coupling terms caused by wing flexibility. In this chapter the quadratic nonlinear terms are accounted for by including the in-plane bending motion into the BBT equations. The NATAm wing model is treated in this chapter. The model has linear store terms regardless of the store-induced nonlinearities. Two stiffness ratios considered in this chapter are $\beta_z = 44$ and $\beta_z = 10$. The effect of individual and combined nonlinearities are studied. For the system with only one type of nonlinearity, the possibility of internal resonance is examined by using the Method of Multiple Scales (MMS) and the effect of the velocity change is investigated through bifurcation diagrams. The bifurcation diagrams consist of Poincare maps obtained by the sampling rules $\dot{w} = 0.0$ and/or $\dot{\alpha} = 0.0$. The effect of store parameters such as M_s , I_{sy} , x_s , and z_s , are investigated. The effect of individual store parameter is different from each other. Sub-critical bifurcation is observed. Through this investigation, the dominant factor causing the LCOs at a velocity less than the linear flutter velocity is identified.

A. Systems with only Aerodynamic Nonlinearities

Aerodynamic nonlinearities are introduced by a stall model. Approximate solutions are obtained by using the Method of Multiple Scales, and response characteristics are

investigated through time simulations and a bifurcation diagram.

1. Equations of Motion

The equations of motion for a system with only aerodynamic nonlinearities are obtained from Eqs. (2.42), (2.43), and (2.44), by neglecting the store-induced and structural nonlinear terms.

$$C_{uw1}\ddot{u}_i + \beta_z C_{uw2}u_i = 0 \quad (6.1)$$

$$\begin{aligned} & C_{ww1}\ddot{w}_j - e^*\ddot{\alpha}_k + C_{wwq}w_j \\ & - \mu * V^* C_{wa1}\dot{\alpha}_k + \mu \frac{C_{L\alpha_k}}{\pi} V^* \left[\frac{1}{b^* V^*} \dot{w} - \alpha - V^* \left(\frac{1}{2} - a \right) \dot{\alpha}_k \right] \\ & = -\mu \frac{C_{L\alpha}}{\pi} V^{*2} c_3 \int_0^s W_r \alpha_{eff}^3 ds \end{aligned} \quad (6.2)$$

$$\begin{aligned} & C_{aw1}\ddot{\alpha}_k - \frac{e^*}{I_y^*} \ddot{w}_j + \frac{1}{I_y^*} \beta_y C_{aw2} \alpha_k - \frac{1}{I_y^*} \mu b^* \left(\frac{1}{2} - a \right) V^* C_{aa1} \dot{\alpha}_k \\ & + \frac{1}{I_y^*} \mu \frac{C_{m\alpha_k}}{\pi} V^{*2} \left[\frac{1}{V^*} C_{aa2} \dot{w} - C_{aa3} \alpha_k - b^* \left(\frac{1}{2} - a \right) \frac{1}{V^*} C_{aa4} \dot{\alpha} \right] \\ & = -\frac{1}{I_y^*} \mu \frac{C_{m\alpha}}{\pi} V^{*2} c_3 \int_0^1 \alpha_{eff}^3 ds \end{aligned} \quad (6.3)$$

The above equations can be rewritten in matrix form as follows,

$$[M]\{\ddot{q}\} + [C]\{\dot{q}\} + [K]\{q\} = \{NL_A\} \quad (6.4)$$

In these expressions, the nonlinear aerodynamics terms are included in the vector $\{NL_A\}$ on the right-hand side. The expression for these nonlinear terms is

$$\int_0^s W_r \alpha_{eff}^3 ds = C_{wa5}(\alpha^3)$$

$$\begin{aligned}
& + \frac{1}{V^*} \left[-3C_{wa6}\alpha\alpha\dot{w} + 3b^* \left(\frac{1}{2} - a \right) C_{wa7}\alpha\alpha\dot{\alpha} \right] \\
& + \frac{1}{V^{*2}} \left[3C_{wa8}\alpha\dot{w}\dot{w} - 6b^* \left(\frac{1}{2} - a \right) C_{wa9}\alpha\dot{\alpha}\dot{w} + 3b^{*2} \left(\frac{1}{2} - a \right)^2 C_{wa10}\alpha\dot{\alpha}\dot{\alpha} \right] \\
& + \frac{1}{V^{*3}} \left[-C_{wa11}\dot{w}\dot{w}\dot{w} + 3b^* \left(\frac{1}{2} - a \right) C_{wa12}\dot{\alpha}\dot{w}\dot{w} \right] \\
& + \frac{1}{V^{*3}} \left[-3b^{*2} \left(\frac{1}{2} - a \right)^2 C_{wa13}(\dot{\alpha}\dot{\alpha}\dot{w}) + b^{*3} \left(\frac{1}{2} - a \right)^3 C_{wa14}\dot{\alpha}^3 \right] \quad (6.5)
\end{aligned}$$

$$\begin{aligned}
\int_0^1 \alpha_{eff}^3 ds & = C_{aa5}(\alpha^3) \\
& + \frac{1}{V^*} \left[-3C_{aa6}\alpha\alpha\dot{w} + 3b^* \left(\frac{1}{2} - a \right) C_{aa7}\alpha\alpha\dot{\alpha} \right] \\
& + \frac{1}{V^{*2}} \left[3C_{aa8}\alpha\dot{w}\dot{w} - 6b^* \left(\frac{1}{2} - a \right) C_{aa9}\alpha\dot{\alpha}\dot{w} + 3b^{*2} \left(\frac{1}{2} - a \right)^2 C_{aa10}\alpha\dot{\alpha}\dot{\alpha} \right] \\
& + \frac{1}{V^{*3}} \left[-C_{aa11}\dot{w}\dot{w}\dot{w} + 3b^* \left(\frac{1}{2} - a \right) C_{aa12}\dot{\alpha}\dot{w}\dot{w} \right] \\
& + \frac{1}{V^{*3}} \left[-3b^{*2} \left(\frac{1}{2} - a \right)^2 C_{aa13}(\dot{\alpha}\dot{\alpha}\dot{w}) + b^{*3} \left(\frac{1}{2} - a \right)^3 C_{aa14}\dot{\alpha}^3 \right] \quad (6.6)
\end{aligned}$$

As suggested by these equations, the aerodynamic loads considered in this section do not provide any aerodynamic force related to the in-plane motion. Thus, there is no interaction between the in-plane motion and other motions. Therefore, the in-plane motion is excluded in the following analysis by the Method of Multiple Scales since the response is simply one degree of freedom response due to an initial condition.

In order to uncouple the linear mass and stiffness matrices, higher order terms and damping terms in Eq. (6.4) are relocated to the right-hand side as follows,

$$[M]\{\ddot{q}\} + [K]\{q\} = -[C]\{\dot{q}\} + \{NL_A\} \quad (6.7)$$

2. Analysis by the Method of Multiple Scales

Because there is no coupling with the in-plane motion, the simplified modal matrix is obtained from Eq. (4.19 by removing the column and row associated with the in-plane bending motion as follows,

$$[P_2] = \begin{bmatrix} 1 & 1 \\ 0 & \tau \end{bmatrix} \quad (6.8)$$

Using the simplified modal matrix, $[P_2]$ Eq. (6.7) is rewritten.

$$[I]\{\ddot{\eta}\} + [\Lambda]\{\eta\} = -[P_2]^{-1}[C][P_2]\{\dot{\eta}\} + [P_2]^{-1}\{NL_A(\eta)\} \quad (6.9)$$

The linear terms are already determined, thus, the nonlinear aerodynamic terms are developed in this section. The linear damping terms placed on the right-hand side are perturbed as follows,

$$[I]\{\ddot{\eta}\} + [\Lambda]\{\eta\} = -\epsilon^2[P_2]^{-1}[C][P_2]\{\dot{\eta}\} + [P_2]^{-1}\{NL_A(\eta)\} \quad (6.10)$$

and included in the first non-homogeneous expression with $O(\epsilon^3)$. A new independent variable $T_n = \epsilon^n t$, and a notation $D_n = \partial/\partial T_n$, are introduced to obtain approximate solutions. The time derivatives with respect to 't' are rewritten in terms of partial derivatives with respect to the new variable T_n , such that

$$\begin{aligned} \frac{d}{dt} &= \frac{dT_0}{dt} \frac{\partial}{\partial T_0} + \frac{dT_1}{dt} \frac{\partial}{\partial T_1} + \dots = D_0 + \epsilon D_1 + \epsilon^2 D_2 + \dots \\ \frac{d^2}{dt^2} &= D_0^2 + 2\epsilon D_0 D_1 + \epsilon^2 (D_1^2 + 2D_0 D_2) \end{aligned} \quad (6.11)$$

Because all nonlinear terms are cubic, the approximate solution can be expressed in the form

$$\eta = \epsilon \eta_1(T_0, T_2, \dots) + \epsilon^3 \eta_3(T_0, T_2, \dots) + \dots \quad (6.12)$$

Substituting the new variable, T_n , and Eq. (6.12), and applying Eq. (6.11), we get the following expression,

$$\begin{pmatrix} \epsilon ([I]\{\ddot{\eta}_1\} + [\Lambda]\{\eta_0\}) \\ \epsilon^3 ([I]\{\ddot{\eta}_3\} + [\Lambda]\{\eta_2\}) \end{pmatrix} = -\epsilon^3 \left([P_2]^{-1}[C][P_2]\{\dot{\eta}_0\} + [P_2]^{-1}\{NL_A(\eta_0)\} \right) \quad (6.13)$$

Equating terms of the same order of ϵ , two sets of order equations are obtained as

Order(ϵ^1):

$$[I]\{\ddot{\eta}_1\} + [\Lambda]\{\eta_1\} = 0 \quad (6.14)$$

Order(ϵ^3):

$$[I]\{\ddot{\eta}_3\} + [\Lambda]\{\eta_3\} = [P_2]^{-1}[C][P_2]\{\dot{\eta}_1\} + [P_2]^{-1}\{NL_A(\eta_1)\} \quad (6.15)$$

As shown in these equations, the solution of Eq. (6.14) can be written in the following form because the lowest order equation Eq. (6.14), is homogeneous.

$$\eta_{1k} = A_k(T_2)e^{i\omega_k T_0} + \bar{A}_k(T_2)e^{-i\omega_k T_0} \quad (6.16)$$

Because the right-hand side of the first non-homogeneous order equation, Eq. (6.15) consists of η_{1k} , the right-hand side of Eq. (6.15) can be rewritten.

Equations (6.5) and (6.6) are modified as follows,

$$\begin{aligned} \int_0^1 W_r \alpha_{eff}^3 ds &= C_{www1}^w e^{i3\omega_w T_0} + C_{www2}^w e^{i\omega_w T_0} \\ &+ C_{ww\alpha 1}^w e^{i(\omega_\alpha + 2\omega_w)T_0} + C_{ww\alpha 2}^w e^{i\omega_\alpha T_0} + C_{ww\alpha 3}^w e^{i(\omega_\alpha - 2\omega_w)T_0} \\ &+ C_{w\alpha\alpha 1}^w e^{i(2\omega_\alpha + \omega_w)T_0} + C_{w\alpha\alpha 2}^w e^{i\omega_w T_0} + C_{w\alpha\alpha 3}^w e^{i(-2\omega_\alpha + \omega_w)T_0} \\ &+ C_{\alpha\alpha\alpha 1}^w e^{i3\omega_\alpha T_0} + C_{\alpha\alpha\alpha 2}^w e^{i\omega_\alpha T_0} \end{aligned} \quad (6.17)$$

$$\begin{aligned}
\int_0^1 A_r \alpha_{eff}^3 ds &= C_{www1}^\alpha e^{i3\omega_w T_0} + C_{www2}^\alpha e^{i\omega_w T_0} \\
&+ C_{ww\alpha1}^\alpha e^{i(\omega_\alpha + 2\omega_w)T_0} + C_{ww\alpha2}^\alpha e^{i\omega_\alpha T_0} + C_{ww\alpha3}^\alpha e^{i(\omega_\alpha - 2\omega_w)T_0} \\
&+ C_{w\alpha\alpha1}^\alpha e^{i(2\omega_\alpha + \omega_w)T_0} + C_{w\alpha\alpha2}^\alpha e^{i\omega_w T_0} + C_{w\alpha\alpha3}^\alpha e^{i(-2\omega_\alpha + \omega_w)T_0} \\
&+ C_{\alpha\alpha\alpha1}^\alpha e^{i3\omega_\alpha T_0} + C_{\alpha\alpha\alpha2}^\alpha e^{i\omega_\alpha T_0}
\end{aligned} \tag{6.18}$$

For a case of $A_k = \text{constant}$, the corresponding particular solutions are assumed as

$$\begin{aligned}
\eta_{w1p} &= g_{w1} e^{i\omega_w T_0} + g_{w2} e^{i3\omega_w T_0} + g_{w3} e^{i(\omega_w + 2\omega_\alpha)T_0} + g_{w4} e^{i(\omega_\alpha + 2\omega_w)T_0} \\
&+ g_{w5} e^{i(\omega_w - 2\omega_\alpha)T_0} + g_{w6} e^{i(\omega_\alpha - 2\omega_w)T_0} + g_{w7} e^{i3\omega_\alpha T_0} + g_{w8} e^{i\omega_\alpha T_0}
\end{aligned} \tag{6.19}$$

$$\begin{aligned}
\eta_{\alpha1p} &= g_{\alpha1} e^{i\omega_w T_0} + g_{\alpha2} e^{i3\omega_w T_0} + g_{\alpha3} e^{i(\omega_w + 2\omega_\alpha)T_0} + g_{\alpha4} e^{i(\omega_\alpha + 2\omega_w)T_0} \\
&+ g_{\alpha5} e^{i(\omega_w - 2\omega_\alpha)T_0} + g_{\alpha6} e^{i(\omega_\alpha - 2\omega_w)T_0} + g_{\alpha7} e^{i3\omega_\alpha T_0} + g_{\alpha8} e^{i\omega_\alpha T_0}
\end{aligned} \tag{6.20}$$

where g_{qi} are constant coefficients of the particular solutions. Substituting these assumed solutions into the left hand side of Eq. (6.15) and equating terms of the same exponential components, we can determine the coefficients of the assumed solutions. As shown in the denominator (as singularities) of the following expression, some coefficients may contribute to internal resonance mechanism.

$$\begin{aligned}
g_{w5} &= \frac{1}{(\omega_\alpha - \omega_w)(\omega_\alpha - 3\omega_w)} c_3^w C_{ww\alpha3}^w \\
g_{w7} &= \frac{1}{(\omega_w + 3\omega_\alpha)(\omega_w - 3\omega_\alpha)} c_3^w C_{\alpha\alpha\alpha1}^w \\
g_{\alpha2} &= \frac{1}{(\omega_\alpha + 3\omega_w)(\omega_\alpha - 3\omega_w)} c_3^\alpha C_{www1}^\alpha \\
g_{\alpha6} &= \frac{1}{(\omega_w - \omega_\alpha)(\omega_w - 3\omega_\alpha)} c_3^\alpha C_{w\alpha\alpha3}^\alpha
\end{aligned} \tag{6.21}$$

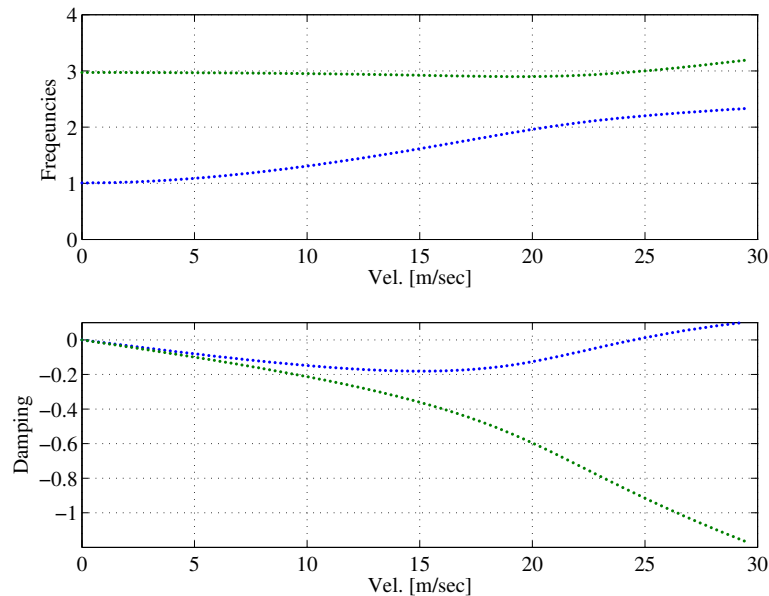


Fig. 60. V-f and V-g plots for a wing with an external store (BBT1)

where c_3^w and c_3^α are functions of system parameters. This equation shows that there are at least two possible internal resonance (IR) conditions, $\omega_\alpha : \omega_w = 1 : 3$ and $\omega_\alpha : \omega_w = 3 : 1$.

3. Numerical Simulations and Bifurcation Analysis

Time simulation is performed to study the effects of nonlinear aerodynamic terms. In this section, the possibility of 3:1 IR and additional response characteristics are studied. One reference wing based on NATAm having a store is considered. The wing model is named ‘BBT1’. The store parameters are $M_s = 0.1mL$, $I_{sy} = 0.1I_yL$, and $x_s = z_s = 0.0$. The stiffness ratio, β_z , is ‘44’. V-f and V-g plots are presented in Fig. 60. For this case, $V_F = 24.5102$ m/sec. As shown in this figure, the maximum frequency ratio ω_w/ω_α is 2.7 and the maximum occurs at $V=0$. Because the ratio is less than 3 and $\omega_w > \omega_\alpha$, internal resonance is not present in this wing model.

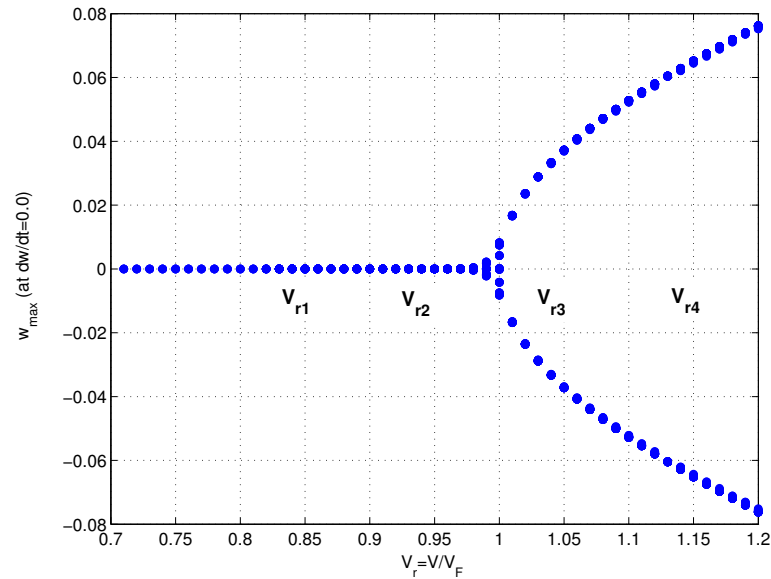


Fig. 61. Bifurcation diagram for a wing with aerodynamic nonlinearities (w_{max})

Bifurcation analysis is performed. Using the Poincare map, bifurcation diagrams are obtained. Because the aeroelastic system considered is autonomous, there is not any specified sampling condition. Therefore, two sampling conditions, $\partial w/\partial t = 0.0$ and $\partial \alpha/\partial t = 0.0$, are applied, and the corresponding bifurcation diagrams are shown in Figs. 61 and 62, respectively. It can be seen from these figures that there are two fixed points for $Vr = V/V_f > 1.0$ and there is only one fixed point for $Vr < 1.0$. In the region of $Vr > 1.0$, the two fixed points are symmetric with respect to the x-axis and they have a non-zero value. In the other region, $Vr < 1.0$, the only fixed point has the value of zero.

The two sampling conditions are investigated through an example in detail. For a velocity condition, $Vr = 1.1 > 1.0$, a part of the time histories is shown in Fig. 63. In this figure, the amplitudes corresponding to two sampling conditions are C_{Fw1} and $A_{F\alpha 1}$. If a sampling condition, $\partial w/\partial t = 0.0$, is applied to the torsional motion,

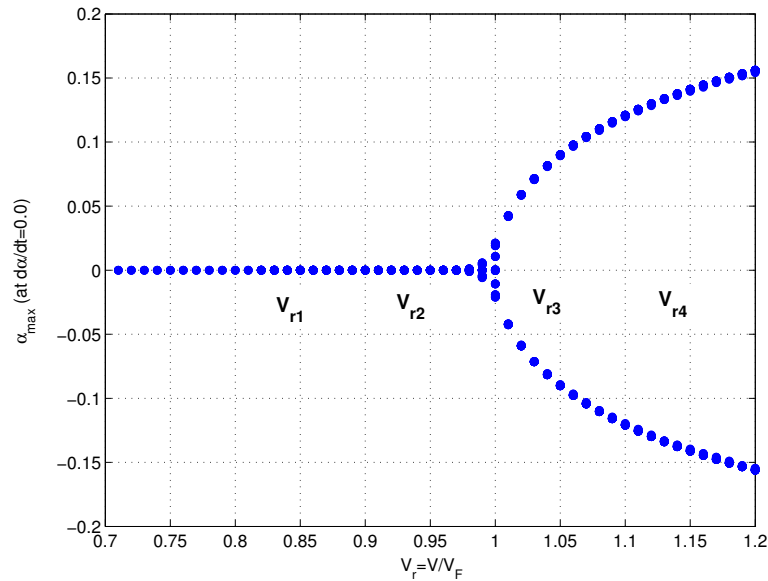


Fig. 62. Bifurcation diagram for a wing with aerodynamic nonlinearities (a_{max})

the corresponding point is A_{Fw1} . As shown in this figure, the two points, $A_{F\alpha1}$ and A_{Fw1} , have slightly different values. This means that the bending motion and the torsional motion have a small phase angle. The corresponding phase portrait and Poincare maps are shown in Fig. 64. The fixed points indicated by $A_{F\alpha1}$, B_{Fw1} , $B_{F\alpha1}$ and A_{Fw1} are the same as those in Fig. 63. The fixed points corresponding to the sampling rules are different from each other. This result shows that the two sampling rules are not satisfied simultaneously. The other points in the phase plane are not fixed points because they are not repeated. Depending upon the the sampling rule, two different symbols, 'O' and ' \diamond ', are adopted. In order to identify the relative motion between the bending and torsional motions, two responses for these two motions are examined in the time history. But, in the phase plane, the relative motion is identified by applying a different sampling rule. For example, when a sampling rule, $dw/dt = 0$, is applied to the torsional motion, the corresponding fixed points have non-zero $\dot{\alpha}$ as indicated by A_{Fw1} and B_{Fw1} in Fig. 64. For a bounded response, there

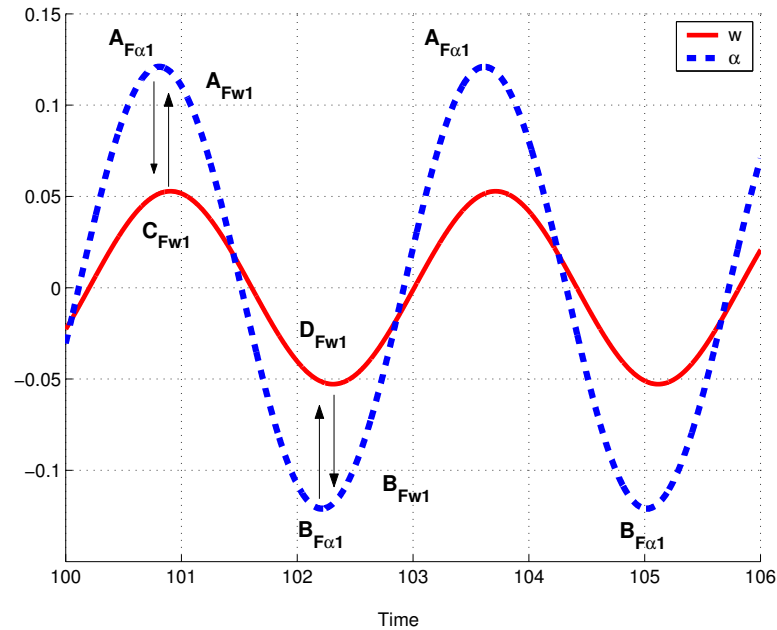


Fig. 63. Time histories for a wing with aerodynamic nonlinearities ($V_r=1.1$)

is a pair of fixed points because there are two cases satisfying the sampling conditions; one case occurs when $d()/dt$ changes from ‘positive’ to ‘negative’ and the other case occurs when the sign is reversed. For another velocity condition, $V_r = 0.85 < 1.0$, the responses are simple, as shown in Fig. 65. There is only one fixed point, and this is zero. As shown in these phase plane, the motion in the upper half-plane, $y = \dot{\alpha} > 0$, must proceed to the right because the variable in x-axis (α) must increase in time for $\dot{\alpha} > 0$, and vice versa for $\dot{\alpha} < 0$.⁵³ This is valid for the case $d\alpha/dt = y$. If $d\alpha/dt = -y$ is adopted, then the direction must be reversed.

For a set of velocity conditions, the change of frequency content is shown in Fig. 66. The aeroelastic frequencies are indicated by ‘P1’, ‘P2’, and ‘P3’ which correspond to the out-of-bending, torsion, and in-plane bending frequencies, respectively. For a case of $V_r = 0.85$, these components could be identified. In figure 66 (a), ‘P1’, ‘P2’,

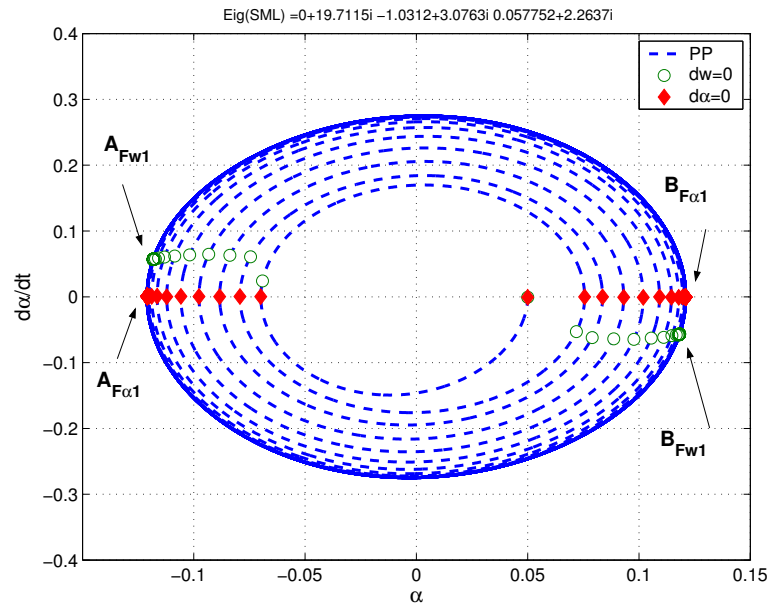


Fig. 64. Phase portrait and Poincaré maps for a wing with aerodynamic nonlinearities ($V_r=1.1$)

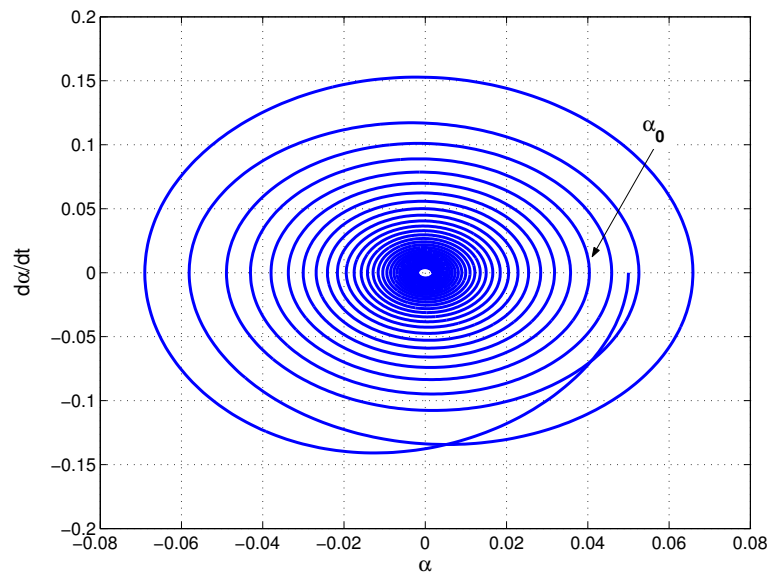


Fig. 65. Phase portrait and Poincaré maps for a wing with aerodynamic nonlinearities ($V_r=0.9$)

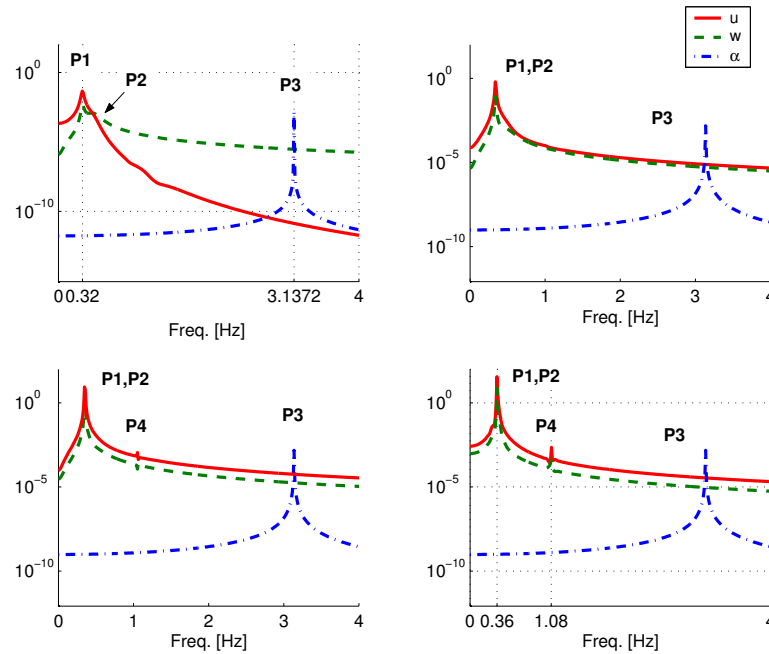


Fig. 66. FFT for a wing with aerodynamic nonlinearities: (a) $V_r=0.85$ (Left, Upper), (b) $V_r=0.95$ (Right, Upper), (c) $V_r=1.05$ (Left, Lower), (d) $V_r=1.15$ (Right, Lower)

and ‘P3’ are 0.32, 0.46, and 3.13 Hz. As velocity increases, the strength of ‘P2’ is weakened. For $V_r > 1.0$ (see (c) and (d) in Fig. 66), there is another component, ‘P4’, which corresponds to ‘ $3 \times P1$ ’. This kind of component could be caused by the cubic term included in the stall nonlinearities. This result shows that the stall nonlinearity contributes to the limit cycle oscillation at $V_r > 0$.

B. Systems with Structural Nonlinearities

For the second case of bending-bending-torsional systems, a system with only structural nonlinearities is considered. This system has both quadratic and cubic nonlinearities.

1. Equations of Motion

The equations of motion are obtained from Eqs. (2.42), (2.43), and (2.44) by neglecting the store-induced and aerodynamic nonlinear terms. The equations of motion for the system are expressed in matrix form.

$$[M]\{\ddot{q}\} + [C]\{\dot{q}\} + [K]\{q\} = \{G_{q0}\} \quad (6.22)$$

where,

$$[M] = \begin{bmatrix} C_{uw1} & 0 & 0 \\ 0 & C_{ww1} & -e^*C_{uw21} \\ 0 & -\frac{e^*}{I_y^*}C_{aw21} & C_{aw1} \end{bmatrix} \quad (6.23)$$

$$[C] = \begin{bmatrix} 0 & 0 & 0 \\ 0 & \mu\frac{C_{L\alpha}}{\pi}C_{uw1} & -\mu V^*C_{wa1} - \mu\frac{C_{L\alpha}}{\pi}V^{*2}\left(\frac{1}{2} - a\right)C_{wa4} \\ 0 & \mu\frac{1}{I_y^*}\frac{C_{m\alpha}}{\pi}V^*C_{aa2} & -\frac{1}{I_y^*}(C_{aa1} + C_{m\alpha}\pi C_{aa4})\mu V^{*2}b^*\left(\frac{1}{2} - a\right) \end{bmatrix} \quad (6.24)$$

$$[K] = \begin{bmatrix} \beta_z C_{uw2} & 0 & 0 \\ 0 & C_{ww2} & -\mu\frac{C_{L\alpha}}{\pi}V^*C_{ww2} \\ 0 & 0 & \frac{1}{I_y^*}\left(\beta_y C_{aw2} - \mu\frac{C_{M\alpha}}{\pi}V^{*2}C_{aa3}\right) \end{bmatrix} \quad (6.25)$$

The structural nonlinear terms are included in $\{G_{q0}\}$. In order to distinguish these nonlinear terms from the entire combination of nonlinear expressions, an additional subscript '0' is added. The detail components are

$$\begin{aligned} G_{u0} &= \beta_y C_{uw3}\alpha_k w_j - \beta_z [C_{uw4}u_i u_p u_q + C_{uw5}u_i w_j w_p] \\ &+ (\beta_z - 1) [(C_{uw6}w_j \alpha_k + C_{uw7}u_i \alpha_k \alpha_p) - C_{uw8}w_j u_i w_p] + I_z^* C_{uw9}\ddot{u}_i \\ &- [C_{uw10}u_i (\ddot{w}_j w_p + \dot{w}_j \dot{w}_p) + C_{uw11}u_i (\ddot{u}_p u_q + \dot{u}_p \dot{u}_q)] \\ &+ e^* C_{uw21}u_i \ddot{u}_p \end{aligned}$$

$$+e^* \left[\frac{1}{2} (C_{uw22} \alpha_k \ddot{\alpha}_p - C_{uw23} w_j \ddot{w}_p) - C_{uw24} u_i \ddot{u}_p - C_{uw25} w_j \ddot{w}_p \right] \quad (6.26)$$

$$\begin{aligned} G_{w0} &= -\beta_y C_{ww3} (\alpha_k u_i) - [C_{ww4} w_j (w_p w_q) + C_{ww5} w_j (u_i u_p)] \\ &+ (\beta_z - 1) [(C_{ww6} u_i \alpha_k - C_{ww7} w_j \alpha_k \alpha_p) - C_{ww8} u_i w_j u_p] + I_z^* C_{ww9} \ddot{w}_j \\ &- [C_{ww10} w_j (\ddot{w}_p w_q + \dot{w}_p \dot{w}_q) + C_{ww11} w_j (\ddot{u}_i u_p + \dot{u}_i \dot{u}_p)] - e^* C_{ww22} w_j \ddot{u}_i \\ &- e^* C_{ww23} u_i \ddot{w}_j \end{aligned} \quad (6.27)$$

$$\begin{aligned} G_{a0} &= -\frac{1}{I_y^*} (\beta_z - 1) [(C_{aw3} w_j w_p - C_{aw4} u_i u_p) \alpha_k - C_{aw5} w_j u_i] \\ &+ \frac{1}{I_y^*} I_y^* [C_{aw6} (\ddot{w}_j u_i + 2\dot{w}_j \dot{u}_i + w_j \ddot{u}_i) - C_{aw7} (\dot{w}_j \dot{u}_i + \ddot{w}_j u_i)] \\ &+ \frac{1}{I_y^*} (I_z^* - I_x^*) [(C_{aw8} \dot{w}_j \dot{w}_p - C_{aw9} \dot{u}_i \dot{u}_p) \alpha_k - C_{aw10} \dot{u}_i \dot{w}_j] \\ &+ \frac{1}{I_y^*} \frac{1}{2} e^* [-\ddot{w}_j (C_{aw22} w_p w_q + C_{aw23} \alpha_k \alpha_p) + C_{aw24} w_j \ddot{w}_p w_q + C_{aw25} u_i \ddot{u}_p] \\ &+ \frac{1}{I_y^*} e^* \ddot{u}_i (C_{aw26} \alpha_k - C_{aw27} u_p w_j) \end{aligned} \quad (6.28)$$

In the above expressions, the coefficient terms such as C_{uw3} , and C_{aw27} are defined in Appendix A.

2. Analysis by the Method of Multiple Scales

In order to obtain approximate solutions, linear damping terms are relocated in the right-hand side as

$$[M]\{\ddot{q}\} + [K]\{q\} = -[C]\{\dot{q}\} + \{G_{q0}\} \quad (6.29)$$

In order that the lowest order equations are homogeneous, the matrices on the left-hand side are uncoupled using the modal matrix, $[P]$, shown in Chapter III. In this

process, the coordinates are also transformed as follows,

$$\{q\} = [P]\{\eta\}$$

Eq. (6.29) is pre-multiplied by $[P]^{-1}$. The uncoupled equations of motion are

$$[I]\{\ddot{\eta}\} + [\Lambda]\{\eta\} = -[P]^{-1}[C][P]\{\dot{\eta}\} + [P]^{-1}\{G_\eta\} \quad (6.30)$$

The nonlinear terms are rewritten using Eqs. (6.26) ~ (6.28).

$$[P]^{-1}\{G_\eta\} = \begin{Bmatrix} G_{u0} \\ G_{w0} - \frac{1}{\tau}G_{a0} \\ \frac{1}{\tau}G_{a0} \end{Bmatrix} \quad (6.31)$$

For simplicity, it is assumed that the nonlinear effect of nonlinear inertia terms can be neglected. Because Crespo da Silva and Glynn²⁸ mentioned that the nonlinear curvature terms are more important than the nonlinear inertia term in their study, this type of assumption may be possible. Based on this assumption, the time derivatives terms are removed and the following simplified expressions are obtained.

$$\begin{aligned} G_{u0}^s &= \beta_y C_{uw3} \alpha_k w_j - \beta_z [C_{uw4} u_i u_p u_q + C_{uw5} u_i w_j w_p] \\ &+ (\beta_z - 1) [(C_{uw6} w_j \alpha_k + C_{uw7} u_i \alpha_k \alpha_p) - C_{uw8} w_j u_i w_p] \end{aligned} \quad (6.32)$$

$$\begin{aligned} G_{w0}^s &= -\beta_y C_{ww3} (\alpha_k u_i) - [C_{ww4} w_j (w_p w_q) + C_{ww5} w_j (u_i u_p)] \\ &+ (\beta_z - 1) [(C_{ww6} u_i \alpha_k - C_{ww7} w_j \alpha_k \alpha_p) - C_{ww8} u_i w_j u_p] \end{aligned} \quad (6.33)$$

$$G_{a0}^s = -\frac{1}{I_y^*} (\beta_z - 1) [(C_{aw3} w_j w_p - C_{aw4} u_i u_p) \alpha_k - C_{aw5} w_j u_i] \quad (6.34)$$

Because these expressions are simplified, the superscript ‘s’ is introduced. Applying the coordinate transformation to these expressions gives

$$\begin{aligned}
G_{u0}^s(\eta) &= \beta_y C_{uw3} \tau \eta_\alpha (\eta_w + \eta_\alpha) - \beta_z \left[C_{uw4} \eta_u^3 + C_{uw5} \eta_u (\eta_w + \eta_\alpha)^2 \right] \\
&\quad + (\beta_z - 1) \left[\left(C_{uw6} (\eta_w + \eta_\alpha) \tau \eta_\alpha + C_{uw7} \eta_u \tau^2 \eta_\alpha^2 \right) - C_{uw8} (\eta_w + \eta_\alpha)^2 \eta_u \right]
\end{aligned} \tag{6.35}$$

$$\begin{aligned}
G_{w0}^s(\eta) &= -\beta_y C_{ww3} (\tau \eta_\alpha \eta_u) - \left[C_{ww4} (\eta_w + \eta_\alpha) + C_{ww5} (\eta_w + \eta_\alpha) \eta_u^2 \right] \\
&\quad + (\beta_z - 1) \left[\left(C_{ww6} \eta_u \tau \eta_\alpha - C_{ww7} (\eta_w + \eta_\alpha) \tau^2 \eta_\alpha^2 \right) - C_{ww8} \eta_u^2 (\eta_w + \eta_\alpha) \right]
\end{aligned} \tag{6.36}$$

$$G_{\alpha 0}^s(\eta) = -\frac{1}{I_y^*} (\beta_z - 1) \left[\left(C_{aw3} (\eta_w + \eta_\alpha)^2 - C_{aw4} \eta_u \right) \tau \eta_\alpha - C_{aw5} (\eta_w + \eta_\alpha) \eta_u \right] \tag{6.37}$$

Introducing a new independent parameter $T_n = \epsilon^n t$ and a notation $D_n = \partial / \partial T_n$ gives

$$[I]\{\ddot{\eta}\} + [\Lambda]\{\eta\} = -[\bar{C}]\{\dot{\eta}\} + [T]^{-1}\{NL_w(\eta)\} \tag{6.38}$$

where $\{NL_w(\eta)\}$ represents structural nonlinearities. Because the nonlinear vector consists of quadratic and cubic nonlinearities, the first non-homogeneous order equations having $Order(\epsilon^n)$ for $n \neq 1$ may have different terms depending upon the adopted time scales. As the first case, the approximate solution can be expressed as follows,

$$\eta = \epsilon \eta_0(T_0, T_1, T_2, \dots) + \epsilon^2 \eta_1(T_0, T_1, T_2, \dots) + \epsilon^3 \eta_2(T_0, T_1, T_2, \dots) + \dots \tag{6.39}$$

When this approximation is applied, the first non-homogeneous order equations having $Order(\epsilon^2)$ consist of only quadratic nonlinearities, not cubic terms. In the second

case, the ϵ^2 terms are removed from Eq.(6.39). In this case, the quadratic nonlinear terms could not be included in the order equations corresponding to $Order(\epsilon)$ and $Order(\epsilon^3)$. In the Method of Multiple Scales, the approximation solutions are specified in the first non-homogeneous order equation. In order to include both quadratic and cubic nonlinearities into the first non-homogeneous order equation, the quadratic nonlinear terms and the linear damping terms should be perturbed by ϵ and ϵ^2 , respectively. After that, the approximate solution is assumed as

$$\eta = \epsilon\eta_0(T_0, T_1, T_2, \dots) + \epsilon^3\eta_2(T_0, T_1, T_2, \dots) + \dots \quad (6.40)$$

Substituting this approximation into Eq.(6.41) gives

$$\begin{aligned} [I]\{\ddot{\eta}_0\} + [\Lambda]\{\eta_0\} \\ + \epsilon^3[I]\{\ddot{\eta}_2\} + \epsilon^3[\Lambda]\{\eta_2\} = -\epsilon^3[\bar{C}]\{\dot{\eta}_0\} + \epsilon^3[T]^{-1}\{NL_w(\eta_0)\} \end{aligned} \quad (6.41)$$

Equating terms of the same order of ϵ leads to the following equations.

$Order(\epsilon)$:

$$D_0^2\ddot{\eta}_{u0} + \omega_u^2\eta_{u0} = 0 \quad (6.42)$$

$$D_0^2\ddot{\eta}_{w0} + \omega_w^2\eta_{w0} = 0 \quad (6.43)$$

$$D_0^2\ddot{\eta}_{\alpha 0} + \omega_\alpha^2\eta_{\alpha 0} = 0 \quad (6.44)$$

$Order(\epsilon^3)$:

$$D_0^2\ddot{\eta}_{u2} + \omega_u^2\eta_{u2} = G_{u0}^s \quad (6.45)$$

$$D_0^2\ddot{\eta}_{w2} + \omega_w^2\eta_{w2} = -\bar{C}_{22}\eta_{w0} - \bar{C}_{23}\eta_{\alpha 0} + G_{w0}^s - \frac{1}{\tau}G_{\alpha 0}^s \quad (6.46)$$

$$D_0^2\ddot{\eta}_{\alpha 2} + \omega_\alpha^2\eta_{\alpha 2} = -\bar{C}_{32}\eta_{w0} - \bar{C}_{33}\eta_{\alpha 0} + \frac{1}{\tau}G_{\alpha 0}^s \quad (6.47)$$

where the nonlinear terms are expressed as follows,

$$\begin{aligned}
G_{u0}^s &= \beta_y C_{uw3} \tau (\eta_{\alpha 0} \eta_{w0} + \eta_{\alpha 0}^2) \\
&\quad - \beta_z [C_{uw4} \eta_{w0}^3 + C_{uw5} (\eta_{u0} \eta_{w0}^2 + 2\eta_{u0} \eta_{w0} \eta_{\alpha 0} + \eta_{u0} \eta_{\alpha 0}^2)] \\
&\quad + (\beta_z - 1) \begin{pmatrix} C_{uw6} \tau (\eta_{\alpha 0} \eta_{w0} + \eta_{\alpha 0}^2) + C_{uw7} \tau^2 \eta_{u0} \eta_{\alpha 0}^2 \\ -C_{uw8} (\eta_{u0} \eta_{w0}^2 + 2\eta_{u0} \eta_{w0} \eta_{\alpha 0} + \eta_{u0} \eta_{\alpha 0}^2) \end{pmatrix} \quad (6.48)
\end{aligned}$$

$$\begin{aligned}
G_{w0}^s &= -\beta_y C_{ww3} \tau (\eta_{\alpha 0} \eta_{u0}) \\
&\quad - \begin{pmatrix} C_{ww4} (\eta_{w0}^3 + 3\eta_{w0}^2 \eta_{\alpha 0} + 3\eta_{w0} \eta_{\alpha 0}^2 + \eta_{\alpha 0}^3) \\ + C_{ww5} (\eta_{w0} \eta_{u0}^2 + \eta_{\alpha 0} \eta_{u0}^2) \end{pmatrix} \\
&\quad + (\beta_z - 1) \begin{pmatrix} C_{ww6} \tau (\eta_{\alpha 0} \eta_{u0}) - C_{ww7} \tau^2 (\eta_{w0} \eta_{\alpha 0}^2 + \eta_{\alpha 0}^3) \\ -C_{ww8} (\eta_{u0} \eta_{w0}^2 + \eta_{u0}^2 \eta_{\alpha 0}) \end{pmatrix} \quad (6.49)
\end{aligned}$$

$$G_{\alpha 0}^s = -\frac{1}{I_y^*} (\beta_z - 1) \begin{pmatrix} C_{aw3} \tau (\eta_{w0}^2 \eta_{\alpha 0} + 2\eta_{w0} \eta_{\alpha 0}^2 + \eta_{\alpha 0}^3) \\ -C_{aw4} \tau (\eta_{u0}^2 \eta_{\alpha 0}) \\ -C_{aw5} (\eta_{w0} \eta_{u0} + \eta_{\alpha 0} \eta_{u0}) \end{pmatrix} \quad (6.50)$$

The solution for the first-order equations is

$$\eta_k = A_k(T_2) e^{i\omega_k T_0} + \bar{A}_k(T_2) e^{-i\omega_k T_0} \quad (6.51)$$

where \bar{A}_k is the complex conjugate of A_k . This solution is then substituted into the nonlinear terms in Eqs.(6.48)-(6.50), and the following expressions are obtained.

$$\begin{aligned}
G_{u0}^s(\eta_0) &= C_{w\alpha 1}^u e^{i(\omega_\alpha + \omega_w) T_0} + C_{w\alpha 2}^u e^{i(\omega_\alpha - \omega_w) T_0} \\
&\quad + C_{\alpha\alpha 1}^u e^{i(2\omega_\alpha) T_0} + C_{\alpha\alpha 2}^u A_\alpha \bar{A}_\alpha \\
&\quad + C_{uuu 1}^u e^{i(3\omega_u) T_0} + C_{uuu 2}^u e^{i(\omega_u) T_0} \\
&\quad + C_{uww 1}^u e^{i(\omega_u + 2\omega_w) T_0} + C_{uww 2}^u e^{i(\omega_u) T_0} + C_{uww 3}^u e^{i(\omega_u - 2\omega_w) T_0}
\end{aligned}$$

$$\begin{aligned}
& + C_{u\alpha\alpha 1}^u e^{i(\omega_u+2\omega_\alpha)T_0} + C_{u\alpha\alpha 2}^u e^{i(\omega_u)T_0} + C_{u\alpha\alpha 3}^u e^{i(\omega_u-2\omega_\alpha)T_0} \\
& + C_{uw\alpha 1}^u e^{i(\omega_u+\omega_w+\omega_\alpha)T_0} + C_{uw\alpha 1}^u e^{i(\omega_u+\omega_w-\omega_\alpha)T_0} + C_{uw\alpha 3}^u e^{i(\omega_u-\omega_w+\omega_\alpha)T_0}
\end{aligned} \tag{6.52}$$

$$\begin{aligned}
G_{w0}^s(\eta_0) & = C_{u\alpha 1}^w e^{i(\omega_u\omega_\alpha)T_0} + C_{u\alpha 2}^w e^{i(\omega_u-\omega_\alpha)T_0} \\
& C_{uuw 1}^w e^{i(2\omega_u+\omega_w)T_0} + C_{uuw 2}^w e^{i(\omega_w)T_0} + C_{uuw 3}^w e^{i(\omega_w-2\omega_u)T_0} \\
& C_{uu\alpha 1}^w e^{i(2\omega_u+\omega_\alpha)T_0} + C_{uu\alpha 2}^w e^{i(\omega_\alpha)T_0} + C_{uu\alpha 3}^w e^{i(-2\omega_u+\omega_\alpha)T_0} \\
& C_{www 1}^w e^{i(3\omega_w)T_0} + C_{www 2}^w e^{i(\omega_w)T_0} \\
& C_{ww\alpha 1}^w e^{i(2\omega_w+\omega_\alpha)T_0} + C_{ww\alpha 2}^w e^{i(\omega_\alpha)T_0} + C_{ww\alpha 3}^w e^{i(\omega_\alpha-2\omega_w)T_0} \\
& C_{w\alpha\alpha 1}^w e^{i(\omega_w+2\omega_\alpha)T_0} + C_{w\alpha\alpha}^w e^{i(\omega_w)T_0} + C_{w\alpha\alpha 3}^w e^{i(\omega_w-2\omega_\alpha)T_0} \\
& C_{\alpha\alpha\alpha 1}^w e^{i(3\omega_\alpha)T_0} + C_{\alpha\alpha\alpha 2}^w e^{i(\omega_\alpha)T_0}
\end{aligned} \tag{6.53}$$

$$\begin{aligned}
G_{\alpha 0}^s(\eta_0) & = C_{u\alpha 1}^\alpha e^{i(\omega_u+\omega_\alpha)T_0} + C_{u\alpha 2}^\alpha e^{i(\omega_u-\omega_\alpha)T_0} \\
& C_{uw 1}^\alpha e^{i(\omega_u+\omega_w)T_0} + C_{uw 2}^\alpha e^{i(\omega_u-\omega_w)T_0} \\
& C_{uu\alpha 1}^\alpha e^{i(2\omega_u+\omega_\alpha)T_0} + C_{uu\alpha 2}^\alpha e^{i(\omega_\alpha)T_0} + C_{uu\alpha 3}^\alpha e^{i(\omega_\alpha-2\omega_u)T_0} \\
& C_{ww\alpha 1}^\alpha e^{i(2\omega_w+\omega_\alpha)T_0} + C_{ww\alpha 2}^\alpha e^{i(\omega_\alpha)T_0} + C_{ww\alpha 3}^\alpha e^{i(\omega_\alpha-2\omega_w)T_0} \\
& C_{w\alpha\alpha 1}^\alpha e^{i(2\omega_\alpha+\omega_w)T_0} + C_{w\alpha\alpha 2}^\alpha e^{i(\omega_w)T_0} + C_{w\alpha\alpha 3}^\alpha e^{i(\omega_w-2\omega_\alpha)T_0} \\
& C_{\alpha\alpha\alpha 1}^\alpha e^{i(3\omega_\alpha)T_0} + C_{\alpha\alpha\alpha 2}^\alpha e^{i(\omega_\alpha)T_0}
\end{aligned} \tag{6.54}$$

If A_k are not functions of time T_2 , but constants, then particular solutions can be written in the following forms

$$\begin{aligned}
\eta_{up0} & = g_{u1} e^{i(\omega_u)T_0} + g_{u2} e^{i(\omega_\alpha+\omega_w)T_0} + g_{u3} e^{i(\omega_\alpha-\omega_w)T_0} \\
& + g_{u4} e^{i(2\omega_\alpha)T_0} + g_{u5} e^{i(3\omega_u)T_0} + g_{u6} e^{i(\omega_u+2\omega_w)T_0} \\
& + g_{u7} e^{i(\omega_u-2\omega_w)T_0} + g_{u8} e^{i(\omega_u+2\omega_w)T_0} + g_{u9} e^{i(\omega_u-\omega_w)T_0}
\end{aligned}$$

$$\begin{aligned}
& g_{u10}e^{i(\omega_u+\omega_w+\omega_\alpha)T_0} + g_{u11}e^{i(\omega_u-\omega_w+\omega_\alpha)T_0} + g_{u12}e^{i(\omega_u+\omega_w-\omega_\alpha)T_0} \\
& g_{u13}e^{i(\omega_u-\omega_w-\omega_\alpha)T_0}
\end{aligned} \tag{6.55}$$

$$\begin{aligned}
\eta_{up0} = & g_{w1}e^{i(\omega_w)T_0} + g_{w2}e^{i(\omega_\alpha)T_0} + g_{w3}e^{i(\omega_u+\omega_\alpha)T_0} \\
& + g_{w4}e^{i(\omega_u-\omega_\alpha)T_0} + g_{w5}e^{i(3\omega_\alpha)T_0} + g_{w6}e^{i(3\omega_w)T_0} \\
& + g_{w7}e^{i(2\omega_u+\omega_w)T_0} + g_{w8}e^{i(\omega_u-\omega_w)T_0} + g_{w9}e^{i(2\omega_u+\omega_\alpha)T_0} \\
& g_{w10}e^{i(2\omega_u-\omega_\alpha)T_0} + g_{w11}e^{i(2\omega_w+\omega_\alpha)T_0} + g_{w12}e^{i(2\omega_w-\omega_\alpha)T_0} \\
& g_{w13}e^{i(\omega_w+2\omega_\alpha)T_0} + g_{w14}e^{i(\omega_w-2\omega_\alpha)T_0}
\end{aligned} \tag{6.56}$$

$$\begin{aligned}
\eta_{up0} = & g_{a1}e^{i(\omega_w)T_0} + g_{a2}e^{i(\omega_\alpha)T_0} + g_{a3}e^{i(\omega_u+\omega_\alpha)T_0} \\
& + g_{a4}e^{i(\omega_u-\omega_\alpha)T_0} + g_{a5}e^{i(\omega_u+\omega_w)T_0} + g_{a6}e^{i(\omega_u-\omega_w)T_0} \\
& + g_{a7}e^{i(3\omega_\alpha)T_0} + g_{a8}e^{i(2\omega_u+\omega_\alpha)T_0} + g_{a9}e^{i(\omega_\alpha-2\omega_u)T_0} \\
& + g_{a10}e^{i(2\omega_w+\omega_\alpha)T_0} + g_{a11}e^{i(\omega_\alpha-2\omega_w)T_0} + g_{a12}e^{i(2\omega_\alpha+\omega_w)T_0} \\
& + g_{a13}e^{i(\omega_w-2\omega_\alpha)T_0}
\end{aligned} \tag{6.57}$$

Substituting these particular solutions into the left-hand side of the third-order equations and equating the coefficients of same exponential function, the coefficients of the particular solutions could be determined. All terms which exhibit internal resonance are represented as follows,

$$\begin{aligned}
g_{u2} &= \frac{C_{w\alpha 1}^u}{(\omega_u + \omega_w + \omega_\alpha)(\omega_u - \omega_w - \omega_\alpha)} \\
g_{u4} &= \frac{C_{\alpha\alpha 1}^u}{(\omega_u + 2\omega_\alpha)(\omega_u - 2\omega_\alpha)} \\
g_{w4} &= \frac{C_{u\alpha 2}^w}{(\omega_u + \omega_w + \omega_\alpha)(\omega_u - \omega_w + \omega_\alpha)} \\
g_{w5} &= \frac{C_{\alpha\alpha\alpha 1}^w}{(3\omega_\alpha + \omega_w)(3\omega_\alpha - \omega_w)}
\end{aligned}$$

$$\begin{aligned}
g_{a4} &= \frac{C_{u\alpha 2}^\alpha}{(\omega_u - 2\omega_\alpha)} \\
g_{a6} &= \frac{C_{uw 2}^\alpha}{\omega_w(\omega_w - 2\omega_\alpha)} \\
g_{a13} &= \frac{C_{u\alpha\alpha 3}^\alpha}{(3\omega_\alpha - \omega_w)(\omega_\alpha - \omega_w)}
\end{aligned} \tag{6.58}$$

where only the singularities associated with the resonance are shown. From these results, three possible internal resonance conditions are identified; $\omega_w = 3\omega_\alpha$, $\omega_u = 2\omega_\alpha$, and $\omega_u = \omega_w + \omega_\alpha$. The first internal resonance is caused by cubic nonlinearities. Quadratic nonlinearities caused the other two internal resonances in which the in-plane motion is included.

3. Numerical Simulations and Bifurcation Analysis

A wing system based on NATAm wing model is considered. The wing system is described in the previous section. Although store-induced nonlinearities are not included, the linear store terms are considered. The store parameters are $M_s = 0.1mL$, $I_{sy} = 0.1I_yL$, and $x_s = z_s = 0.0$. The stiffness ratio, β_z , is ‘44’. As shown in Fig. 23, the NATAm model does not satisfy any IR conditions such as $\omega_u = 2\omega_\alpha$, and $\omega_u = \omega_w + \omega_\alpha$. Another internal resonance condition, $\omega_w = 3\omega_\alpha$, also is not satisfied because of $\omega_w = 2.7\omega_\alpha$, as mentioned in the previous section. Thus, IR responses are not expected in this wing model.

For the system with only structural nonlinearity, bifurcation diagrams are shown in Figs. 67 and 68. These two bifurcation diagrams are obtained by applying two different sampling rules, $\dot{w} = 0.0$ and $\dot{\alpha} = 0.0$, respectively. As shown in these figures, zero and non-zero points are included in the velocity region $0.91 \leq Vr \leq 1.0$. This

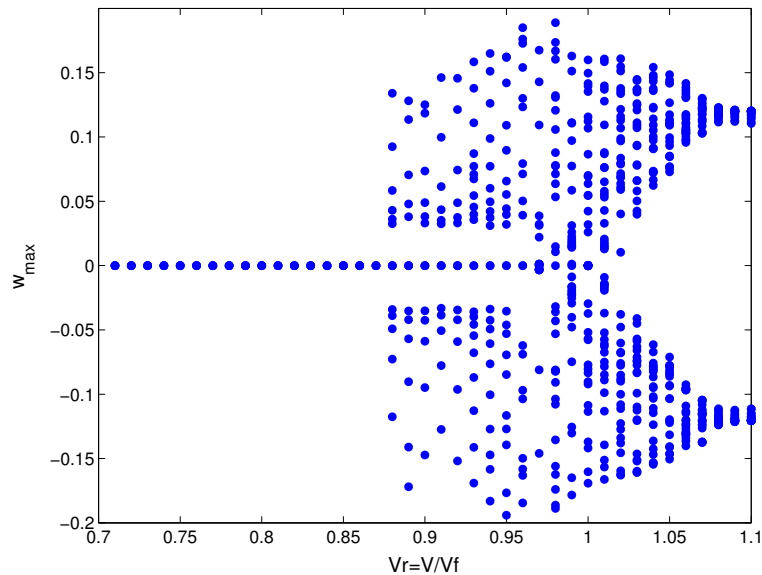


Fig. 67. Bifurcation diagram for a wing (w_{max})

result implies that there is a subcritical bifurcation. As shown in these bifurcation diagrams, nonzero points are shown from $Vr = 0.88$. For $Vr > 1$, zero fixed points disappear. This result shows that the structural nonlinearity may be one source causing LCO responses for velocity less than V_F . More detail discussion will be provided later.

C. The System with Store Nonlinearities

The third nonlinearity is induced by the attached store and the effect of the store-induced nonlinearity is investigated in this section.

1. Equations of Motion

Equations of motion for the system having only store-induced nonlinearity are obtained from Eqs. (2.42), (2.43), and (2.44).

$$C_{uw1}\ddot{u}_i + \beta_z C_{uw2}u_i + M_s^* (C_{us1}\ddot{u}_i + z_s^* C_{us2}\ddot{\alpha}_k)$$

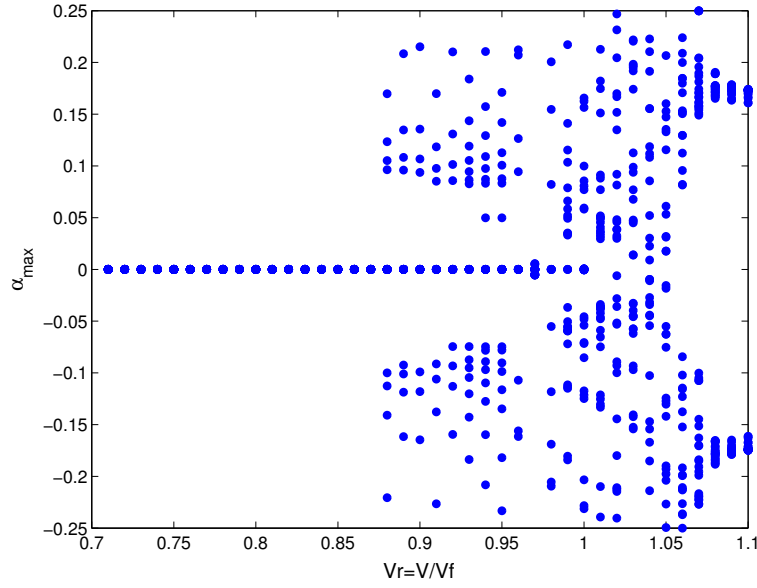


Fig. 68. Bifurcation diagram for a wing (α_{max})

$$\begin{aligned}
 &= M_s^* x_s^* [C_{us3}(\ddot{u}_i u_p + \dot{u}_i \dot{u}_p) + C_{us4}(\ddot{\alpha}_k \alpha_p + \dot{\alpha}_k \dot{\alpha}_p)] \\
 &+ M_s^* z_s^* [C_{us5}(\ddot{w}_j u_i + 2\dot{w}_j \dot{u}_i + \ddot{u}_i w_j)]
 \end{aligned} \tag{6.59}$$

$$\begin{aligned}
 &C_{ww1} \ddot{w}_j - e^* C_{we1} \ddot{\alpha}_k + C_{ww2} w_j + M_s^* (C_{ws1} \ddot{w}_j - x_s^* C_{ws2} \ddot{\alpha}_k) \\
 &- \mu * V^* C_{wa1} \dot{\alpha}_k + \mu \frac{C_{L\alpha_k}}{\pi} V^* \left[\frac{1}{b^* V^*} C_{wa2} \dot{w} - C_{wa3} \alpha - V^* \left(\frac{1}{2} - a \right) C_{wa4} \dot{\alpha} \right] \\
 &= M_s^* z_s^* [C_{ws3}(\ddot{w}_j w_p + \dot{w}_j \dot{w}_p) + C_{ws4}(\ddot{\alpha}_k \alpha_p + \dot{\alpha}_k \dot{\alpha}_p)] \\
 &+ M_s^* x_s^* [C_{ws5}(\ddot{u}_i w_j + 2\dot{u}_i \dot{w}_j + \ddot{w}_j u_i)] \\
 &- \mu \frac{C_{L\alpha}}{\pi} V^{*2} c_3 \int_0^s W_r \alpha_{eff}^3 ds
 \end{aligned} \tag{6.60}$$

$$\begin{aligned}
 &C_{aw1} \ddot{\alpha}_k - \frac{e^*}{I_y^*} C_{ae1} \ddot{w}_j + \frac{1}{I_y^*} \beta_y C_{aw2} \alpha_k \\
 &+ \frac{1}{I_y^*} \left[(I_{sy}^* + M_S^* z_S^{*2} + M_S^* x_S^{*2}) \ddot{\alpha}_k + M_s^* (-x_s^* \ddot{w}_j + z_s^* \ddot{u}) \right] \\
 &- \frac{1}{I_y^*} \mu b^* \left(\frac{1}{2} - a \right) V^* C_{aa1} \dot{\alpha}_k
 \end{aligned}$$

$$\begin{aligned}
& + \frac{1}{I_y^*} \mu \frac{C_{m\alpha_k}}{\pi} V^{*2} \left[\frac{1}{V^*} C_{aa2} \dot{w} - C_{aa3} \alpha_k - b^* \left(\frac{1}{2} - a \right) \frac{1}{V^*} C_{aa4} \dot{\alpha} \right] \\
& = + \frac{1}{I_y^*} M_s^* \ddot{w}_j \left[-\frac{1}{2} x_s^* (C_{as4} w_p w_q + C_{as5} \alpha_k \alpha_p) + z_s^* (C_{as6} \alpha_k - C_{as7} w_p u_i + C_{as8} u_i w_p) \right] \\
& + \frac{1}{I_y^*} M_s^* \ddot{u}_i \left[x_s^* (C_{as9} \alpha_k - C_{as10} w_j u_p) + \frac{1}{2} z_s^* (C_{as11} \alpha_k \alpha_p + C_{as12} u_p u_q) \right] \\
& - \frac{1}{I_y^*} M_s^* x_s^* z_s^* [-C_{as13} \dot{u}_i \dot{u}_p + 2C_{as14} \dot{u}_i \dot{w}_j \alpha_k] \\
& - \frac{1}{I_y^*} M_s^* x_s^* [C_{as15} (\ddot{w}_j w_p + \dot{w}_j \dot{w}_p) w_p + C_{as16} (2\ddot{u}_i u_p + 2\dot{u}_i \dot{u}_p) w_j] \\
& - \frac{1}{I_y^*} M_s^* z_s^* [C_{as17} (\ddot{w}_j w_p + \dot{w}_j \dot{w}_p) u_i + C_{as18} (2\ddot{u}_i u_p + 2\dot{u}_i \dot{u}_p) u_q] \\
& + \frac{1}{I_y^*} (I_{sz}^* - I_{sx}^*) [(C_{as19} \dot{w}_j \dot{w}_p - C_{as20} \dot{u}_i \dot{u}_p) \alpha_k - C_{as21} \dot{u}_i \dot{w}_j] \\
& + \frac{1}{I_y^*} I_{sy}^* [C_{as22} (\ddot{w}_j u_i + 2\dot{w}_j \dot{u}_i + w_j \ddot{u}_i) - C_{as23} (\dot{w}_j \dot{u}_i + \ddot{w}_j u_i)] \\
& - \frac{1}{I_y^*} \mu \frac{C_{m\alpha}}{\pi} V^{*2} c_3 \int_0^1 \alpha_{eff}^3 ds \tag{6.61}
\end{aligned}$$

2. Analysis by the Method of Multiple Scales

The nonlinear inertia terms are neglected to simplify the expression as was performed in the previous section. Crespo da Silva²⁸ stated that the nonlinear curvature terms are relatively important when compared to the nonlinear inertia terms. As shown in Eqs. (6.59), (6.60) and (6.61), the store-induced nonlinearities consist of time derivative terms. Therefore, resonance analysis by the Method of Multiple Scales is not performed.

3. Numerical Simulations and Bifurcation Analysis

A specified case is examined to investigate the effect of store-induced nonlinearities. The store parameters are $M_s = 0.1mL$, $I_{sy} = 0.1I_yL$, and $x_s = z_s = 0.0$. The stiffness ratio, β_z , is '44'. Bifurcation analysis is performed for the system. Although the result can be affected by the physical parameters, there is not any result of significant

interest in the specified case. The responses at $Vr < 1$ simply go to zero, and the responses at $Vr > 1$ diverge like a linear system.

D. The System with All Nonlinearities

As shown in previous sections, the aerodynamic nonlinearities cause LCO responses at $Vr > 1$, the structural nonlinearities show possible LCO responses at $Vr < 1$, and the store shows no remarkable response at $Vr < 1$. These characteristics were not predicted by the Method of Multiple Scales. For the wing system with only structural nonlinearity, the responses may exceed the limitation of linear aerodynamics. Aerodynamic nonlinearity is required to account the situation exceeding the linear aerodynamic range. Although the store-induced nonlinearity shown in previous section does not contribute to LCO response at $Vr < 1$, the nonlinearity may have a role when it is combined with other nonlinearities. Therefore, all nonlinearities are considered in this section.

1. Equations of Motion

The equations of motion having all nonlinearities are obtained from Eqs. (2.42), (2.43), and (2.44).

$$\begin{aligned}
& C_{uw1}\ddot{u}_i + \beta_z C_{uw2}u_i + M_s^* (C_{us1}\ddot{u}_i + z_s^* C_{us2}\ddot{\alpha}_k) \\
& = \beta_y C_{uw3}\alpha_k w_j - \beta_z [C_{uw4}u_i u_p u_q + C_{uw5}u_i w_j w_p] \\
& + (\beta_z - 1) [(C_{uw6}w_j \alpha_k + C_{uw7}u_i \alpha_k \alpha_p) - C_{uw8}w_j u_i u_p] + I_z^* C_{uw9}\ddot{u}_i \\
& - [C_{uw10}u_i (\ddot{w}_j w_p + \dot{w}_j \dot{w}_p) + C_{uw11}u_i (\ddot{u}_p u_q + \dot{u}_p \dot{u}_q)] \\
& + e^* C_{uw21}u_i \ddot{u}_p \\
& + e^* \left[\frac{1}{2} (C_{uw22}\alpha_k \ddot{\alpha}_p - C_{uw23}w_j \ddot{w}_p) - C_{uw24}u_i \ddot{u}_p - C_{uw25}w_j \ddot{w}_p \right]
\end{aligned}$$

$$\begin{aligned}
& +M_s^* x_s^* [C_{us3}(\ddot{u}_i u_p + \dot{u}_i \dot{u}_p) + C_{us4}(\ddot{\alpha}_k \alpha_p + \dot{\alpha}_j \dot{\alpha}_p)] \\
& +M_s^* z_s^* [C_{us5}(\ddot{w}_j u_i + 2\dot{w}_j \dot{u}_i + \ddot{u}_i w_j)]
\end{aligned} \tag{6.62}$$

$$\begin{aligned}
& C_{ww1} \ddot{w}_j - e^* C_{we1} \ddot{\alpha}_k + C_{ww2} w_j + M_s^* (C_{ws1} \ddot{w}_j - x_s^* C_{ws2} \ddot{\alpha}_k) \\
& -\mu * V^* C_{wa1} \dot{\alpha}_k + \mu \frac{C_{L\alpha_k}}{\pi} V^* \left[\frac{1}{b^* V^*} C_{wa2} \dot{w} - C_{wa3} \alpha - V^* \left(\frac{1}{2} - a \right) C_{wa4} \dot{\alpha} \right] \\
& = -\beta_y C_{ww3} (\alpha_k u_i) - [C_{ww4} w_j (w_p w_q) + C_{ww5} w_j (u_i u_p)] \\
& +(\beta_z - 1) [(C_{ww6} u_i \alpha_k - C_{ww7} w_j \alpha_k \alpha_p) - C_{ww8} u_i w_j u_p] + I_z^* C_{ww9} \ddot{w}_j \\
& - [C_{ww10} w_j (\ddot{w}_p w_q + \dot{w}_p \dot{w}_q) + C_{ww11} w_j (\ddot{u}_i u_p + \dot{u}_i \dot{u}_p)] - e^* C_{ww22} w_j \ddot{u}_i \\
& - e^* C_{ww23} u_i \ddot{w}_j \\
& +M_s^* z_s^* [C_{ws3}(\ddot{w}_j w_p + \dot{w}_j \dot{w}_p) + C_{ws4}(\ddot{\alpha}_k \alpha_p + \dot{\alpha}_k \dot{\alpha}_p)] \\
& +M_s^* x_s^* [C_{ws5}(\ddot{u}_i w_j + 2\dot{u}_i \dot{w}_j + \ddot{w}_j u_i)] \\
& -\mu \frac{C_{L\alpha}}{\pi} V^{*2} c_3 \int_0^s W_r \alpha_{eff}^3 ds
\end{aligned} \tag{6.63}$$

$$\begin{aligned}
& C_{aw1} \ddot{\alpha}_k - \frac{e^*}{I_y^*} C_{ae1} \ddot{w}_j + \frac{1}{I_y^*} \beta_y C_{aw2} \alpha_k \\
& + \frac{1}{I_y^*} \left[(I_{sy}^* + M_S^* z_S^{*2} + M_S^* x_s^{*2}) \ddot{\alpha}_k + M_s^* (-x_s^* \ddot{w}_j + z_s^* \ddot{u}) \right] \\
& - \frac{1}{I_y^*} \mu b^* \left(\frac{1}{2} - a \right) V^* C_{aa1} \dot{\alpha}_k \\
& + \frac{1}{I_y^*} \mu \frac{C_{m\alpha_k}}{\pi} V^{*2} \left[\frac{1}{V^*} C_{aa2} \dot{w} - C_{aa3} \alpha_k - b^* \left(\frac{1}{2} - a \right) \frac{1}{V^*} C_{aa4} \dot{\alpha} \right] \\
& = -\frac{1}{I_y^*} (\beta_z - 1) [(C_{aw3} w_j w_p - C_{aw4} u_i u_p) \alpha_k - C_{aw5} w_j u_i] \\
& + \frac{1}{I_y^*} I_y^* [C_{aw6} (\ddot{w}_j u_i + 2\dot{w}_j \dot{u}_i + w_j \ddot{u}_i) - C_{aw7} (\dot{w}_j \dot{u}_i + \ddot{w}_j u_i)] \\
& + \frac{1}{I_y^*} (I_z^* - I_x^*) [(C_{aw8} \dot{w}_j \dot{w}_p - C_{aw9} \dot{u}_i \dot{u}_p) \alpha_k - C_{aw10} \dot{u}_i \dot{w}_j] \\
& + \frac{1}{I_y^*} \frac{1}{2} e^* [-\ddot{w}_j (C_{aw22} w_p w_q + C_{aw23} \alpha_k \alpha_p) + C_{aw24} w_j \ddot{w}_p w_q + C_{aw25} u_i \ddot{u}_p]
\end{aligned}$$

$$\begin{aligned}
& + \frac{1}{I_y^*} e^* \ddot{u}_i (C_{aw26} \alpha_k - C_{aw27} u_p w_j) \\
& + \frac{1}{I_y^*} M_s^* \ddot{w}_j \left[-\frac{1}{2} x_s^* (C_{as4} w_p w_q + C_{as5} \alpha_k \alpha_p) + z_s^* (C_{as6} \alpha_k - C_{as7} w_p u_i + C_{as8} u_i w_p) \right] \\
& + \frac{1}{I_y^*} M_s^* \ddot{u}_i \left[x_s^* (C_{as9} \alpha_k - C_{as10} w_j u_p) + \frac{1}{2} z_s^* (C_{as11} \alpha_k \alpha_p + C_{as12} u_p u_q) \right] \\
& - \frac{1}{I_y^*} M_s^* x_s^* z_s^* [-C_{as13} \dot{u}_i \dot{u}_p + 2C_{as14} \dot{u}_i \dot{w}_j \alpha_k] \\
& - \frac{1}{I_y^*} M_s^* x_s^* [C_{as15} (\ddot{w}_j w_p + \dot{w}_j \dot{w}_p) w_p + C_{as16} (2\ddot{u}_i u_p + 2\dot{u}_i \dot{u}_p) w_j] \\
& - \frac{1}{I_y^*} M_s^* z_s^* [C_{as17} (\ddot{w}_j w_p + \dot{w}_j \dot{w}_p) u_i + C_{as18} (2\ddot{u}_i u_p + 2\dot{u}_i \dot{u}_p) u_q] \\
& + \frac{1}{I_y^*} (I_{sz}^* - I_{sx}^*) [(C_{as19} \dot{w}_j \dot{w}_p - C_{as20} \dot{u}_i \dot{u}_p) \alpha_k - C_{as21} \dot{u}_i \dot{w}_j] \\
& + \frac{1}{I_y^*} I_{sy}^* [C_{as22} (\ddot{w}_j u_i + 2\dot{w}_j \dot{u}_i + w_j \ddot{u}_i) - C_{as23} (\dot{w}_j \dot{u}_i + \ddot{w}_j u_i)] \\
& - \frac{1}{I_y^*} \mu \frac{C_{m\alpha}}{\pi} V^{*2} c_3 \int_0^1 \alpha_{eff}^3 ds
\end{aligned} \tag{6.64}$$

where the nonlinear terms are placed on the right-hand side. The aerodynamic nonlinear terms appear in the out-of-plane bending and torsional equations. The last terms having the term V are the aerodynamic terms. Simplifying the α_{eff} term is not fully expanded in these equations. The store-induced terms have the subscripts 's'. The other terms which do not have both V and the subscript 's' are caused by wing flexibility.

2. Analysis by the Method of Multiple Scales

For a bending-bending-torsion system, the aerodynamic nonlinearity may cause $\omega_\alpha \approx 3\omega_w$ and $\omega_w \approx 3\omega_\alpha$. Three possible internal resonance conditions may be caused by the structural nonlinearity; $\omega_w \approx 3\omega_\alpha$, $\omega_u \approx 2\omega_\alpha$, and $\omega_u \approx \omega_w + \omega_\alpha$. The internal resonance condition $\omega_w \approx 3\omega_\alpha$ may be caused by both nonlinearities. Although 5 cases of internal resonance conditions are suggested by aerodynamic and structural

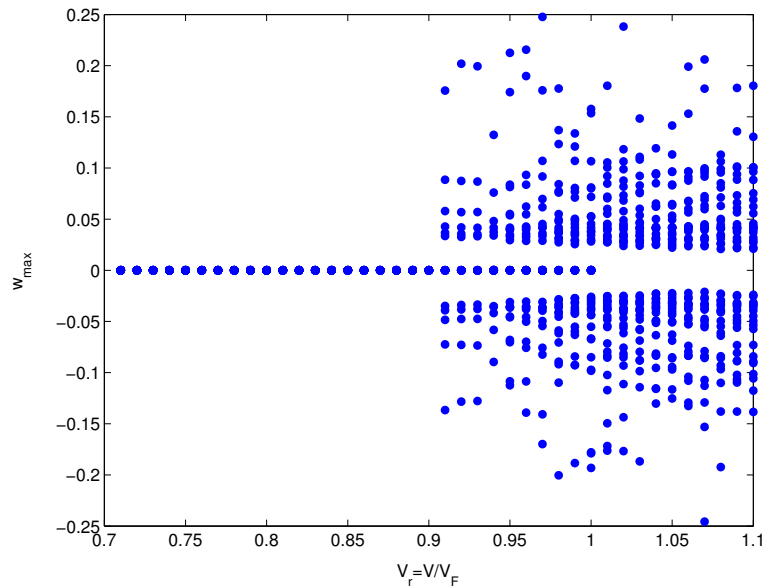


Fig. 69. Bifurcation diagram for a wing [$M_s = 0.1mL$, $I_{sy} = 0.1I_yL$, $x_s = z_s = 0.0$, and $\beta_z = 44$], (w_{max})

nonlinearities, it can be said that there are 4 possible internal resonance conditions because one condition is duplicated. As already mentioned in previous sections, the internal resonances are not possible in the considered wing model based on NATAm.

3. Numerical Simulation and Bifurcation Analysis

Possible sources causing LCO responses at $V_R < 1.0$ are investigated in detail. The effect of store parameters and the stiffness ratio is studied. If the stiffness ratio is not specified in this section, then the stiffness ratio, β_z , is ‘44’. The bifurcation diagram for the NATAm wing model with store parameters $M_s = 0.1mL$, $I_{sy} = 0.1I_yL$, $x_s = z_s = 0.0$ is depicted in Fig. 69. The shape of this diagram is somewhat different from the previous diagrams Fig. 67. This result shows that although the nonlinearities are simply added, the responses may not be obtained by linearly adding each response.

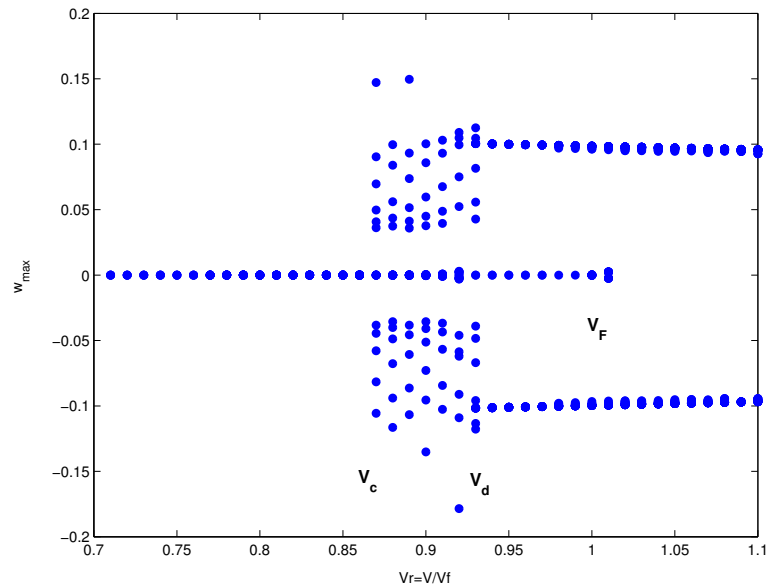


Fig. 70. Bifurcation diagram for a wing [$M_s = 0.2mL$, $I_{sy} = 0.1I_yL$, $x_s = -0.2b$, $z_s = 0.0$, $\beta_z = 44$], (w_{max})

Using another wing model having different store characteristics, the existence of LCO response at $Vr < 1$ is investigated. When mass ratio is increased from ‘0.1’ to ‘0.2’, and the x-coordinate of the store position, x_s , is moved from ‘0.0b’ to ‘-0.2b’, the bifurcation diagrams are simple, as shown in Figs.70 and 71. For $Vr \leq 1.0$, there are three velocity regions showing different characteristics. The region is divided by two velocities, V_c and V_d . The lowest velocity showing non-zero Poincare map is denoted by V_c , and the highest velocity showing multiple Poincare maps is expressed by V_d . In the region $V_c < Vr < V_d$, the number of Poincare maps is greater than 4. When $Vr < V_c = 0.87$, there is only one fixed point which has a zero amplitude. In the region $V_d = 0.93 \leq Vr \leq 1.0$, there is one zero point and two non-zero points. The non-zero points are symmetric. In the other region ($V_c \leq Vr \leq V_d$), there are multi-points including a zero point. Regardless of the velocity condition, the fact

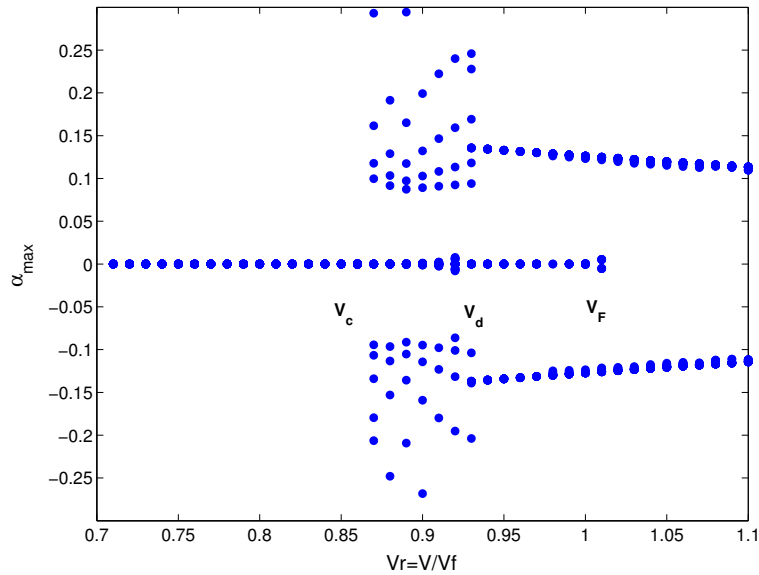


Fig. 71. Bifurcation diagram for a wing [Store parameters $M_s = 0.2mL$, $I_{sy} = 0.1I_yL$, $x_s = -0.2b$, $z_s = 0.0$, $\beta_z = 44$], (α_{max})

that a zero-fixed point exists and non-zero points are exist in the bifurcation diagram of Poincare map implies that there is a subcritical bifurcation. Depending upon the initial condition, the response goes to either zero amplitude or non-zero states. The velocity V_C is one of the important velocities. The velocity condition $V_C < 1.0$ implies that there is a subcritical bifurcation. If we can find the case satisfying $V_C \geq 1.0$, then we can identify the dominant factor causing LCO responses at $V_r < 1.0$.

When store mass increases, the area $V_c < Vr < V_d$ disappears (Fig. 72). There are only three fixed points at $Vr < V_F$, including one zero point which is not included in the region $Vr > V_F$. The two stable fixed points imply that there are unstable points between the points. The unstable equilibrium points could not be directly determined in time simulation because the responses went to stable states. In order to identify the unstable status, the rule of trial and error is applied. At $Vr > V_F$, the zero amplitudes correspond to the unstable equilibrium points. At

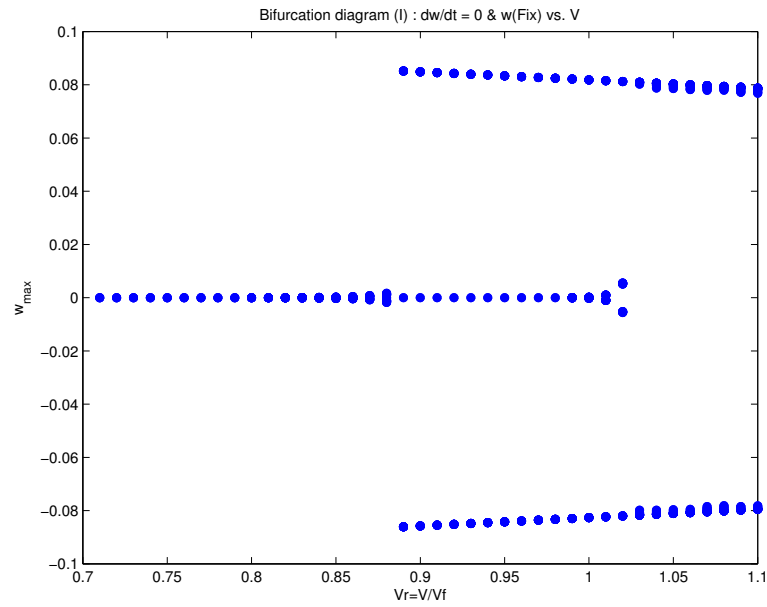


Fig. 72. Bifurcation diagram for a wing [$M_s = 0.3mL$, $I_{sy} = 0.1I_yL$, $x_s = -0.2b$, $z_s = 0.0$, $\beta_z = 44$], (w_{max})

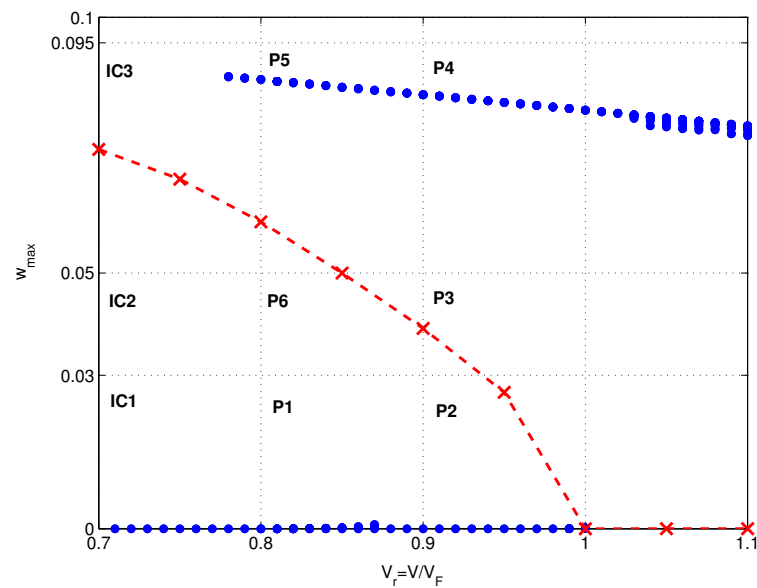


Fig. 73. Subcritical Bifurcation for a wing [$M_s = 0.3mL$, $I_{sy} = 0.1I_yL$, $x_s = -0.2b$, $z_s = 0.0$, $\beta_z = 44$], (w_{max})

$Vr < V_F$, the unstable condition has non-zero amplitude because one of stable condition has zero-amplitude. The subcritical bifurcation diagram for this case is shown in Fig. 73. In this figure, stable fixed points are expressed by ‘filled circles’ and the unstable solutions are depicted by the dashed line with a symbol ‘ \times ’. The subcritical bifurcation has locally unstable solutions on both sides of bifurcation.⁵⁴

Time responses for various initial conditions and velocity conditions are considered. As shown in Fig 73, three initial conditions ‘IC1’, ‘IC2’, and ‘IC3’, and two velocity conditions ‘ $V_r = 0.8$ ’ and ‘ $V_r = 0.9$ ’, are selected. The corresponding points are expressed by ‘ P_i ’ ($i = 1, 2, \dots, 6$). The correspondence to these points are shown in Fig. 74. The responses at $V_r = 0.8$ are placed on the left-hand side, and the responses at $V_r = 0.9$ are located on the right-hand side. The responses for ‘P1’ and ‘P2’ show that for a small initial condition, ‘IC1’, the responses go to zero regardless of the velocity conditions considered. For another initial condition ‘IC2’, the responses for ‘P6’ and ‘P3’ show different shapes. Because ‘P6’ is lower than the unstable solution at $V_r = 0.8$, the response goes to a zero equilibrium point. The response for ‘P3’ goes to a non-zero stable solution because the condition ‘P3’ is higher than the unstable solution at $V_r = 0.9$. The responses for ‘P4’ and ‘P5’ go to non-zero solutions. If the velocity is reduced to $V_r = 0.6$, then the initial condition ‘IC3’, corresponding to ‘P4’ and ‘P5’, does not cause a limit cycle oscillation. The response goes to zero. Although the shape of responses are different from each other, they converge to stable solutions: the responses for the condition below the unstable solutions decay to zero and the responses for the condition above the unstable solutions go to non-zero solutions showing Limit Cycle Oscillations (LCOs).

For a velocity condition $Vr = 0.95$, time history and frequency content for these

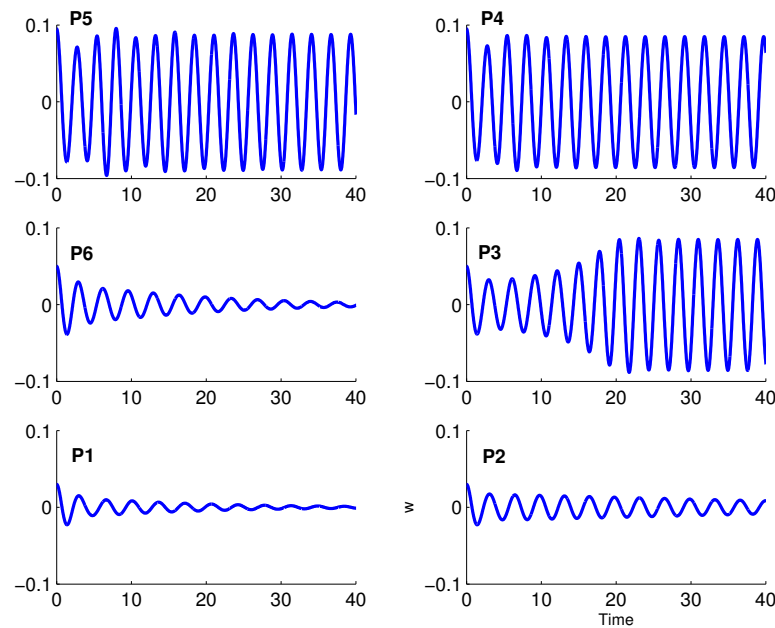


Fig. 74. Time histories of w for various initial conditions and velocities: $V_r = 0.8$ (Left) and $V_r = 0.9$ (Right)

two initial conditions are shown in Fig. 75. At velocity condition $V_r = 0.95$, the responses depend upon the initial conditions. As shown in this figure, the response for a small initial condition is damped and there are three peak frequencies in the frequency content. The peak, ‘P1’, corresponds to the out-of-bending frequency and the other frequencies ‘P3-P1’, and ‘P3+p1’, means the frequencies combined with the in-plane bending frequency. For the initial condition close to ‘IC2’, the response slightly increase for $t < 80$. In the time region $80 < t < 100$, the response is abruptly increased and the increased amplitude is maintained. From the signal, we could find one more peak frequency, ‘3P1’. This frequency corresponds to the three times of ‘P1’. This type of component might be caused by cubic nonlinear terms.

In order to investigate the spectral variations with time, the results are presented in Figs. 76 and 77. In these 3-Dimensional spectral maps, the additional axis (x-

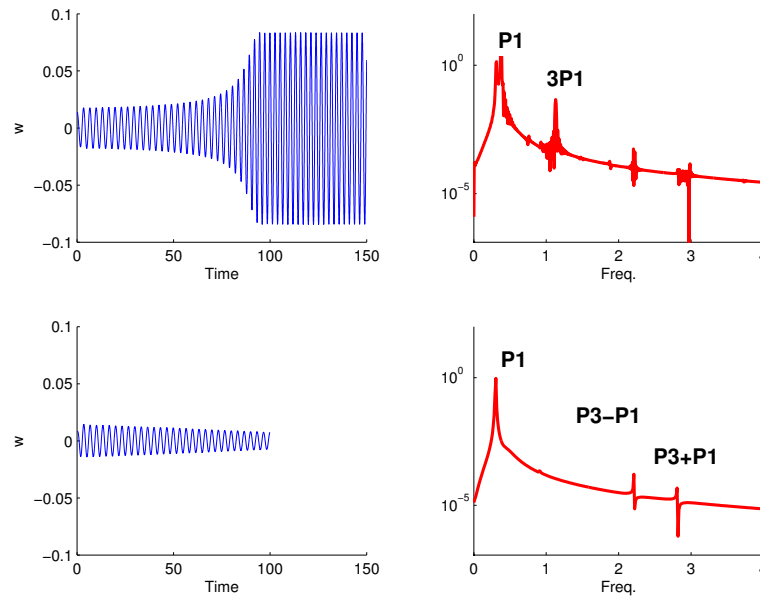


Fig. 75. Time history and frequency content for two initial conditions IC2 (lower) and IC3(upper) [$M_s = 0.3mL$, $I_{sy} = 0.1I_yL$, $x_s = -0.2b$, $z_s = 0.0$, $\beta_z = 44$], (w_{max}

axis) is time sequence. At first ($x=1$), the dominant frequency component of the responses w and α is ‘P1’. As time increases, there are additional frequency components such as ‘3P1’ and ‘P3-P1’ which are caused by nonlinear terms. In the response for the out-of-bending motion, the magnitude of the ‘3P1’ component is relatively small. But, in the torsion motion, the effect of nonlinear terms is increased.

The region $V_c < Vr < V_d$, having multiple points, increases as the store inertia increases. V_c is slightly increased from 0.87 to 0.89, as shown in Fig. 78. Another bifurcation diagram is shown in Fig. 79. When the store position, x_s , is changed from $-0.2b$ to $-0.4b$, the bifurcation diagram consists of two non-zero fixed points and one zero-fixed point at $Vr < 1$. Although store position, z_s , is increased, the shape of the bifurcation diagram is slightly changed as shown in Fig. 80. As shown in previous bifurcation diagrams, the change of store parameters causes different responses. Non-zero Poincare maps exist at $Vr < 1$. Therefore, it is not easy to isolate the main

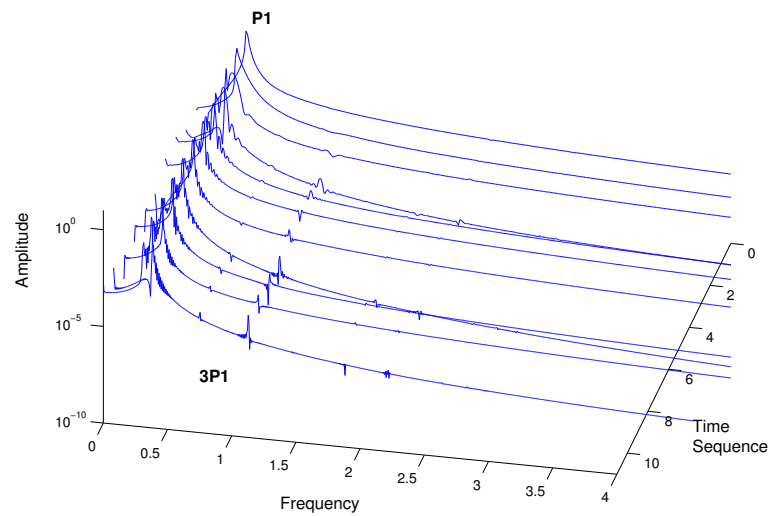


Fig. 76. Three dimensional spectral map (or Waterfall plot) for an initial condition IC3 [$M_s = 0.3mL$, $I_{sy} = 0.1I_yL$, $x_s = -0.2b$, $z_s = 0.0$, $\beta_z = 44$], (w - motion)

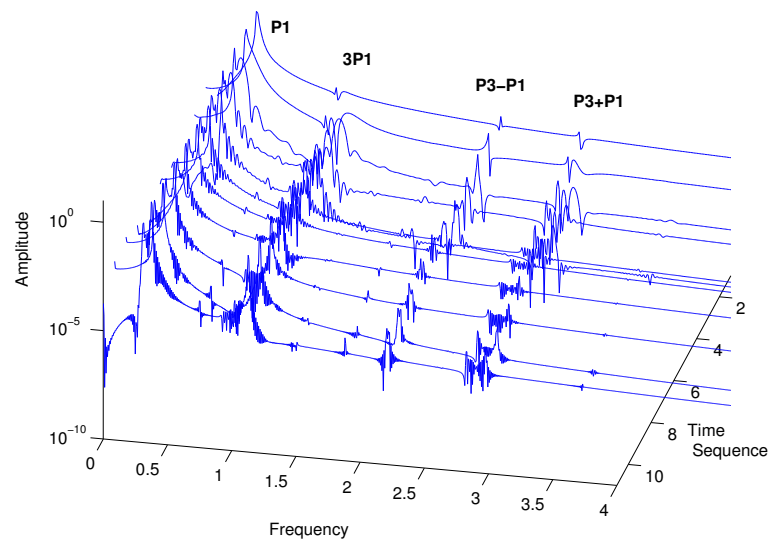


Fig. 77. Three dimensional spectral map (or Waterfall plot) for an initial condition IC3 [$M_s = 0.3mL$, $I_{sy} = 0.1I_yL$, $x_s = -0.2b$, $z_s = 0.0$, $\beta_z = 44$], (α - motion)

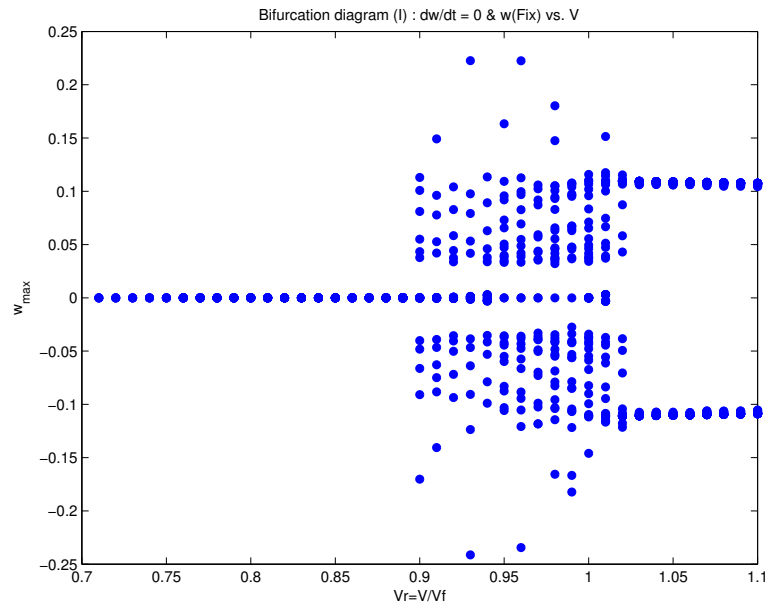


Fig. 78. Bifurcation diagram for a wing [$M_s = 0.2mL$, $I_{sy} = 0.3I_yL$, $x_s = -0.2b$, $z_s = 0.0$, $\beta_z = 44$], (w_{max})

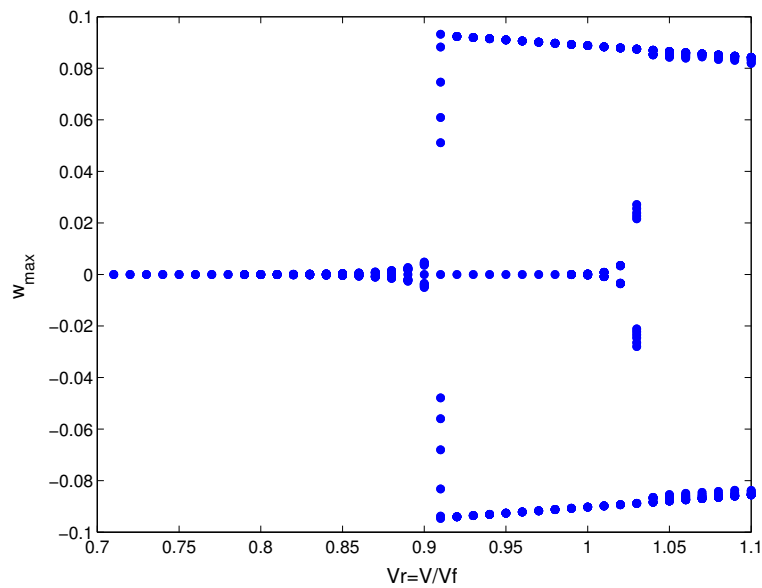


Fig. 79. Bifurcation diagram for a wing [$M_s = 0.2mL$, $I_{sy} = 0.1I_yL$, $x_s = -0.4b$, $z_s = 0.0$, $\beta_z = 44$], (w_{max})

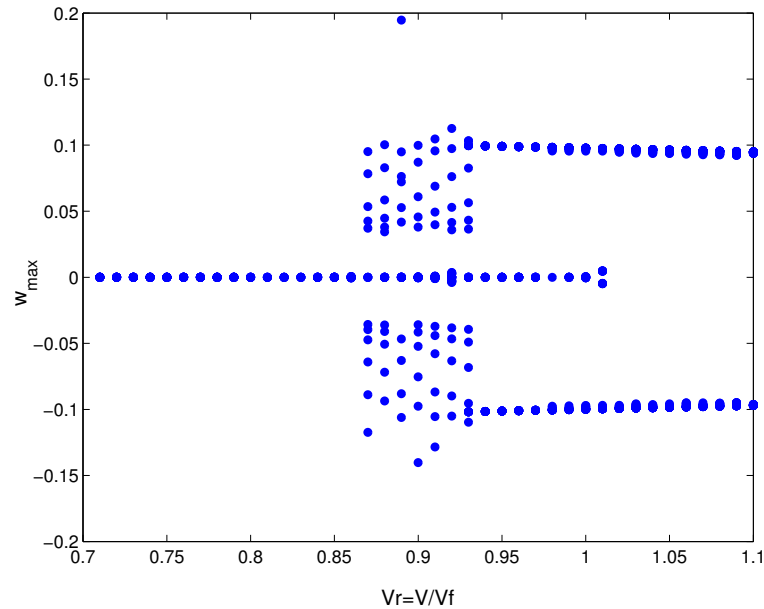


Fig. 80. Bifurcation diagram for a wing [$M_s = 0.2mL$, $I_{sy} = 0.1I_yL$, $x_s = -0.2b$, $z_s = 0.3b$, $\beta_z = 44$], (w_{max})

factor causing LCO responses.

We examine another case which has different store parameters. As shown in Fig. 81, the combination of store parameters does not reduce in the region $Vr < 1$. V_c is still less than V_F . This result shows that it is not easy to find the main factor causing the subcritical bifurcation through the combination of store parameters.

Another possible cause of LCO is investigated by changing the stiffness ratio, β_z ; the ratio is reduced from '44' to '10'. The corresponding bifurcation diagrams are shown in Figs. 82 and 83. Non-zero fixed points are observed in the vicinity of $Vr = 1.0$. The region showing three fixed points disappears. Additionally, the effect of the moment of inertia of the attached store is shown in Fig. 84 and 85. At a velocity condition $Vr < 1.0$, it is not easy to determine non-zero fixed points. Two fixed

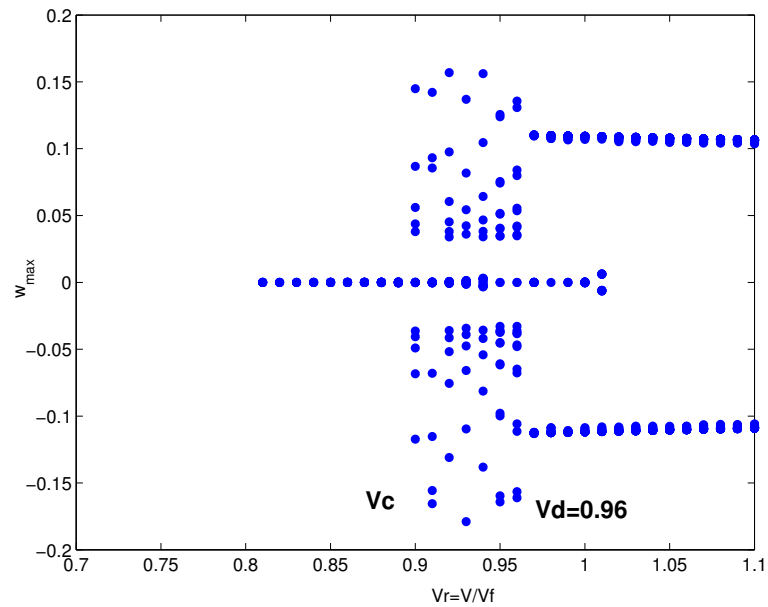


Fig. 81. Bifurcation diagram for a wing [$M_s = 0.2mL$, $I_{sy} = 0.3I_yL$, $x_s = -0.2b$, $z_s = 0.3b$, $\beta_z = 44$], (w_{max})

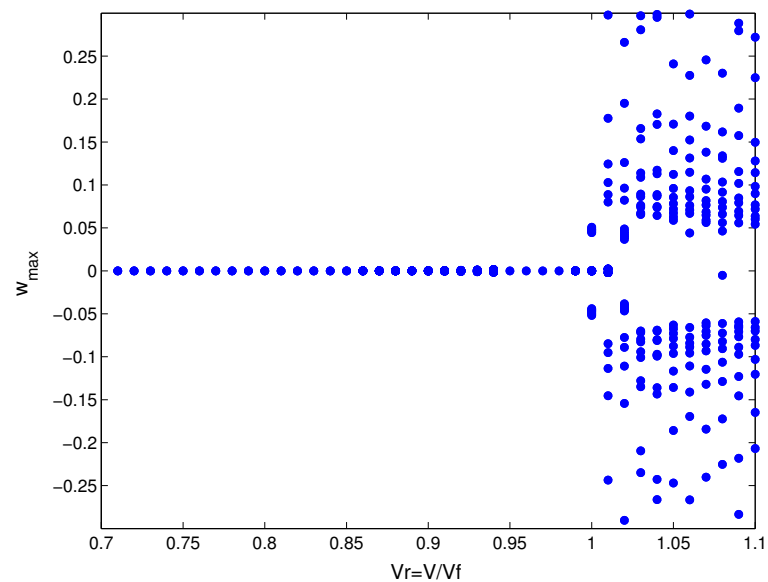


Fig. 82. Bifurcation diagram for a wing [$M_s = 0.2mL$, $I_{sy} = 0.1I_yL$, $x_s = -0.2b$, $z_s = 0.0b$, $\beta_z = 10$], (w_{max})

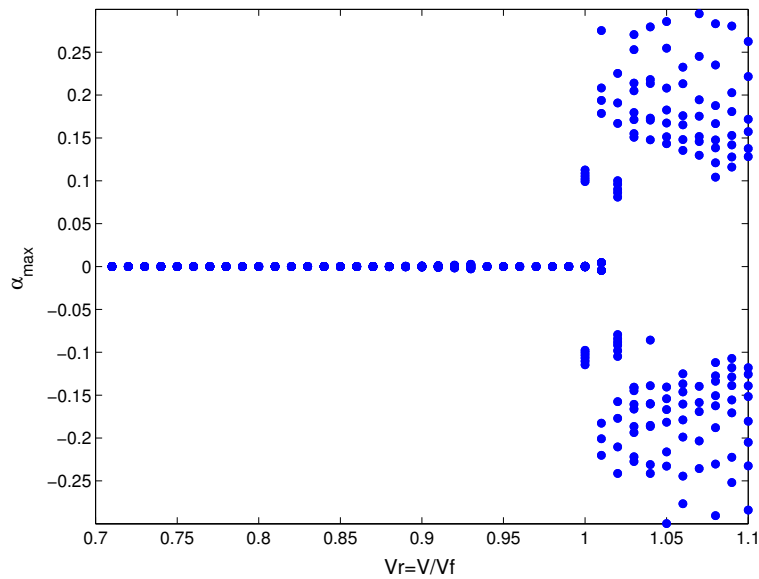


Fig. 83. Bifurcation diagram for a wing [$M_s = 0.2mL$, $I_{sy} = 0.1I_yL$, $x_s = -0.2b$, $z_s = 0.0b$, $\beta_z = 10$, α_{max}]

points appear in region $1.0 < Vr < 1.04$. For higher velocities ($Vr > 1.05$), there are multi Poincare maps. These two cases show that the stiffness ratio, β_z , is a main factor causing LCO responses at the velocity less than the flutter velocity.

E. Discussion

Using the bending-bending-torsion equations of motion, nonlinear aeroelastic analyses are performed. Internal resonance conditions are anticipated by the Method of Multiple Scales. Two internal resonance conditions, $\omega_\alpha : \omega_w = 1 : 3$ and $\omega_\alpha : \omega_w = 3 : 1$, are caused by the aerodynamic nonlinearities, and three internal resonance conditions $\omega_w = 3\omega_\alpha$, $\omega_u = 2\omega_\alpha$, and $\omega_u = \omega_w + \omega_\alpha$, are caused by the structural nonlinearities. Because one condition, $\omega_w = 3\omega_\alpha$, is duplicated, there are four internal resonance conditions. Among them, two conditions, $\omega_\alpha : \omega_w = 1 : 3$ and $\omega_\alpha : \omega_w = 3 : 1$, are related to the cubic nonlinearity, and the other two conditions, $\omega_u = 2\omega_\alpha$, and

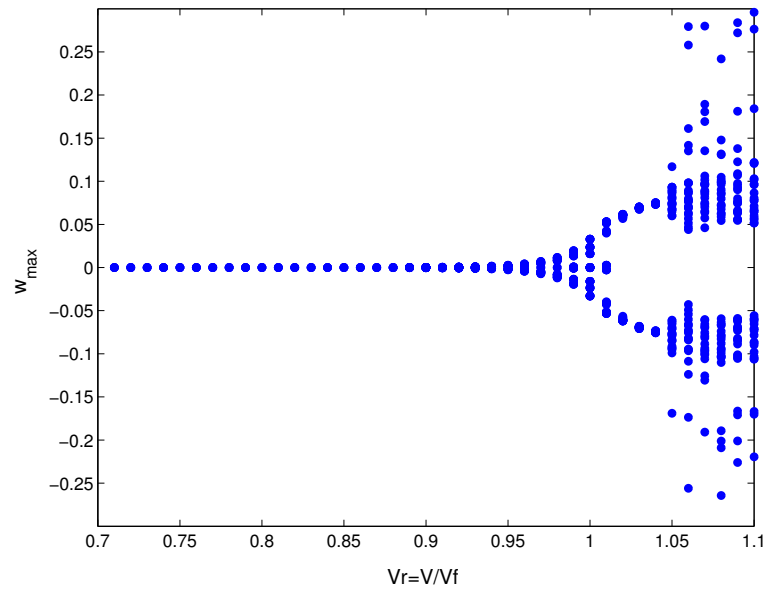


Fig. 84. Bifurcation diagram for a wing [$M_s = 0.2mL$, $I_{sy} = 0.3I_yL$, $x_s = -0.2b$, $z_s = 0.0b$, $\beta_z = 44$], (w_{max})

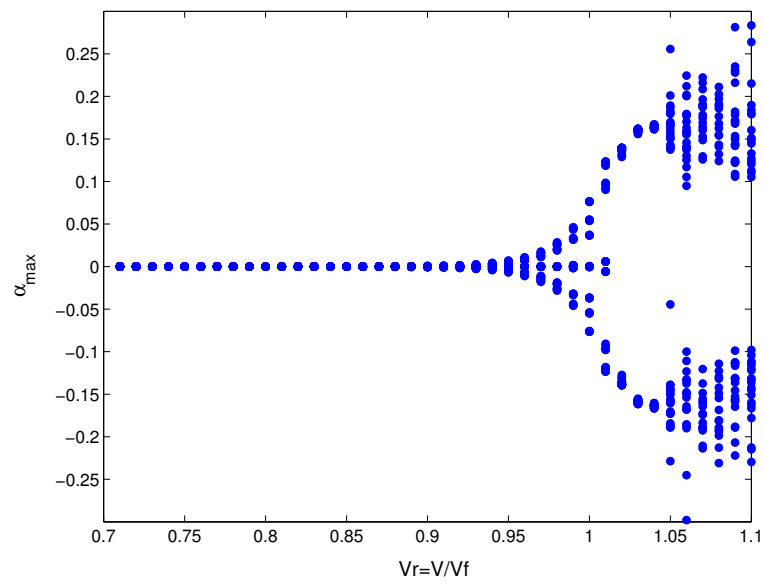


Fig. 85. Bifurcation diagram for a wing [$M_s = 0.2mL$, $I_{sy} = 0.3I_yL$, $x_s = -0.2b$, $z_s = 0.0b$, $\beta_z = 10$], (α_{max})

$\omega_u = \omega_w + \omega_\alpha$, are caused by the quadratic nonlinearities. These resonance conditions are investigated through the wing model based on NATAm with a store. The stiffness ratio β_z is '44', and the store parameters are $M_s = 0.1mL$, $I_{sy} = 0.1I_yL$, and $x_s = z_s = 0.0$. The wing model considered herein does not satisfy the resonance condition because the maximum frequency ratio ω_w/ω_α is 2.7, which occurs at $V=0$.

Possible causes of LCO responses of aircraft wings are investigated through wing models based on the NATAm wing model. For a specified case, the effect of individual nonlinearity is investigated. The stiffness ratio β_z is '44', and the store parameters are $M_s = 0.1mL$, $I_{sy} = 0.1I_yL$, and $x_s = z_s = 0.0$. The effect of velocity change is presented in bifurcation diagrams. The bifurcation diagrams consist of Poincare maps. The bifurcation diagram for a system with aerodynamic nonlinearity shows the supercritical bifurcation. Stable solutions exist in both velocity regions $V_r < 0$ and $V_r > 0$. For the case wing structural nonlinearity, the subcritical bifurcation is observed. But the torsional angle is too high to be accommodated by linear aerodynamics. This situation must be improved by adding a nonlinear aerodynamic model. The effect of store-induced nonlinearity is studied through the above specified case. There are no results of significant interest in this specified case. The responses at $Vr < 1$ simply go to zero, and the responses at $Vr > 1$ diverge like a linear system.

Using the systems with all three nonlinearities, the effect of store parameters are investigated. Although no significant results of interest are observed for the specified system with only store-induced nonlinearity, the store-induced nonlinearity is included because the responses could be affected by the physical store parameters. For the wing systems with $\beta_z = 44$, subcritical bifurcations are observed at many cases. When store inertia, I_{sy} increases, V_C increases. Through two example cases, the effect of the stiffness ratio (β_z) is studied. When the stiffness ratio is reduced from

'44' to '10', the subcritical bifurcation is not present in the velocity region $V_r < 1$. Additionally, the supercritical bifurcation is explicitly observed by the increased store inertia. This result shows that the stiffness ration is the dominant factor causing the LCO at $V_r < 1$, and store parameters could slightly affect the LCO response.

CHAPTER VII

CONCLUSIONS

A nonlinear structural model for a cantilever wing with a store is derived by using the extended Hamilton principle. The bending-bending-torsion equations of motion include up to the third order. A store model having nonlinear terms is included in the equations by introducing the Dirac delta function. The nonlinear aerodynamics with subsonic stall is also included in the equations to describe aeroelastic responses of the considered wing.

In order to understand the responses characteristics of nonlinear aeroelastic system, several nonlinear approaches are considered. Perturbation methods such as the Method of Multiple Scales are useful for nonlinear analysis. For an example based on the Duffing's equation, a software package AUTO2000 provides a simple bifurcation diagram, but the bifurcation diagram based on Poincare map generates a more complex diagram. Although they appear different from each other, the stable periodic solutions show good agreement.

In this dissertation, the bifurcation characteristics are investigated by the bifurcation diagram based on Poincare map. A bifurcation diagram for a bending-torsion system is compared the bifurcation diagram obtained by AUTO2000. The shapes are analogous to each other, and the existence of LCO responses below flutter velocity is conformed. For the system having all three nonlinearities, the responses depend upon the store parameters such as store mass, inertia, and store positions. In all cases of bending-torsion systems considered, subcritical bifurcations are observed. For bending-torsion systems with $\beta_z = 100$, the subcritical bifurcation characteristics

of the system are not affected by the change of store parameters.

The bending-bending-torsion system has quadratic nonlinear terms. They are not present in the bending-torsion system because they are related to the in-plane bending motion.

According to resonance analysis by the Method of Multiple Scales, there are at least two internal resonances are possible. Two resonance conditions $\omega_u = 2 \times \omega_\alpha$ and $\omega_u = \omega_w + \omega_\alpha$ are predicted. These resonance cases are investigated through the Heavy Goland Wing. Depending upon the uncoupling process, the number of anticipated resonance conditions is different. Because the effect of wing span on the bending and the torsion frequencies are different, and the aeroelastic frequencies are functions of flow velocity, these condition could be satisfied by changing the wing span and the velocity. When the wing span (L) is increased from 20 to 36 (and 60) ft, the frequencies are close to the resonance conditions. This larger wing span is expected in future air vehicle including UAVs. For these two cases having increased wing spans, modulated responses showing internal resonance are observed. It is necessary to consider the internal resonance as one possible aeroelastic phenomena of interest.

Using the bending-bending-torsion equations, the possible causes of LCO responses are studied. Depending upon the store condition, the shape of the bifurcation diagrams changes. When store mass and/or store position is changed increased, there are multiple Poincare maps at $V < V_F$ showing stable periodic motion. The main factor causing subcritical bifurcation is the stiffness ratio. When the stiffness ratio is changed, the subcritical bifurcation is changed to a supercritical bifurcation.

Herein, the supercritical bifurcation is usually caused by nonlinear aerodynamics due to stall, it is observed that the nonlinear responses are dominated by the nonlinear aerodynamics rather than the nonlinearity caused by the wing flexibility reflected by the stiffness ratio. This result shows that the stiffness ratio is a main factor causing subcritical bifurcation and LCO responses.

REFERENCES

- ¹ Denegri, C., Limit Cycle Oscillation Flight Test Results of a Fighter with External Stores, *Journal of Aircraft*, Vol. 37, No. 5, April 2000, pp. 761–769.
- ² Stearman, R., Powers, E., Schwartz, J., and Yurkovich, R., editors, *Aeroelastic System Identification of Advanced Technology Aircraft Through Higher Order Signal Processing*. in Proceedings of the 9th International Modal Analysis Conference, 1991.
- ³ Bunton, R. and Denegri, C., Limit Cycle Oscillation Characteristics of Fighter Aircraft, *Journal of Aircraft*, Vol. 37, No. 5, 2000, pp. 916–918.
- ⁴ Norton, W. J., Limit Cycle Oscillation and Flight Flutter Testing, *Proceedings of the 21st Annual Symposium*, 1990, pp. 3.4.1–3.4.12.
- ⁵ Denegri, C. J. and Cutchins, M., Evaluation of Classical Flutter Analysis for the Prediction of Limit Cycle Oscillations, *38th AIAA Structures, Structural Dynamics, and Materials Conference*, AIAA-1997-1021, April 1997.
- ⁶ Tang, D. and Dowell, E., Experimental and Theoretical Study for Nonlinear Aeroelastic Behavior of a Flexible Rotor Blade, *AIAA Journal*, Vol. 31, No. 6, 1993, pp. 1133–1142.
- ⁷ Kim, S. and Lee, I., Aeroelastic Analysis of a Flexible Airfoil with a Freeplay Nonlinearity, *Journal of Sound and Vibration*, Vol. 194, No. 4, 1996, pp. 823–846.
- ⁸ Chen, P., Sarhaddi, D., and Liu, D., Limit Cycle Oscillation Studies of a Fighter with External Stores, *39th AIAA Structures, Structural Dynamics, and Materials Conference*, AIAA Paper 98-1727, 1998.

- ⁹ Stearman, R. and Lamb, J., editors, *Applications of Higher-Order Statistics to Aircraft Aeroelastic Stability and Fluid-Structure Interactions*, 1992.
- ¹⁰ Cole, S., Effects of Spoiler Surfaces on the Aeroelastic Behavior of a Low-Aspect Ratio Wing, *Proceedings of the 31st AIAA Structures, Structural Dynamics, and Materials Conference, AIAA Paper 90-0981*, April 1990, pp. 1455–1463.
- ¹¹ Oh, K., Nayfeh, A., and Mook, D., Modal Interactions in the Forced Vibration of a Cantilever Metallic Plate, *Nonlinear and Stochastic Dynamics*, Vol. 192, 1994, pp. 237–247.
- ¹² Pai, P. and Nayfeh, A., Three-Dimensional Nonlinear Vibrations of Composite Beams-I. Equations of Motion, *Nonlinear Dynamics*, Vol. 1, 1990, pp. 477–502.
- ¹³ Gilliatt, H. C., *Investigations of Internal Resonance Phenomena and Related Nonlinear Pathologies in Aeroelastic Systems*, Master's thesis, Texas A&M University, 1997.
- ¹⁴ Thompson, D. and Strganac, T., Store-Induced Limit Cycle Oscillations and Internal Resonance in Aeroelastic Systems, *41st AIAA Structures, Structural Dynamics, and Materials Conference, AIAA Paper 2000-1413*, 2000.
- ¹⁵ Thompson, D., *Nonlinear Analysis of Store Induced Limit Cycle Oscillations*, Master's thesis, Texas A&M University, 2001.
- ¹⁶ Ko, J., Kurdila, A., , and Strganac, T., Nonlinear Control Theory for a Class of Structural Nonlinearities in a Prototypical Wing Section, *the 35th AIAA Structures, Structural Dynamics, and Materials Conference, AIAA Paper*, 1994.
- ¹⁷ O'Neil, T., Gilliatt, H., and Strganac, T., Investigations of Aeroelastic Response for a System with Continuous Structural Nonlinearities, *the 35th AIAA Structures,*

- Structural Dynamics, and Materials Conference, AIAA Paper 96-1390*, 1996.
- ¹⁸ Block, J. and Gilliatt, H., Active Control of an Aeroelastic structure, *35th Aerospace Science Meeting & Exhibit, AIAA Paper 97-0016*, 1997.
- ¹⁹ Tang, D. and Dowell, E., Experimental and Theoretical Study on Aeroelastic Response of High-Aspect-Ratio Wings, *AIAA Journal*, Vol. 39, No. 8, 2001, pp. 1430–1441.
- ²⁰ Patil, M. and Hodges, D., Nonlinear Aeroelastic Analysis of Complete Aircraft in Subsonic Flow, *Journal of Aircraft*, Vol. 37, No. 5, Sep.-Oct. 2000, pp. 753–760.
- ²¹ Kim, K. and Strganac, T., editors, *Nonlinear Responses of a Cantilever Wing with an External Store*, AIAA Paper 2003-1708, Norfolk, VA, Apr 2003, 44th AIAA Structures, Structural Dynamics, and Materials Conference.
- ²² Hodges, D. and Dowell, E., Nonlinear Equations of Motion for the Elastic Bending and Torsion of Twisted Nonuniform Rotor Blades, *NASA TN D-7818*, 1974.
- ²³ Dowell, E.H., T. J. and Hodges, D., An Experimental-Theoretical Correlation Study of Nonlinear Bending and Torsion Deformations of a Cantilever beam, *Journal of Sound and Vibration*, Vol. 50, 1977, pp. 533–544.
- ²⁴ Hodges, D., Crespo da Silva, M., and Peters, D., Nonlinear Effects in the Static and Dynamic Behavior of Beams and Rotor Blades, *Vertica*, Vol. 12, No. 3, 1988, pp. 243–256.
- ²⁵ Rosen, A. and Friedmann, P., The Nonlinear Behavior of Elastic Slender Straight Beams Undergoing Small Strains and Moderate Rotations, *Journal of Applied Mechanics*, Vol. 46, 1979, pp. 161–168.

- ²⁶ Rosen, A., Loewy, R., and Mathew, M., Nonlinear Analysis of Pretwisted Rods Using "Principal Curvature Transformation Part I: Theoretical Derivation", *Journal of Applied Mechanics*, Vol. 25, No. 3.
- ²⁷ Crespo da Silva, M. and Glynn, C., Nonlinear Flexural-Flexural-Torsional Dynamics of Inextensional Beams-I. Equations of Motions, *Journal of Structural Mechanics*, Vol. 6, No. 4, 1978, pp. 437–448.
- ²⁸ Crespo da Silva, M. and Glynn, C., Nonlinear Flexural-Flexural-Torsional Dynamics of Inextensional Beams-II. Forced Motions, *Journal of Structural Mechanics*, Vol. 6, No. 4, 1978, pp. 449–461.
- ²⁹ Kim, K., Nonlinear Equations, *private communication*, 2003.
- ³⁰ D.W.Jordan and Smith, P., *Nonlinear Ordinary Differential Equations*, Oxford University Press, Oxford, 1999.
- ³¹ Nayfeh, A. H. and Mook, D. T., *Nonlinear Oscillations*, John Wiley & Sons, Inc., New York, 1979.
- ³² Guckenheimer, A., Meloon, B., Myers, M., Wicklin, F., and Worfolk, P., *DsTool: A Dynamic System Toolkit with an Interactive Graphical Interface User's Manual*, Center for Applied Mathematics, Cornell University, Ithaca NY 14853, December 1997.
- ³³ Doedel, E., Affenroth, R., Champneys, A., Fairgrieve, T., Kuznetsov, Y., Sandstede, B., and Wan, X., *AUTO2000: Continuation and Bifurcation Software for Ordinary Differential Equations (with Hom-Cont)*, <http://www.enm.bris.ac.uk/staff/hinke/dss/continuation/auto.html>,

- <http://www.math.ohio-state.edu/~sandsted/publications/auto2000.pdf>, November 5 2003.
- ³⁴ Schaub, H. and Junkins, J. J., *Analytical Mechanics of Space Systems*, AIAA Education Series, 2003.
- ³⁵ Bisplinghoff, R., Ashley, H., and Halfman, R., *Aeroelasticity*, Dover, New York, 1955.
- ³⁶ Strganac, T. W., *Lecture Notes on Aeroelasticity*.
- ³⁷ Lee, B. and Price, S., Nonlinear Aeroelastic Analysis of Airfoils : Bifurcation and Chaos, *Progress in Aerospace Sciences*, Vol. 35, 1999, pp. 205–334.
- ³⁸ Poirel, D. and Price, S., Post-instability behavior of a structurally nonlinear airfoil in longitudinal turbulence, *Journal of Aircraft*, Vol. 34, 1997, pp. 619–626.
- ³⁹ Tang, D. and Dowell, E., Nonlinear Response of a Non-Rotating Rotor Blade to a Periodic Gust, *Journal of Fluids and Structures*, Vol. 10.
- ⁴⁰ Kim, S., *Aeroelastic Analysis for Control Surface of Flight Vehicle with Structural Nonlinearities*, Ph.D. Dissertation, Korean Advanced Institute of Science and Technology, 1994.
- ⁴¹ S.H. Kim and I. Lee , *Aeroelastic Analysis of a Flexible Airfoil with a Freeplay Non-linearity*, *Journal of Sound and Vibration*, Vol. 194, 1996, pp. 823-846.
- ⁴² Nayfeh, A. H. and Balachadran, B., *Applied Nonlinear Dynamics*, John Wiley & Sons, Inc., New York, 1995.
- ⁴³ Slotine, J.-J. E. and Li, W., *Applied Nonlinear Control*, Prentice Hall, Inc., New York.

- ⁴⁴ Greenberg, M., *Advanced Engineering Mathematics*, Prentice Hall, Inc., New York.
- ⁴⁵ Moon, F. C., *Chaotic Vibrations*, John Wiley & Sons, Inc., New York, 1987.
- ⁴⁶ Strganac, T., Ko, J., and Thompson, D., Identification and Control of Limit Cycle Oscillations in Aeroelastic Systems, *Journal of Guidance, Control, and Dynamics*, Vol. 23, Nov.-Dec., 2000, pp. 1127–1133.
- ⁴⁷ Eastep, F., Transonic Flutter Analysis of a Rectangular Wing with Conventional Airfoil Sections, *AIAA Journal*, Vol. 18, No. 10, Oct. 1986, pp. 1159–1164.
- ⁴⁸ Beran, P., Khot, N., Eastep, R. S., Zweber, J., Huttzell, L., and Scott, J., editors, *The Dependence of Store-Induced Limit-Cycle Oscillation Predictions on Modelling Fidelity*, Presented at the RTO Applied Vehicle Technology Panel Symposium, Apr 2002.
- ⁴⁹ Beran, P. S., Strganac, T. W., and Kim, K., editors, *Studies of Store-Induced Limit-Cycle Oscillations Using a Model with Full System Nonlinearities*, Norfolk, VA, Apr. 7-10 2003, 44th AIAA/ASME/ASCE/AHS/ASC Structures, Structural Dynamics, and Materials Conference.
- ⁵⁰ Hall, B. D., Mook, D. T., and Nayfeh, A., Novel Strategy for Suppressing the Flutter Oscillations of Aircraft Wings, *AIAA Journal*, Vol. 39, No. 10, October 2001, pp. 1843–1850.
- ⁵¹ Pai, P.-J. F., *Nonlinear Flexural-Flexural-Torsional Dynamics of Metallic and Composite Beams*, Ph.D. Dissertation, Virginia Polytechnic Institute and State University, 1990.
- ⁵² Nickkawde, C., Nonlinear Responses of a Cantilever Wing with an External Store, AIAA 2003-1708, *Nonlinear Vibrations: Project Report*, 2003.

- ⁵³ Rand, R. H., *Lecture Notes on Nonlinear Vibrations (version 45)*, Dept. Theoretical & Applied Mechanics, Cornell University, <http://www.tam.cornell.edu/randdocs>, 2003.
- ⁵⁴ Seydel, R., *From Equilibrium to Chaos: Practical Bifurcation and Stability Analysis*, Elsevier Science publishing Co., Inc., New York, 10017, 1988.
- ⁵⁵ Nayfeh, A. H., *Introduction to Perturbation Techniques*, John Wiley & Sons, Inc., New York, 1981.
- ⁵⁶ Bush, A. W., *Perturbation Methods for Engineer and Scientist*, CRC Press, Inc., Boca Raton Florida, 1992.
- ⁵⁷ Kim, J., *Nonlinear Beam Equations, private communication*, 2001.
- ⁵⁸ Craig, R. R., *Structural Dynamics: An introduction to Computer Methods*, John Wiley & Sons, Inc., Edison, NJ 08817, 1981.
- ⁵⁹ Meirovitch, L., *Computational Methods in Structural Dynamics*, Kluwer Academic Publishers, Hingham, MA 02018-0358, 1980.

APPENDIX I

DEFINITIONS FOR EQUATIONS OF MOTION

Kinematics As shown in Figs. 1 and 2, let P_d be an arbitrary position in the local coordinate system with the inertial position vector R_w , and the external store has the inertial position vector R_s . A point $P_e^0 = (0, \hat{s}, 0)$ on the elastic axis in the inertial frame $X - Y - Z$ is located at $P_e = (u, \hat{s} + v, w)$ after deformation. This point is denoted by another inertial position vector R_e . In the local coordinate system $\xi - \eta - \zeta$, the points P_d , the store mass and an arbitrary position in the store have local position vectors, r_w , r_{sc} , and r_s , respectively. Additionally, the position vector r_s can be expressed by r_{sc} and r_{sl} , in which r_{sl} is a position vector in the local store coordinate system $\xi_s - \eta_s - \zeta_s$.

$$\begin{aligned}
R_w &= \overrightarrow{OP}_d = R_e + r_w = u\hat{i} + (\hat{s} + v)\hat{j} + w\hat{k} + [\xi\hat{e}_\xi + 0\hat{e}_\eta + \zeta\hat{e}_\zeta] \\
R_s &= \overrightarrow{OP}_{sd} = R_e + r_s = R_e + r_{sc} + r_{sl} \\
&= u\hat{i} + (\hat{s} + v)\hat{j} + w\hat{k} + [\xi_s\hat{e}_\xi + 0\hat{e}_\eta + \zeta_s\hat{e}_\zeta]
\end{aligned} \tag{A.1}$$

Using the transformation matrix, $[T]$, and taking the time derivatives of R_w and R_s , we find

$$\begin{aligned}
\dot{R}_w &= \dot{R}_e + \dot{r}_w \\
&= \dot{u}\hat{i} + \dot{v}\hat{j} + \dot{w}\hat{k} + [(\xi\dot{T}_{11} + \eta\dot{T}_{31})\hat{i} + (\xi\dot{T}_{12} + \eta\dot{T}_{32})\hat{j} + (\xi\dot{T}_{13} + \eta\dot{T}_{33})\hat{k}] \\
\dot{R}_s &= \dot{R}_e + \dot{r}_s \\
&= \dot{u}\hat{i} + \dot{v}\hat{j} + \dot{w}\hat{k} + [(\xi_s\dot{T}_{11} + \eta_s\dot{T}_{31})\hat{i} + (\xi_s\dot{T}_{12} + \eta_s\dot{T}_{32})\hat{j} + (\xi_s\dot{T}_{13} + \eta_s\dot{T}_{33})\hat{k}]
\end{aligned} \tag{A.2}$$

When these time derivatives are instituted into the kinetic energy , the following inner product terms are required.

$$\begin{aligned}\dot{R}_w \cdot \dot{R}_w &= (\dot{R}_e + \dot{r}_w) \cdot (\dot{R}_e + \dot{r}_w) \\ &= (\dot{R}_e \cdot \dot{R}_e + \dot{R}_e \cdot \dot{r}_w + \dot{r}_w \cdot \dot{R}_e + \dot{r}_w \cdot \dot{r}_w)\end{aligned}\quad (\text{A.3})$$

$$\begin{aligned}\dot{R}_s \cdot \dot{R}_s &= (\dot{R}_e + \dot{r}_s) \cdot (\dot{R}_e + \dot{r}_s) \\ &= (\dot{R}_e \cdot \dot{R}_e + \dot{R}_e \cdot \dot{r}_s + \dot{r}_s \cdot \dot{R}_e + \dot{r}_s \cdot \dot{r}_s)\end{aligned}\quad (\text{A.4})$$

In the above expression, the rotational energy term of the rigid store can be rewritten in terms of the local store coordinates.

$$\begin{aligned}\dot{r}_s \cdot \dot{r}_s &= (\dot{r}_{sc} + \dot{r}_{sl}) \cdot (\dot{r}_{sc} + \dot{r}_{sl}) \\ &= (\dot{r}_{sc} \cdot \dot{r}_{sc} + 2\dot{r}_{sc} \cdot \dot{r}_{sl} + \dot{r}_{sl} \cdot \dot{r}_{sl})\end{aligned}\quad (\text{A.5})$$

When these terms are integrated over the given domain, the following material properties can be defined.

$$\begin{aligned}m &= \int \rho_w d\xi d\zeta \\ me_x &= \int \rho_w \xi d\xi d\zeta \\ me_z &= \int \rho_w \zeta d\xi d\zeta \\ I_\xi &= \int \rho_w \xi^2 d\xi d\zeta \\ I_\eta &= \int \rho_w \eta^2 d\xi d\zeta \\ I_\zeta &= \int \rho_w \zeta^2 d\xi d\zeta \\ I_{\xi\zeta} &= \int \rho_w \xi \zeta d\xi d\zeta\end{aligned}\quad (\text{A.6})$$

$$M_s = \int \rho_s d\xi_s d\zeta_s$$

$$\begin{aligned}
M_s x_s &= \int \rho_s \xi_s d\xi_s d\zeta_s \\
M_s z_s &= \int \rho_s \zeta_s d\xi_s d\zeta_s \\
I_{s\xi} &= \int \rho_s \xi_s^2 d\xi_s d\zeta_s \\
I_{s\eta} &= \int \rho_s \eta_s^2 d\xi_s d\zeta_s \\
I_{s\zeta} &= \int \rho_s \zeta_s^2 d\xi_s d\zeta_s \\
I_{s\xi\zeta} &= \int \rho_s \xi_s \zeta_s d\xi_s d\zeta_s
\end{aligned} \tag{A.7}$$

where ρ_w and ρ_s are the material density of wing and store, respectively.

Euler Angles and Displacements The direction cosine matrix (or transformation matrix) is the most fundamental method of describing a relative orientation.³⁴ Using Figures 1 and 2, the transformation from the undeformed $X - Y - Z$ coordinate system (the inertial frame) to the deformed coordinate system $\xi - \eta - \zeta$ (the local frame) can be expressed as

$$\{E\} = [T] \{N\} \tag{A.8}$$

Depending upon the used Euler angles, the expressions for transformation matrix can be changed. But, their final expression in terms of displacements should be unique.²⁴ In terms of the (1-3-2) Euler angles (ϕ, ψ, θ) , the direction cosine matrix is written as

$$[T] = T_{ij} = \begin{bmatrix} c\theta c\psi & c\theta s\psi c\phi + s\theta s\phi & c\theta s\psi s\phi - s\theta c\psi \\ -s\psi & c\psi c\phi & c\psi s\phi \\ s\theta c\psi & s\theta s\psi c\phi - c\theta s\phi & s\theta s\psi s\phi + c\theta c\phi \end{bmatrix} \tag{A.9}$$

In this matrix, the terms having Euler angles ϕ or ψ can be represented in terms of the derivatives of displacements as follows,

$$\cos \phi = \frac{1 + v'}{\sqrt{(1 + v')^2 + w'^2}}$$

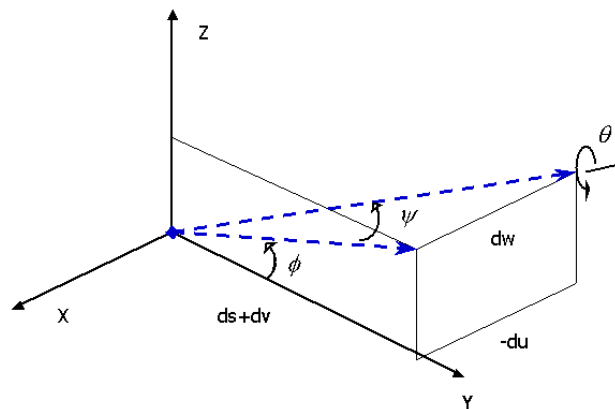


Fig. 86. Euler Angles and the derivatives of displacements

$$\begin{aligned}
 \sin \phi &= \frac{w'}{\sqrt{(1+v')^2 + w'^2}} \\
 \cos \psi &= \frac{\sqrt{(1+v')^2 + w'^2}}{\sqrt{(1+v')^2 + u'^2 + w'^2}} \\
 \sin \psi &= \frac{-u}{\sqrt{(1+v')^2 + u'^2 + w'^2}}
 \end{aligned} \tag{A.10}$$

These ex are obtained from Fig. 86. Using Taylor-Series expansions of sin and cos functions, and keeping terms up to $O(\epsilon^3)$ gives

$$\begin{aligned}
 \cos \phi &= 1 - \frac{1}{2}w'^2 + w'^2v' \\
 \sin \phi &= w' - w'v' + w'v'^2 - \frac{1}{2}w'^3 \\
 \cos \psi &= 1 - \frac{1}{2}u'^2 + u'^2v' \\
 \sin \psi &= -u' + u'v' - u'v'^2 + \frac{1}{2}u'w'^2 + \frac{1}{2}u'^3 \\
 \cos \theta &= 1 - \frac{1}{2}\theta^2 \\
 \sin \theta &= \theta - \frac{1}{6}\theta^3
 \end{aligned} \tag{A.11}$$

or,

$$\phi = w' - w'v' + w'v'^2 - \frac{1}{3}w'^3 + H.O.T \quad (\text{A.12})$$

$$\psi = -u' + u'v' - u'v'^2 + \frac{1}{2}u'w'^2 + \frac{1}{3}u'^3 + H.O.T \quad (\text{A.13})$$

The derivatives of ϕ and ψ are

$$\frac{\partial \phi}{\partial u'} = 0 \quad (\text{A.14})$$

$$\frac{\partial \phi}{\partial v'} = -w' + 2w'v' \quad (\text{A.15})$$

$$\frac{\partial \phi}{\partial w'} = 1 - v' + v'^2 - w'^2 \quad (\text{A.16})$$

$$\frac{\partial \psi}{\partial u'} = -1 + v' - v'^2 + \frac{1}{2}w'^2 + u'^2 \quad (\text{A.17})$$

$$\frac{\partial \psi}{\partial v'} = u' - 2u'v' \quad (\text{A.18})$$

$$\frac{\partial \psi}{\partial w'} = u'w' \quad (\text{A.19})$$

For ease of formulation in the following expressions, the expressions for some combined cases are summarized as follows.

$$\cos \phi \cos \theta = 1 - \frac{1}{2}(w'^2 + \theta^2) + w'^2v'$$

$$\cos \phi \cos \psi = 1 - \frac{1}{2}(u'^2 + w'^2) + w'^2v' + u'^2v'$$

$$\cos \phi \sin \theta = \theta - \left(\frac{1}{2}\theta w'^2 + \frac{1}{6}\theta^3 \right)$$

$$\cos \phi \sin \psi = -u' + u'v' - u'(v'^2 + w'^2) + \frac{1}{2}u'^3$$

$$\cos \theta \cos \psi = 1 - \frac{1}{2}(\theta^2 + u'^2) + u'^2v'$$

$$\cos \theta \sin \psi = -u' + u'v' + \frac{1}{2}\theta^2u' - u'v'^2 + \frac{1}{2}u'(w'^2 + u'^2)$$

$$\sin \phi \cos \theta = w' - w'v' + w'v'^2 - \frac{1}{2}w'(w'^2 + \theta^2)$$

$$\sin \phi \cos \psi = w' - w'v' + w'v'^2 - \frac{1}{2}w'(w'^3 + u'^2)$$

$$\begin{aligned}
\sin \phi \sin \theta &= w' \theta - w' v' \theta \\
\sin \phi \sin \psi &= -w' u' + 2w' v' u' \\
\sin \theta \cos \psi &= \theta - \frac{1}{2} u'^2 \theta - \frac{1}{6} \theta^3 \\
\sin \theta \sin \psi &= -u' \theta + u' v' \theta \\
\cos \phi \cos \theta \cos \psi &= 1 - \frac{1}{2} u'^2 + u'^2 v' - \frac{1}{2} (w'^2 + \theta^2) + w'^2 v' \\
\cos \phi \cos \theta \sin \psi &= -u' + u' v' + \frac{1}{2} u' (w'^2 + \theta^2) - u' v'^2 + \frac{1}{2} u' (u'^2 + w'^2) \\
\cos \phi \sin \theta \cos \psi &= \theta - \frac{1}{2} \theta (u'^2 + w'^2) - \frac{1}{6} \theta^3 \\
\cos \phi \sin \theta \sin \psi &= -u' \theta + u' v' \theta \\
\sin \phi \cos \theta \cos \psi &= w' - w' v' + w' v'^2 - \frac{1}{2} (w'^3 + w' \theta^2) \\
\sin \phi \cos \theta \sin \psi &= -u' w' + 2u' w' v' \\
\sin \phi \sin \theta \cos \psi &= w' \theta - w' v' \theta \\
\sin \phi \sin \theta \sin \psi &= -w' u' \theta
\end{aligned} \tag{A.20}$$

Substituting Eq. (A.11) into Eq. (A.9), we obtain the following expressions for the components.

$$\begin{aligned}
T_{11} &= 1 - \frac{1}{2} (u'^2 + \theta^2) + u'^2 v' \\
T_{12} &= -u' + (u' v' + w' \theta) + (-u' v'^2 + u' w'^2 + \frac{1}{2} u'^3 + \frac{1}{2} u' \theta^2 - w' v' \theta) \\
T_{13} &= -\theta - u' w' + (2u' v' w' + \frac{1}{2} w'^2 \theta + \frac{1}{6} \theta^3) \\
T_{21} &= u' - u' v' + u' v'^2 - \frac{1}{2} u' w'^2 - \frac{1}{2} u'^3 \\
T_{22} &= 1 - \frac{1}{2} (w'^2 + u'^2) + v' (w'^2 + u'^2) \\
T_{23} &= \theta - \frac{1}{2} u'^2 \theta - \frac{1}{6} \theta^3 \\
T_{31} &= \theta - \frac{1}{6} \theta^3 - \frac{1}{2} u'^2 \theta \\
T_{32} &= -w' - u' \theta + w' v' + (u' v' \theta - w' v'^2 + \frac{1}{2} w'^3 + \frac{1}{2} \theta^2 w')
\end{aligned}$$

$$T_{33} = 1 - \frac{1}{2}(\theta^2 + w'^2) + (w'^2 v' - \theta u' w') \quad (\text{A.21})$$

Based on these expressions, the expressions for derivatives with respect to time and space can be obtained as

$$\begin{aligned} \dot{T}_{11} &= -\frac{1}{2}(u'^2 + \theta^2)' + (u'^2 v')' \\ \dot{T}_{12} &= -\dot{u}' + (u'v' + w'\theta)' + (-u'v'^2 + u'w'^2 + \frac{1}{2}u'^3 + \frac{1}{2}u'\theta^2 - w'v'\theta)' \\ \dot{T}_{13} &= -\dot{\theta} - (u'w')' + (2u'v'w' + \frac{1}{2}w'^2\theta + \frac{1}{6}\theta^3)' \\ \ddot{T}_{11} &= -\frac{1}{2}(u'^2 + \theta^2)'' + (u'^2 v')'' \\ \ddot{T}_{12} &= -\ddot{u}' + (u'v' + w'\theta)'' + (-u'v'^2 + u'w'^2 + \frac{1}{2}u'^3 + \frac{1}{2}u'\theta^2 - w'v'\theta)'' \\ \ddot{T}_{13} &= -\ddot{\theta} - (u'w')'' + (2u'v'w' + \frac{1}{2}w'^2\theta + \frac{1}{6}\theta^3)'' \\ \frac{\partial \dot{T}_{11}}{\partial \theta} &= -\theta \\ \frac{\partial \dot{T}_{12}}{\partial \theta} &= w' + \theta u' - w'v' \\ \frac{\partial \dot{T}_{13}}{\partial \theta} &= -1 + \frac{1}{2}(w'^2 + \theta^2) \\ \frac{d}{dt} \frac{\partial \dot{T}_{11}}{\partial \theta} &= \dot{\theta} \\ \frac{d}{dt} \frac{\partial \dot{T}_{12}}{\partial \theta} &= \dot{w}' + (\theta u' - w'v')' \\ \frac{d}{dt} \frac{\partial \dot{T}_{13}}{\partial \theta} &= \frac{1}{2}(w'^2 + \theta^2)' \end{aligned} \quad (\text{A.22})$$

$$\begin{aligned} \dot{T}_{31} &= \dot{\theta} - \frac{1}{2}\dot{\theta}\theta^2 - \frac{1}{2}(u'^2\theta)' \\ \dot{T}_{32} &= -\dot{w}' - (u'\theta + w'v')' + \left(u'v'\theta - w'v'^2 + \frac{1}{2}w'^3 + \frac{1}{2}\theta^2 w'\right)' \\ \dot{T}_{33} &= -\frac{1}{2}(\theta^2 + w'^2)' + (w'^2 v' - \theta u' w')' \\ \ddot{T}_{31} &= \ddot{\theta} - \frac{1}{2}\ddot{\theta}\theta^2 - \frac{1}{2}(u'^2\theta)'' \\ \ddot{T}_{32} &= -\ddot{w}' - (u'\theta + w'v')'' + \left(u'v'\theta - w'v'^2 + \frac{1}{2}w'^3 + \frac{1}{2}\theta^2 w'\right)'' \\ \ddot{T}_{33} &= -\frac{1}{2}(\theta^2 + w'^2)'' + (w'^2 v' - \theta u' w')'' \end{aligned}$$

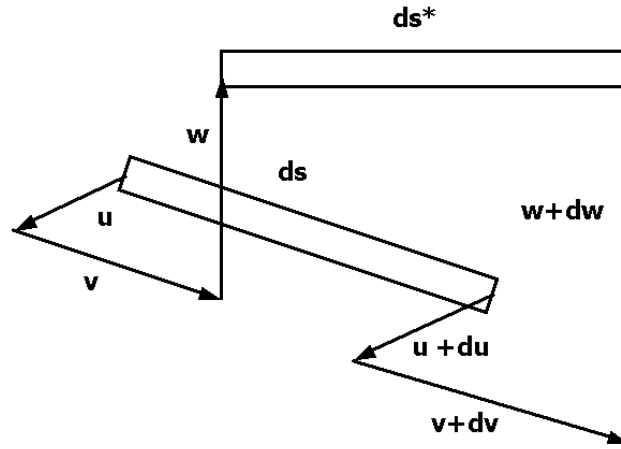


Fig. 87. A differential element of the beam

$$\begin{aligned}
 \frac{\partial \dot{T}_{31}}{\partial \theta} &= 1 - \frac{1}{2}\theta^2 - \frac{1}{2}u'^2 \\
 \frac{\partial \dot{T}_{32}}{\partial \theta} &= -u' + u'v' + w'\theta \\
 \frac{\partial \dot{T}_{33}}{\partial \theta} &= -\theta - u'w' \\
 \frac{d}{dt} \frac{\partial \dot{T}_{31}}{\partial \theta} &= -\theta\dot{\theta} - \dot{u}'u' \\
 \frac{d}{dt} \frac{\partial \dot{T}_{32}}{\partial \theta} &= -\dot{u}' + \dot{u}'v' + \dot{\theta}w' + \theta w' \\
 \frac{d}{dt} \frac{\partial \dot{T}_{33}}{\partial \theta} &= -\dot{\theta} - \dot{u}'w' - u'\dot{w}'
 \end{aligned} \tag{A.23}$$

Inextensibility Condition For an inextensional beam, a differential element of the beam is considered. As shown in Fig. 87, its undeformed length is ds and the deformed length is ds^* . From this figure, the deformed length ds^* is obtained as follows,

$$\begin{aligned}
 ds^* &= \sqrt{[(ds + u + du - u)^2 + (v + dv - v)^2 + (w + dw - w)^2]} \\
 &= \sqrt{[(1 + u')^2 + v'^2 + w'^2] ds^2}
 \end{aligned} \tag{A.24}$$

The difference between ds^* and ds is determined as follows,

$$\begin{aligned} |ds^*|^2 - |ds|^2 &= (|ds^*| - |ds|)(|ds^*| + |ds|) \\ &= \left[(1 + u')^2 + v'^2 + w'^2 \right] ds^2 - ds^2 \end{aligned} \quad (\text{A.25})$$

or

$$|ds^*| - |ds| = \left\{ \left[(1 + u')^2 + v'^2 + w'^2 \right] - 1 \right\} \frac{ds^2}{(|ds^*| + |ds|)} \quad (\text{A.26})$$

For an inextensional beam, the difference must be zero because there is no axial stretch. Thus, the equation satisfying the inextensional condition is

$$\left[(1 + u')^2 + v'^2 + w'^2 \right] - 1 = 0 \quad (\text{A.27})$$

Angular Velocity and Curvature The instantaneous angular velocity vector ω of local frame relative to the inertial frame is simply

$$\omega = \omega_\xi \hat{e}_\xi + \omega_\eta \hat{e}_\eta + \omega_\zeta \hat{e}_\zeta = \dot{\phi} \hat{i} + \dot{\psi} \hat{k}_1 + \dot{\theta} \hat{j}_2 \quad (\text{A.28})$$

where the dot means $\partial()/\partial t$, Using the transformation matrix and its property, each component of the angular velocity vector can be determined as

$$\begin{aligned} \omega_\xi &= \dot{\phi} \cos \theta \cos \psi - \dot{\psi} \sin \theta \\ \omega_\eta &= -\dot{\phi} \sin \psi + \dot{\theta} \\ \omega_\zeta &= \dot{\phi} \sin \theta \cos \psi + \dot{\psi} \cos \theta \end{aligned} \quad (\text{A.29})$$

According to Kirchoff's kinetic analogy,^{12,27} the curvature can be obtained from ω by replacing $\partial/\partial t()$ with $\partial/\partial s()$.

$$\rho = \rho_\xi \hat{e}_\xi + \rho_\eta \hat{e}_\eta + \rho_\zeta \hat{e}_\zeta \quad (\text{A.30})$$

and

$$\begin{aligned}
 \rho_\xi &= \phi' \cos \theta \cos \psi - \psi' \sin \theta \\
 \rho_\eta &= -\phi' \sin \psi + \theta' \\
 \rho_\zeta &= \phi' \sin \theta \cos \psi + \psi' \cos \theta
 \end{aligned} \tag{A.31}$$

Using these expressions for angular velocities and curvatures, their derivatives are obtained as follows,

$$\frac{\partial \omega_\xi}{\partial \phi} = 0 \tag{A.32}$$

$$\frac{\partial \omega_\xi}{\partial \theta} = \dot{\phi} \sin \theta \cos \psi - \dot{\psi} \cos \theta \tag{A.33}$$

$$\frac{\partial \omega_\xi}{\partial \psi} = -\dot{\phi} \cos \theta \sin \psi \tag{A.34}$$

$$\frac{\partial \omega_\xi}{\partial \dot{\phi}} = \cos \theta \cos \psi \tag{A.35}$$

$$\frac{\partial \omega_\xi}{\partial \dot{\theta}} = 0 \tag{A.36}$$

$$\frac{\partial \omega_\xi}{\partial \dot{\psi}} = -\sin \theta \tag{A.37}$$

$$\frac{\partial \omega_\eta}{\partial \phi} = 0 \tag{A.38}$$

$$\frac{\partial \omega_\eta}{\partial \theta} = 0 \tag{A.39}$$

$$\frac{\partial \omega_\eta}{\partial \psi} = -\dot{\phi} \cos \psi \tag{A.40}$$

$$\frac{\partial \omega_\eta}{\partial \dot{\phi}} = -\sin \psi \tag{A.41}$$

$$\frac{\partial \omega_\eta}{\partial \dot{\theta}} = 1 \tag{A.42}$$

$$\frac{\partial \omega_\eta}{\partial \dot{\psi}} = 0 \tag{A.43}$$

$$\frac{\partial \omega_\zeta}{\partial \phi} = 0 \quad (\text{A.44})$$

$$\frac{\partial \omega_\zeta}{\partial \theta} = -\dot{\phi} \cos \theta \cos \psi - \dot{\psi} \sin \theta \quad (\text{A.45})$$

$$\frac{\partial \omega_\zeta}{\partial \psi} = -\dot{\phi} \sin \theta \sin \psi \quad (\text{A.46})$$

$$\frac{\partial \omega_\zeta}{\partial \dot{\phi}} = \sin \theta \cos \psi \quad (\text{A.47})$$

$$\frac{\partial \omega_\zeta}{\partial \dot{\theta}} = 0 \quad (\text{A.48})$$

$$\frac{\partial \omega_\zeta}{\partial \dot{\psi}} = \cos \theta \quad (\text{A.49})$$

$$\frac{\partial \rho_\xi}{\partial \phi} = 0 \quad (\text{A.50})$$

$$\frac{\partial \rho_\xi}{\partial \theta} = -\phi' \sin \theta \cos \psi - \psi' \cos \theta \quad (\text{A.51})$$

$$\frac{\partial \rho_\xi}{\partial \psi} = -\phi' \cos \theta \sin \psi \quad (\text{A.52})$$

$$\frac{\partial \rho_\xi}{\partial \phi'} = \cos \theta \cos \psi \quad (\text{A.53})$$

$$\frac{\partial \rho_\xi}{\partial \theta'} = 0 \quad (\text{A.54})$$

$$\frac{\partial \rho_\xi}{\partial \psi'} = -\sin \theta \quad (\text{A.55})$$

$$\frac{\partial \rho_\eta}{\partial \phi} = 0 \quad (\text{A.56})$$

$$\frac{\partial \rho_\eta}{\partial \theta} = 0 \quad (\text{A.57})$$

$$\frac{\partial \rho_\eta}{\partial \psi} = -\phi' \cos \psi \quad (\text{A.58})$$

$$\frac{\partial \rho_\eta}{\partial \phi'} = -\sin \psi \quad (\text{A.59})$$

$$\frac{\partial \rho_\eta}{\partial \theta'} = 1 \quad (\text{A.60})$$

$$\frac{\partial \rho_\eta}{\partial \psi'} = 0 \quad (\text{A.61})$$

$$\frac{\partial \rho_\zeta}{\partial \phi} = 0 \quad (\text{A.62})$$

$$\frac{\partial \rho_\zeta}{\partial \theta} = \phi' \cos \theta \cos \psi - \psi' \sin \theta \quad (\text{A.63})$$

$$\frac{\partial \rho_\zeta}{\partial \psi} = -\phi' \sin \theta \sin \psi \quad (\text{A.64})$$

$$\frac{\partial \rho_\zeta}{\partial \phi'} = \sin \theta \cos \psi \quad (\text{A.65})$$

$$\frac{\partial \rho_\zeta}{\partial \theta'} = 0 \quad (\text{A.66})$$

$$\frac{\partial \rho_\zeta}{\partial \psi'} = \cos \theta \quad (\text{A.67})$$

Substituting the Euler angles into Eqs. (A.29) and (A.31), and keeping up to $O(\epsilon^3)$, we obtain

$$\begin{aligned} \omega_\xi &= \dot{w}' - (w'v') + w'^2 \dot{w}' - \frac{1}{2} \dot{w}'(\theta^2 + u'^2) + \dot{u}'\theta - \theta(u'v') \\ \omega_\eta &= \dot{\theta} + \dot{w}'u' - u'(w'v') - \dot{w}'(u'v') \\ \omega_\zeta &= -\dot{u}' + (u'v') + \dot{w}'\theta - \theta \dot{w}'v' - \theta w'\dot{v}' - (u'v'^2) + \left(\frac{1}{2}u'w'^2 + \frac{1}{3}u'^3 \right) + \frac{1}{2}\dot{u}'\theta^2 \end{aligned} \quad (\text{A.68})$$

Partial Derivatives of L_T The partial derivatives of $L_T = L_W + L_s$ shown in Eqs. (2.8) and (2.18), are defined in this section.

$$\begin{aligned} \frac{d}{dt} \left(\frac{\partial L_W}{\partial \dot{u}} \right) &= \frac{d}{dt} \left(\frac{\partial T_{w1}}{\partial \dot{u}} + \frac{\partial T_{w2}}{\partial \dot{u}} \right) = m\ddot{u} + me\ddot{T}_{11} \\ &= m\ddot{u} + me \left[-\frac{1}{2}(u'^2 + \theta^2)'' + (u'^2v')'' \right] \end{aligned} \quad (\text{A.69})$$

$$\begin{aligned} \frac{d}{dt} \left(\frac{\partial L_W}{\partial \dot{v}} \right) &= \frac{d}{dt} \left(\frac{\partial T_{w1}}{\partial \dot{v}} + \frac{\partial T_{w2}}{\partial \dot{v}} \right) = m\ddot{v} + me\ddot{T}_{12} \\ &= me \{ -\ddot{u}' + (u'v' + w'\theta)'' + \left(-u'v'^2 + u'w'^2 + \frac{1}{2}u'^3 + \frac{1}{2}\theta^2u - \theta w'v' \right)'' \} \end{aligned}$$

$$\begin{aligned} \frac{d}{dt} \left(\frac{\partial L_W}{\partial \dot{w}} \right) &= \frac{d}{dt} \left(\frac{\partial T_{w1}}{\partial \dot{w}} + \frac{\partial T_{w2}}{\partial \dot{w}} \right) = m\ddot{w} + me\ddot{T}_{13} \\ &= me \{ -\ddot{\theta} - (u'w')'' + \left(2u'v'w' + \frac{1}{2}\theta^3 + \frac{1}{2}\theta w'^2 \right)'' \} \end{aligned} \quad (\text{A.70})$$

$$\frac{\partial L_T}{\partial u} = \frac{\partial L_T}{\partial v} = \frac{\partial L_T}{\partial w} = 0 \quad (\text{A.71})$$

$$\begin{aligned} \frac{\partial L_W}{\partial \theta} &= \frac{\partial T_{w2}}{\partial \theta} + \frac{\partial T_{w3}}{\partial \theta} - \frac{\partial V_w}{\partial \theta} \\ &= me \left(\frac{\partial \dot{T}_{11}}{\partial \theta} \dot{u} + \frac{\partial \dot{T}_{12}}{\partial \theta} \dot{v} + \frac{\partial \dot{T}_{13}}{\partial \theta} \dot{w} \right) \\ &\quad + I_\xi \omega_\xi \frac{\partial \omega_\xi}{\partial \theta} + I_\eta \omega_\eta \frac{\partial \omega_\eta}{\partial \theta} + I_\zeta \omega_\zeta \frac{\partial \omega_\zeta}{\partial \theta} \\ &\quad - D_\xi \rho_\xi \frac{\partial \rho_\xi}{\partial \theta} - D_\eta \rho_\eta \frac{\partial \rho_\eta}{\partial \theta} - D_\zeta \rho_\zeta \frac{\partial \rho_\zeta}{\partial \theta} \end{aligned} \quad (\text{A.72})$$

$$\begin{aligned} \frac{d}{dt} \left(\frac{\partial L_W}{\partial \dot{\theta}} \right) &= \frac{d}{dt} \left(\frac{\partial T_{w2}}{\partial \dot{\theta}} + \frac{\partial T_{w3}}{\partial \dot{\theta}} \right) \\ &= \frac{d}{dt} \left\{ me \left(\frac{\partial \dot{T}_{11}}{\partial \dot{\theta}} \dot{u} + \frac{\partial \dot{T}_{12}}{\partial \dot{\theta}} \dot{v} + \frac{\partial \dot{T}_{13}}{\partial \dot{\theta}} \dot{w} \right) \right. \\ &\quad \left. + I_\xi \omega_\xi \frac{\partial \omega_\xi}{\partial \dot{\theta}} + I_\eta \omega_\eta \frac{\partial \omega_\eta}{\partial \dot{\theta}} + I_\zeta \omega_\zeta \frac{\partial \omega_\zeta}{\partial \dot{\theta}} \right\} \end{aligned} \quad (\text{A.73})$$

$$\begin{aligned} \frac{d}{ds} \left(\frac{\partial L_W}{\partial \theta'} \right) &= -\frac{d}{ds} \left(\frac{\partial V_w}{\partial \theta'} \right) \\ &= -\frac{d}{ds} \left\{ D_\xi \rho_\xi \frac{\partial \rho_\xi}{\partial \theta} + D_\eta \rho_\eta \frac{\partial \rho_\eta}{\partial \theta} + D_\zeta \rho_\zeta \frac{\partial \rho_\zeta}{\partial \theta} \right\} \end{aligned} \quad (\text{A.74})$$

$$\begin{aligned} A_\theta &= -I_2 \ddot{\theta} + me \ddot{w} + D_2 \theta'' - I_2 (u' \dot{w}') + D_2 (w'' u')' \\ &\quad - me \left[-\theta \ddot{u} - \frac{1}{2} \int (u'^2 + w'^2) \ddot{u} ds + \frac{1}{2} me (w'^2 + \theta^2) \ddot{w} \right] \\ &\quad + (I_3 - I_1) (\theta \dot{w}'^2 - \theta \dot{u}'^2 - \dot{w}' \dot{u}') \\ &\quad - (D_3 - D_1) (\theta w''^2 - \theta u''^2 - w'' u'') \end{aligned} \quad (\text{A.75})$$

From the above expression and the condition, $A_\theta = 0$, the following result is obtained.

$$-I_2 \ddot{\theta} + me \ddot{w} + D_2 \theta'' - I_2 (u' \dot{w}') + D_2 (w'' u')'$$

$$\begin{aligned}
&= -me \left[-\theta |ddotu - \frac{1}{2} \int (u'^2 + w'^2)'' ds + \frac{1}{2} me (w'^2 + \theta^2) \ddot{w} \right] \\
&\quad + (I_3 - I_1) (\theta \dot{w}'^2 - \theta \dot{u}'^2 - \dot{w}' \dot{u}') \\
&\quad - (D_3 - D_1) (\theta w''^2 - \theta u''^2 - w'' u'')
\end{aligned} \tag{A.76}$$

$$\begin{aligned}
\frac{\partial L_W}{\partial \phi} &= \frac{\partial T_{w2}}{\partial \phi} + \frac{\partial T_{w3}}{\partial \phi} - \frac{\partial V_w}{\partial \phi} \\
&= me \left(\frac{\partial \dot{T}_{11}}{\partial \theta} \dot{u} + \frac{\partial \dot{T}_{12}}{\partial \theta} \dot{v} + \frac{\partial \dot{T}_{13}}{\partial \theta} \dot{w} \right) \\
&\quad + I_\xi \omega_\xi \frac{\partial \omega_\xi}{\partial \phi} + I_\eta \omega_\eta \frac{\partial \omega_\eta}{\partial \phi} + I_\zeta \omega_\zeta \frac{\partial \omega_\zeta}{\partial \phi} \\
&\quad - D_\xi \rho_\xi \frac{\partial \rho_\xi}{\partial \phi} - D_\eta \rho_\eta \frac{\partial \rho_\eta}{\partial \phi} - D_\zeta \rho_\zeta \frac{\partial \rho_\zeta}{\partial \phi}
\end{aligned} \tag{A.77}$$

$$\begin{aligned}
\frac{d}{dt} \left(\frac{\partial L_W}{\partial \dot{\phi}} \right) &= \frac{d}{dt} \left(\frac{\partial T_{w2}}{\partial \dot{\phi}} + \frac{\partial T_{w3}}{\partial \dot{\phi}} \right) \\
&= \frac{d}{dt} \left\{ me \left(\frac{\partial \dot{T}_{11}}{\partial \dot{\phi}} \dot{u} + \frac{\partial \dot{T}_{12}}{\partial \dot{\phi}} \dot{v} + \frac{\partial \dot{T}_{13}}{\partial \dot{\phi}} \dot{w} \right) \right. \\
&\quad \left. + I_\xi \omega_\xi \frac{\partial \omega_\xi}{\partial \dot{\phi}} + I_\eta \omega_\eta \frac{\partial \omega_\eta}{\partial \dot{\phi}} + I_\zeta \omega_\zeta \frac{\partial \omega_\zeta}{\partial \dot{\phi}} \right\}
\end{aligned} \tag{A.78}$$

$$\begin{aligned}
\frac{d}{ds} \left(\frac{\partial L_W}{\partial \phi'} \right) &= -\frac{d}{ds} \left(\frac{\partial V_w}{\partial \phi'} \right) \\
&= -\frac{d}{ds} \left\{ D_\xi \rho_\xi \frac{\partial \rho_\xi}{\partial \phi'} + D_\eta \rho_\eta \frac{\partial \rho_\eta}{\partial \phi'} + D_\zeta \rho_\zeta \frac{\partial \rho_\zeta}{\partial \phi'} \right\}
\end{aligned} \tag{A.79}$$

$$\begin{aligned}
A_\phi &= -I_2 (\dot{\theta} \dot{w}' + \dot{w}'^2 u') \\
&\quad + D_2 (\theta' \dot{w}' + w''^2 u') \\
&\quad + I_1 (\dot{w}'^2 u') - D_1 (w''^2 u') \\
&\quad + \frac{1}{2} me (u'^2 + w'^2)'' - me (u' \ddot{u} + w' \ddot{w}) - \frac{1}{2} me (-w'^2 - u'^2 - \theta^2)' \\
&\quad + I_3 \ddot{u}' + \frac{1}{2} I_3 (\dot{u}' u'^2)' - D_3 u''' - \frac{1}{2} D_3 (u'' u'^2)' \\
&\quad - (I_3 - I_1) (\dot{w}' \theta + \dot{u}' \theta^2)' + (D_3 - D_1) (w'' \theta + u'' \theta^2)'
\end{aligned} \tag{A.80}$$

$$\begin{aligned}
\frac{\partial L_W}{\partial \psi} &= \frac{\partial T_{w2}}{\partial \psi} + \frac{\partial T_{w3}}{\partial \psi} - \frac{\partial V_w}{\partial \psi} \\
&= me \left(\frac{\partial \dot{T}_{11}}{\partial \psi} \dot{u} + \frac{\partial \dot{T}_{12}}{\partial \psi} \dot{v} + \frac{\partial \dot{T}_{13}}{\partial \psi} \dot{w} \right) \\
&\quad + I_\xi \omega_\xi \frac{\partial \omega_\xi}{\partial \psi} + I_\eta \omega_\eta \frac{\partial \omega_\eta}{\partial \psi} + I_\zeta \omega_\zeta \frac{\partial \omega_\zeta}{\partial \psi} \\
&\quad - D_\xi \rho_\xi \frac{\partial \rho_\xi}{\partial \psi} - D_\eta \rho_\eta \frac{\partial \rho_\eta}{\partial \psi} - D_\zeta \rho_\zeta \frac{\partial \rho_\zeta}{\partial \psi}
\end{aligned} \tag{A.81}$$

$$\begin{aligned}
\frac{d}{dt} \left(\frac{\partial L_W}{\partial \dot{\psi}} \right) &= \frac{d}{dt} \left(\frac{\partial T_{w2}}{\partial \dot{\psi}} + \frac{\partial T_{w3}}{\partial \dot{\psi}} \right) \\
&= \frac{d}{dt} \left\{ me \left(\frac{\partial \dot{T}_{11}}{\partial \dot{\psi}} \dot{u} + \frac{\partial \dot{T}_{12}}{\partial \dot{\psi}} \dot{v} + \frac{\partial \dot{T}_{13}}{\partial \dot{\psi}} \dot{w} \right) \right. \\
&\quad \left. + I_\xi \omega_\xi \frac{\partial \omega_\xi}{\partial \dot{\psi}} + I_\eta \omega_\eta \frac{\partial \omega_\eta}{\partial \dot{\psi}} + I_\zeta \omega_\zeta \frac{\partial \omega_\zeta}{\partial \dot{\psi}} \right\}
\end{aligned} \tag{A.82}$$

$$\begin{aligned}
\frac{d}{ds} \left(\frac{\partial L_W}{\partial \psi'} \right) &= - \frac{d}{ds} \left(\frac{\partial V_w}{\partial \psi'} \right) \\
&= - \frac{d}{ds} \left\{ D_\xi \rho_\xi \frac{\partial \rho_\xi}{\partial \psi'} + D_\eta \rho_\eta \frac{\partial \rho_\eta}{\partial \psi'} + D_\zeta \rho_\zeta \frac{\partial \rho_\zeta}{\partial \psi'} \right\}
\end{aligned} \tag{A.83}$$

$$\begin{aligned}
A_\psi &= -I_2 \ddot{\theta} + me \ddot{w} + D_2 \theta'' - I_2 (u' \dot{w}') + D_2 (w'' u') \\
&\quad - me \left[-\theta \ddot{u} - \frac{1}{2} \int (u^2 + w^2)'' ds + \frac{1}{2} me (w'^2 + \theta^2) \ddot{w} \right] \\
&\quad + (I_3 - I_1) (\theta \dot{w}'^2 + \theta \dot{u}'^2 - \dot{w}' \dot{u}') \\
&\quad - (D_3 - D_1) (\theta w''^2 + \theta u''^2 - w'' u'')
\end{aligned} \tag{A.84}$$

$$\begin{aligned}
\frac{d}{dt} \left(\frac{\partial L_s}{\partial \dot{u}} \right) &= \frac{d}{dt} \left(\frac{\partial T_{s1}}{\partial \dot{u}} + \frac{\partial T_{s2}}{\partial \dot{u}} \right) \\
&= M_s \ddot{u} + M_s x_s \ddot{T}_{11} + M_s z_s \ddot{T}_{31}
\end{aligned} \tag{A.85}$$

$$\begin{aligned}
\frac{d}{dt} \left(\frac{\partial L_s}{\partial \dot{v}} \right) &= \frac{d}{dt} \left(\frac{\partial T_{s1}}{\partial \dot{v}} + \frac{\partial T_{s2}}{\partial \dot{v}} \right) \\
&= M_s \ddot{v} + M_s x_s \ddot{T}_{12} + M_s z_s \ddot{T}_{32}
\end{aligned} \tag{A.86}$$

$$\begin{aligned}
\frac{d}{dt} \left(\frac{\partial L_s}{\partial \dot{w}} \right) &= \frac{d}{dt} \left(\frac{\partial T_{s1}}{\partial \dot{w}} + \frac{\partial T_{s2}}{\partial \dot{w}} \right) \\
&= M_s \ddot{w} + M_s x_s \ddot{T}_{13} + M_s z_s \ddot{T}_{33}
\end{aligned} \tag{A.87}$$

$$\begin{aligned}
\frac{\partial L_s}{\partial \theta} &= \frac{\partial T_{s2}}{\partial \theta} + \frac{\partial T_{s3}}{\partial \theta} \\
&= \dot{u} \left(M_s x_s \frac{\partial \dot{T}_{11}}{\partial \theta} + M_s z_s \frac{\partial \dot{T}_{31}}{\partial \theta} \right) \\
&\quad + \dot{v} \left(M_s x_s \frac{\partial \dot{T}_{12}}{\partial \theta} + M_s z_s \frac{\partial \dot{T}_{32}}{\partial \theta} \right) \\
&\quad + \dot{w} \left(M_s x_s \frac{\partial \dot{T}_{13}}{\partial \theta} + M_s z_s \frac{\partial \dot{T}_{33}}{\partial \theta} \right) \\
&\quad + I_{s\xi} \omega_\xi \frac{\partial \omega_\xi}{\partial \theta} + I_{s\eta} \omega_\eta \frac{\partial \omega_\eta}{\partial \theta} + I_{s\zeta} \omega_\zeta \frac{\partial \omega_\zeta}{\partial \theta} \\
&\quad + M_s x_s z_s \left(\omega_\zeta \frac{\partial \omega_\xi}{\partial \theta} + \omega_\xi \frac{\partial \omega_\zeta}{\partial \theta} \right)
\end{aligned} \tag{A.88}$$

$$\begin{aligned}
\frac{d}{dt} \left(\frac{\partial L_s}{\partial \dot{\theta}} \right) &= \frac{d}{dt} \left(\frac{\partial T_{s2}}{\partial \dot{\theta}} + \frac{\partial T_{s3}}{\partial \dot{\theta}} \right) \\
&= \frac{d}{dt} \left\{ \dot{u} \left(M_s x_s \frac{\partial \dot{T}_{11}}{\partial \dot{\theta}} + M_s z_s \frac{\partial \dot{T}_{31}}{\partial \dot{\theta}} \right) \right. \\
&\quad + \dot{v} \left(M_s x_s \frac{\partial \dot{T}_{12}}{\partial \dot{\theta}} + M_s z_s \frac{\partial \dot{T}_{32}}{\partial \dot{\theta}} \right) \\
&\quad \left. + \dot{w} \left(M_s x_s \frac{\partial \dot{T}_{13}}{\partial \dot{\theta}} + M_s z_s \frac{\partial \dot{T}_{33}}{\partial \dot{\theta}} \right) \right\} \\
&\quad + \frac{d}{dt} \left\{ I_{s\xi} \omega_\xi \frac{\partial \omega_\xi}{\partial \dot{\theta}} + I_{s\eta} \omega_\eta \frac{\partial \omega_\eta}{\partial \dot{\theta}} + I_{s\zeta} \omega_\zeta \frac{\partial \omega_\zeta}{\partial \dot{\theta}} \right. \\
&\quad \left. + M_s x_s z_s \left(\omega_\zeta \frac{\partial \omega_\xi}{\partial \dot{\theta}} + \omega_\xi \frac{\partial \omega_\zeta}{\partial \dot{\theta}} \right) \right\}
\end{aligned} \tag{A.89}$$

Ordering Scheme In developing a set of nonlinear equations of motion, one must determine the order of magnitude. It is recommended by Nayfeh⁵⁵ that even if one is not interested in approximations, one should perform the dimensional analysis before analyzing the system. Through the process, the order of magnitude of each term

Table IX. Order of Terms Used in the Hodges-Dowell Equations²²

Property	Dimensionless terms	Order
Axial coordinate	x/R	$O(1)$
Bending deflections	$v/R, w/R$	$O(\epsilon)$
Elastic twist	ϕ	$O(\epsilon)$
Lateral coordinates	$\eta/R, \zeta/R$	$O(\epsilon)$
Axial deflection	u/R	$O(\epsilon^2)$
Mass moment of inertia	$mk_m^2 \ddot{\phi}$	$O(\epsilon^3)$

could be determined. Depending upon the order, some terms may be retained, and others may be ignored. The letter ‘ O ’ (upper case, big ‘ o ’) is an order symbol. This order symbol has the following properties.⁵⁶

Summation:

$$O(\epsilon^2) + O(\epsilon^3) = O(\epsilon^2) \text{ as } \epsilon \rightarrow 0$$

while

$$O(\epsilon^2) + O(\epsilon^3) = O(\epsilon^3) \text{ as } \epsilon \rightarrow \infty$$

Multiplication:

For a constant C , $C \cdot O(\epsilon^n) = O(\epsilon^n)$ as $\epsilon \rightarrow 0$.

$$O(\epsilon^n) \cdot O(\epsilon^m) = O(\epsilon^{n+m})$$

$$\frac{O(\epsilon^n)}{O(\epsilon^m)} = O(\epsilon^{n-m})$$

$$[O(\epsilon^n)]^p = O(\epsilon^{np})$$

The order of terms used in developing the Hodges-Dowell equations²² is shown in Table IX. It should be noted that the symbols used in Table IX are different from those in Chapter II because the used coordinate systems are different. In this table, k_m is mass radius of gyration of blade cross section and R is the length of blade.

Table X. Order of Terms Used in the Pai & Nayfeh Equations¹²

Property	Dimensionless terms	Order
Bending deflections	$v/R, w/R$	$O(\epsilon)$
Elastic twist	ϕ	$O(\epsilon)$
Axial deflection	u/R	$O(\epsilon)$ or $O(\epsilon^2)$
Rotary inertia	$j_1, j_2, \text{ and } j_3$	$O(\epsilon^2)$

The lateral coordinates are of the same order as the chord c and the thickness t , respectively. Because the mass centroid offset from the elastic axis e is defined in the lateral coordinate, it may be of similar order with the chord c . Kim⁵⁷ extended the Hodges-Dowell equation to the case of composite beams. In his development, the mass centroid offset terms e_g are $O(\epsilon^{3/2})$. He also used the order rule shown in Table IX. In the Hodges-Dowell equations²² and Kim's equations,⁵⁷ terms up to second order are retained. But some third order terms related to elastic twist including $mk_m^2 \ddot{\phi}$ are also retained because they are important for configurations with low torsion stiffness.

Similar ordering scheme is used by Pai and Nayfeh.¹² As shown in Table X, the order of terms are very similar with those used in the Hodges-Dowell equations. For example, the axial deformation u , can be $O(\epsilon)$ or $O(\epsilon^2)$. For the case of inextensional beams, u is $O(\epsilon^2)$ because $u' = -1/2(v'^2 + w'^2)$. The order of rotary inertia is examined through a beam with a rectangular cross-section. For this beam, the rotary inertia satisfies $j_1 = j_2 + j_3 = 1/12(b/L)^2 + 1/12(h/L)$. Because the nondimensional lateral coordinate is $O(\epsilon)$ as shown in Table IX, (b/L) and (h/L) are $O(\epsilon)$ and the rotary inertia terms could be $O(\epsilon^2)$. Based on this example case, they assumed that the rotary inertia terms are second-order quantities. Based upon this ordering scheme, terms up to third order are retained in the nonlinear equations shown in Chapter II.

Coefficients for BBT Ordinary Differential Equations

$$\begin{aligned}
C_{uw1} &= \int_0^1 U_r U_i ds = \delta_{ri} \\
C_{uw2} &= \int_0^1 U_r U_i^{IV} ds = \beta_i^4 \delta_{ri} \\
C_{uw3} &= \int_0^1 U_r (A'_k W''_j)' ds = \int_0^1 F_r (A'_k F''_j)' ds \\
C_{uw4} &= \int_0^1 U_r [U'_i (U'_p U''_q)]' ds = \int_0^1 F_r [F'_i (F'_p F''_q)]' ds \\
C_{uw5} &= \int_0^1 U_r [U'_i (W'_j W''_p)]' ds = \int_0^1 U_r [U'_i (U'_p U''_q)]' ds \\
C_{uw6} &= \int_0^1 U_r (W''_j A_k)'' ds \\
C_{uw7} &= \int_0^1 U_r (U''_i A_k A_p)'' ds \\
C_{uw8} &= \int_0^1 U_r \left(W''_j \int_0^s U''_i W'_p ds \right) ds \\
C_{uw9} &= \int_0^1 U_r U''_i ds \\
C_{uw10} &= \int_0^1 U_r \left[U'_i \int_1^s \left(\int_0^s W'_j W'_p ds \right) \right]' ds \\
C_{uw11} &= \int_0^1 U_r \left[U'_i \int_1^s \left(\int_0^s U'_p U'_q ds \right) \right]' ds \\
C_{uw21} &= \int_0^1 U_r \left[U'_i \int_1^s U'_p ds \right]' ds \\
C_{uw22} &= \int_0^1 U_r (A_k A_p) ds \\
C_{uw23} &= \int_0^1 U_r (W'_j W'_p) ds \\
C_{uw24} &= \int_0^1 U_r (U'_i U_p)' ds \\
C_{uw25} &= \int_0^1 U_r (W'_k W_p)' ds
\end{aligned}$$

(A.90)

$$\begin{aligned}
C_{ua1} &= \int_0^1 ds \\
C_{ua2} &= \int_0^1 ds
\end{aligned}$$

$$\begin{aligned}
C_{us1} &= \int_0^1 U_r U_i L \delta(y - y_s) ds = \int_0^L U_r U_i \delta(y - y_s) d\hat{s} = U_r U_i |_{y=y_s} \\
C_{us2} &= \int_0^1 U_r A_k L \delta(y - y_s) ds = \int_0^L U_r A_k \delta(y - y_s) d\hat{s} = U_r A_k |_{y=y_s} \\
C_{us3} &= \int_0^1 U_r (U_i' U_p') L \delta(y - y_s) ds = \int_0^L U_r (U_i' U_p') \delta(y - y_s) d\hat{s} = U_r (U_i' U_p') |_{y=y_s} \\
C_{us4} &= \int_0^1 U_r (A_k A_p) L \delta(y - y_s) ds = \int_0^L U_r (A_k A_p) \delta(y - y_s) d\hat{s} = U_r (A_k A_p) |_{y=y_s} \\
C_{us5} &= \int_0^1 U_r \left(\int_0^s W_j'' U_i' \right) L \delta(y - y_s) ds = \int_0^1 U_r \left(\int_0^s W_j'' U_i' \right) \delta(y - y_s) d\hat{s} \\
&= U_r \left(\int_0^s W_j'' U_i' \right) |_{y=y_s} \tag{A.91}
\end{aligned}$$

$$\begin{aligned}
C_{ww1} &= \int_0^1 W_r W_j ds = \delta_{rj} \\
C_{ww2} &= \int_0^1 W_r W_j^{IV} ds = \beta_j^4 \delta_{rj} \\
C_{ww3} &= \int_0^1 W_r (A_k' U_i'')' ds = \int_0^1 F_r (A_k' F_i'')' ds \\
C_{ww4} &= \int_0^1 W_r [W_j' (W_p' W_q'')] ds = \int_0^1 F_r [F_j' (F_p' F_q'')] ds \\
C_{ww5} &= \int_0^1 W_r [W_j' (U_i' U_p'')] ds = \int_0^1 W_r [W_j' (U_i' U_p'')] ds \\
C_{ww6} &= \int_0^1 W_r (U_i'' A_k)'' ds \\
C_{ww7} &= \int_0^1 W_r (W_j'' A_k A_p)'' ds \\
C_{ww8} &= \int_0^1 W_r \left(U_j''' \int_0^s W_j'' U_p' ds \right) ds \\
C_{ww9} &= \int_0^1 W_r W_j'' ds \\
C_{ww10} &= \int_0^1 W_r \left[W_j' \int_1^s \left(\int_0^s W_p' W_q' ds \right) \right]' ds \\
C_{ww11} &= \int_0^1 W_r \left[W_j' \int_1^s \left(\int_0^s U_i' U_p' ds \right) \right]' ds \\
C_{ww21} &= \int_0^1 W_r A_k ds \\
C_{ww22} &= \int_0^1 W_r \left[W_j' \int_1^s U_i' ds \right]' ds \\
C_{ww23} &= \int_0^1 W_r \left[U_i'' \int_0^s U_i'' W_j' ds \right]' ds
\end{aligned}$$

(A.92)

$$\begin{aligned}
C_{wa1} &= \int_0^1 W_r A_k ds = C_{wa3} = C_{wa4} \\
C_{wa2} &= \int_0^1 W_r W_j ds = \delta_{rj} = C_{ww1} \\
C_{wa3} &= \int_0^1 W_r A_k ds = C_{wa1} \\
C_{wa4} &= \int_0^1 W_r A_k ds = C_{wa3} \\
C_{wa5} &= \int_0^1 W_r (A_k A_p A_q) ds = C_{wa7} = C_{wa10} = C_{wa14} \\
C_{wa6} &= \int_0^1 W_r (A_k A_p W_j) ds = C_{wa9} = C_{wa13} \\
C_{wa8} &= \int_0^1 W_r (A_k W_j W_p) ds = C_{wa12} \\
C_{wa11} &= \int_0^1 W_r (W_j W_p W_q) ds
\end{aligned} \tag{A.93}$$

$$\begin{aligned}
C_{ws1} &= \int_0^1 W_r W_j L \delta(y - y_s) ds = \int_0^L W_r W_j \delta(y - y_s) d\hat{s} = W_r W_j |_{y=y_s} \\
C_{ws2} &= \int_0^1 W_r A_k L \delta(y - y_s) ds = \int_0^L W_r A_k \delta(y - y_s) d\hat{s} = W_r A_k |_{y=y_s} \\
C_{ws3} &= \int_0^1 W_r (W_j' W_p') L \delta(y - y_s) ds = \int_0^L W_r (W_j' W_p') \delta(y - y_s) d\hat{s} = W_r (W_j' W_p') |_{y=y_s} \\
C_{ws4} &= \int_0^1 W_r (A_k A_p) L \delta(y - y_s) ds = \int_0^1 W_r (A_k A_p) \delta(y - y_s) d\hat{s} = W_r (A_k A_p) |_{y=y_s} \\
C_{ws5} &= \int_0^1 W_r \left(\int_0^s U_i'' W_j' \right) L \delta(y - y_s) ds = \int_0^1 U_r \left(\int_0^s U_i'' W_j' \right) \delta(y - y_s) d\hat{s} \\
&= W_r \left(\int_0^s U_i'' W_j' \right) |_{y=y_s}
\end{aligned} \tag{A.94}$$

$$\begin{aligned}
C_{aw1} &= \int_0^1 A_r A_k ds = \delta_{rk} \\
C_{aw2} &= \int_0^1 A_r A_k'' ds = -\gamma_k^2 \delta_{rk} \\
C_{aw3} &= \int_0^1 A_r (W_j'' W_p'' A_k) ds \\
C_{aw4} &= \int_0^1 A_r (U_i'' U_p'' A_k) ds \\
C_{aw5} &= \int_0^1 A_r (W_k'' U_i'') ds \\
C_{aw6} &= \int_0^1 A_r \left(\int_0^s W_j'' U_i' \right) ds
\end{aligned}$$

$$\begin{aligned}
C_{aw7} &= \int_0^1 A_r (W_j' U_i') ds \\
C_{aw8} &= \int_0^1 A_r (W_j' W_p' A_k) ds \\
C_{aw9} &= \int_0^1 A_r (W_j W_p A_k) ds
\end{aligned} \tag{A.95}$$

$$\begin{aligned}
C_{aw21} &= \int_0^1 A_k W_j ds \\
C_{aw22} &= \int_0^1 A_k [W_j W_p' W_q'] ds \\
C_{aw23} &= \int_0^1 A_k [W_j A_k A_p] ds \\
C_{aw24} &= \int_0^1 A_k \left[W_q' \int_0^s W_j' W_p' ds \right] ds \\
C_{aw25} &= \int_0^1 A_k \left[W_j' \int_0^s U_i' U_p' ds \right] ds \\
C_{aw26} &= \int_0^1 A_k U_i A_k ds \\
C_{aw27} &= \int_0^1 A_k \left[U_i \int_0^s W_j'' U_p' ds \right]' ds
\end{aligned} \tag{A.96}$$

$$\begin{aligned}
C_{aa1} &= C_{aw1} = C_{aa3} = C_{aa4} \\
C_{aa2} &= \int_0^1 A_r W_j ds \\
C_{aa5} &= \int_0^1 A_r (A_k A_p A_q) ds = C_{aa7} = C_{aa10} = C_{aa14} \\
C_{aa6} &= \int_0^1 A_r (A_k A_p W_j) ds = C_{aa9} = C_{aa13} \\
C_{aa8} &= \int_0^1 A_r (A_k W_j W_p) ds = C_{aa12} \\
C_{aa11} &= \int_0^1 A_r (W_j W_p W_q) ds
\end{aligned} \tag{A.97}$$

$$\begin{aligned}
C_{as1} &= \int_0^1 A_r A_k L \delta(y - y_s) ds = \int_0^1 A_r A_k \delta(y = y_s) d\hat{s} = A_r A_k |_{y=y_s} \\
C_{as2} &= \int_0^1 A_r W_j L \delta(y - y_s) ds = \int_0^1 A_r W_j \delta(y = y_s) d\hat{s} = A_r W_j |_{y=y_s}
\end{aligned}$$

$$\begin{aligned}
C_{as3} &= \int_0^1 A_r U_i L \delta(y - y_s) ds = \int_0^1 A_r U_i \delta(y = y_s) d\hat{s} = A_r U_i |_{y=y_s} \\
C_{as4} &= \int_0^1 A_r (W_j W'_p W'_q) L \delta(y = y_s) ds = \int_0^1 A_r (W_j W'_p W'_q) \delta(y = y_s) d\hat{s} \\
&= A_r (W_j W'_p W'_q) |_{y=y_s} \tag{A.98}
\end{aligned}$$

$$\begin{aligned}
C_{as5} &= \int_0^1 A_r (W_j A_k A_p) L \delta(y - y_s) ds = \int_0^1 A_r (W_j A_k A_p) \delta(y - y_s) d\hat{s} \\
&= A_r W_j A_k A_p |_{y=y_s} \tag{A.99}
\end{aligned}$$

$$\begin{aligned}
C_{as6} &= \int_0^1 A_r (W_j A_k) L \delta(y - y_s) ds = \int_0^1 A_r (W_j A_k A_p) \delta(y - y_s) d\hat{s} \\
&= A_r W_j A_k A_p |_{y=y_s} \tag{A.100}
\end{aligned}$$

$$\begin{aligned}
C_{as7} &= \int_0^1 A_r \left(W_j \int_0^s W''_p U'_i ds \right) L \delta(y - y_s) ds \\
&= \int_0^1 A_r \left(W_j \int_0^s W''_p U'_i ds \right) \delta(y - y_s) d\hat{s} = A_r W_j \int_0^s W''_p U'_i ds |_{y=y_s}
\end{aligned}$$

$$\begin{aligned}
C_{as8} &= \int_0^1 A_r (W_j U'_i W'_p) L \delta(y - y_s) ds = \int_0^1 A_r (W_j U'_i W'_p) \delta(y - y_s) d\hat{s} \\
&= A_r W_j U'_i W'_p |_{y=y_s}
\end{aligned}$$

$$C_{as9} = \int_0^1 A_r (U_i A_k) L \delta(y - y_s) ds = \int_0^1 A_r (U_i A_k) \delta(y - y_s) d\hat{s} = A_r U_i A_k |_{y=y_s}$$

$$\begin{aligned}
C_{as10} &= \int_0^1 A_r \left(U_i \int_0^s U''_p W'_j ds \right) L \delta(y - y_s) ds \\
&= \int_0^1 A_r \left(U_i \int_0^s U''_p W'_j ds \right) \delta(y - y_s) d\hat{s} = A_r U_i \int_0^s U''_p W'_j ds |_{y=y_s}
\end{aligned}$$

$$\begin{aligned}
C_{as11} &= \int_0^1 A_r (U_i A_k A_p) L \delta(y - y_s) ds = \int_0^1 A_r (U_i A_k A_p) \delta(y - y_s) d\hat{s} \\
&= A_r U_i A_k A_p |_{y=y_s}
\end{aligned}$$

$$\begin{aligned}
C_{as12} &= \int_0^1 A_r (U_i U'_p U'_q) L \delta(y - y_s) ds = \int_0^1 A_r (U_i U'_p U'_q) \delta(y - y_s) d\hat{s} \\
&= A_r U_i U'_p U'_q |_{y=y_s}
\end{aligned}$$

$$C_{as13} = \int_0^1 A_r (U'_i U'_p) L \delta(y - y_s) ds = \int_0^1 A_r (U'_i U'_p) \delta(y - y_s) d\hat{s} = A_r U'_i U'_p |_{y=y_s}$$

$$\begin{aligned}
C_{as14} &= \int_0^1 A_r (U'_i W'_j A_k) L \delta(y - y_s) ds = \int_0^1 A_r (U'_i W'_j A_k) \delta(y - y_s) d\hat{s} \\
&= A_r U'_i W'_j A_k |_{y=y_s}
\end{aligned}$$

$$C_{as15} = \int_0^1 A_r \left(W'_q \int_0^s W'_j W'_p ds \right) L \delta(y - y_s) ds$$

$$\begin{aligned}
&= \int_0^1 A_r \left(W'_q \int_0^s W'_j W'_p ds \right) \delta(y - y_s) d\hat{s} = A_r W'_q \int_0^s W'_j W'_p ds|_{y=y_s} \\
C_{as16} &= \int_0^1 A_r \left(W'_q \int_0^s U'_i U'_p ds \right) L \delta(y - y_s) ds \\
&= \int_0^1 A_r \left(W'_q \int_0^s U'_i U'_p ds \right) \delta(y - y_s) d\hat{s} = A_r W'_q \int_0^s U'_i U'_p ds|_{y=y_s} \\
C_{as17} &= \int_0^1 A_r \left(U'_i \int_0^s W'_j W'_p ds \right) L \delta(y - y_s) ds \\
&= \int_0^1 A_r \left(U'_i \int_0^s W'_j W'_p ds \right) \delta(y - y_s) d\hat{s} = A_r U'_i \int_0^s W'_j W'_p ds|_{y=y_s} \\
C_{as18} &= \int_0^1 A_r \left(U'_q \int_0^s U'_i U'_p ds \right) L \delta(y - y_s) ds \\
&= \int_0^1 A_r \left(U'_q \int_0^s U'_i U'_p ds \right) \delta(y - y_s) d\hat{s} = A_r U'_q \int_0^s U'_i U'_p ds|_{y=y_s} \\
C_{as19} &= \int_0^1 A_r \left(W'_j W'_p A_k \right) L \delta(y - y_s) ds = \int_0^1 A_r \left(W'_j W'_p A_k \right) \delta(y - y_s) d\hat{s} \\
&= A_r W'_j W'_p A_k|_{y=y_s} \\
C_{as20} &= \int_0^1 A_r \left(U'_i U'_p A_k \right) L \delta(y - y_s) ds = \int_0^1 A_r \left(U'_i U'_p A_k \right) \delta(y - y_s) d\hat{s} \\
&= A_r U'_i U'_p A_k|_{y=y_s} \\
C_{as21} &= \int_0^1 A_r \left(W'_j U'_i \right) L \delta(y - y_s) ds = \int_0^1 A_r \left(W'_j U'_i \right) \delta(y - y_s) d\hat{s} \\
&= A_r W'_j U'_i|_{y=y_s} \\
C_{as22} &= \int_0^1 A_r \left(\int_0^s W'_j U'_i ds \right) L \delta(y - y_s) ds \\
&= \int_0^1 A_r \left(\int_0^s W'_j U'_i ds \right) \delta(y - y_s) d\hat{s} = A_r \int_0^s W'_j U'_i ds|_{y=y_s} \tag{A.101}
\end{aligned}$$

Matrices, M , C , and K Matrices shown in the ordinary differential equations are summarized in this appendix.

$$[M]_L = \begin{bmatrix} C_{uw1} + M_s^* C_{us1} & 0 & M_s^* z_s^* C_{us2} \\ 0 & C_{ww1} + M_s^* C_{ws1} & -e^* C_{ww21} \\ M_s^* z_s^* C_{as3} & -e^* C_{aw21} & -M_s^* x_s^* C_{ws2} \\ & -M_s^* x_s^* C_{as2} & I_y^* C_{aw1} \\ & & + (I_{sy}^* + M_s^* x_s^{*2} + M_s^* z_s^{*2}) C_{as1} \end{bmatrix}_L \quad (\text{A.102})$$

$$[C]_L = \begin{bmatrix} 0 & 0 & 0 \\ 0 & \mu \frac{C_{L\alpha}}{\pi} \frac{V^*}{b^*} C_{wa2} & -\mu V^* C_{wa1} - \mu \frac{C_{L\alpha}}{\pi} V^* \left(\frac{1}{2} - a\right) C_{wa4} \\ 0 & \mu \frac{C_{m\alpha}}{\pi} V^* C_{aa2} & \mu b^* \left(\frac{1}{2} - a\right) C_{aa1} - \mu \frac{C_{m\alpha}}{\pi} V^* b^* \left(\frac{1}{2} - a\right) C_{aa4} \end{bmatrix}_L \quad (\text{A.103})$$

$$[K]_L = \begin{bmatrix} \beta_z C_{uw2} & 0 & 0 \\ 0 & C_{ww2} & -\mu \frac{C_{L\alpha}}{\pi} \frac{V^{*2}}{b^*} C_{wa3} \\ 0 & 0 & -\beta_y C_{aw2} - \mu \frac{C_{m\alpha}}{\pi} V^{*2} C_{aa3} \end{bmatrix}_L \quad (\text{A.104})$$

$$\begin{aligned} [M]_{NL} &= [M]_{NLw} + [M]_{NLs} \\ &= \begin{bmatrix} M_{11nw} & M_{12nw} & M_{13nw} \\ M_{21nw} & M_{22nw} & M_{23nw} \\ M_{31nw} & M_{32nw} & M_{33nw} \end{bmatrix}_{NLw} + \begin{bmatrix} M_{11ns} & M_{12ns} & M_{13ns} \\ M_{21ns} & M_{22ns} & M_{23ns} \\ M_{31ns} & M_{32ns} & M_{33ns} \end{bmatrix}_{NLs} \end{aligned} \quad (\text{A.105})$$

$$\begin{aligned} M_{11n} &= I_z^* C_{uw9} - \frac{1}{2} C_{uw11} u_i (u_p + u_q) + e^* [C_{uw21} u_i - C_{uw24} u_i] \\ &\quad + \frac{1}{2} M_s^* x_s^* C_{us3} (u_p + u_q) + M_s^* z_s^* C_{us5} w_j \end{aligned} \quad (\text{A.106})$$

$$\begin{aligned} M_{12n} &= -\frac{1}{2} C_{uw10} u_i (w_p + w_i) + e^* [-C_{uw23} w_p - C_{uw25} w_j] \\ &\quad + M_s^* z_s^* C_{us5} u_i \end{aligned} \quad (\text{A.107})$$

$$M_{13n} = \frac{1}{2}M_s^*x_s^*C_{us4}(\alpha_p + \alpha_k) + e^*C_{uw22}\alpha_p \quad (\text{A.108})$$

$$M_{21n} = -\frac{1}{2}C_{ww11}w_j(u_p + u_i) - e^*(C_{ww22} + C_{ww23})w_j \\ + M_s^*x_s^*C_{ws5}w_j \quad (\text{A.109})$$

$$M_{22n} = I_x^*C_{ww9} - \frac{1}{2}C_{ww10}w_j(w_p + w_q) - e^*C_{ww23}u_i \\ + M_s^*z_s^*C_{ws3}w_j + M_s^*x_s^*C_{ws5}u_i \quad (\text{A.110})$$

$$M_{23n} = M_s^*z_s^*C_{ws4}\alpha_k \quad (\text{A.111})$$

$$M_{31n} = I_y^*C_{aw6}w_j \\ + e^*[C_{aw25}u_pw_j + C_{aw26}\alpha_k - C_{aw27}w_ju_p] \\ + M_s^*\left\{x_s^*[C_{as9}\alpha_k - C_{as10}w_ju_p] + \frac{1}{2}z_s^*[C_{as11}\alpha_k\alpha_p + C_{as12}u_pu_q]\right\} \\ + M_s^*\{x_s^*C_{as16}u_pw_j - z_s^*C_{as18}u_pu_q\} \\ + I_{sy}^*C_{as22}w_j \quad (\text{A.112})$$

$$M_{32n} = I_y^*(C_{aw6}u_i - C_{aw7}u_i) \\ + e^*\left[-\frac{1}{2}C_{aw22}w_pw_q - \frac{1}{2}C_{aw23}\alpha_k\alpha_p + C_{aw24}w_pw_q\right] \\ + M_s^*\left\{-\frac{1}{2}x_s^*[C_{as4}w_pw_q + C_{as5}\alpha_k\alpha_p] + z_s^*[C_{as6}\alpha_k - C_{as7}w_pu_i + C_{as8}u_iw_p]\right\} \\ + M_s^*\{x_s^*C_{as15}w_pw_j - z_s^*C_{as17}w_pu_i\} \\ + I_{sy}^*[C_{as22}u_i - C_{as23}u_i] \quad (\text{A.113})$$

$$M_{33n} = 0 \quad (\text{A.114})$$

$$[C]_{NL} = [C]_{NLw} + [C]_{NLa} \\ = \begin{bmatrix} C_{11nw} & C_{12nw} & C_{13nw} \\ C_{21nw} & C_{22nw} & C_{23nw} \\ C_{31nw} & C_{32nw} & C_{33nw} \end{bmatrix}_{NLw} + \begin{bmatrix} 0 & 0 & 0 \\ 0 & C_{22na} & C_{23na} \\ 0 & C_{32na} & C_{33na} \end{bmatrix}_{NLa} \quad (\text{A.115})$$

$$\begin{aligned}
C_{11nw} &= -\frac{1}{2}C_{uw11}u_i2\dot{u}_p \\
&\quad + \frac{1}{2}M_s^*x_s^*C_{us3}2\dot{u}_p + M_s^*z_s^*C_{us5}2\dot{w}_j
\end{aligned} \tag{A.116}$$

$$\begin{aligned}
C_{12nw} &= -\frac{1}{2}C_{uw10}u_i2\dot{w}_p \\
&\quad + e^*(-C_{uw23}\dot{w}_p)
\end{aligned} \tag{A.117}$$

$$\begin{aligned}
C_{13nw} &= \frac{1}{2}M_s^*x_s^*C_{us4}2\dot{\alpha}_p \\
&\quad + e^*C_{uw22}\dot{\alpha}_p
\end{aligned} \tag{A.118}$$

$$\begin{aligned}
C_{21nw} &= -\frac{1}{2}C_{ww11}2\dot{u}_p \\
&\quad - e^*C_{ww23}2\dot{w}_j \\
&\quad + M_s^*x_s^*C_{ws5}2\dot{w}_q
\end{aligned} \tag{A.119}$$

$$\begin{aligned}
C_{22nw} &= -\frac{1}{2}C_{ww10}2\dot{w}_pw_j \\
&\quad + M_s^*z_s^*C_{ws3}2\dot{w}_p
\end{aligned} \tag{A.120}$$

$$C_{23nw} = 0 \tag{A.121}$$

$$\begin{aligned}
C_{31nw} &= I_y^*(2C_{aw6}\dot{w}_j - C_{aw7}\dot{w}_j) + (I_z^* - I_x^*)[-C_{aw9}\dot{u}_p\alpha_k - C_{aw10}\dot{w}_j] \\
&\quad + e^*C_{aw25}\dot{u}_pw_j \\
&\quad - M_s^*\{x_s^*z_s^*[-C_{as13}\dot{u}_p + 2C_{as14}w_j\alpha_k] - x_s^*C_{as16}\dot{u}_pw_j + z_s^*C_{as18}\dot{u}_pu_q\} \\
&\quad + I_{sy}^*[2C_{as22}\dot{w}_j - C_{as23}\dot{w}_j] + (I_{sz}^* - I_{sx}^*)[-C_{as20}\dot{u}_p\alpha_k - C_{as21}\dot{w}_j]
\end{aligned} \tag{A.122}$$

$$\begin{aligned}
C_{32nw} &= (I_z^* - I_x^*)C_{aw8}\dot{w}_p\alpha_k \\
&\quad + e^*C_{aw24}\dot{w}_pw_q \\
&\quad - M_s^*\{-x_s^*C_{as15}\dot{w}_pw_j + z_s^*C_{as17}\dot{w}_pu_i\} + (I_{sz}^* - I_{sx}^*)C_{as19}\dot{w}_p\alpha_k
\end{aligned} \tag{A.123}$$

$$C_{33nw} = 0 \tag{A.124}$$

$$\begin{aligned}
C_{22na} &= -\mu\frac{C_{L\alpha}}{\pi}\frac{V^{*2}}{b^*}c_3\left\{\frac{1}{V^*}[-3C_{wa6}\alpha_k\alpha_p]\right. \\
&\quad \left. + \frac{1}{V^{*2}}\left[3C_{wa8}\alpha_k\dot{w}_p - 6b^*\left(\frac{1}{2} - a\right)C_{wa9}\alpha_k\dot{\alpha}_p\right]\right\}
\end{aligned}$$

$$\begin{aligned}
& + \frac{1}{V^{*3}} \left[-C_{wa11} \dot{w}_p \dot{w}_q + 3b^{*2} \left(\frac{1}{2} - a \right) C_{wa12} \dot{\alpha} \dot{w}_p - 3b^{*2} \left(\frac{1}{2} - a \right)^2 C_{wa13} \dot{\alpha}_k \dot{\alpha}_p \right] \} \\
C_{23na} & = -\mu \frac{C_{L\alpha} V^{*2}}{\pi b^*} c_3 \left\{ \frac{1}{V^*} \left[3b^* \left(\frac{1}{2} - a \right) C_{wa7} \alpha_k \alpha_p \right] \right. \\
& \left. + \frac{1}{V^{*2}} \left[3b^{*2} \left(\frac{1}{2} - a \right)^2 C_{wa10} \alpha_k \dot{\alpha}_p \right] + \frac{1}{V^{*3}} \left[b^{*3} \left(\frac{1}{2} - a \right)^3 C_{wa14} \dot{\alpha}_k \dot{\alpha}_p \right] \right\} \quad (A.125) \\
C_{32na} & = -\mu \frac{C_{m\alpha} V^{*2}}{\pi} c_3 \left\{ \frac{1}{V^*} \left[-3C_{aa6} \alpha_k \alpha_p \right] + \frac{1}{V^{*2}} \left[3C_{aa8} \alpha_k \dot{w}_p - 6b^* \left(\frac{1}{2} - a \right) C_{aa9} \alpha_k \dot{\alpha}_p \right] \right. \\
& \left. + \frac{1}{V^{*3}} \left[-C_{aa11} \dot{w}_p \dot{w}_q + 3b^* \left(\frac{1}{2} - a \right) C_{aa12} \dot{\alpha} \dot{w}_p - 3b^{*2} \left(\frac{1}{2} - a \right)^2 C_{aa13} \dot{\alpha}_k \dot{\alpha}_p \right] \right\} \\
C_{33na} & = -\mu \frac{C_{m\alpha} V^{*2}}{\pi} c_3 \left\{ \frac{1}{V^*} \left[3b^* \left(\frac{1}{2} - a \right) C_{aa7} \alpha_k \alpha_p \right] \right. \\
& \left. + \frac{1}{V^{*2}} \left[3b^{*2} \left(\frac{1}{2} - a \right)^2 C_{aa10} \alpha_k \dot{\alpha}_p \right] + \frac{1}{V^{*3}} \left[b^{*3} \left(\frac{1}{2} - a \right)^3 C_{aa14} \dot{\alpha}_k \dot{\alpha}_p \right] \right\} \quad (A.126)
\end{aligned}$$

$$\begin{aligned}
[K]_{NL} & = \begin{bmatrix} K_{11nw} & K_{12nw} & K_{13nw} \\ K_{21nw} & K_{22nw} & K_{23nw} \\ K_{31nw} & K_{32nw} & K_{33nw} \end{bmatrix}_{NLw} + \begin{bmatrix} K_{11na} & K_{12na} & K_{13na} \\ K_{21na} & K_{22na} & K_{23na} \\ K_{31na} & K_{32na} & K_{33na} \end{bmatrix}_{NLa} \\
& = \begin{bmatrix} -\beta_z [C_{uw4} u_p u_q + C_{uw5} w_j w_p] & \beta_y [C_{uw3} \alpha_k] & 0 \\ +(\beta_z - 1) [C_{uw7} \alpha_k \alpha_p - C_{uw8} w_j w_p] & +(\beta_z - 1) [C_{uw2} \alpha_k] & 0 \\ -\beta_y C_{ww3} \alpha_k - C_{ww5} w_j u_p & -C_{ww4} w_p w_q & 0 \\ +(\beta_z - 1) [C_{ww6} \alpha_k - C_{ww8} w_j u_p] & -(\beta_z - 1) C_{ww7} \alpha_k \alpha_p & 0 \\ -(\beta_z - 1) [-C_{aw4} u_p \alpha_k - C_{aw5} w_j] & -(\beta_z - 1) C_{aw3} \alpha_k \alpha_p & 0 \end{bmatrix} \\
& + \begin{bmatrix} 0 & 0 & 0 \\ 0 & 0 & -\mu \frac{C_{L\alpha} V^{*2}}{\pi b^*} c_3 C_{wa5} \alpha_p \alpha_q \\ 0 & 0 & -\mu \frac{C_{m\alpha} V^{*2}}{\pi} c_3 C_{aa5} \alpha_p \alpha_q \end{bmatrix} \quad (A.127)
\end{aligned}$$

APPENDIX II

BENDING-TORSION EQUATIONS

For a simple beam, it may be assumed that the effect of the distributed mass moment of inertia is negligible.²⁸ But for an aeroelastic system, the effect of the torsion motion could not be neglected. Aeroelastic behavior of aircraft wings are usually described by the out-of-plane bending and torsion. In order to investigate the nonlinear characteristics of aeroelastic systems, it is required to form a set of nonlinear bending-torsion equations of motion. Two approaches are considered to obtain the nonlinear bending-torsion equations.

Approach 1 The first approach is to derive the bending-torsion equation from the bending-bending-torsion equations. If the flexural rigidity in the in-plane motion is relatively high, then the frequency of the in-plane bending motion is much greater than the other frequencies in the out-of-plane bending and torsion motion. This means that the in-plane bending motion cannot be excited by other motions. Additionally, if there is no external force in the in-plane bending motion, then the deflection u is only induced by the torsional angle and/or the out-of-plane bending deflection.

Based on this concept, a set of nonlinear bending-torsion equations is derived from Eqs. (2.25). The induced in-plane bending deflection can be found from the in-plane bending equation. By setting all terms with time derivatives in the equations equal to zero, we obtain

$$D_z u^{IV} = D_y (\alpha' w'')' + (D_z - D_x) (w'' \alpha)'' + H.O.T \quad (\text{B.1})$$

where *H.O.T.* means the higher order terms. In the above equation, $O(\epsilon^3)$ terms are neglected because the u terms shown in the out-of-plane bending and torsion motion are at least quadratic. Integration of Eq. (B.1) is

$$D_z u''' = D_y \int_0^s (\alpha' w'')' ds + (D_z - D_x) \int_0^s (w'' \alpha)'' ds + C1 \quad (\text{B.2})$$

From a boundary condition $u'''(1) = 0$ for a cantilever beam, $C1$ is determined as follows,

$$C1 = D_y \int_1^0 (\alpha' w'')' ds + (D_z - D_x) \int_1^0 (w'' \alpha)'' ds \quad (\text{B.3})$$

Substituting Eq. B.3 into Eq. B.2, and integration over the domain $[0, s]$, we obtain

$$D_z u'' = D_y \int_0^s \int_1^s (\alpha' w'')' ds + (D_z - D_x) \int_0^s \int_1^s (w'' \alpha)'' ds + C2 \quad (\text{B.4})$$

From the boundary condition $u''(1) = 0$, it can be realized that $C2 = 0$. Performing two more steps of integration, and applying the other boundary conditions such as $u'(0) = 0$ and $u(0) = 0$, we obtain

$$D_z u = D_y \int_0^s \int_0^s \int_0^s \int_1^s (\alpha' w'')' ds + (D_z - D_x) \int_0^s \int_0^s \int_0^s \int_1^s (w'' \alpha)'' ds \quad (\text{B.5})$$

If $D_z \gg D_y$ and $D_z \gg D_x$, then the expression could be represented simply,

$$D_z u = D_z \int_0^s \int_0^s \int_0^s \int_1^s (w'' \alpha)'' ds \quad (\text{B.6})$$

Substituting these results into the other equations in the bending-bending-torsion equations, we can obtain the bending-torsion equations with cubic nonlinearities. Because u and u'' have the order of ϵ^2 , the quadratic nonlinear term having only one u term, can be changed to cubic nonlinear terms. Other nonlinear terms which have either two u terms or cubic terms do not contribute the nonlinear bending torsion equations. As shown in Eqs. (B.7) and (B.8), the bending-torsion equations consist

of cubic terms.

$$\begin{aligned}
& m\ddot{w} - m\epsilon\ddot{\alpha} + D_x w^{IV} + M_s(\ddot{w} - x_s\ddot{\alpha})\delta(y - y_s) \\
& - \pi\rho b^2 V\dot{\alpha} + \rho V b C_{L\alpha} \left[\dot{w} - V\alpha - b\left(\frac{1}{2} - a\right)\dot{\alpha} \right] = G_w^{BT1} \\
& I_y\ddot{\alpha} - m\epsilon\ddot{w} - D_y\alpha'' + \left[(I_{sy} + M_s(x_s^2 + z_s^2))\ddot{\alpha} - M_s x_s \ddot{w} + M_s z_s \ddot{u} \right] \delta(y - y_s) \\
& + \pi\rho b^2 V b \left(\frac{1}{2} - a\right)\dot{\alpha} + \rho V b^2 C_{m\alpha} \left[\dot{w} - V\alpha - b\left(\frac{1}{2} - a\right)\dot{\alpha} \right] = G_\alpha^{BT1} \quad (B.7)
\end{aligned}$$

where

$$\begin{aligned}
G_w &= -D_y (\alpha' u_u'')' - D_x [w' (w' w'')]'' \\
& + (D_z - D_x) \left[(u_u'' \alpha - w'' \alpha^2)' \right]' + I_x \ddot{w}'' \\
& - \left\{ \frac{1}{2} w' \int_L^s m \left[\int_o^{\hat{s}} (w'^2) ds \right]'' d\hat{s} \right\}' \\
& + [M_s z_s (\alpha \dot{\alpha} + w' \dot{w}')] \delta(y - y_s) \\
& - \rho V^2 b C_{L\alpha} c_3 \alpha_{eff}^3 \quad (B.8)
\end{aligned}$$

$$\begin{aligned}
G_\alpha &= -(D_z - D_x) [(w'^2)\alpha - w'' u_u''] \\
& + I_y \left[\left(\int_0^s w'' u_u' ds \right)'' - (\dot{w}' u_u') \bullet \right] + (I_z - I_x) [(\dot{w}'^2)\alpha - \dot{u}'_u \dot{w}'] \\
& + m\epsilon \left\{ -\frac{1}{2} \ddot{w} (w'^2 + \alpha^2) + \frac{1}{2} w' \left(\int_0^s (w'^2) ds \right)'' + \ddot{u}_u(\alpha) \right\} \\
& + M_s \ddot{w} \left[-\frac{1}{2} x_s (w'^2 + \alpha^2) + z_s(\alpha) \right] \delta(y - y_s) \\
& + M_s \ddot{u} \left[x_s (\alpha - \int_0^s w'' u' ds) + \frac{1}{2} z_s (\alpha^2 + u'^2) \right] \delta(y - y_s) \\
& + M_s \left\{ -\frac{1}{2} \left[\int_0^s (w'^2) \right]'' (x_s w') \right\} \delta(y - y_s) \\
& + \left\{ I_{sy} \left[\left(\int_0^s w'' u_u' ds \right)'' - (\dot{w}' u_u') \bullet \right] + (I_{sz} - I_{sx}) [(\dot{w}'^2)\alpha - \dot{u}'_u \dot{w}'] \right\} \delta(y - y_s) \\
& - \rho V^2 b^2 C_{m\alpha} c_3 \alpha_{eff}^3 \quad (B.9)
\end{aligned}$$

The induced in-plane bending deflection u_u terms are defined as

$$u_u'' = \frac{1}{D_z} \left[D_y \int_0^s \int_1^s (\alpha' w'')' ds + (D_z - D_x) \int_0^s \int_1^s (w'' \alpha)'' ds \right] \quad (\text{B.10})$$

$$u_u' = \frac{1}{D_z} \left[D_y \int_0^s \int_0^s \int_1^s (\alpha' w'')' ds + (D_z - D_x) \int_0^s \int_0^s \int_1^s (w'' \alpha)'' ds \right] \quad (\text{B.11})$$

Here is another example. The following equations are derived from the Hodges-Dowell equations and used by Tang and Dowell.^{19,39} Depending upon the considered cases, they included the associated terms.

$$EI_2 v'''' + (EI_2 - EI_1)(\phi w'')'' + m\ddot{v} = \frac{dF_v}{dx} \quad (\text{B.12})$$

$$EI_1 w'''' + (EI_2 - EI_1)(\phi v'')'' + m\ddot{w} = \frac{dF_w}{dx} \quad (\text{B.13})$$

$$-GJ\phi'' + (EI_2 - EI_1)(w'' v'')'' + mK_m^2 \ddot{\phi} = \frac{dM_x}{dx} \quad (\text{B.14})$$

where v is the chordwise (in-plane bending) deflection, w is the span-wise (out-of-plane bending) deflection, and ϕ represent the twist angle with respect to deformed elastic axis. It is noted that the most important geometric structural nonlinear terms retained from the Hodges-Dowell equations and third-and higher order nonlinear terms are neglected.

The nonlinear bending-bending-torsion equations could be reduced to the bending-torsion equations by applying the above procedure. From Eq. B.12, we obtain

$$EI_2 v'''' = -(EI_2 - EI_1)(\phi w'')'' \quad (\text{B.15})$$

Applying two boundary conditions $v'''(1) = v''(1) = 0$, the expression for v'' can be determined. It can be expressed simply ' $v'' = C_v f(\phi w)$ '. Substituting the resulting

expression into the other equations Eqs. (B.13) and (B.14), we obtain

$$\begin{aligned} EI_1 w'''' + (EI_2 - EI_1) \underline{(\phi C_v f(\phi w))''} + m\ddot{w} &= \frac{dF_w}{dx} \\ -GJ\phi'' + (EI_2 - EI_1) \underline{(w'' C_v f(\phi w))''} + mK_m^2 \ddot{\phi} &= \frac{dM_x}{dx} \end{aligned} \quad (\text{B.16})$$

As shown Eq. (B.16), the underlined terms are third order. In developing the Hodges-Dowell equations, the third order terms are neglected if there is no special reason. Therefore, the third order terms could be removed from Eq. (B.16). The resulting bending-bending equations are not nonlinear, but linear.

Approach 2 Another procedure to obtain more simplified expressions for the bending-torsion system is considered. In the previous section, the bending-torsion equations are derived from the bending-bending-torsion equations by removing the in-plane bending terms. In this section, the terms associated with the in-plane bending motion is excluded from energy expressions.

In the following examples, the adopted energy expressions are different depending upon the focused motion. A cantilever beam with a concentrated mass is the first example.⁵⁸ In order to investigate the out-of-plane bending deflection w , the following energy expressions are adopted. The strain energy is

$$V = \frac{1}{2} \int_0^L EI (w'')^2 dx + \frac{1}{2} k_i w_i^2 \quad (\text{B.17})$$

and the kinetic energy is

$$T = \frac{1}{2} \int_0^L \rho A \dot{w}^2 dx + \frac{1}{2} m_s \dot{w}_s^2. \quad (\text{B.18})$$

The second example is a rod undergoing torsional deformation.⁵⁸ The corresponding potential energy and kinetic energy are

$$V = \frac{1}{2} \int_0^L GJ(\theta')^2 dx \quad (\text{B.19})$$

and

$$T = \frac{1}{2} \int_0^L \rho I_p \dot{\theta}^2 dx \quad (\text{B.20})$$

Another example is a bar attached to a shaft, rotating uniformly with the angular velocity Ω .⁵⁹ Because it is focused on the out-of-plane bending deflection, w , the potential energy and kinetic energy are expressed by w as follows,

$$V(t) = \frac{1}{2} \int_0^L EI(w'')^2 dx + \int_0^L P(ds - dx) \quad (\text{B.21})$$

and

$$T(t) = \frac{1}{2} \int_0^L m\dot{w}^2 dx + \frac{1}{2} \int_0^L J(\dot{w}')^2 dx \quad (\text{B.22})$$

Substituting these energy expressions into the Hamilton's principle, equations of motion for each example can be obtained.

Based on these examples, another set of nonlinear bending-torsion equations can be obtained. For a cantilever wing, the potential energy and kinetic energy are expressed in terms of the out-of-plane bending, torsion motion and associated terms as follows,

$$V = \frac{1}{2} D_\xi \rho_\xi^2 + \frac{1}{2} D_\eta \rho_\eta^2 \quad (\text{B.23})$$

and

$$T_W = \frac{1}{2} \int_0^L m\dot{w}^2 d\hat{s} + \int_0^L m\dot{T}_{13}\dot{w}^2 d\hat{s} + \frac{1}{2} \int_0^L (I_\xi \omega_\xi^2 + I_\eta \omega_\eta^2) d\hat{s} \quad (\text{B.24})$$

Because these expressions can be obtained from Eqs. (2.5) and (2.4) by neglecting the in-plane bending and axial deflection terms, the corresponding nonlinear bending-torsion equations can be derived from Eqs. (2.27) and (2.28).

$$G_w^w = -D_x [w' (w' w'')] + D_x (w'' \alpha^2)'' + I_x \ddot{w}'' \quad (\text{B.25})$$

$$G_\alpha^w = D_x [(w''^2) \alpha] - I_x [(\dot{w}^2) \alpha] \quad (\text{B.26})$$

where the superscript w means that these nonlinear terms are caused by the wing(W) flexibility. When e and x_s have the order of ϵ^0 , and the integral terms shown in Eqs. (2.27) and (2.28) are neglected, the nonlinear terms including the external store and mass imbalance terms are

$$\begin{aligned} & m\ddot{w} - me\ddot{\alpha} + D_x w^{IV} + M_s(\ddot{w} - x_s \ddot{\alpha}) \delta(y - y_s) \\ & - \pi \rho b^2 V \dot{\alpha} + \rho V b C_{L\alpha} \left[\dot{w} - V\alpha - b\left(\frac{1}{2} - a\right) \dot{\alpha} \right] = G_w^{BT2} \\ & I_y \ddot{\alpha} - me\ddot{w} - D_y \alpha'' + \left[(I_{sy} + M_s(x_s^2 + z_s^2)) \ddot{\alpha} - M_s x_s \ddot{w} \right] \delta(y - y_s) \\ & + \pi \rho b^2 V b \left(\frac{1}{2} - a\right) \dot{\alpha} + \rho V b^2 C_{m\alpha} \left[\dot{w} - V\alpha - b\left(\frac{1}{2} - a\right) \dot{\alpha} \right] = G_\alpha^{BT2} \quad (\text{B.27}) \end{aligned}$$

where

$$\begin{aligned} G_w^{BT2} &= -D_x [w' (w' w'')] + D_x (w'' \alpha^2)'' + I_x \ddot{w}'' \\ & - \frac{1}{2} me \left[(\dot{\alpha} w'^2 + 2\alpha w' \dot{w}' + \alpha^2 \dot{\alpha}) \dot{} + (\dot{w}^2 - 2(\ddot{w} \alpha w')) \right] \\ & - \frac{1}{2} M_s x_s (\dot{\alpha} w'^2 + 2\alpha w' \dot{w}' + \alpha^2 \dot{\alpha}) \dot{} \delta(y - y_s) \\ & + [M_s z_s (\alpha \dot{\alpha} + w' \dot{w}')] \delta(y - y_s) \quad (\text{B.28}) \end{aligned}$$

$$\begin{aligned} G_\alpha^{BT2} &= D_x [(w''^2) \alpha] - I_x [(\dot{w}^2) \alpha] - \frac{1}{2} me [\ddot{w} (w'^2 + \alpha^2)] \\ & + M_s \ddot{w} \left[-\frac{1}{2} x_s (w'^2 + \alpha^2) + z_s (\alpha) \right] \delta(y - y_s) \end{aligned}$$

$$-I_{sx}(\dot{w}^2)\alpha\delta(y - y_s) \tag{B.29}$$

APPENDIX III

PROGRAM LISTS

Main Program

```

%   Nonlinear Bending-(Bending-) Torsion Program
%       [ui,wj,alphak] i=j=k=1 case
%
%
%                               KIUN KIM
%
clear all

%   Part I. global data
%----- global -----
global p1 p2 p3 p4 p5 p6 p7 p8 p9 p10 p11 p12 p13
global MatD MatND                % for BBT_mat.m
global NLmodel IDsys global V Vs IDEq Vfg global IDwing
global IDana IDmodel Uf N        % for BT_k
global ML CL KL SML global UR eii eir
global MNL CNL KNL SM           % for BBT_sub
global IDsol global fid fidc fidi fidout
global IR WQC
global iPPu iPPw iPPa          % For Phase Portraits
global iPMu iPMw iPMa          % For Poincare Maps
global iBIFuu iBIFuw iBIFua iBIFwu iBIFfw iBIFwa iBIFau iBIFaw
iBIFaa global pmw pmw2 pmwt pmwt2 pma pma2 pmat pmat2 global Vr

```

```

f_Bif y0 iIC
% ----- End of Part I
% === Part II. Select Model =====
%
% Select Wing Model & System
%   IDmodel = (1,2) = (NATA, HGW)
%   NLmodel = (0,1,2,3,4,5,6,7) = (L,W,A,S,WA,WS,SA,WAS)
%
%           L ~ Linear model
%           W ~ Wing, A~ Aero, S~Store
%   IDsys   = (1,2) = (BT, BBT)
%   IDsol   = (1,2) = (RK4, ode45)
%
%   IDmodel = 1;
%   NLmodel = 0;
%   IDsys   = 2;   IDEq = IDsys;
%   IDsol   = 2;
%
% Select Solution approach
%   IDana = (0,1,2,3,4,5,6) =(TR, NM, F1, F2, PP, Pm, Bif)
%
%           TR ~ TRansient analysis
%           NM ~ Normal Mode Analysis
%           F1 ~ Flutter analysis 1 (k-method)
%           F2 ~ Flutter analysis 2 (Eig. of SM)
%           PP ~ Phase portraits for various IC's
%           Pm ~ Poincare Maps
%           Bif~ Bifurcation diagram
%

```

```

IDana = 2          % if possible, DO NOT use IDana = 3 option
ID_Bif = 1;

        N = 1;

        NV = 2;

        IR = 1; % default = 1 [if IR = 0, then C may be zero ]
% ----- Select Model -----
% NATAm Model
if (IDmodel ==1)
xsr = 0.0 ; ysr = 1.; zsr = 0.0; ap = 1; st = 0;
msr = 0.1; Isyr = 0.1 ; elseif (IDmodel ==2)
% HGW Model
xsr = -1.75/3 ; ysr = 1.; zsr = 0.0;          ap =
1; st = 0; msr = 0.1; Isyr = 50.340/(25.170*20) ; Dz_sf = 12.0 ;
Model = 1 ; SCw = 1/1; SCa=1/1; end
% Define parameters -----
%%%      p[0] = Velocity, p1= aero_linear, La,
%      p[2] = store_linear, Ls
%      p3 = Wing_Nonliner(NLw), p4=aero_nonlinear(NLa),
%      p5=store_nonlinear(NLs),
%      p[6] = xs, p7 = ys, p8 = zs, store position
%      p9 = Ms (store Mass), p[10] = Isy (Store inertia)
%      p11= IDmodel (0,1) = ( my model bassed on NATA, HGW) */
%      p12 = bz
%      p13 = L
La = 1; Ls = 1; NLw = 0 ; NLa = 0; NLs = 1;
p13 = 1.0; % Scale Factor for Wing Span L , L = AR(=p13)*L (original)

```

```

                % p13 = 1 (default)
WQC = 1      %
bz = 44.0;
% -----
p1 = La; p2 = Ls; p3 = NLw; p4 = NLa; p5 = NLS; p6 = xsr; p7 =
ysr; p8 = zsr; p9 = msr; p10= Isyr; p12 = bz;
% ===== End of parameters
%
%                Record for input data
% -----
dat = 022704; %(N=NATA,H=HGW)  MMDDYY
fname =sprintf('tN00S_m1I1x0z0_bz44BBT%.0fPa.dat',dat) %
fid = fopen(fname,'w');
if (ID_Bif == 1)
    fn_Bif =sprintf('tN00S_NWAS_m1I1x0z0_bz44BBT_Bif%.0fPa.dat',dat)
    f_Bif = fopen(fn_Bif,'w')      ;
    fprintf(f_Bif,'%% Bifurcation diagram data for a system -----> \n');
    fprintf(f_Bif,'%% Model = %2i (1,2) = (KIM=NATA, HGW)\n',IDmodel);
    fprintf(f_Bif,'%% System Parameters La = %2i, La = %2i, NLw = %2i,
                NLa = %2i, NLS = %2i \n',La,Ls,NLw,NLa,NLS);
    fprintf(f_Bif,'%% Scale factor for Wing span (p13) = %5.2 & bz =
                %5.2 \n',p13,bz);
    fprintf(f_Bif,'%% WQC (= NLw option) = %2i ; (0,1)=(Quad,Cubic)\n',
                WQC);
    fprintf(f_Bif,'%% Store Conditions ----- \n');
    fprintf(f_Bif,'%% Msr = %6.2f Isr = %6.2f xsr = %6.2f zsr = %6.2f
                \n',msr,Isyr,xsr,zsr);

```

```

        fprintf(f_Bif, '%% ----- \n');
end

fprintf(fid, ' Check the Model data ----- %7i
          (IDmodel =(1,2)=(NATA,HGW))', IDmodel)

% ----- End of Part II
% Call BBT_mat.m           ~ Wing, Aero. and Store properties
%   MatD(i) = L,      c,   b,   a, ea, cg, mass, me, Dx, Dy ;
%   MatD(1i) = Dz,   Iy0,  Ix,  Iy, Iz      <-- Wing
%   MatD(2i) = rhoa, Cla, Cma, c3          <-- Aero terms
%   MatD(3i) = Mass,  xs,  ys,  zs, Isx, Isy, Isz ; <-- Store
% -----
%
%   MatD = BBT_mat(IDmodel);
% -----
% Call BT_k.m             ~ Flutter Analysis (k-method) for the
% -----
%
%   Vfg = BT_k(IDmodel);
%
% -----
% === Part III. Select Simulation Conditions
%
%   t0 = initial time
%   dt = increment
%   tmax = maximum time
%   nplot = # of point (ode45 option)
%

```

```

% Vr = Velocity Ratio to the flutter velocity (Vf) = V/Vf
%
% y0 = [u,w,alpha,du,dw,d_alpha]^T
%       for BT case, u=du=0
%
ti = 0.0;
tmax0 = 150.0;
tmax = tmax0;
te = tmax0;
dt = 0.01;      nplot = 2048*2^2+1;
% -----
Vr = [ 0.71;0.72;0.73;0.74;0.75;0.76;0.77;0.78;0.79; 0.8; ...
      0.81;0.82;0.83;0.84;0.85;0.86;0.87;0.88;0.89; 0.9; ...
      0.91;0.92;0.93;0.94; 0.95;0.96;0.97;0.98;0.99; 1.0;...
      1.01;1.02; 1.03; 1.04; 1.05; 1.06; 1.07; 1.08; 1.09; 1.1 ];
LVr = length(Vr);
% Vr = 1.02 ; LVr = 1 ;      %
%
%===== Velocity Loop -----
% NV : # of Vel. conditions ==> LVr
% Vr : Velocity ratio = V/Vfg
%
for iV = 1: LVr
V = Vr(iV) * Vfg;
fidc = 1;      % Record initial conditions including SM
% IDs for figures

```



```

iPPu = 300 + iV; iPPw = 400 + iV; iPPa = 500 + iV; % for Pm
iPMu = 600 + iV; iPMw = 700 + iV; iPMa = 800 + iV; % for PP
iBIFuu = 911 ; iBIFuw = 912 ; iBIFua = 913 ; % For du = 0 & (u,w,a)
iBIFwu = 921 ; iBIFww = 922 ; iBIFwa = 923 ; % For dw = 0 & (u,w,a)
iBIFau = 931 ; iBIFaw = 932 ; iBIFaa = 933 ; % For da = 0 & (u,w,a)
% ===== IC loop
%           NIC : # of Initial conditions
NIC = 1 ;
    L = MatD(1);
    umax = 0.001/L;    wmax = 0.05/L*1.    ; amax = 0.15/3*1.0;
    du = 0.0;        dw = 0.05/L*0    ; da = 0.05*0; %
    du = 0.0;        dw = wmax/NIC; da = amax/NIC; %
    du0= 0.0;        dw0 = 0.0/L    ; da0 = 0.0;
NICs = (NIC+1)*(NIC+1);
NICw = NIC+1;
NICa = 1;
IDTH = 0;
%   NICs = 1; NICw = 1; IDTH = 1 % For a specified case
for iIC = 1 : NICs
% ----- Initial Conditions
ui = umax;
if (iIC <= NICw )
    ai = amax - da*(NICa -1);
else
    ai = amax - da*(NICa );
    NICw = NICw + (NIC+1);

```

```

        NICa = NICa + 1;
    end
    wi = wmax - dw*(NICw*1 - iIC) ; % 011904
    aiwi = ai + wi;
    dVr = abs(Vr - 1.0);
    if (aiwi <= 0.001 & dVr <=0.1 | wi == 0)
        wi = wi + 0.0002;
        ai = ai + 0.0002;
        te = 6 * tmax0; %nplot = 2048*2^3+1
        tmax = te;
    else
        te = 1.0 * tmax0; %nplot = 2048*2^3+1
        tmax = te;
    end
    if ( dVr < 0.07 & wi >=wmax)
        te = 5 * tmax0; %nplot = 2048*2^3+1
        tmax = te;
    end
    if (tmax > 1200) te = 1197; tmax = 1197; end
    y(1,1) = ui ; y(2,1) = wi; y(3,1) = ai;
    y(4,1) = du0; y(5,1)=dw0 ; y(6,1)= da0 ;
% -----
    y0 = [ui,wi,ai,du0,dw0,da0]; yi = y0;
    Today = dat;
% -----
%=== Part IV. Numerical Integration (2)

```

```

%   IDsol = (1,2)   = (4th order Runge-Kutta, ode45)
%
%   IDsol = 1;
% -----
%
nt = 1 if (IDsol == 1)
    fprintf(' IDsol is %4i', IDsol)
    for t = ti : dt : te
        rk1 = dt*BBT_sub_WQC_h011804(t, y(:,nt)      );
        rk2 = dt*BBT_sub_WQC_h011804(t, y(:,nt)+rk1/2 );
        rk3 = dt*BBT_sub_WQC_h011804(t, y(:,nt)+rk2/2 );
        rk4 = dt*BBT_sub_WQC_h011804(t, y(:,nt)+rk3   );
        y(:,nt+1) = y(:,nt) + 1/6*(rk1+2*rk2+2*rk3+rk4);
        tr(nt+1) = ti+nt*dt; t = ti+nt*dt ;
        nt = nt + 1;
    end
end
%
if (IDsol ==2)
    fprintf(' IDsol is %4i', IDsol)
    tspan = linspace(ti, te ,nplot);
    [tr45,y45] = ode45('BBT_sub_WQC_h011804',tspan,yi);
%
    y = transpose(y45);
    tr = transpose(tr45);
end

```

```

%=== Part V. Post-processor
%end % of IC loop [N_IC] Original position
%
if (IDTH ==1)
    figure
    set(gca,'FontSize',10)
    subplot(221),plot(tr,y(1,:)),xlabel('t'),ylabel(' u ')
    title(['Vr = ',num2str(Vr(iV)),'=(V/Vfg) = (',
          num2str(V),'/',num2str(Vfg),'')'])
    grid
    subplot(222),plot(tr,y(2,:)),xlabel('t'),ylabel(' w ')
    title(['yo = ',num2str(y0)])
    grid
    subplot(223),plot(tr,y(3,:)),xlabel('t'),ylabel(' \alpha ')
    title(['Solver = ',num2str(IDsol)])
    grid
    subplot(224),plot(y(3,:),y(6:8,:)),xlabel('\alpha'),ylabel('d\alpha ')
    Egn = eig(SML);
    title(['Eig(SML) = ',num2str(Egn(1)),' ',num2str(Egn(3)),' ',
          num2str(Egn(5))])
    grid
end
%% ===== Bifurcation Diagram =====
%%

```

```

if (ID_Bif == 1)
    fprintf(f_Bif, '% Vel. ratio, Vr = V/(Vfg=%8.4f) \n', Vfg);
    fprintf(f_Bif, '%BP          Vrp= %8.4f \n', Vr(iV));
    fprintf(f_Bif, '% ----IC(u,w,a,du,dw,da) = (%8.4f,%8.4f,%8.4f,
        %4.2f,%4.2f,%4.2f) \n', y0);

    NF = 10 ;

    I_PM = BBT_PM_F(iV,Vfg,NF,y,tr);
    Lw = I_PM(1); La = I_PM(2);
    I_Bif = BBT_Bif_F021004(iV,NF,Lw,La)
end % of ID_Bif loop
%
end % of IC loop [N_IC]

end % of Vel. loop [iV]
ST = fclose('all') toc

```

Material Peorperty Module : BBT_mat.m

```

function MatD=BBT_mat(IDmodel)
% BBT - Material properties and aerodynamic coefficients
%
global p1 p2 p3 p4 p5 p6 p7 p8 p9 p10 p11 p12 p13 % Store Coefficients
global MatD MatND global V Vs IDEq Vfg p11 = IDmodel; bz = p12;
iDzsf = 1/bz;
    if (p11 == 2)

```

```

%    {
L = 20. ;          %%% wing span, ft */
c  = 6.  ;        %%% wing chord, ft */
b  = c /2. ;      %%% semi chord, ft */
ea = 2.0 ;        %%% Elastic Axis */
cg = 2.6 ;        %%% Center of Gravity, ft from LE */
mass = 11.249 ;   %%% mass per unit length, slug/ft*/
me  = 6.7494 ;   %%% 1st mass moment, slug ft/ft */
Ix = 0.0;        %%% Assumed */
Iy0 = 25.170;
Iy = Iy0 + mass*(cg-ea)*(cg-ea); %%
                                %=29.2196, 2nd mass moment, slug ft^2/ft */
Iz = 0.0;
EI = 23647000;   %%% Bending Rigidity */
GJ = 2389900;    %%% Torsional Rigidity */
%
a = (ea-c/2.)/b;  %%% ND distance midchord to EA */

%% Input Aerodynamic Properties */
%% # include "Aero_HGW.dat" */ %% Aero_HGW.dat */
rhoa = 0.0023769 ; %%% Air density, [lb-sec^2-ft^(-4) */
CLa = 2.*3.141592; %%% Lift slope */
Cma = CLa * (1./2. + a); %%% Moment slope */
%}
else
%    {

```

```

        if( p11 == 1 ) %%% Model 0 => p11 = 0 ~ My model based on NATA */
%   {
    L = 1.20 ;    %%% span */
    c = 0.135*2. ;    %%% chord */
    b = 0.135      ;    %%% semi-chord */
    mass = 1.644*1.2 ; %%% mass per unit length */
    me = mass* 0.0 * b; %%% 1st mass moment */
    a = -0.8; %%% a = (ea-c/2.)/b; => ea = a*b+b */
    ea = (a+1.0)*b;
    cg = ea + me/mass;
%           Dz_sf = 10 ; % Assumed value {4/(1/3)=12 for HGW)
    EI = 476.928 ;% *SCw ;
    Ix = 0.0;
    Iy0 = 0.05265;
    Iy = Iy0 + mass*( cg-ea) * (cg-ea);
           Iz = Iy0 /(1.0+1.0*iDzsf^2); % [020203]
           Ix = 1.0*iDzsf^2*Iz;
    GJ = 3.9878 ;%* SCa;
%
    rhoa = 1.225 ;    %%% Air density, [lb-sec^2-ft^(-4) */
%   CLa = 0.123466*180./3.141592;    %%% Lift slope */
    CLa = 0.123466*180/pi ;% [022003]
    Cma = CLa * (1./2. + a); %%% Moment slope */
%   }
end    % of Model 0 {NATA)
%   };

```

```

end      % of Model 1 (HGW)
% -----
      Dx = EI ; Dy = GJ;
% -----
%   Modify Wing span, L
      L = p13 * L;
% -----
Mass = p9*(mass*L);   %%% 22.496 for p9=0.1, 0.0<p[0]<1.0 */;
Isx = 0.0;
Isy = p10*(Iy0*L);   %%% 50.340 for p[10] = 0.1 */;
Isz = 0.0;
xs = p6*b ;         %%% -1.0 <= p6 <= 1.0*/
ys = p7*L;         %%%  0.0 <= p7 <= 1.0*/
zs = p8*b;         %%% -1.0 <= p8 <= 1.0*/
%%% ===== End of Geometric and Material */
%   c3 = 0.00034189 * (180.0/3.141592)^3/CLa ;
c3 = 0.00034189 * (180.0/pi)^3/CLa ;
%
% =====
% Nondimensional parameters
%       Characteristic time and length are
%               sqrt(mass L^4/Dx), L
%-----
% Vs = V/Vf, ux = u/L, wx = w/L
es = me/mass/L ;           MatND(1) = es; Ixs =
Ix/(mass*L^2);           MatND(2) = Ixs; Iys = Iy/(mass*L^2);

```



```

MatND(3) = Iys; Izs = Iz/(mass*L^2);           MatND(4) =
Izs;
%
Dz = Dx * bz;                               MatND(5) = Dz;
%bz = Dz/Dx;           % = (EIz/EIx)
by = Dy/Dx;                               MatND(6) = by; bs = b / L;
MatND(7) = bs;

MatND(8) = a;
MatND(9) = bz;
MatND(11) = mu;% Aero
Mss = Mass/(mass*L);                       MatND(21) = Mss; xss = xs/L;
MatND(22) = xss; zss = zs/L;                MatND(23) =
zss; Isxs = Isx/mass/L^3;                   MatND(24) = Isxs; Isys =
Isy/mass/L^3;                               MatND(25) = Isys; Iszs =
Isz/mass/L^3;                               MatND(26) = Iszs;
% =====
%       Save the material properties and aerodynamic coefficients
%       MatD(i)~ Dimensional properties;
%       MatND(i)~ Non-dimensional properties
% -----
%   Wing properties
MatD = zeros(40,1) % Set zero
    MatD(1) = L ;   %%% span */
    MatD(2) = c   ;   %%% chord */
    MatD(3) = b   ;   %%% semi-chord */
    MatD(4) = a ; %%% a = (ea-c/2.)/b; => ea = a*b+b */

```

```

MatD(5) = ea ;
MatD(6) = cg ;

%
MatD(7) = mass ;   %%% mass per unit length */
MatD(8) = me ;   %%% 1st mass moment */
MatD(9) = Dx ;
MatD(10) = Dy ;
MatD(11) = Dz ;
MatD(12) = Iy0 ;
MatD(13) = Ix ;
MatD(14) = Iy ;   %[020203]
MatD(15) = Iz ;

% Aerodynamics
MatD(21) = rhoa ;   %%% Air density*/
MatD(22) = CLa ;   % Lift Slope
MatD(23) = Cma ;   %%% Moment slope */
MatD(24) = c3 ;   % Nonlinear Aero. factor

% Store properties
MatD(31) = Mass ;   % Store mass
MatD(32) = xs ;   % Store position (xs,ys,zs)
MatD(33) = ys ;
MatD(34) = zs ;
MatD(35) = Isx ;   % Store Inertia
MatD(36) = Isy ;
MatD(37) = Isz ;

% MatD(i) = L , c , b , a , ea ,cg , mass, me, Dx, Dy ;

```

```

%      MatD(1i) = Dz, Iy0, Ix, Iy ,Iz
%      MatD(2i) = rhoa , Cla, Cma, c3
%      MatD(3i) = Mass , xs, ys, zs, Isx, Isy, Isz ;

Flutter Module : BT_k.m

%  Filename : BT_k.m [020304 Home version]
%      Using the k-method, flutter condition will be calculated.
%      Flutter Analysis Program for a cantilever beam with tip store
%                                     ( Including Heavy Goland wing)
%
%      Test Model : Heavy Goland Wing [ Beran's paper, 2002 ]
%      Aerodynamic Model : Quasi Steady-State Aerodynamics
%                          [ Aeroelasticity by Bisplinghoff, Ashley, and Halfman]
%
%      Analysis Parts 2
%      (1) Search flutter condtion
%      (2) Save the V-fg data
%
%      function Vfg = BT_k(IDmodel);
global p1 p2 p3 p4 p5 p6 p7 p8 p9 p10 p11 p12 global IDana IDmodel
Uf N global M2n C2n K2n SM U global ML CL KL SML global MatD MatND
global UR eii eir global fid fidc fidi fidout p11 = IDmodel;
% =====
% Control Parameters
% -----
% -----

```

```

% Select Analysis option, IDanal
% -----
    IDanal = IDana      % IDanal (sub) = IDana (main) [120603]
                        % 1 ~ Modal Analysis,
                        % 2 ~ Find Vf,
Iter_max = 1 ;          % Default value

Ui = 50.0;              % Velocity for Transient analysis
    if (IDmodel ==1 )
        Umax = 60; % Velocity Range
        Ui = 10;
        kstep = 100; dk = .1; % (1/k)_max = kstep * dk
    elseif (IDmodel ==2)
        Umax = 1000; % Velocity Range
        kstep = 1000; dk = .2;
    end

if IDanal == 1
    U = 0;
    IDfig = 1 ;          % 0 ~ No mode shape, 1 ~ Draw mode shapes

elseif IDanal == 2      % Flutter Analysis
    U0 = 0 ;
    U = Umax; Umax0 = Umax;
    Uf = 0.0;
    Iter_max = 120;

```

```

elseif IDanal == 3
    U = Ui;      % Dummy value
%   kstep = 1000; dk = .2;          % (1/k)_max = kstep * dk
end

% ===== Step 1 : Find Vfg -----
iCTVf = 1; Vm = 0; Vp = Umax; Vstep = 120; dV = (Vp-Vm); Veps =
0.001; V0 = Vp/3; IDpm = 0; while dV > Veps
    % Call Function BBT_Lin
    SML2k = BBT_Lin(Vstep,Veps,V0);

    EGR2 = eig(SML2k); % Damping = real(), Freq. = imag() [111302]

%   gc = min(real(EGR2));
gc = max(real(EGR2));
if (gc < 0.0)
    Vm = V0;
    if (IDpm <=0)
        V0 = Vm + V0;
    elseif (IDpm ==1)
        V0 = (Vm + Vp)/2;
    end
else
    Vp = V0;
    V0 = (Vm + Vp)/2;

```

```

        IDpm = 1;
    end
    dV = (Vp - Vm);
    iCTVf = iCTVf + 1;
    if (iCTVf > 1000) pause; end
end Vfg = V0;
% -----
% ===== Step 2 : Save data -----
NV = 120; for iVR = 1 : NV +1
    V0 = Vfg/100*(iVR-1);
    UR(iVR) = V0;
    SML2k = BBT_Lin(Vstep,Veps,V0);
    EGR2 = eig(SML2k);
    if ( imag(EGR2(1)) > imag(EGR2(3)) )
        eir(iVR,1) = real(EGR2(3));
        eii(iVR,1) = imag(EGR2(3));
        eir(iVR,2) = real(EGR2(1));
        eii(iVR,2) = imag(EGR2(1));
    else
        eir(iVR,1) = real(EGR2(1));
        eii(iVR,1) = imag(EGR2(1));
        eir(iVR,2) = real(EGR2(3));
        eii(iVR,2) = imag(EGR2(3));
    end
end
end
% -----

```

```

% ----- Flutter Analysis (1)
%
%           Check the eigenvalues of system matrix, [SM]
%
%end      % end of while
% -----
%Vfg = Uf;
% =====
if IDanal == 2
    IDmat = 1; IDkp = 0; IDsub = 0;
    fprintf(fid,' ***** BT_k.m ***** \n');
    IDp = BBT_printout(IDmat,IDkp,IDsub)
    fprintf(fid,' ***** BT_k.m *****\n ----
                End of BT_k.m \n');
figure
if (IDmodel == 1)
    subplot(211), plot(UR,eii, '.'), axis([0, 30, 0, 8]), grid,...
        set(gca,'FontSize',14),set(gca,'FontName','times'),...
        xlabel('Vel. [m/sec]'),ylabel('Frequeuncies ')...
        ,title(['V-f & V-g Plots (Vf =',num2str(Vfg),' ft/sec)'])
    subplot(212),plot(UR,eir, '.'), axis([0, 30, -1.2,0.1]),grid,...
        set(gca,'FontSize',14),set(gca,'FontName','times'),...
        xlabel('Vel. [m/sec]'),ylabel('Damping') %...
elseif (IDmodel ==2)
    subplot(211), plot(UR,eii, '.'), axis([0, 200, 0, 8]), grid,...
        set(gca,'FontSize',14),set(gca,'FontName','times'),...
        xlabel('Vel. [ft/sec]'),ylabel('Frequeuncies ')...

```

```

        ,title(['V-f & V-g Plots (Vf =',num2str(Vfg),' ft/sec)
              for L=',num2str(MatD(1))])
subplot(212),plot(UR,eir,'.'), axis([0, 200, -.6,0.1]),grid,...
        set(gca,'FontSize',14),set(gca,'FontName','times'),...
        xlabel('Vel. [ft/sec]'),ylabel('Damping')
title(['N-Freq. : \omega_w & \omega_{\alpha} = ',
       num2str(eii(1,:)),... ' =',num2str(eii(1:)/2/pi)])
    end
end

```

BBT Linear Module : BBT_Lin.m

```

%
%   File name : BBT_Lin.m
%
%   In order to find the flutter velocity, this function file is
%   prepared. This program will be called in BT_k.m.
%
%   Input data : Velocity Condition, material properties {MatD and/or
%   MatND)
%   Output data : SML (System matrix for Linear system), eigenvalues
%
function SML2k = BBT_Lin(Vstep,Veps,V0) global fid fidc fidi
fidout global p1 p2 p3 p4 p5 p6 p7 p8 p9 p10 p11 p12 global V Vs
IDeq Vfg global MatD MatND global ML CL KL SML

% -----

```



```

es = MatND(1) ; Ixs = MatND(2); Iys = MatND(3); Izs = MatND(4) ;
Dz = MatND(5) ; by = MatND(6) ; bs = MatND(7) ; a = MatND(8)
; bz = MatND(9) ;
mu = MatND(11) ;% Aero
rhoa = MatD(21) ; %%% Air density*/
CLa = MatD(22) ; % Lift Slope
Cma = MatD(23) ; %%% Moment slope */
c3 = MatD(24) ;
Mss = MatND(21) ; % Store
xss = MatND(22) ; zss = MatND(23) ; Isxs = MatND(24) ; Isys =
MatND(25) ; Iszs = MatND(26) ;
% -----
L = MatD(1); mass = MatD(7); Dx = MatD(9); V = V0;
%Vs = (V/Vfg)*(Vfg/sqrt(Dx/mass/L^2) );
Vs = (V/sqrt(Dx/mass/L^2) );
% ===== Stall Condition -----
% =====
if (IDeq == 2 )
    ux = 0.0; dux = 0.0;
end
% =====
% Coefficients, Cpqi
% p = (u,w,a), q = (W,A,S), i = 1,2,3,...n
% %-----
% ----- in-plane bending (u)
Cuw1 = 1.0; %0.99983350;

```

```

Cuw2 = 1.8751^4 ;% = 12.3622; 12.35756130 ;
Cuw3 = -6.59670299 ; Cuw4 = 40.40864878 ; Cuw5 = 40.40864878 ;
Cuw6 = 5.03464023 ; Cuw7 = 3.20771918 ; Cuw8 = -11.32343354 ;
Cuw9 = 0.85819664 ; Cuw10 = 4.59531864 ; Cuw11 = 4.59531864 ;
Cuw12 = 0.0; Cuw21 = 4.09855496 ; Cuw22 = 1.21618943 ; Cuw23 =
5.19493449 ; Cuw24 = 5.81481592 ; Cuw25 = 5.81481592 ;

%----- Out-of-plane
Cww1 = 1.0 ;% 0.99983350 ;
Cww2 = 1.8751^4 ;% = 12.3622;12.35756130 ;
Cww3 = -6.59670299 ; Cww4 = 40.40864878 ; Cww5 = 40.40864878 ;
Cww6 = 5.03464023 ; Cww7 = 3.20771918 ; Cww8 = -11.32343358 ;
Cww9 = 0.85819604 ; Cww10 = 4.59531861 ; Cww11 = 4.59531861 ;
Cww12 = 0.0;          Cww13 = 0.0;          Cww14 = 0.0;          % dummy
Cww15 = 0.0;          Cww16 = 0.0;          Cww17 = 0.0; Cww18 = 0.0;
Cww19 = 0.0;          Cww20 = 0.0;
Cww21 = 0.95855948 ; % mass imbalance terms
Cww22 = 4.09855496 ; Cww23 = -7.17869258 ;
Cww24 = 0.0;          Cww25 = 0.0;          Cww26 = 0.0;          % dummy

% ----- torsion (alpha)
Caw1 = 1.0;          % 0.99999979 ;
Caw2 = -(pi/2)^2 ; % = -2.4674; -2.46739956 ;
Caw3 = 3.21320715 ; Caw4 = 3.21320715 ; Caw5 = 5.03852063 ;
Caw6 = 2.67354281 ; Caw7 = 5.34708573 ; Caw8 = 6.50085826 ;
Caw9 = 1.73977627; Caw10 = 0.0; Caw11 = 0.0;          Caw12 = 0.0;
Caw13 = 0.0;          Caw14 = 0.0; Caw15 = 0.0;          Caw16 = 0.0;
Caw17 = 0.0;          Caw18 = 0.0; Caw19 = 0.0;          Caw20 = 0.0;

```

```

Caw21 = 0.95855948; Caw22 = 6.61910722; Caw23 = 1.57648449; Caw24
= 5.25531032; Caw25 = 5.25531032; Caw26 = 1.21618943; Caw27 =
11.05426447;
%----- Aero
Cwa1 = 0.6779*sqrt(2); % = 0.95869; 0.95855948 ; %
Cwa2 = 1.0 ; %0.99983350 ;
Cwa3 = 0.6779*sqrt(2); %0.95855948 ;
Cwa4 = 0.6779*sqrt(2); %0.95855948 ;
Cwa5 = 1.57648449 ; Cwa6 = 1.73977627 ; Cwa7 = 1.57648449 ;
Cwa8 = 1.99231188; Cwa9 = 1.73977627 ;
Cwa10 = 1.57648449; %
Cwa11 = 2.34789947;
Cwa12 = 1.99231188;
Cwa13 = 1.73977627;
Cwa14 = 1.57648449;
% Cwa1(=Cwa3,4),Cwa2,Cwa5(=Cwa7,10,14),Cwa6(=Cwa9,13),Cwa8(=Cwa12)
%-----
Caa1 = 0.99999979 ; Caa2 = 0.95855948 ; Caa3 = 0.99999979 ;
Caa4 = 0.99999979 ; Caa5 = 1.49999948 ; Caa7 = Caa5; Caa10 =
Caa5; Caa14 = Caa5; Caa6 = 1.57648449 ; Caa9 = Caa6;
Caa13 = Caa6; Caa8 = 1.73977627 ; Caa12=Caa8; Caa11 =
1.99231188 ;
%----- Store terms
Cus1 = 3.999389 ; Cus2 = 1.999847 ;
Cus3 = 15.155298 ; Cus4 = 1.999847 ;
Cus5 = 7.577649 ;

```

```

Cws1 = 3.999389 ; Cws2 = 1.999847 ;
Cws3 = 15.155298 ; Cws4 = 1.999847 ;
Cws5 = 7.577649 ;
Cas1 = 1.000000 ; Cas2 = 1.999847 ;
Cas3 = 1.999847 ; Cas4 = 15.155298 ;
Cas5 = 1.999847 ; Cas6 = 1.999847 ;
Cas7 = 7.577649 ; Cas8 = 7.998167 ;
Cas9 = 1.999847 ; Cas10 = 7.577649 ;
Cas11 = 1.999847 ; Cas12 = 15.155298 ;
Cas13 = 7.578228 ; Cas14 = 7.578228 ;
Cas15 = 12.792806 ; Cas16 = 12.792806 ;
Cas17 = 12.792806 ; Cas18 = 12.792806 ;
Cas19 = 7.578228 ; Cas20 = 7.578228 ;
Cas21 = 7.578228 ; Cas22 = 1.999694 ;
Cas23 = 7.998167 ;

%=====
% Nondimensional parameters
%
% =====
% Matrices, M, C, K
% subscripts (L, NL) mean Linear and Nonlinear, respectively
% ----- Wing [M]_L
MLw(1,1) = Cw1; MLw(1,2) = 0.0; MLw(1,3) = 0.0;
MLw(2,1) = 0.0; MLw(2,2) = Cww1; MLw(2,3) = -es*Cww21;
MLw(3,1) = 0.0; MLw(3,2) = -es*Caw21; MLw(3,3) = Iys*Caw1;
% ----- Aero [M]_L

```

```

MLa(1,1) = 0.0; MLa(1,2) = 0.0; MLa(1,3) = 0.0; MLa(2,1) = 0.0;
MLa(2,2) = 0.0; MLa(2,3) = 0.0; MLa(3,1) = 0.0; MLa(3,2) = 0.0;
MLa(3,3) = 0.0;
% ----- Store [M]_L
Isyt = Isys + Mss*(xss^2+zss^2); MLs(1,1) = Mss*Cus1;
MLs(1,2) = 0.0;          MLs(1,3) = Mss*zss*Cus2; MLs(2,1) =
0.0;          MLs(2,2) = Mss*Cws1;          MLs(2,3) =
-Mss*xss*Cws2;
MLs(3,1) = Mss*zss*Cas3;  MLs(3,2) = -Mss*xss*Cas2; %
MLs(3,3) = Isys*Cas1;
%-----
% ----- Wing [C]_L
CwL(1,1) = 0.0; CwL(1,2) = 0.0; CwL(1,3) = 0.0; CwL(2,1) = 0.0;
CwL(2,2) = 0.0; CwL(2,3) = 0.0; CwL(3,1) = 0.0; CwL(3,2) = 0.0;
CwL(3,3) = 0.0;
% ----- Aero [C]_L
CaL(1,1) = 0.0; CaL(1,2) = 0.0; CaL(1,3) = 0.0; CaL(2,1) = 0.0;
CaL(2,2) = mu*CLa/pi*Vs/bs*Cwa2 ;
CaL(2,3) = -mu*Vs*Cwa1 - mu*CLa/pi*Vs*(1.0/2.0-a)*Cwa4; %[010503]
CaL(3,1) = 0.0;
CaL(3,2) = mu*Cma/pi*Vs*Caa2; % [010604 20:40]
CaL(3,3) =
mu*bs*(1.0/2.0-a)*Vs*Caa1-mu*Cma/pi*Vs*bs*(1.0/2.0-a)*Caa4;
% ----- Store [C]_L
CsL(1,1) = 0.0; CsL(1,2) = 0.0; CsL(1,3) = 0.0; CsL(2,1) = 0.0;
CsL(2,2) = 0.0; CsL(2,3) = 0.0; CsL(3,1) = 0.0; CsL(3,2) = 0.0;

```

```

CsL(3,3) = 0.0;
% -----
% ----- Wing [K]_L
KLw(1,1) = bz*Cuw2;    KLw(1,2) = 0.0;    KLw(1,3) = 0.0;
KLw(2,1) = 0.0;      KLw(2,2) = Cww2;    KLw(2,3) = 0.0;
KLw(3,1) = 0.0;      KLw(3,2) = 0.0;    KLw(3,3) = -by*Caw2;
% ----- Aero [K]_L
KLa(1,1) = 0.0; KLa(1,2) = 0.0; KLa(1,3) = 0.0;
KLa(2,1) = 0.0; KLa(2,2) = 0.0; KLa(2,3) = -mu*CLa/pi/bs*Vs^2*Cwa3;%
KLa(3,1) = 0.0; KLa(3,2) = 0.0; KLa(3,3) = -mu*Cma/pi*Vs^2*Caa3;
% ----- Store [K]_L
KLS(1,1) = 0.0; KLS(1,2) = 0.0; KLS(1,3) = 0.0; KLS(2,1) = 0.0;
KLS(2,2) = 0.0; KLS(2,3) = 0.0; KLS(3,1) = 0.0; KLS(3,2) = 0.0;
KLS(3,3) = 0.0;
%-----
if (Vs == 0)
    iVs = 0;
else
    iVs = 1/Vs;
end
%
%=====
% Summation
% -----
for MCKi = 1:3
    for MCKj = 1:3

```

```

ML(MCKi, MCKj) = MLw(MCKi, MCKj) + p1*MLa(MCKi, MCKj)
                                     + p2*MLs(MCKi, MCKj);
%-----
CL(MCKi, MCKj) = CwL(MCKi, MCKj) + p1*CaL(MCKi, MCKj)
                                     + p2*CsL(MCKi, MCKj);
% -----
KL(MCKi, MCKj) = KLw(MCKi, MCKj) + p1*KLa(MCKi, MCKj)
                                     + p2*KLs(MCKi, MCKj);
% ===== Nonlinear
%=====
end      % of MCKj
end      % of MCKi
% =====
% Inverse matrix of [M]
iML = inv(ML);
% =====
%
for MiKi = 1:3
    for MiKj = 1:3
        MiKL(MiKi,MiKj) = iML(MiKi,1)*KL(1,MiKj)+iML(MiKi,2)*KL(2,MiKj)
                        +iML(MiKi,3)*KL(3,MiKj) ;
        MiCL(MiKi,MiKj) = iML(MiKi,1)*CL(1,MiKj)+iML(MiKi,2)*CL(2,MiKj)
                        +iML(MiKi,3)*CL(3,MiKj) ;
    end      % of MiKj
end      % of KiKi

```

```

%=====
%
z3 = zeros(3,3); I3 = eye(3,3); for iSM = 1 : 3
    for jSM = 1 : 3
        SML(iSM,jSM)    = z3(iSM,jSM);
        SML(iSM,jSM+3)  = I3(iSM,jSM);
        SML(iSM+3,jSM)  = -MiKL(iSM,jSM);
        SML(iSM+3,jSM+3)= -MiCL(iSM,jSM);
        % Nonlinear
    end
end
end
% -----
%=====
% Summation (2)
% -----
for MCKi = 2:3
    for MCKj = 2:3
        ML2(MCKi-1, MCKj-1) = MLw(MCKi, MCKj) + p1*MLa(MCKi, MCKj)
                                + p2*MLs(MCKi, MCKj);
        %-----
        CL2(MCKi-1, MCKj-1) = CwL(MCKi, MCKj) + p1*CaL(MCKi, MCKj)
                                + p2*CsL(MCKi, MCKj);
        % -----
        KL2(MCKi-1, MCKj-1) = KLw(MCKi, MCKj) + p1*KLa(MCKi, MCKj)
                                + p2*KLs(MCKi, MCKj);
        % ===== Nonlinear
    end
end

```



```

%=====
end      % of MCKj
end      % of MCKi
% =====
% Inverse matrix of [M]
iML2 = inv(ML2);
% =====
%
for MiKi = 1:2
    for MiKj = 1:2
        MiKL2(MiKi,MiKj) = iML2(MiKi,1)*KL2(1,MiKj)
                           +iML2(MiKi,2)*KL2(2,MiKj) ;
        MiCL2(MiKi,MiKj) = iML2(MiKi,1)*CL2(1,MiKj)
                           +iML2(MiKi,2)*CL2(2,MiKj) ;
    end      % of MiKj
end      % of KiKi
%=====
z2 = zeros(2,2); I2 = eye(2,2); for iSM = 1 : 2
    for jSM = 1 : 2
        SML2(iSM,jSM)      = z2(iSM,jSM);
        SML2(iSM,jSM+2)    = I2(iSM,jSM);
        SML2(iSM+2,jSM)    = -MiKL2(iSM,jSM);
        SML2(iSM+2,jSM+2)= -MiCL2(iSM,jSM);
        % Nonlinear
    end
end
end

```

```

% =====
%f = SM* y;
SML2k = SML2;
%===== End of Subroutine

```

Nonlinear Formulation Module : BBT_sub.m

```

%
% BBT Function
%
%           function f = BBT_sub(t,y)
%   Input data
%   y = [1,1,1,0,0,0]
%   IDEq = (2,3,4) = (BT, BBT, BBTC)
%       eu = eta_u(t), deu = d(eta_u)/d(tau)
%
%function f = BBT_sub(t,y)
function f = BBT_sub_WQC_h011804(t,y) global fid fidc fidi fidout
global p1 p2 p3 p4 p5 p6 p7 p8 p9 p10 p11 p12 global V Vs IDEq Vfg
global MatD MatND global ML CL KL SML global MNL CNL KNL global Mt
Ct Kt SM
global IR WQC           % Add WQC option [011504]
ux = y(1); dux = y(4); wx = y(2); dwx = y(5); ax = y(3); dax =
y(6);
% -----
es = MatND(1) ; Ixs = MatND(2); Iys = MatND(3); Izs = MatND(4) ;
Dz = MatND(5) ; by = MatND(6) ; bs = MatND(7) ; a = MatND(8)

```

```

; bz = MatND(9) ;
mu   = MatND(11) ;% Aero
rhoa = MatD(21) ;   %%% Air density*/
CLa  = MatD(22) ;   % Lift Slope
Cma  = MatD(23) ;   %%% Moment slope */
c3   = MatD(24) ;

Mss  = MatND(21) ; % Store
xss  = MatND(22) ; zss  = MatND(23) ; Isxs = MatND(24) ; Isys =
MatND(25) ; Iszs = MatND(26) ;
% -----
L = MatD(1); mass = MatD(7); Dx = MatD(9);
%Vs  = (V/Vfg);%*(Vfg/sqrt(Dx/mass/L^2) );
Vs   = (V/Vfg)*(Vfg/sqrt(Dx/mass/L^2) );
% ===== Stall Condition -----
AoA = ax;
%
    if ( abs(AoA) >= 0.1920 & p4 ==1 )
%     {
%     AoA = aeff
        c3 = 0.0
            CLa = 0.0; %[020804]
            Cma = 0.0;
            ap_st = 0;   %
        end
% =====
%if (IDeq == 2 ) % <-- Did it work?

```

```

if (IDeq == 1 )    % [011504]
    ux = 0.0; dux = 0.0;
end
% =====
%   Coefficients, Cpqi
%           p = (u,w,a), q = (W,A,S), i = 1,2,3,...n
% %-----
% ----- in-plane bending (u)
Cuw1 = 1.0; %0.99983350;
Cuw2 = 1.8751^4 ;% = 12.3622; 12.35756130 ;
Cuw3 = -6.59670299 ; Cuw4 = 40.40864878 ; Cuw5 = 40.40864878 ;
Cuw6 = 5.03464023 ; Cuw7 = 3.20771918 ; Cuw8 = -11.32343354 ;
Cuw9 = 0.85819664 ; Cuw10 = 4.59531864 ; Cuw11 = 4.59531864 ;
Cuw12 = 0.0; Cuw21 = 4.09855496 ; Cuw22 = 1.21618943 ; Cuw23 =
5.19493449 ; Cuw24 = 5.81481592 ; Cuw25 = 5.81481592 ;
%----- Out-of-plane
Cww1 = 1.0 ;% 0.99983350 ;
Cww2 = 1.8751^4 ;% = 12.3622;12.35756130 ;
Cww3 = -6.59670299 ; Cww4 = 40.40864878 ; Cww5 = 40.40864878 ;
Cww6 = 5.03464023 ; Cww7 = 3.20771918 ; Cww8 = -11.32343358 ;
Cww9 = 0.85819604 ; Cww10 = 4.59531861 ; Cww11 = 4.59531861 ;
Cww12 = 0.0;          Cww13 = 0.0;          Cww14 = 0.0;    % dummy
Cww15 = 0.0;          Cww16 = 0.0;          Cww17 = 0.0; Cww18 = 0.0;
Cww19 = 0.0;          Cww20 = 0.0;
Cww21 = 0.95855948 ;    % mass imbalance terms
Cww22 = 4.09855496 ; Cww23 = -7.17869258 ;

```

```

Cww24 = 0.0;          Cww25 = 0.0;          Cww26 = 0.0;          % dummy
% ----- torsion (alpha)
Caw1 = 1.0;          % 0.99999979 ;
Caw2 = -(pi/2)^2 ;   % = -2.4674; -2.46739956 ;
Caw3 = 3.21320715 ; Caw4 = 3.21320715 ; Caw5 = 5.03852063 ;
Caw6 = 2.67354281 ; Caw7 = 5.34708573 ; Caw8 = 6.50085826 ;
Caw9 = 1.73977627; Caw10 = 0.0; Caw11 = 0.0;          Caw12 = 0.0;
Caw13 = 0.0;          Caw14 = 0.0; Caw15 = 0.0;          Caw16 = 0.0;
Caw17 = 0.0;          Caw18 = 0.0; Caw19 = 0.0;          Caw20 = 0.0;
Caw21 = 0.95855948; Caw22 = 6.61910722; Caw23 = 1.57648449; Caw24
= 5.25531032; Caw25 = 5.25531032; Caw26 = 1.21618943; Caw27 =
11.05426447;
%----- Aero
Cwa1 = 0.6779*sqrt(2); % = 0.95869; 0.95855948 ; %
Cwa2 = 1.0           ; %0.99983350 ;
Cwa3 = 0.6779*sqrt(2); %0.95855948 ;
Cwa4 = 0.6779*sqrt(2); %0.95855948 ;
Cwa5 = 1.57648449 ;   Cwa6 = 1.73977627 ; Cwa7 = 1.57648449 ;
Cwa8 = 1.99231188; Cwa9 = 1.73977627 ;
Cwa10 = 1.57648449; % should be updated [122003]
Cwa11 = 2.34789947;
Cwa12 = 1.99231188;
Cwa13 = 1.73977627;
Cwa14 = 1.57648449;
%      Cwa1(=Cwa3,4),Cwa2,Cwa5(=Cwa7,10,14),Cwa6(=Cwa9,13),Cwa8(=Cwa12)
%-----

```

```

Caa1 = 0.99999979 ; Caa2 = 0.95855948 ; Caa3 = 0.99999979 ;
Caa4 = 0.99999979 ; Caa5 = 1.49999948 ; Caa7 = Caa5; Caa10 =
Caa5; Caa14 = Caa5; Caa6 = 1.57648449 ; Caa9 = Caa6;
Caa13 = Caa6; Caa8 = 1.73977627 ; Caa12=Caa8; Caa11 =
1.99231188 ;

```

```

%----- Store terms

```

```

Cus1 = 3.999389 ; Cus2 = 1.999847 ;
Cus3 = 15.155298 ; Cus4 = 1.999847 ;
Cus5 = 7.577649 ;
Cws1 = 3.999389 ; Cws2 = 1.999847 ;
Cws3 = 15.155298 ; Cws4 = 1.999847 ;
Cws5 = 7.577649 ;
Cas1 = 1.000000 ; Cas2 = 1.999847 ;
Cas3 = 1.999847 ; Cas4 = 15.155298 ;
Cas5 = 1.999847 ; Cas6 = 1.999847 ;
Cas7 = 7.577649 ; Cas8 = 7.998167 ;
Cas9 = 1.999847 ; Cas10 = 7.577649 ;
Cas11 = 1.999847 ; Cas12 = 15.155298 ;
Cas13 = 7.578228 ; Cas14 = 7.578228 ;
Cas15 = 12.792806 ; Cas16 = 12.792806 ;
Cas17 = 12.792806 ; Cas18 = 12.792806 ;
Cas19 = 7.578228 ; Cas20 = 7.578228 ;
Cas21 = 7.578228 ; Cas22 = 1.999694 ;
Cas23 = 7.998167 ;

```

```

%=====

```

```

% Nondimensional parameters

```

```

%
% =====
%   Matrices, M, C, K
%   subscripts (L, NL) mean Linear and Nonlinear, respectively
%   ----- Wing [M]_L
MLw(1,1) = Cw1;   MLw(1,2) = 0.0;   MLw(1,3) = 0.0;
MLw(2,1) = 0.0;   MLw(2,2) = Cw1;   MLw(2,3) = -es*Cw21;
MLw(3,1) = 0.0;   MLw(3,2) = -es*Caw21; MLw(3,3) = Iys*Caw1;
%   ----- Aero [M]_L
MLa(1,1) = 0.0; MLa(1,2) = 0.0; MLa(1,3) = 0.0; MLa(2,1) = 0.0;
MLa(2,2) = 0.0; MLa(2,3) = 0.0; MLa(3,1) = 0.0; MLa(3,2) = 0.0;
MLa(3,3) = 0.0;
%   ----- Store [M]_L
Isyt = Isys + Mss*(xss^2+zss^2); % See definition for 'Isy'
MLs(1,1) = Mss*Cus1;   MLs(1,2) = 0.0;   MLs(1,3) =
Mss*zss*Cus2; MLs(2,1) = 0.0;   MLs(2,2) = Mss*Cws1;
MLs(2,3) = -Mss*xss*Cws2;
MLs(3,1) = Mss*zss*Cas3; MLs(3,2) = -Mss*xss*Cas2; %MLs(3,3) = Isyt*Cas1;
MLs(3,3) = Isys*Cas1; % 012804
%-----
%   ----- Wing [C]_L
CwL(1,1) = 0.0; CwL(1,2) = 0.0; CwL(1,3) = 0.0; CwL(2,1) = 0.0;
CwL(2,2) = 0.0; CwL(2,3) = 0.0; CwL(3,1) = 0.0; CwL(3,2) = 0.0;
CwL(3,3) = 0.0;
%   ----- Aero [C]_L
CaL(1,1) = 0.0; CaL(1,2) = 0.0; CaL(1,3) = 0.0; CaL(2,1) = 0.0;

```

```

CaL(2,2) = mu*CLa/pi*Vs/bs*Cwa2 ;
CaL(2,3) = -mu*Vs*Cwa1 - mu*CLa/pi*Vs*(1.0/2.0-a)*Cwa4; %
CaL(3,1) = 0.0;
CaL(3,2) = mu*Cma/pi*Vs*Caa2; % [010604 20:40]
CaL(3,3) =
mu*bs*(1.0/2.0-a)*Vs*Caa1-mu*Cma/pi*Vs*bs*(1.0/2.0-a)*Caa4;
% ----- Store [C]_L
CsL(1,1) = 0.0; CsL(1,2) = 0.0; CsL(1,3) = 0.0; CsL(2,1) = 0.0;
CsL(2,2) = 0.0; CsL(2,3) = 0.0; CsL(3,1) = 0.0; CsL(3,2) = 0.0;
CsL(3,3) = 0.0;
% -----
% ----- Wing [K]_L
KLw(1,1) = bz*Cuw2;    KLw(1,2) = 0.0;    KLw(1,3) = 0.0;
KLw(2,1) = 0.0;       KLw(2,2) = Cww2;    KLw(2,3) = 0.0;
KLw(3,1) = 0.0;       KLw(3,2) = 0.0;    KLw(3,3) = -by*Caw2;
% ----- Aero [K]_L
KLa(1,1) = 0.0; KLa(1,2) = 0.0; KLa(1,3) = 0.0;
%KLa(2,1) = 0.0; KLa(2,2) = 0.0; KLa(2,3) = -mu*CLa/pi*Vs^2*Cwa3;
KLa(2,1) = 0.0; KLa(2,2) = 0.0; KLa(2,3) = -mu*CLa/pi/bs*Vs^2*Cwa3;%
KLa(3,1) = 0.0; KLa(3,2) = 0.0; KLa(3,3) = -mu*Cma/pi*Vs^2*Caa3;
% ----- Store [K]_L
KLS(1,1) = 0.0; KLS(1,2) = 0.0; KLS(1,3) = 0.0; KLS(2,1) = 0.0;
KLS(2,2) = 0.0; KLS(2,3) = 0.0; KLS(3,1) = 0.0; KLS(3,2) = 0.0;
KLS(3,3) = 0.0;
%----- Nonlinear Terms + H.O.T
% ----- Wing [M]_NL

```



```

MNLw(1,1) = Izs*Cuw9*WQC-1./2.*Cuw11*ux*(ux+ux)*WQC
           +es*(Cuw21*ux-Cuw24*ux)*WQC;%011604
MNLw(1,2) = -1./2.*Cuw10*ux*(wx+wx)*WQC +
es*(-Cuw23*wx-Cuw25*wx)*WQC; MNLw(1,3) = es*Cuw22*ax*WQC;
MNLw(2,1) = -1./2.*Cww11*wx*(ux+ux)*WQC-es*(Cww22-Cww23)*wx*WQC;
MNLw(2,2) = Ixs*Cww9*WQC -1./2.*Cww10*wx*(wx+wx)*WQC
-es*Cww23*ux*WQC; MNLw(2,3) = 0.0; MNLw(3,1) = Iys*Caw6*wx*WQC+
es*(Caw25*ux*wx+Caw26*ax-Caw27*wx*ux)*WQC; MNLw(3,2) =
Iys*(Caw6*ux - Caw7*ux)*WQC ...
    + es*(-1./2.*Caw22*wx*wx-1./2.*Caw23*ax*ax+Caw24*wx*wx)*WQC;
MNLw(3,3) = 0.0 ;
% ----- Aero [M]_NL
MNLa(1,1) = 0.0; MNLa(1,2) = 0.0; MNLa(1,3) = 0.0; MNLa(2,1) =
0.0; MNLa(2,2) = 0.0; MNLa(2,3) = 0.0; MNLa(3,1) = 0.0; MNLa(3,2)
= 0.0; MNLa(3,3) = 0.0;
% ----- Store [M]_NL
MNLs(1,1) = 1./2.*Mss*xss*Cus3*(ux+ux) + Mss*zss*Cus5*wx;
MNLs(1,2) = Mss*zss*Cus5*ux; MNLs(1,3) =
1./2.*Mss*xss*Cus4*(ax+ax); MNLs(2,1) = Mss*xss*Cws5*wx;
MNLs(2,2) = Mss*zss*Cws3*wx + Mss*xss*Cws5*ux; MNLs(2,3) =
Mss*zss*Cws4*ax; MNLs(3,1) = Mss*(xss*(Cas9*ax-Cas10*wx*ux) ...
    + 1./2.*zss*(Cas11*ax*ax+Cas11*ux*ux)) ...
    +Mss*(xss*Cas16*ux*wx - zss*Cas18*ux*ux) ...
    + Isys*Cas22*wx;
MNLs(3,2) = Mss*(-1./2.*xss*(Cas4*wx*wx+Cas5*ax*ax) ...
    + zss*(Cas6*ax-Cas7*wx*ux+Cas8*ux*wx) ) ...

```

```

    + Mss *(xss*Cas15*wx*wx -zss*Cas17*wx*ux) ...
    + Isys*(Cas22*ux-Cas23*ux);
MNLs(3,3) = 0.0;
%-----
% ----- Wing [C]_NL
CNLw(1,1) = -1./2.*Cuw11*ux*2*dux*WQC; CNLw(1,2) =
-1./2.*Cuw10*ux*2*dwx*WQC + es*(-Cuw23*dwx)*WQC; CNLw(1,3) =
es*Cuw22*dax*WQC; CNLw(2,1) = -1./2.*Cww11*2*dux*WQC
-es*Cww23*2*dwx*WQC;
%CNLw(2,2) = -1./2.*Cww10*2*dwx;
CNLw(2,2) = -1./2.*Cww10*2*dwx*wx *WQC; % 011604
CNLw(2,3) = 0.0; CNLw(3,1) = Iys*(2*Caw6*dwx -Caw7*dwx)*WQC ...
    +(Izs-Ixs)*(-Caw9*dux*ax *WQC -Caw10*dwx) ...
    + es*Caw25*dux*wx *WQC;
CNLw(3,2) = (Izs-Ixs)*Caw8*dwx*ax *WQC + es*Caw24*dwx*wx *WQC;
CNLw(3,3) = 0.0;
% ----- Aero [C]_NL
if (Vs == 0)
    iVs = 0;
else
    iVs = 1/Vs;
end
%
CNLa(1,1) = 0.0; CNLa(1,2) = 0.0; CNLa(1,3) = 0.0; CNLa(2,1) =
0.0;
CNLa(2,2) = -mu*CLa/pi*Vs^2/bs*c3* ( iVs*(-3*Cwa6*ax*ax) ... %

```

```

+ iVs^2*(3*Cwa8*ax*dwx-6*bs*(1./2.-a)*Cwa9*ax*dax) ...
+ iVs^3*(-Cwa11*dwx*dwx+3*bs*(1./2.-a)*Cwa12*dax*dwx
-3*bs*(1./2.-a)^2*Cwa13*dax*dax) );
%CNLa(2,3) = -mu*CLa/pi*Vs^2*c3* ( iVs*(bs*(1./2.-a)*Cwa7*ax*ax) ...
%CNLa(2,3) = -mu*CLa/pi*Vs^2*c3* ( iVs*(3*bs*(1./2.-a)*Cwa7*ax*ax) ...%
CNLa(2,3) = -mu*CLa/pi*Vs^2/bs*c3* ( iVs*(3*bs*(1./2.-a)*Cwa7*ax*ax)...%
+ iVs^2*(3*bs^2*(1./2.-a)^2*Cwa10*ax*dax) ...
+ iVs^3*(bs^3*(1./2.-a)^3*Cwa14*dax*dax) );
CNLa(3,1) = 0.0; CNLa(3,2) = -mu*Cma/pi*Vs^2*c3* (
iVs*(-3*Caa6*ax*ax) ...
+ iVs^2*(3*Caa8*ax*dwx-6*bs*(1./2.-a)*Caa9*ax*dax) ...
+ iVs^3*(-Caa11*dwx*dwx+3*bs*(1./2.-a)*Caa12*dax*dwx
-3*bs^2*(1./2.-a)^2*Caa13*dax*dax) );
CNLa(3,3) = -mu*Cma/pi*Vs^2*c3* ( iVs*(3*bs*(1./2.-a)*Caa7*ax*ax)
...
+ iVs^2*(3*bs^2*(1./2.-a)^2*Caa10*ax*dax) ...
+ iVs^3*(bs^3*(1./2.-a)^2*Caa14*dax*dax) );
% ----- Store [C]_NL
CNLs(1,1) = Mss*xss*Cus3*w*x*dux + Mss*zss*Cus5*2*dwx; CNLs(1,2) =
0.0; CNLs(1,3) = 1./2.*Mss*xss*Cus4*2*dax; CNLs(2,1) =
Mss*xss*Cws5*2*dwx; CNLs(2,2) = Mss*xss*Cws3*2*dwx; CNLs(2,3) =
0.0; CNLs(3,1) = -Mss*(xss*zss*(-Cas13*dux+2*Cas14*w*x*ax)...
-xss*Cas16*dux*w*x + zss*Cas18*dux*u*x) ...
+ Isys*(2*Cas22*dwx - Cas23*dwx) ...
+ (Iszs-Isxs)*(-Cas20*dux*ax-Cas21*dwx) ;
CNLs(3,2) = -Mss*(-xss*Cas15*dwx*w*x + zss*Cas17*dwx*u*x) ...

```

```

      +(Iszs-Isxs)*Cas19*dwx*ax;
CNLs(3,3) = 0.0;
% -----
% ----- Wing [K]_NL
KNLw(1,1) = -bz*(Cuw4*ux*ux + Cuw5*wx*wx) *WQC ...
      +(bz-1)*(Cuw7*ax*ax - Cuw8*wx*wx) *WQC;
KNLw(1,2) = by*Cuw3*ax + (bz-1)*Cuw6*ax; %
KNLw(1,3) = 0.0; KNLw(2,1) = -by*Cww3*ax - Cww5*wx*ux *WQC ...
      +(bz-1)*(Cww6*ax - Cww8*wx*ux *WQC) ; %
KNLw(2,2) = -Cww4*wx*wx *WQC - (bz-1)* Cww7*ax*ax *WQC; KNLw(2,3)
= 0.0;
%KNLw(3,1) = -(bz-1)*(Caw4*ux*ax *WQC - Caw5*wx);
KNLw(3,1) = -(bz-1)*(-Caw4*ux*ax *WQC - Caw5*wx); %
%KNLw(3,2) = -(bz-1)*Caw3*ax*ax *WQC;
KNLw(3,2) = -(bz-1)*Caw3*wx*ax *WQC; % 011604
KNLw(3,3) = 0.0;
% ----- Aero [K]_NL
KNLa(1,1) = 0.0; KNLa(1,2) = 0.0; KNLa(1,3) = 0.0;
%KNLa(2,1) = 0.0; KNLa(2,2) = 0.0;
      KNLa(2,3) = -mu*CLa/pi*Vs^2*c3*Cwa5*ax*ax;
KNLa(2,1) = 0.0; KNLa(2,2) = 0.0;
      KNLa(2,3) = -mu*CLa/pi*Vs^2/bs*c3*Cwa5*ax*ax; % '04
KNLa(3,1) = 0.0; KNLa(3,2) = 0.0; KNLa(3,3) =
-mu*Cma/pi*Vs^2*c3*Caa5*ax*ax;
% ----- Store [K]_NL = zeros(3)
KNLs(1,1) = 0.0; KNLs(1,2) = 0.0; KNLs(1,3) = 0.0; KNLs(2,1) =

```

```

0.0; KNLs(2,2) = 0.0; KNLs(2,3) = 0.0; KNLs(3,1) = 0.0; KNLs(3,2)
= 0.0; KNLs(3,3) = 0.0;
%=====
% Summation
% -----
for MCKi = 1:3
    for MCKj = 1:3
        ML(MCKi, MCKj) = MLw(MCKi, MCKj) + p1*MLa(MCKi, MCKj)
                                + p2*MLs(MCKi, MCKj);
        %-----
        CL(MCKi, MCKj) = CwL(MCKi, MCKj) + IR*p1*CaL(MCKi, MCKj)
                                + p2*CsL(MCKi, MCKj);
        % -----
        KL(MCKi, MCKj) = KLw(MCKi, MCKj) + p1*KLa(MCKi, MCKj) + p2*KLs(MCKi, MCKj);
        % ===== Nonlinear
        MNL(MCKi, MCKj) = p3*MNLw(MCKi, MCKj) + p1*p4*MNLa(MCKi, MCKj)
                                + p2*p5*MNLs(MCKi, MCKj);
        %-----
        CNL(MCKi, MCKj) = p3*CNLw(MCKi, MCKj) + p1*p4*CNLa(MCKi, MCKj)
                                + p2*p5*CNLs(MCKi, MCKj); %011403
        % -----
        KNL(MCKi, MCKj) = p3*KNLw(MCKi, MCKj) + p1*p4*KNLa(MCKi, MCKj)
                                + p2*p5*KNLs(MCKi, MCKj);
        %-----
        % -----
        Mt(MCKi, MCKj) = ML(MCKi, MCKj) - MNL(MCKi, MCKj); % [010704 00:02~] + -->

```

```

%-----
Ct(MCKi, MCKj) = CL(MCKi, MCKj) - CNL(MCKi, MCKj);
%-----
Kt(MCKi, MCKj) = KL(MCKi, MCKj) - KNL(MCKi, MCKj);
%=====

end      % of MCKj
end      % of MCKi
% =====
% Inverse matrix of [M]
iML = inv(ML);
detMt = Mt(1,1)*Mt(2,2)*Mt(3,3) - Mt(1,1)*Mt(2,3)*Mt(3,2) -
Mt(2,1)*Mt(1,2)*Mt(3,3) ...
      +Mt(2,1)*Mt(1,3)*Mt(3,2) + Mt(3,1)*Mt(1,2)*Mt(2,3)
      - Mt(3,1)*Mt(1,3)*Mt(2,2);
iMt = inv(Mt);
% =====
%
for MiKi = 1:3
  for MiKj = 1:3
    MiKL(MiKi,MiKj) = iML(MiKi,1)*KL(1,MiKj)+iML(MiKi,2)*KL(2,MiKj)
                    +iML(MiKi,3)*KL(3,MiKj) ;
    MiCL(MiKi,MiKj) = iML(MiKi,1)*CL(1,MiKj)+iML(MiKi,2)*CL(2,MiKj)
                    +iML(MiKi,3)*CL(3,MiKj) ;
%
    MiK(MiKi,MiKj) = iMt(MiKi,1)*Kt(1,MiKj)+iMt(MiKi,2)*Kt(2,MiKj)
                    +iMt(MiKi,3)*Kt(3,MiKj) ;

```

```

        MiC(MiKi,MiKj) = iMt(MiKi,1)*Ct(1,MiKj)+iMt(MiKi,2)*Ct(2,MiKj)
                        +iMt(MiKi,3)*Ct(3,MiKj) ;

    end      % of MiKj
end         % of KiKi

%=====
%
z3 = zeros(3,3); I3 = eye(3,3); for iSM = 1 : 3
    for jSM = 1 : 3
        SML(iSM,jSM)      = z3(iSM,jSM);
        SML(iSM,jSM+3)    = I3(iSM,jSM);
        SML(iSM+3,jSM)    = -MiKL(iSM,jSM);
        SML(iSM+3,jSM+3)= -MiCL(iSM,jSM);

        % Nonlinear
        SM(iSM,jSM)       = z3(iSM,jSM);
        SM(iSM,jSM+3)     = I3(iSM,jSM);
        SM(iSM+3,jSM)     = -MiK(iSM,jSM);
        SM(iSM+3,jSM+3)= -MiC(iSM,jSM);

    end

end

%
% =====
f = SM * y;

% ----- Summarize basic data
%%%      p[0] = Velocity, p1= aero_linear, La,
%        p[2] = store_linear, Ls

```

```

%           p3 = Wing_Nonlinear(NLw), p4=aero_nonlinear(NLa),
%           p5=store_nonlinear(NLs),
%           p[6] = xs, p7 = ys, p8 = zs, store position
%           p9 = Ms (store Mass), p[10] = Isy (Store inertia)
%           p11= IDmodel (0,1) = ( my model based on NATA, HGW) */
if (fidc ==1)
    IDmat = 1; IDkp = 0; IDsub = 1;
    IDp = BBT_printout(IDmat,IDkp,IDsub)
fprintf(fid,'\n===== Nonlinear Options
=====\n');
    fprintf(fid,' Vel. ratio = %8.2f  IDmodel(1,2)=(NATA,HGW)= %4i \n',Vs,p11);
    fprintf(fid,' La=%4i Ls=%4i NLw=%4i NLa=%4i NLS=%4i \n',p1,p2,p3,p4,p5);
    fprintf(fid,' ----- Store parameters -----\n');
    fprintf(fid,' xs=%4i ys=%4i zs=%4i Isy=%4i Ms=%4i \n',p6,p7,p8,p9,p10);
    fprintf(fid,'Matrices M C K and SM components are ... \n');
    fprintf(fid,'System Matric, SM(i,j) ... (Linear) \n');
    fprintf(fid,' %10.4e %10.4e %10.4e %10.4e %10.4e %10.4e \n',SM(1,1),
    SM(1,2),SM(1,3),SM(1,4),SM(1,5),SM(1,6));
    fprintf(fid,' %10.4e %10.4e %10.4e %10.4e %10.4e %10.4e \n',SM(2,1),
    SM(2,2),SM(2,3),SM(2,4),SM(2,5),SM(2,6));
    fprintf(fid,' %10.4e %10.4e %10.4e %10.4e %10.4e %10.4e \n',SM(3,1),
    SM(3,2),SM(3,3),SM(3,4),SM(3,5),SM(3,6));
    fprintf(fid,' %10.4e %10.4e %10.4e %10.4e %10.4e %10.4e \n',SM(4,1),
    SM(4,2),SM(4,3),SM(4,4),SM(4,5),SM(4,6));
    fprintf(fid,' %10.4e %10.4e %10.4e %10.4e %10.4e %10.4e \n',SM(5,1),
    SM(5,2),SM(5,3),SM(5,4),SM(5,5),SM(5,6));

```



```

fprintf(fid,' %10.4e %10.4e %10.4e %10.4e %10.4e %10.4e \n',SM(6,1),
SM(6,2),SM(6,3),SM(6,4),SM(6,5),SM(6,6));
fprintf(fid,'----- Non-Linear terms
----- \n'); fprintf(fid,'System Matric, SM(i,j) ...
(Non-Linear) \n');
fprintf(fid,' %10.4e %10.4e %10.4e %10.4e %10.4e %10.4e \n',SM(1,1),
SM(1,2),SM(1,3),SM(1,4),SM(1,5),SM(1,6));
fprintf(fid,' %10.4e %10.4e %10.4e %10.4e %10.4e %10.4e \n',SM(2,1),
SM(2,2),SM(2,3),SM(2,4),SM(2,5),SM(2,6));
fprintf(fid,' %10.4e %10.4e %10.4e %10.4e %10.4e %10.4e \n',SM(3,1),
SM(3,2),SM(3,3),SM(3,4),SM(3,5),SM(3,6));
fprintf(fid,' %10.4e %10.4e %10.4e %10.4e %10.4e %10.4e \n',SM(4,1),
SM(4,2),SM(4,3),SM(4,4),SM(4,5),SM(4,6));
fprintf(fid,' %10.4e %10.4e %10.4e %10.4e %10.4e %10.4e \n',SM(5,1),
SM(5,2),SM(5,3),SM(5,4),SM(5,5),SM(5,6));
fprintf(fid,' %10.4e %10.4e %10.4e %10.4e %10.4e %10.4e \n',SM(6,1),
SM(6,2),SM(6,3),SM(6,4),SM(6,5),SM(6,6));

fidc = fidc + 1; end

%===== End of Subroutine

```

Poincare Map Module : BT_Pm_F.m

```

% Poincare Map for BBT system [012104] + alpha
% ad = 0.0 condition is added. [052803]
% wd = 0.0

```

```

%
%function I_PM = BBT_PM_F(iV,Vfg,NF,y,tr,Lw,La)
function I_PM = BBT_PM_F(iV,Vfg,NF,y,tr,Lw,La)

global pmw pmw2 pmwt pmwt2 pma pma2 pmat pmat2
global iPPu iPPw iPPa % For Phase Portraits
global iPMu iPMw iPMa % For Poincare Maps
global ML CL KL SML %
global MNL CNL KNL SM % for BBT_sub
global Vr f_Bif y0
ado = 0.0 ; % zero setting
wdo = 0.0 t = tr;
IDc = 0 ; % Select Pm condition, IDc = (0,1) = (wdn = 0, adn=0)
scr = size(y); leng = scr(2); count = 1 ; countw = 1 ; counta
= 1; kcount = 1 ; kcountw = 1; kcounta= 1; for i = 1 : leng
% if (IDc == 1)
    wdn = y(5,i);
    wd_ind = wdo * wdn;
    % else
    adn = y(6,i);
    ad_ind = ado * adn;
    % end
NDOF = 3 ; % for BBT systems
if i ~= 1
    if (wd_ind <=0.0 ) %& wdn <=0.0)
        prw(kcountw) = countw;

```

```

    for jpm = 1 : 2*NDOF
        pmw(jpm,kcountw) = y(jpm,i);
        pmw2(jpm,kcountw) = (y(jpm,i)+y(jpm,i-1))/2;
    end
    pmwt(kcountw) = t(i);
    pmwt2(kcountw) = (t(i)+t(i-1))/2      ;
    kcountw = kcountw + 1 ;
end
if (ad_ind <=0.0 ) %& wdn <=0.0)
    pra(kcounta) = counta;
    for jpm = 1 : 2*NDOF
        pma(jpm,kcounta) = y(jpm,i);
        pma2(jpm,kcounta) = (y(jpm,i)+y(jpm,i-1))/2;
    end
    pmat(kcounta) = t(i);
    pmat2(kcounta) = (t(i)+t(i-1))/2      ;
    kcounta = kcounta + 1 ;
end
end
wdo = wdn;
ado = adn; % for da/dt = 0.0
count = count + 1;
%   count = count + 1;
end
%
figure(iPPu)

```

```

subplot(221),plot(y(1,:),y(4,:),pmw(1,:),pmw(4,:), 'o',pmw2(1,:),
                ,pmw2(4,:), 'x'), title('trajectories and Poincare Map
(du/dt=0.0)') legend('trajectoreis','Poincare
Map(1)', 'PoincareMap(2)') ,xlabel('u') , ylabel('du/dt') grid

subplot(222),plot(y(2,:),y(5,:),pmw(2,:),pmw(5,:), 'o',pmw2(2,:),
                ,pmw2(5,:), 'x'),
title(['(dw/dt=0.0) Vr = ',num2str(Vr(iV))]) xlabel('w') ,
ylabel('dw/dt') grid

subplot(223),plot(y(3,:),y(6,:),pma(3,:),pma(6,:), 'o',pma2(3,:),
                ,pma2(6,:), 'x'),
title('(d\alpha/dt=0.0)') xlabel('\alpha') , ylabel('d\alpha/dt')
grid Egn = eig(SML);
subplot(224),plot(y(3,:),y(6,:),pmw(3,:),pmw(6,:), 'o',pma(3,:)
                ,pma(6,:), 'x'),
title('(d\alpha & dw=0.0)'), hold on xlabel('\alpha') ,
ylabel('d\alpha/dt') title(['Eig(SML) =',num2str(Egn(1)),',
',num2str(Egn(3)),', ',num2str(Egn(5))])
legend('PP','dw=0','d\alpha=0') grid

I_PM(1) = kcountw -1; I_PM(2) = kcounta -1;
%I_PM = 1;

Bifurcation Module : BBT_Bif.m

% Bifurcation Diagram

```

```

%
function Bif = BBT_Bif_F(iV, NF, Lw, La)
%
global pmw pmw2 pmwt pmwt2 pma pma2 pmat pmat2
global iPPu iPPw iPPa % For Phase Portraits
global iPMu iPMw iPMa % For Poincare Maps
global iBIFuu iBIFuw iBIFua iBIFwu iBIFww iBIFwa iBIFau iBIFaw
iBIFaa global Vr f_Bif y0
%Nf = 20; % # of selected fixed points
%% ===== dw/dt = 0 =====
%Lw = length(pmw);
%if (Lw >= NF)
if (Lw > NF)
    LwNF = Lw - NF;
else
    LwNF = 1;
end Vbifw = Vr(iV) * ones(Lw,1) ;
% -----
figure(iBIFww)
plot(Vbifw(LwNF:Lw),pmw(2,LwNF:Lw),'bo','LineWidth',2,'MarkerSize',4,
'MarkerFaceColor','b','MarkerEdgeColor','b'),
hold on title(['Bifurcation diagram (I) : dw/dt = 0 & w(Fix) vs. V
' ]) figure(iBIFwa)
plot(Vbifw(LwNF:Lw),pmw(3,LwNF:Lw),'bo','LineWidth',2,'MarkerSize',4,
'MarkerFaceColor','b','MarkerEdgeColor','b'),
hold on title(['Bifurcation diagram (I) : dw/dt = 0 & a(Fix) vs. V

```

```

' ])
%% ===== da/dt = 0 =====
%La = length(pma);
%if (La >= NF)
if (La > NF)
    LaNF = La - NF;
else
    LaNF = 1;
end % LaNF = La - NF;
Vbifa = Vr(iV) * ones(La,1) ;
%-----
figure(iBIFaw)
plot(Vbifa(LaNF:La),pma(2,LaNF:La),'bo','LineWidth',2,'MarkerSize',4,
'MarkerFaceColor','b','MarkerEdgeColor','b'),
hold on title('Bifurcation diagram (II) : da/dt = 0 & w(Fix) vs. V
' ) figure(iBIFaa)
plot(Vbifa(LaNF:La),pma(3,LaNF:La),'bo','LineWidth',2,'MarkerSize',4,
'MarkerFaceColor','b','MarkerEdgeColor','b'),
hold on title('Bifurcation diagram (II) : da/dt = 0 & a(Fix) vs. V
')
%

fprintf(f_Bif,' %% ===== Poincare maps at dw/dt = 0.0 \n')
fprintf(f_Bif,' %% ===u=== ===w=== ===a=== ==du=== ==dw=== ==da===
\n')

for iw = LwNF : Lw

```

```

    fprintf(f_Bif,' %8.4f %8.4f %8.4f %8.4f %8.4f %8.4f \n',pmw(:,iw))
%   fprintf(f_Bif,' %8.4f %8.4f %8.4f %8.4f %8.4f %8.4f \n',pma(1,iw)
        ,pma(2,iw),pma(3,iw),pma(4,iw),pma(5,iw),pma(6,iw))
end
fprintf(f_Bif,' %% ===== Poincare maps at da/dt = 0.0 \n')
for ia = LaNF : La
    fprintf(f_Bif,' %8.4f %8.4f %8.4f %8.4f %8.4f %8.4f \n',pma(:,ia))
%   fprintf(f_Bif,' %8.4f %8.4f %8.4f %8.4f %8.4f %8.4f \n',pma(1,iw)
        ,pma(2,iw),pma(3,iw),pma(4,iw),pma(5,iw),pma(6,iw))
end
fprintf(f_Bif,' %% ===== End of Poincare maps \n')

Bif = 1;

```

VITA

Kiun Kim was born on Feb. 10, 1966 in Cheju, Korea. He is the fifth child of DongMin Kim and Gongsun Kang. He attended Cheju Cheil high school in Cheju and graduated in 1984. He attended Inha University in the city of Incheon in 1984, studied aerospace engineering, and received his Bachelor of Science (B.S.) degree in 1988. He received his Master of Science (M.S.) in aerospace engineering from Inha University in 1990. He started his career as a part of the military service at ADD, Teajon from 1990 to 1995 as Research Engineer. After finishing his military service, he worked as Senior Researcher at ADD until 2000. In 2000, he pursued his study in the Department of Aerospace Engineering at Texas A&M University. In May 2004, he received a Doctor of Philosophy (Ph.D) degree in aerospace engineering.

His permanent address is SamDo 1-Dong 259-51 (14/4), Cheju, Cheju Do, South Korea.